Co-funded by the

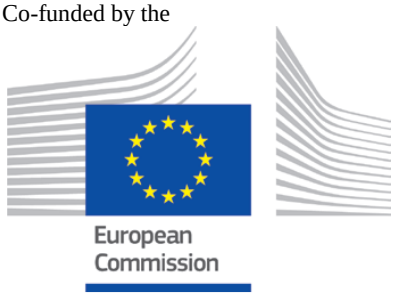

CEBAMA

➢ (Contract Number: 662147)

Deliverable n°D4.19

Draft of the 4rth and Final Project Workshop Proceeding

Editors: Amphos 21 and KIT

Date of issue of this report: May 2019

Report number of pages: 222

Start date of project: 01/06/2015 Duration: 48 Months

Project co-funded by the European Commission under the Euratom Research and Training Programme on Nuclear Energy within the Horizon 2020 Framework Programme		
Dissemination Level		
PU	Public	x
PP	Restricted to other programme participants (including the Commission Services)	
RE	Restricted to a group specified by the partners of the CEBAMA project	
CO	Confidential, only for partners of the CEBAMA project	

ABSTRACT:

The deliverable presents the draft of the 4th and Final Workshop Proceedings.

RESPONSIBLE:

Amphos 21

FOREWORD

The present document contains the proceedings of the 4th and Final Workshop of the EURATOM H2020 Collaborative Project CEBAMA (Cement-based materials, properties, evolution, barrier functions). The electronic version of these proceedings is available on the webpage of the project (*http://www.cebama.eu/*) and at KIT Scientific Publishing (*www.ksp.kit.edu*). The project started in June 2015 and had a duration of four years. The project was implemented by a consortium with 27 Beneficiaries, from 9 EURATOM Signatory States, Japan and Switzerland. National Waste Management Organizations contributed to the running project by participation in the End-User Group, by co-funding Beneficiaries, and providing for knowledge and information transfer.

These proceedings serve for several purposes. The key purpose is to document and make available the progress of the CEBAMA project to a broad scientific community. For this purpose, a considerable part of the project activity is reported by the proceedings, together with scientific-technical summaries containing details of the work developed during the project. The present proceedings are summarizing main efforts and results obtained by the individual contributing groups performed in the three technical Workpackages of CEBAMA. The project facilitated training mobility measures for students, and the Final Workshop also served to communicate the outcome of the CEBAMA mobility grants. Additional purposes of the proceedings are to ensure the documentation of the project outcome, promote systematic scientific-technical development throughout the project and to allow thorough review of the project progress and outcome.

All Scientific and Technical work developed in the project was closely followed by the EUG (End-User-Group) of CEBAMA. The EUG was specifically established within the project representing the interest of the national waste management and/or national regulatory organizations that may use the results of the project for their Safety Cases. For this reason, this EUG had a strong involvement on guiding the priorities of the activities of the project and it is a very useful tool to guarantee that the research is done in a way that allows for future knowledge transfer.

The proceedings give only very brief information about the project structure and the different activities around the project. This type of information is available in detail under *http://www.cebama.eu*. Public deliverables are likewise available at the project website.

The editors of the proceedings want to thank all contributors to the project, especially those submitting contributions to the proceedings, and the workpackage leaders who provided the summary of the different workpackages for publication in these proceedings. Special thanks are given to the the members of the EUG, whose effort and work reflected their commitment and dedication to the project and contribute to a high quality of the research performed within CEBAMA.

Table of Contents

FOREWORD I

THE PROJECT 1

FINAL (4TH) ANNUAL WORKSHOP 3

WP OVERVIEW 5

Overview of Work Package 1 7

Overview of Work Package 2 11

Overview of Work Package 3 13

TECHNICAL SUMMARIES 15

Technical Summary – KIT-INE – WP1 17

Technical Summary – British Geological Survey – WP1 25

Technical Summary – CIEMAT, CSIC, UAM – WP1 31

Technical Summary – SCK·CEN & BRGM – WP1 53

Technical Summary – UJV & CTU – WP1 59

Technical Summary – University of Sheffield – WP1 67

Technical Summary – VTT – WP1 73

Technical Summary – HZDR – WP1 77

Technical Summary – University of Lille – WP1 & WP3 83

Technical Summary – ANDRA – WP1 87

Technical Summary – University of Bern – WP1 91

Technical Summary – IRSN – WP1 97

Technical Summary – University of Surrey – WP1 103

Technical Summary – KIT-INE – WP2 111

Technical Summary – AMPHOS 21 – WP2 117

Technical Summary – BRGM – WP2 125

Technical Summary – JUELICH – WP2 129

Technical Summary – RATEN – WP2 133

Technical Summary – Armines/Subatech – WP2 139

Technical Summary – CTU – WP2 145

Technical Summary – PSI & EMPA – WP2 153
Technical Summary – University of Surrey – WP2 159
Technical Summary – KIT-INE – WP3 165
Technical Summary – AMPHOS 21 – WP3 175
Technical Summary – BRGM – WP3 177
Technical Summary – JUELICH – WP3 181
Technical Summary – NRG – WP3 187
Technical Summary – SKC·CEN – WP3 189
Technical Summary – UDC – WP3 195
Technical Summary – CTU –WP3 201
Technical Summary – VTT – WP3 209
Technical Summary – ANDRA– WP3 215
Technical Summary – PSI – WP3 217

THE PROJECT

CEBAMA was a Collaborative Project funded by the European Commission under the Horizon 2020 Reasearch and Training Programme of the European Atomic Energy Community (EURATOM) (H2020-NFRP-2014/2015), section B - Contribute to the Development of Solutions for the Management of Ultimate Radioactive Waste, Topic NFRP 6 - 2014: Supporting the implementation of the first-of-the-kind geological repositories).

The Collaborative Project CEBAMA addressed key issues of relevance for long term safety and key scientific questions related to the use of cement-based materials in nuclear waste disposal applications. These materials are key components in the barrier system of repositories, independent on the actual host rocks. They are used as waste forms, liners and structural components as well as sealing materials in a broad variety of applications. Waste forms and their behaviour as well as the technical feasibility and long-term performance of repository components are key topics detailed in the Strategic Research Agenda (SRA) of the Implementing Geological Disposal Technology Platform (IGD-TP) and cover studies related with: (a) the release of radionuclides, (b) long-term behaviour of seals and plugs, (c) evolution of cement-based seals, (d) interaction of cement with clays and (e) optimisation aspects.

The overall objective of CEBAMA was to support the implementation of geological disposal by improving significantly the knowledge base for the Safety Case for European repository concepts. The research planned in CEBAMA was largely independent of specific disposal concepts and addressed different types of host rocks in addition to bentonite. CEBAMA was not focusing on one specific cement material but aimed to study a variety of important cement-based materials in order to provide insight on general processes and phenomena.

The ambition of CEBAMA was the development of comprehensive models for predicting the alteration processes and their impact on transport characteristics such as porosity, permeability and diffusion parameters of different cement-based materials in contact with the engineered and natural barriers of repositories in crystalline and argillaceous host rocks. Dedicated studies on radionuclide retention processes on relevant hydrated cement phases, concrete and alteration products were also part of this advanced approach.

The project started on 1st June 2015 and lasted 4 years until end of May 2019. The project was implemented by a consortium with 27 Beneficiaries, from 9 EURATOM Signatory States, Japan and Switzerland. National Waste Management Organizations (WMO) contributed to the running project by participation in the End-User Group, by co-funding Beneficiaries, and providing for knowledge and information transfer.

Indispensable for CEBAMA is the documentation of the scientific and technical state of knowledge and the dissemination of the generated knowledge not only to the WMO but also to the general scientific community and other interested parties. This dissemination strategy was implemented by presentations at international conferences and publications in peer-reviewed journals. Interaction with social stakeholders is of relevance for facilitating global understanding for the need of research in nuclear waste management, and CEBAMA aimed at helping to bridge this communication process. The aspect of training and education of the next generation of waste management professionals was specifically addressed in CEBAMA.

FINAL (4th) ANNUAL WORKSHOP

The Final Workshop of the Collaborative Project CEBAMA was held in Karlsruhe (Germany), 28th – 29th March 2019. The workshop was hosted by KIT-INE at the ACHAT Plaza hotel. There were 66 attendees, including beneficiaries, End-User-Group members, Associated Group organizations and project external organizations. The workshop was organized in two days and the agenda is shown in Figure 1.

Agenda *(28th - 29th March 2019)*

Thursday 28th March 2019

8:00-9:30	1st ExCom meeting *(restricted to ExCom members)*
9:30-9:45	Welcome + Presentation by the Coordination Team
9:45-12:00	PhD Session (PhD presentations, 10 min each)
12:00-13:00	*LUNCH*
13:00-14:00	WP1 Summary Session
14:00-14:45	WP2 Summary Session
14:45-15:15	*Coffee break*
15:15-16:15	WP3 Summary Session
16:15-17:15	**Reporting & Project closure**
19:00	*-- Workshop DINNER --*

Friday 29th March 2019

8:00-8:45	ExCom & EUG meeting (in parallel) *(restricted to ExCom/EUG members)*
8:45-9:30	ExCom & EUG meeting (join meeting) *(restricted to ExCom/EUG members)*
9:30-11:00	Topical Session + Stakeholder Panel (Topic: **Future EU Projects**)
11:00-12:00	**EUG** feedback **+ General Assembly**

Figure 1: *Agenda of the Final Workshop of CEBAMA.*

The objectives of the workshop are presented below.

- Promoting joint research activities within CEBAMA.
- Providing for detailed agreements on the work program, activities and training measures.
- Communicating the status of the different project activities, work and state of progress between all project partners including non-technical stakeholders.
- Discussing the status of the work programme and decide on next steps for closing the project
- Preparing for organization of public Workshop Proceedings for effective documentation and communication of the project achievements.

The Final Workshop included several sessions/meetings such as the ExCom/EUG meetings, WP sessions and General Assembly. A topical session and Stakeholder Panel were also organized.

ExCom and EUG meetings took place the first and second day of the workshop and were focused on the project management and discussion with EUG on the project progress and closure.

The Stakeholder Panel was organized as a Topical Session. The topical session provides an overview on future EU projects. The following presentations were given:

- *Bernd Grambow* (Subatech/Armines) General overview on EURAD project and the EURADScience network
- *Francis Claret* (BRGM) DONUT, Development and improvement Of NUmerical methods and Tools for modelling coupled processes
- *Marcus Altmaier* (KIT-INE) CORI, Cement Organic Radionuclide Interaction
- *Guido Deissman* (JUELICH) on behalf of *Dirk Bosbach*, FUTURE, Fundamental understanding of radionuclide retention

Plenary sessions of WP1, WP2 and WP3 consisted on an overview of the work progress given by the workpackage leader of each technical WP. The three presentations gave an insight on the topics listed below with the aim of providing a complete and integrated view of the work developed during the 4-years of the project.

- Objectives of the workpackage and the partners involved in the investigation studies,
- Summary of the obtained results in an integrated manner,
- Dissemination of the obtained results (mainly conferences and publications),
- Integration between technical workpackages,
- Future needs and impact on the Safety Assessment.

At the end of the workshop, Seif Ben Hadj Hassine (EUG chairman) gave feedback to CEBAMA partners on behalf of the EUG about the progress and main results of the project. Following, the *general assembly* closed the final workshop of the CEBAMA project.

WP OVERVIEW

Overview of Work Package 1

Experiments on interface processes and the impact on physical properties

WP leaders:
Erika Holt (VTT)
Francis Claret (BRGM)
Urs Mäder (*UNIBERN*)

The largest amount of resources (~ 50%) and the most work effort was used for WP1 with 19 institutions participating, led by VTT (Finland), BRGM (France) and the University of Bern (Switzerland). The main objectives were: (i) to perform experimental investigations to better understand and quantify the alteration processes between cement-based materials and different host rocks of interest to Waste Management Organizations (i.e. crystalline rock, Boom Clay, Opalinus Clay (OPA), Callovo-Oxfordian (COX), Toarcian mudstone, Borrowdale Volcanic Group) or engineered barrier components (bentonite backfill) and (ii) to assess their impact on physical (i.e. diffusivity, hydraulic conductivity, porosity, strength,…) and chemical (i.e. porewater composition, mineralogy) properties.

Two types of cementitious materials (based on ordinary Portland cement (OPC), and/or "low-pH cement") were studied, which were in contact with either aged or fresh interfaces (i.e. claystone, bentonite, other rock types) or with model pore water / groundwater solutions. A key source for aged interface materials were ongoing experiments from existing underground research labs (URLs, samples up to 10+ years old) from 6 European URLs in Switzerland, France, Czech Republic and Belgium (i.e. Grimsel test site, Mont Terri laboratory, HADES, Tournemire, Meuse/Haute, Josef) and from Japan. The work of the partners in WP1 focused on five main topics:

- Quantifying transport parameters of altered and unaltered cement-based samples by performing through- and in-diffusion experiments and development of new non-invasive techniques (i.e. GeoPET method).
- Study of hydro-mechanical processes in the interface cement - Callovo Oxfordian claystone, measuring the evolution of flow and strength properties of different cementitious-based materials (i.e. low-pH concrete).
- Study of thermo-hydro-geochemical processes in the interface cement-clay, measuring changes on transport properties due to mineralogical alteration and microstructure changes (e.g. Ca leaching, carbonation).
- Analyses of interface reactions, with respect to changes in mineralogy and porosity evolution, between different materials in contact with solutions with different compositions (i.e. pH, redox, carbonate, sulphate concentration, salinity) by percolation and leaching experiments.
- Manufacturing and characterisation of the reference materials of the CEBAMA project as a benchmark to other studies by various partners.

As reference materials within the CEBAMA project, ternary low-pH concrete (RCM) and a paste (RPM) were manufactured, setting a specific focus on high-performance low-pH materials. Mixtures were cast at VTT in March 2016 and distributed among several CEBAMA partners early in the project. This reference material was also used in WP2 and WP3 of CEBAMA, thus further exploiting synergies between the partners and different WPs in CEBAMA.

The reference mix designs and materials were characterised by different partners in CEBAMA using several techniques (i.e. XRD, XRF, TG/DTA, ^{29}Si and ^{27}Al MAS NMR, X-CT, SEM/EDX, XAS, ICP-OES, etc.) providing complementary information on mechanical, chemical, transport properties and microstructure. Table 1 provides an overview of the applied characterisation methods used by the partners. Most of the results were in agreement but also some disparities were observed. Mineralogical composition, diffusion coefficient and pore solution pH were determined with multiple methods. The results enable comparison between different experimental set-ups and increases cohesion of individual experiments. Low diffusion coefficients (RPM: $10^{-(12\text{-}13)}$ [mol(HTO)/(m^2/s)] and high compression strengths (RCM: 115 MPa, RPM: 150 MPa) were determined with multiple methods. The results confirmed that nanoporosity has a large effect in high performance cementitious materials' total porosity and thus long-term performance. In the studies, the importance of curing temperature on pH development was observed, meaning that pH decreases significantly slower in cold environments.

Table 1: *CEBAMA reference concrete and paste characterisation methods.*

Quality	Partner	Paste (RPM)	Concrete (RCM)
Fresh-stage properties			
Workability	VTT	yes	yes
Air Content	VTT	no	yes
Heat of hydration	USFD	yes	no
Setting	USFD	yes	no
Mechanical properties			
Compression strength	VTT, USFD, CTU, UJV	yes	yes
Chemical composition			
X-ray diffraction (XRD)	KIT, USFD, JUELICH, SURREY, CSIC, UAM	yes	yes
X-ray fluorescence (XRF)	SURREY	initial materials	
Thermogravimetry (TG/DTA)	KIT, USFD, CSIC, UAM	yes	yes
^{29}Si and ^{27}Al MAS NMR	KIT	yes	no
Energy dispersive microscopy (SEM, Back Scattering+ EDS)	KIT, CSIC, USFD, JUELICH	yes	yes
X-ray absorption spectroscopy (XAS, Fe and Cl K-edge)	KIT	yes	yes
Pore solution pH	KIT, VTT, CSIC	yes	yes
Microstructure			
Scanning electron microscopy (SEM)	KIT, CSIC, USFD, JUELICH	yes	yes
Porosity	CSIC, USFD, UJV, BRGM	yes	yes
X-ray computed tomography	USFD	yes	no
Transport properties			
Leaching	VTT	yes	yes
Percolation	USFD, SURREY, CSIC, CTU, UJV	yes	yes
Diffusion	JUELICH, CSIC, UAM, KIT	yes	yes
Other			
Density	VTT, USFD	yes	yes
Spectral induced polarization (SIP)	JUELICH and BRGM	yes	no

Overview of Work Package 2

Radionuclide retention in high pH concrete

WP *leader:*
Bernd Grambow (ARMINES)

There were 10 institutions working in WP2 of CEBAMA which was led by ARMINES/SUBATECH (France). The work of the partners n WP2 was focused on radionuclide retention/migration processes. The main efforts were dedicated to (i) high pH cementitious environments characteristic for cementitious materials, (ii) relevant individual hydrated cement phases and cement pastes and (iii) aged cement pastes. Additionally, the low-pH reference materials of the CEBAMA project as developed in WP1 were considered. The investigations in WP2 include retention or sorption, diffusion, solubility and co-precipitation studies. Focus was put on elements and nuclides for which only insufficient information was available before CEBAMA was started and rather large related uncertainties existed. Work performed by partners in WP2 is divided into the following topics:

- Detailed solid characterisation performed on the experiments with radionuclides using several complementary analytical techniques. (e.g. XRD, XRF, BET, SEM/EDS, TG-DSC and ^{29}Si NMR).
- Solubility experiments with Be, Mo and Se under high pH conditions. Providing for realistic solubility limits and radionuclide speciation schemes was a prerequisite for meaningful sorption studies allowing to derive advanced models on radionuclide retention.
- Sorption/desorption experiments were carried out using various radionuclides or toxic elements (i.e. Be, Mo, Ra, Tc, I^-, IO_3^-, SeO_3^{2-}/SeO_4^{2-}, Cl^-, Ra, Sr and ^{14}C) and various hardened cement paste formulations as well as individual cement phases.
- Solid solutions formation between various radionuclides in a range of oxidation states (Se, I and Mo) and main components (OH, S, Cl…) in cementitious phases (AFm).
- Diffusion experiments were performed with various anionic species ($^{36}Cl^-$, $^{99}TcO_4^-$, $^{125}I^-$, ^{14}C) or sorbing radionuclides (Ra, Sr) through saturated hardened cement pastes considering as well partially water saturated conditions.

As examples of research performed within WP2 of CEBAMA, studies on Se and Be retention are summarised in Figure 1. The joint research performed by CEBAMA partners offered a significantly improved description of Se retention in a variety of systems, while studies on Be within CEBAMA give clear experimental evidence of a strong Be retention in cementitious system, contrary to previous assumptions.

(i)

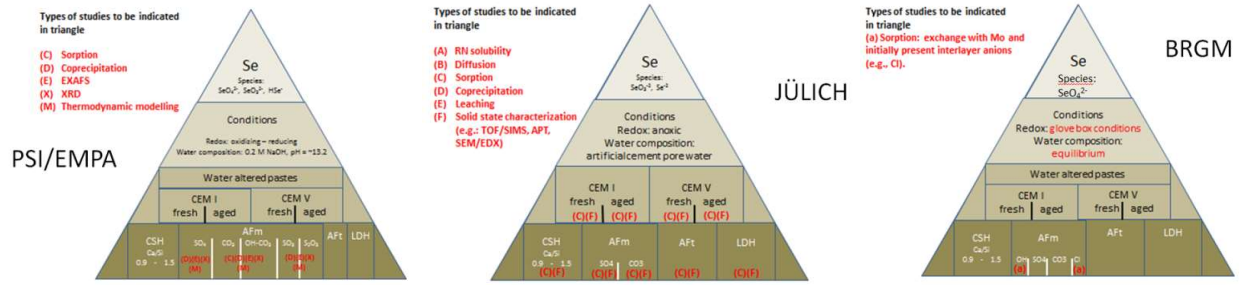

(ii)

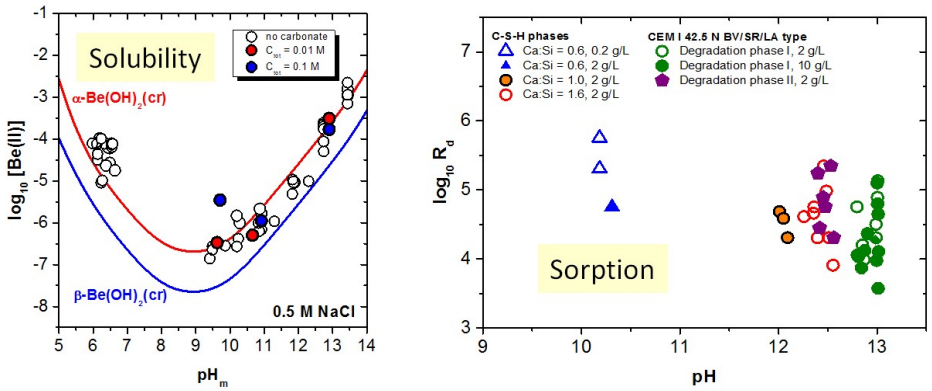

Figure 1: (i) *Overview on the specific systems studied in CEBAMA on Se retention by PSI/EMPA, JUELICH and BRGM. (ii) Studies on Be retention by KIT indicate strong Be retention in cementitious systems.*

Overview of Work Package 3

Interpretation & modelling

WP leader:
Andrés Idiart (AMPHOS21)

In WP3 of CEBAMA, advanced modelling approaches were developed and improved to predict coupled THMC processes at the interface between cement-based materials and engineered or natural barriers in crystalline and argillaceous host rocks. A total of 13 partners were working in this WP led by AMPHOS21. Activities within this WP were mainly dedicated to the modelling and interpretation of experimental data, also generated within CEBAMA in WP1 and WP2. WP3 was additionally contributing to extrapolate modelling to system-level for Safety Case applications and validate different modelling tools. Main modelling work was focused on four main tasks:

- Development of modelling tools with pore- and continuum-scale applications including new capabilities (i.e. Poisson-Nernst-Planck equations, Poisson-Boltzmann equations, coupling with geochemical solvers, coupling between chemistry and mechanics, etc.) in already existing or new codes (i.e. iCP, ORCHESTRA, MATLAB, iPP, Yantra, etc.).
- Modelling work with application to WP1 and WP2 experiments (i.e. through-diffusion tests, leaching tests, cement-clay interaction, etc.), including reactive and mass transport simulations, cement hydration models, solubility calculations and hydromechanical simulations.
- Long-term modelling of concrete-clay interactions including reactive transport and hydro-mechanical-chemical coupled analyses.

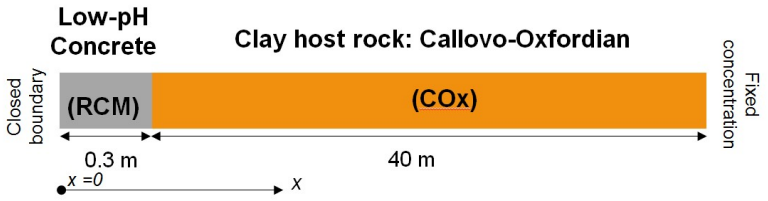

Material	Porosity	Pore diffusivity (m^2/s)	Effective diffusivity (m^2/s)
COx claystone	0.18	$1.44 \cdot 10^{-10}$	$2.60 \cdot 10^{-11}$
Low-pH concrete	0.04	$2.50 \cdot 10^{-11}$	$1.00 \cdot 10^{-12}$

Figure 2: *Geometry and key parameter of the system investigated within the Common Modelling Task.*

To optimize the integration of different modelling approaches and the experimental data obtained in CEBAMA, a Common Modelling Task was developed within the project. The goal of this task, which was supported by 8 different partners, was to cluster WP3 activities around a common long-term simulation case, using a low-pH cement (CEBAMA reference material) / clay interface, based on the set-up shown in Figure 2.

The figure shows the geometry used in the simulations. The interface investigated is resolved with cm-scale elements at both sides of the interface. Initial properties and composition of the low-pH cement used in the simulation were based on the experimental findings obtained for the reference ternary low-pH concrete. The Common Modelling Task helped to increase confidence in the consistency of the different modelling approaches (see contribution to EURADWASTE by A. Idiart et al.) for the simulation of the long-term behaviour of low-pH cementitious materials with reactive transport tools.

Technical Summaries

Technical Summary – KIT-INE – WP1

1. Introduction & Objectives

Cement and clay materials will be used as backfill/ barrier material in deep geological facilities for nuclear waste disposal. During the prolonged period of post disposal, cementitious and clay materials will undergo alterations, possibly changing the chemical and physical (i.e. porosity, permeability) properties of these barriers and developing spatial heterogeneities. One important process that could reduce the durability of the concrete is the leaching/degradation of the solid, especially at the cement/clay interface due to the contact of clay pore water with the cementitious material. In order to minimize the interaction between "classical" ordinary Portland cement (OPC) and the bentonite porewater (pH ~ 7.5), low pH cements were developed within the nuclear waste disposal context in the late 90's. For this reason, the knowledge of low-pH cement systems is much less well advanced that the one of OPC and few studies are available in the literature (Cau Dit Coumes et al. 2006; Codina et al. 2008; García Calvo et al. 2010; Lothenbach et al. 2012; 2014).

In this context, the understanding of the evolution of the interface low pH cements / bentonite over geological time scales and the impact on radionuclide migration requires a detailed knowledge of a series of highly complex coupled Thermo-Hydro-Mechanical-Chemical processes, not investigated in detail in the past. For example, not experimental data on laboratory and field scales were available for the low pH cement / bentonite system when the Cebama project started in 2015. In addition, only in the last years the impact of low pH cement materials on surrounding clay host rocks (i.e. Opalinus clay) has started to be investigated (Savage and Benbow, 2007; Dauzères et al. 2010; 2014; 2016; Jenni et al. 2014; Lerouge et al. 2017) and the impact that these degradation processes can have in radionuclide migration have never been studied before.

Therefore, an urgent need to obtain detailed knowledge and process understanding on the interface low pH cement / clay processes was identified, specially assessing the impact that these processes can have in radionuclide migration. For this reason, the specific objectives of KIT, to contribute to advance in these topics are to acquire in depth knowledge process understanding on:

- Interface chemical processes between low pH cement based materials and bentonite and their specific impact on transport properties and microstructure.
- Radionuclide migration processes (sorption, diffusion) under low pH cement conditions, specially related to anionic radiotracers (i.e. $^{36}Cl^-$, $^{129}I^-$) and tritiated water (HTO) migration.

For achieving the mentioned objectives a combination of different experiments, modelling and techniques have been combined:

- Physicochemical characterization of the cementitious starting materials by different complementary techniques: X-ray diffraction (XRD), thermogravimetric - differential thermal analysis (TG-DTA), Fourier-transformed infrared spectroscopy (FT-IR), ^{29}Si and ^{27}Al magic angle spinning nuclear magnetic resonance spectroscopy (^{29}Si and ^{27}Al MAS NMR), scanning electron microscopy - energy

dispersive X-ray spectroscopy (SEM-EDX), X-ray absorption spectroscopy (XAS), zeta potential measurements, BET analysis and mercury intrusion porosimetry (MIP).

- Kinetic batch sorption experiments and through diffusion experiment of HTO, $^{36}Cl^-$, $^{129}I^-$ on low pH cementitious materials under equilibrated conditions and in contact with MX-80 bentonite porewater.
- Characterization of the alteration process versus time by using techniques like scanning electron microscopy - energy dispersive X-ray spectroscopy (SEM-EDX), and through diffusion experiments among others.

2. Studied system

KIT-INE has mainly worked with low-pH cement pastes, characterizing them and studding the interaction of these material with bentonite water. The characterization includes chemical composition determination, microstructure evaluation and transport properties measurements of 4 different low-pH cement pastes, before and after the interaction with bentonite water.

The four low pH cements investigated consist on three different homogeneous hydrated pastes (MIX 1, MIX 2 and MIX 3) manufactured by KIT-INE and the reference low-pH paste of the project (cebama paste). The water/binder ratio used is 0.60 for the three mixes (MIX 1, MIX 2 and MIX 3). Table 1 gives the composition of the raw materials used to prepare the low pH cement pastes.

Additionally, synthetic low pH cement waters were also prepared and used in the sorption of HTO, $^{36}Cl^-$ and $^{129}I^-$ and diffusion experiments of HTO and $^{36}Cl^-$. To perform alteration studies, an MX-80 bentonite artificial water (BAW) was prepared, on the basis of the synthesis method described in Bradbury and Baeyens 2011 (see Table 2).

Table 1: *Composition (wt.%) of the solid mixtures used to prepare the low pH cement pastes.*

	(wt.%)			
	MIX 1	**MIX 2**	**MIX 3**	**cebama paste**
CEM I	50[a]	40[a]	39[a]	25[b]
Silica fume	50	40	39	27
Limestone filler	-	20	19	-
Superplasticizer	-	-	3c	4d
Blast furnace slag	-	-	-	16
Quartz filler	-	-	-	28
Water/binder ratio		0.6		0.25

[a] CEM I 52.5N SR; [b] CEM I 42.5 MH/SR/LA; [c] Inorganic superplasticizer (SioxX®).

Table 2: *Chemical compositions of the equilibrated solutions of the different cement pastes and bentonite artificial water (BAW).*

mM	**Si**	**Na**	**Ca**	**K**	**Cl**	**SO_4**	**Al**	**Mg**	**Sr**	**CO_3***	**pH**
BAW	$7.5\cdot10^{-2}$	251	14.9	3.2	233	72.3	$4.4\cdot10^{-4}$	9.6	0.10	0.20	8.0

3. Main results – Scientific highlights

3.1. Microstructure and chemical properties of low-pH cements

Various complementary analytical techniques have been used, such as XRD, TG-DTA, FTIR, ^{29}Si and ^{27}Al MAS NMR, SEM-EDX, XAS, zeta potential measurements, BET and MIP to characterize 4 low pH cement pastes defined in section 1.2. Table. 3 gives a summary of the main phases identified/quantified in all the samples. This multi-method approach has, demonstrated that the main hydrated phases are C-A-S-H phases with Ca:Si ratios between 0.6 - 1.1 and Al:Si ratio around 0.05. Additionally, ^{29}Si and ^{27}Al MAS NMR spectra of all the samples (see Figure 1) have shown that Al is tetrahedrally incorporated in the bridging position of the C-S-H phases. Unreacted silica fume is identified as well with SEM-EDX, FT-IR, and ^{29}Si MAS NMR (see Figure 1 with a broad peak at -110 ppm). On the other hand, the presence of unreacted clinker (alite, belite and ferrite) have only been identified in cebama paste together with blast furnace slag, The only minor phase present in all samples is ettringite, clearly seen in the ^{27}Al MAS NMR spectra (Figure 1 with an observed resonances of octahedrally coordinated ^{27}Al). Limestone filler is present in MIX 2 and MIX 3, as it has been added initially for their manufacturing. Finally, the Fe speciation investigated with Fe K-edge XANES, suggests that Fe is located in different phases, such as ettringite, C-S-H (Ca:Si = 1.0), and unreacted clinker (C4AF). For chloride it seems that the speciation in all samples is similar and close to the environment of Cl in the $CaCl_2{\cdot}2H_2O$ salt.

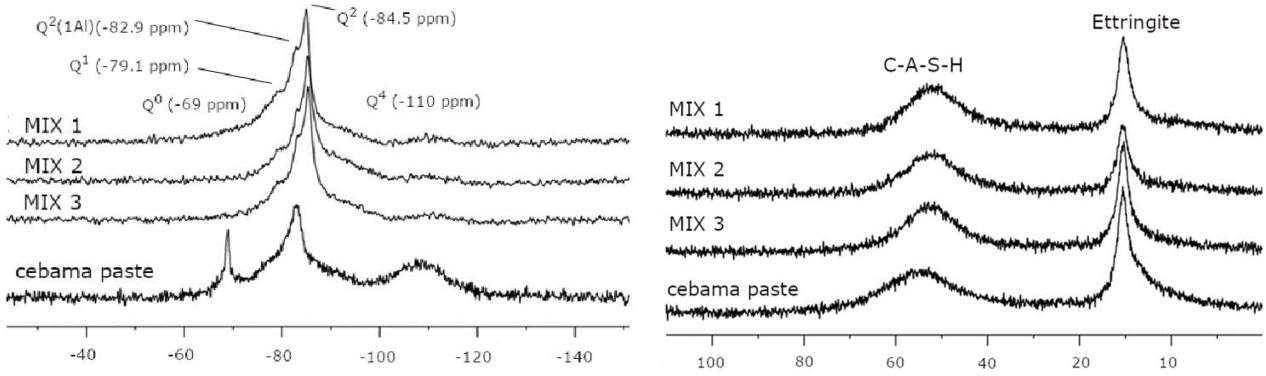

Figure 1: *^{29}Si and ^{27}Al MAS NMR MAS NMR spectra of hydrated cement with assignment the chemical shifts.*

TG-DSC has been applied as well, to measure the bound water in cement samples which correspond to the interlayer water in C-S-H phases, structural water in ettringite, and adsorbed water, but not water in micropores or in larger pores. The amount of bound water was calculated according with the method described in Lothenbach et al. (2012) and is given in Table 3. Additionally, BET analysis has been applied to measure the reactive surface area of the hydrated samples (see Table 3). Comparison of the obtained results with the ones obtained in the literature with a freshly synthetized C-S-H phases (Ca/Si = 1) (Baur et al. 2004), indicate that the reactive surface area of the three samples is correlated with the presence of the C-S-H phases. Finally, the porosity (see Table 3) and pore size distribution were characterized by MIP indicating that the size of the pores in the hydrated cement phases varies from the micro (< 0.04 µm) - to the nanoscale (< 10 nm), attributed to the connected capillary porosity and the C-A-S-H nano-porosity.

Table. 3: *Hydrates and raw materials identified / quantified (wt.%) in the 4 different low pH cement pastes.*

		MIX 1	***MIX 2***	***MIX 3***	***Cebama paste***
Hydrated phases	C-(A)-S-H[a]	92	81.6	83.1	✓
	Al-Ettringite	1.0	1.0	< 1.0	✓
	Fe phases	Fe incorporated in C-S-H + Fe-ettringite			Fe-ettringite +hematite
Raw materials	Silica fume	✓	✓	✓	✓
	Calcite	< 2.0%	11.4%	12.8%	< 2.0%
	Alite, Belite	n.i.			✓
	Ferrites	C4AF			C2F
	Blast furnace slag	n.i.			✓
	Quartz filler	n.i.			✓
	Bound water	29.4	28.5	26.5	10.9
	Bulk density ρ_d (kg/m^3)	1562	1561	1545	2087
	Porosity[b] (%)	35 ± 5	43	24	6.1
	Surface area[c] (m^2/g)	42.6	54.5	46.7	n.m.

.i*n.i. = not identified, n.m. = not measured, [a]C-A-S-H, which could as well include poorly crystalline phases (such as hydrotalcite or monocarbonate) and silica fume, [b]measured with MIP, [c]measured with BET*

Finally, zeta potential measurements of the low pH cement particles, at different concentration of KCl and KI are performed and compared with the one of pure C-S-H phases (Ca/Si = 1.6 - 1.0 - 0.8). The available data indicate a negatively charge surface related with the deprotonated surface silanols of low Ca/Si C-S-H and C-A-S-H phases (main phases of low pH cement).

3.2. Sorption properties of low-pH cements

Kinetics batch sorption experiments of $^{36}Cl^-$, $^{129}I^-$ and HTO in 3 different low-pH cements (MIX 1, MIX 2 and MIX 3) are carried out in a glove box under a controlled Ar atmosphere (O_2 and CO_2 concentrations < 5 ppm), in order to avoid carbonation of the alkaline waters. The uptake studies are realized with a solid-liquid ratio of 133 g·L^{-1} and are followed for a period of 10 - 30 days. Phase separation is achieved with a decantation and a filtration using PVDF filters (0.45 µm pore size). In all cases the results indicates a very weak sorption and the uptake process presents a similar fast mechanism. The determined distribution ratio, R_d value of HTO, $^{36}Cl^-$ and $^{129}I^-$ are 0.40 ± 0.13 L/kg, 0.22 ± 0.15 L/kg and 0.13 ± 0.03 L/kg, respectively. Characterization of the solid sample after 30 days of sorption studies with XRD and TG analysis reveal a no formation of secondary phases, such as Friedel's salt.

The uptake process of Cl and I is probably associated with surface processes in the C-S-H and C-A-S-H phases with competition for sorption sites, between them. In the case of HTO, isotopic exchange with the interlayer water of the C-S-H and the C-A-S-H (associated with the determined bound water) seems to be the main uptake process (Ochs et al. 2016).

3.3. Through diffusion experiments of HTO and $^{36}Cl^-$ in low pH cement paste

Through-diffusion experiments are conducted during 60 days with a cylindrical diffusion cell manufactured in KIT. Diffusion experiments are carried out in a glove box under a controlled Ar atmosphere (O_2 and CO_2 concentrations < 5 ppm), in order to avoid carbonation of the alkaline waters. Three different low pH cement pastes (MIX 1, MIX 3 and Cebama paste (RPM)) have been used in these experiments. The setup consists of a thin cement sample of 10 mm thickness sealed and mounted between two compartments filled with artificial cement water, called upstream and downstream compartment, with total volumes of 50 mL and 3.8 mL, respectively. A gradient of concentration of the two tracers is maintained with a constant concentration of $[HTO]_0 = 1.86 \cdot 10^{-9}$ M and $[^{36}Cl^-]_0 = 4.55 \cdot 10^{-6}$ M, in the upstream, and zero ($C_{down} = 0$) in the downstream compartment.

As illustrative example, the accumulated amounts (mol) of HTO and in the low reservoir and their diffusive fluxes during the diffusion through two RPM samples are shown in Figure 2. Transport parameters of HTO and $^{36}Cl^-$, such as, the effective diffusion coefficient D_e [m^2/s], the capillary porosity, ε [-], and the rock capacity factor, α [-], were obtained by inverse modelling considering Fickian diffusion and using the finite element code Comsol Multiphysics 5.3 to solve the partial differential equations. To verify the applicability of the relationship between porosity and effective diffusivity, the fitting of the experimental data was carried out using two approximations: a modified Archie's law and a multiporosity approach developed in the National Institute of Standards and Technology "NIST" (Bentz et al. 2000).

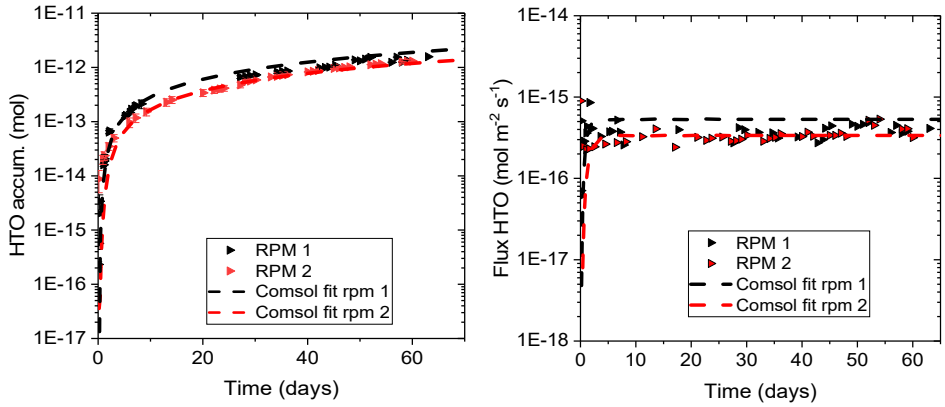

Figure 2: *Accumulated amount of HTO in the low reservoir vs. time and its diffusive flux during diffusion experiments through cebama paste "RPM". $[HTO]_0 = 1.86 \cdot 10^{-9}$ M. Background electrolyte was equilibrated water. Comsol fit from the inverse modelling with the correlation porosity-effective diffusivity developed in NIST.*

3.4. Alteration process between low pH cement pastes and bentonite water

Two different experimental set-ups have been used to study the alteration of low pH cement pastes (MIX 1 and Cebama paste) with bentonite water. Independently of the setup, and prior to the alteration experiments, the cement samples were fully saturated with artificial low-pH cement water. The first setup consist on a cube (10×10×10 mm) sealed with an epoxy resin, except from one side, placed in polyethylene container filled with 40 mL of artificial bentonite water at room temperature. After 6 months in a glove box under a controlled Ar atmosphere (O_2 and CO_2 concentrations < 5 ppm), the low pH cement is immersed in isopropanol in order to displace the water and stop the possible reactions. The alteration zone is then characterized by cutting the cement sample in parallel to the flow direction and identifying the chemical perturbation by SEM-EDX in submillimetre - micrometre scale.

Figure 3 shows the cement phase distributions in false colours (left) overlaying the electron image of cebama paste (right) in contact with the bentonite water. Note that the crack observed in the figure was produced during the cutting of the sample after the degradation experiments. Additionally, hollow shell pores having size range about 1-15 µm have also been identified. These pores are embedded in cement gel and appear to be connected to the continuous capillary pore system by much smaller gel pores. From the images it can be clearly distinguished the initial mineralogical heterogeneity of the sample (in the studied spatial scale) identifying C-(A)-S-H phases, blast furnace slag, quartz filler and initial clinker (belite, ferrite). Additionally, a reacting front of 400 µm from the surface in contact with the bentonite water can be clearly distinguish. ´

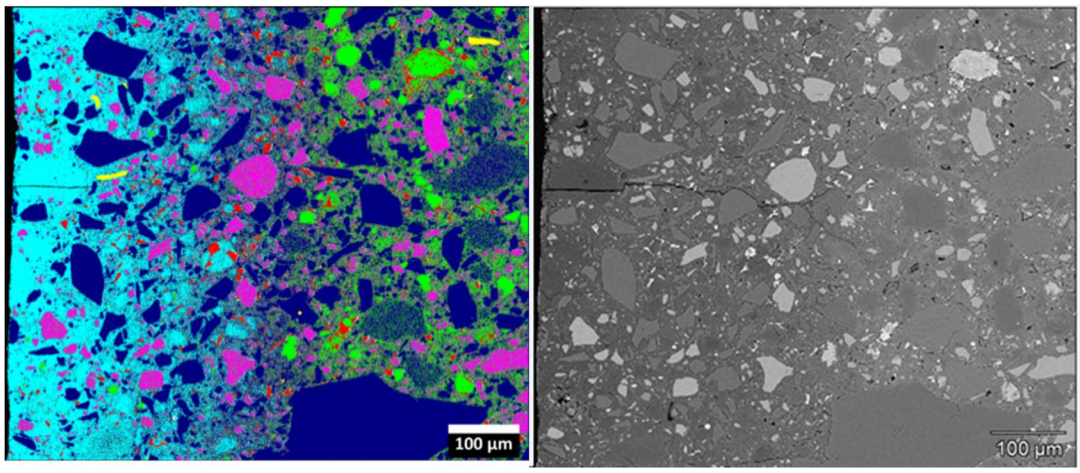

Figure 3: *Left, phase distributions in false colors overlaid on the electron image of a cross-section of low pH cement (Cebama paste) after contact with bentonite pore water (right). Color legend: Mg-exchanged C-S-H (cyan, C/S = 0.17), quartz filler (dark blue), blast furnace slag (pink), belite (shinning green), ferrite (red), muscovite (yellow), C-(A)-S-H (blue/green).*

In order to identify the chemical processes occurring in that area, 700 µm perpendicular to the flow direction is homogenized giving the elemental depth profile depicted in Figure 4. Due to the high gradient of concentration of Mg between the bentonite water and the cement solid, magnesium diffusive to the solid sample and starts to exchange with the calcium present in the C-(A)-S-H phases. For example, magnesium concentration close to the surface is three times higher than calcium suggesting the formation of M-S-H phases by decalcification of the C-S-H phases, this ratio is decreasing with the distance and at 140 µm magnesium calcium ratios are equal. Finally, at 400 µm the magnesium ratio keep constant and equal to the initial Ca:Mg ratio, suggesting that the reactive front during 6 months is only about 400 µm. Other cation exchange with calcium in this case is Na, present in high concentration (~ 0.25 M) in the bentonite water. In addition, the elemental depth profile shows a decrease of sulphate in the altered zone.

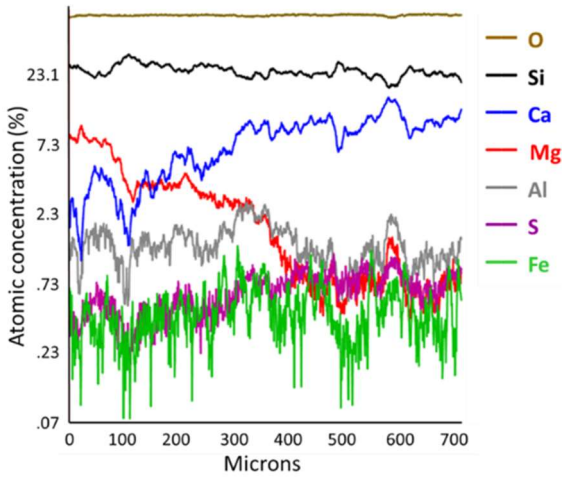

Figure 4: *Elemental depth profile extracted from the data of Figure 3.*

Apart from these main processes, it seems also obvious that clinker (belite, and ferrite) are hydrating/reacting in "the magnesium exchanged zone" (< 400 µm) with the aqueous solution to form magnesium containing phases (i.e. Mg-exchanged C-S-H phases). It can be seen that the blast furnace slag and the quartz filler remain in the sample as non-reactive solid or presenting a slow kinetic dissolution. Finally, precipitation of calcite has only been observed on the holes present in the surface in contact with the bentonite water and not in the porestructure.

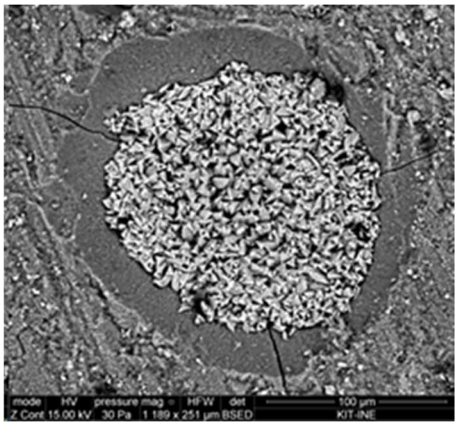

Fiure 5: *Calcite precipitation in the low pH cement.*

The other method used to study the alteration of low pH cement pastes is similar to the one used in the through-diffusion experiments explained in *Sections 1.3.3,* but using bentonite water in the upstream reservoir observing similar processes.

References

Baur, I., Keller, P., Mavrocordatos, D., Wehrli, B., Johnson, C.A. (2004). Dissolution-precipitation behaviour of ettringite, monosulfate, and calcium silicate hydrate. Cement and Concrete Research, 34, 341–348.

Bentz, D.P., Jensen, O.M., Coats, A.M., Glasser, F.P. (2000). Influence of silica fume on diffusivity in cement-based materials: I. Experimental and computer modeling studies on cement pastes. Cement and Concrete Research, 30, 953-962.

Bradbury, M.H. and Baeyens, B. (2011). Physico-Chemical characterisation data and sorption Measurements of Cs, Ni, Eu, Th, U, Cl, I and Se on MX-80 Bentonite. PSI report 11-05, Paul Scherrer Institut, Switzerland.

Cau Dit Coumes, C., Courtois, S., Nectoux, D., Leclercq, S., Bourbon, X. (2006). Formulating a low-alkalinity, high-resistance and low-heat concrete for radioactive waste repositories. Cement and Concrete Research, 36, 2152–2163.

Codina, M., Cau-dit-Coumes, C., Le Bescop, P., Verdier, J., Ollivier, J.P. (2008). Design and characterization of low-heat and low-alkalinity cements. Cement and Concrete Research, 38, 437–448.

Dauzères, A. (2010). Etude experimentale et modelisation des mecanismes physicochimiques des interactions beton-argile dans le contexte du stockage geologique des dechets radioactifs. PhD Thesis. University of Poitiers, France.

Dauzères, A., Le Bescop, P., Cau-Dit-Coumes, C., Brunet, F., Bourbon, X., Timonen, J., Voutilainen, M., Chomat, L., Sardini, P. (2014). On the physico-chemical evolution of low-pH and CEM I cement pastes interacting with Callovo-Oxfordian pore water under its in-situ CO_2 partial pressure. Cement and Concrete Research, 58, 76–88.

Dauzères, A., Achiedo, G., Nied, D., Bernard, E., Alahrache, S., Lothenbach, B. (2016). Magnesium perturbation in low-pH concretes placed in clayey environment—solid characterizations and modeling. Cement and Concrete Research, 79, 137-150.

Jenni, A., Mäder, U., Lerouge, C., Gaboreau, S., Schwyn, B. (2014). In-situ interaction between different concretes and Opalinus Clay. Physics and Chemistry of the Earth Parts ABC, 70, 71–83.

García Calvo, J.L., Hidalgo, A., Alonso, C., Fernández Luco, L. (2010). Development of low-pH cementitious materials for HLRW repositories: Resistance against ground waters aggression. Cement and Concrete Research, 40, 1290–1297.

Lerouge, C., Gaboreau, S., Grangeon, S., Claret, F., Warmont, F., Jenni, A., Cloet, V., Mäder, U. (2017). In-situ interactions between Opalinus Clay and Low Alkali Concrete. Physics and Chemistry of the Earth, Parts A/B/C, 99, 3-21.

Lothenbach, B., Kulik, D.A., Matschei, T., Balonis, M., Baquerizo, L., Dilnesa, B., Miron, G.D., Myers, R.J. (2019). Cemdata18: A chemical thermodynamic database for hydrated Portland cements and alkali-activated materials. Cement and Concrete Research, 115, 472–506.

Lothenbach, B., Le Saout, G., Ben Haha, M., Figi, R., Wieland, E. (2012). Hydration of a low-alkali CEM III/B–SiO_2 cement (LAC). Cement and Concrete Research, 42, 410–423.

Lothenbach, B., Rentsch, D., Wieland, E. (2014). Hydration of a silica fume blended low-alkali shotcrete cement. Physics.and Chemistry of the Hearth Parts ABC, Mechanisms and Modelling of Waste-Cement and Cement-Host Rock Interactions, 70–71, 3–16.

Savage, D. and Benbow, S. (2007). Low pH cements. SKI Report 2007: 32. Swedish Nuclear Power Inspectorate (SKI), Stockholm, Sweden.

Ochs, M., Mallants, D., Wang, L. (2016). Radionuclide and metal sorption on cement and concrete. Springer.

Roosz, C., Vieillard, P., Blanc, P., Gaboreau, S., Gailhanou, H., Braithwaite, D., Montouillout, V., Denoyel, R., Henocq, P., Madé, B. (2018). Thermodynamic properties of C-S-H, C-A-S-H and M-S-H phases: Results from direct measurements and predictive modelling. Applied Geochemistry, 92, 140-156.

Technical Summary – British Geological Survey – WP1

1. Introduction & Objectives

The weakest part of any gallery or deposition hole seal will be at the interface between the sealing components and the host rock. A single seal completion may comprise a number of elements reflecting different design criteria in order to address specific engineering challenges associated with changes in geochemistry and stress. The interaction of these components with the host rock, their evolution in terms of strength/bonding and permeability, and the sensitivity of these properties to an evolving geochemical and physical environment will be key factors in determining the long-term seal performance. In the French repository concept, low pH cement has been proposed as a mechanical support for bentonite seals as they slowly hydrate to isolate sections of the repository system. The interaction between the cement, bentonite and host rock must be defined in order to inform performance assessment. As such, a matrix of bespoke tests using state-of-the-art experimental systems capable of simulating key repository conditions was proposed.

Particular emphasis was placed on defining the temporal evolution of each interface to changes in geochemistry and stress to assess their impact on the development of permeability and strength (shear strength). Diagnostic tests were performed in two heavy duty shear rigs providing real-time data on the hydromechnical and transport behaviour of each interface as it evolved in time and space. This information (including shear strength, fracture transmissivity, volume change, normal and shear stresses etc) was combined with post-test petrological and geochemical analyses to develop a conceptual model describing seal behaviour. This model will be used by Andra to guide and verify future predictive numerical models aimed at repository performance assessment.

Objective: Examine the interaction of low pH cement on Caollovo-Oxfordian claystone seal performance with specific emphasis on the evolution of strength and permeability of key system interfaces.

Main expected outcomes: Gallery/deposition hole seal performance: examine impact of changing geochemical and stress environments on seal integrity; Investigate rates of reaction/interaction and their impact on strength and permeability of seal components; Identify and quantify key processes and reduce uncertainty for inclusion in future predictive numerical codes.

2. Studied system

The experimental programme looked at the concrete/Callovo-Oxfordian claystone interface between two varieties of COx. In the clay-rich variety of COx (UA) the seal at the end of a horizontal drift was simulated. In the high-carbonate variety (USC) a shaft seal was simulated. Figure 1 shows the UA scenario tested. At the end of a horizontal drift a bentonite and concrete system is constructed. At various points shear forces are created between concrete/COx and concrete/concrete. Similar forces are also generated in the shaft seal

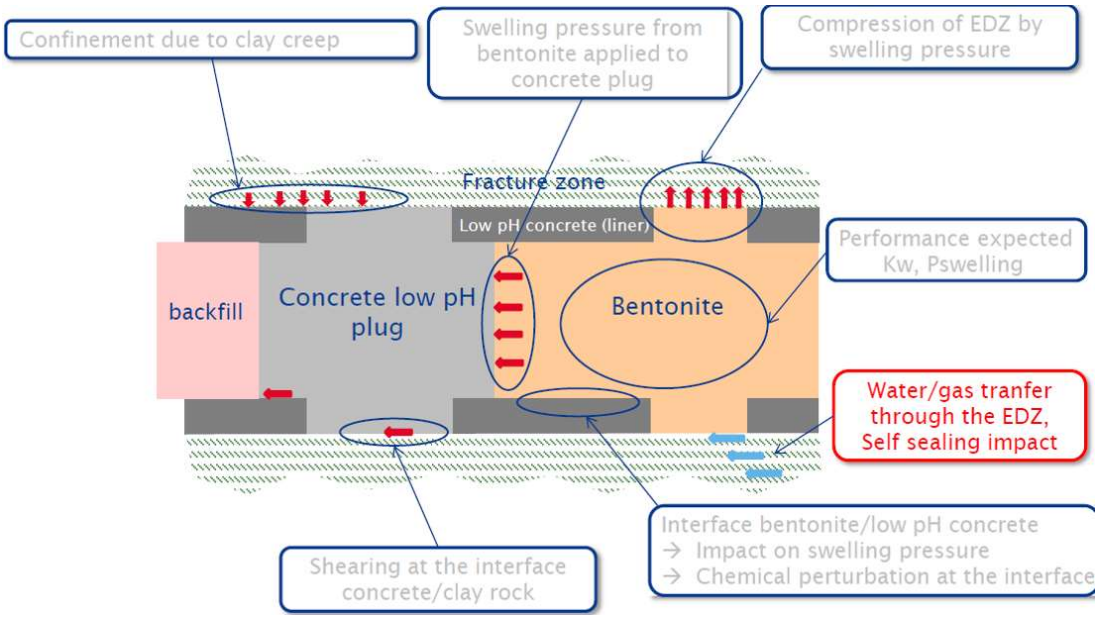

Figure 1: *Scheme of the UA scenario.*

3. Main results – Scientific highlights

This package of work comprised of an experimental study looking at the flow and shear strength properties of two varieties of Callovo-Oxfordian (COx) claystone when in contact with concrete. The two varieties were the so called repository depth clay-rich COx (UA) and the overlying high carbonate variety of COx (USC). These were cast directly with T_L variant ternary blend concrete.

The experimental programme started with the shearing of "intact" UA and USC COx to give baseline shear properties of the two varieties. This also allowed natural variation to be determined and produced realistic rough surfaces to cast concrete on to. In addition, planed samples of UA and USC COx were prepared to allow comparison in shear properties between rough and smooth surfaces of COx with the T_L concrete. All samples were brought to full saturation.

In the T_L ternary binder there was 20% of Portland cement, 32.5% of silica fume and 47.5% of blast furnace slag. The superplasticizer used was Chryso® Optima 175, which is a highly efficient water reducing agent having good compatibility with silica fume.

The highlights of the project are presented in the following lines.

3.1. Uniaxial strength during concrete curing

The uniaxial strength of the concrete samples increased during curing, as expected. However, the rate of strength increase was slower than previously published.

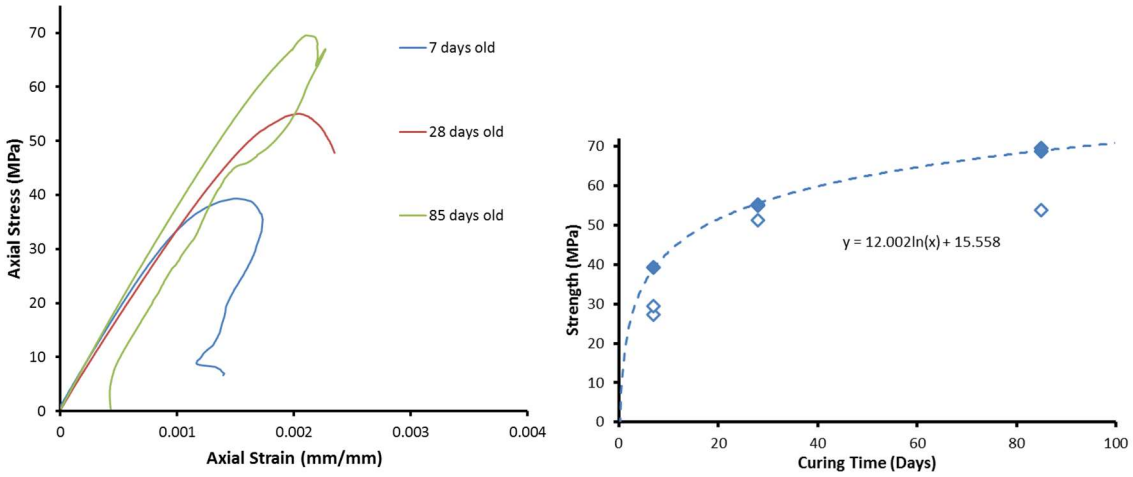

3.2. Strength of intact samples

Considerable strength difference was seen between the UA and USC varieties of COx (a, c). The USC has a shear strength in excess of 20 MPa, whereas the UA variety had a strength closer to 6 MPa. The high clay content variety (UA) showed natural variation in yield, peak, and residual shear stresses (b, c). The two samples of concrete tested showed considerably different shear strengths. In one, a modest strength of approximately 2 MPa was seen, whereas in the other it was approaching 15 MPa.

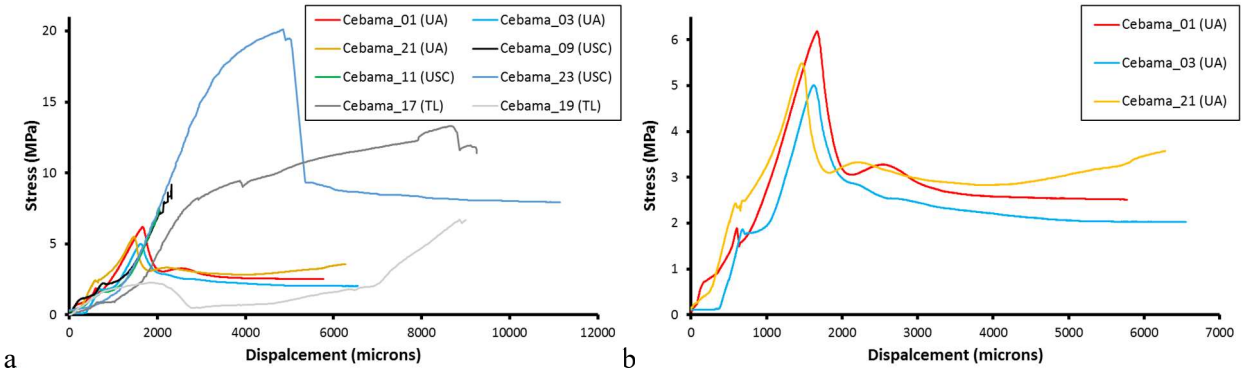

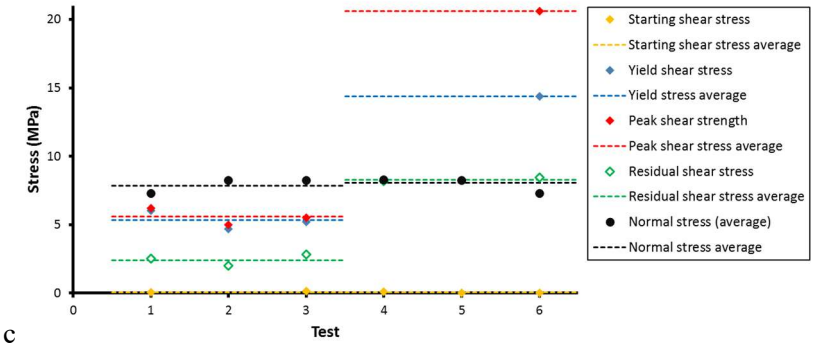

3.3. Strength of interface

In general, when the COx/T_L interface was sheared, the peak strength achieved was similar to the residual strength of the intact rock. Therefore, the interface itself had very little, to no, strength.

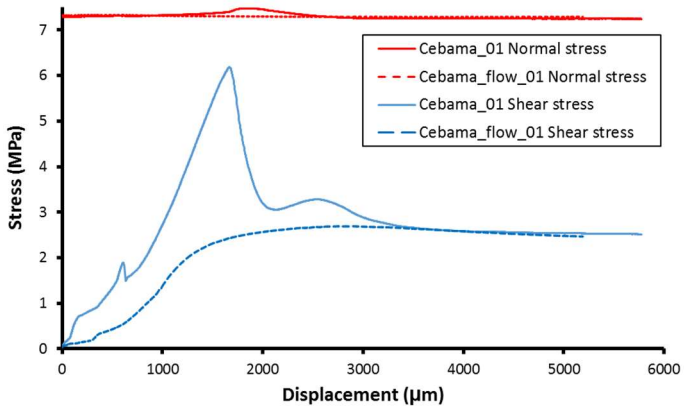

3.4. Increase in strength with time

However, despite the observation that the interface had little strength, there was evidence that the strength of the interface increased with time for the UA variety of COx (a, c, d) with a modest strength increase over a year. It should be noted that the test conducted at approximately 40 weeks showed abnormally high strength that may have derived from accidental drying of the sample. The story in the USC COx (b) is not as clear with the initial test of the fresh material showing the interface had strength, the test after six months showed no strength, and the test after one year showed enhanced strength.

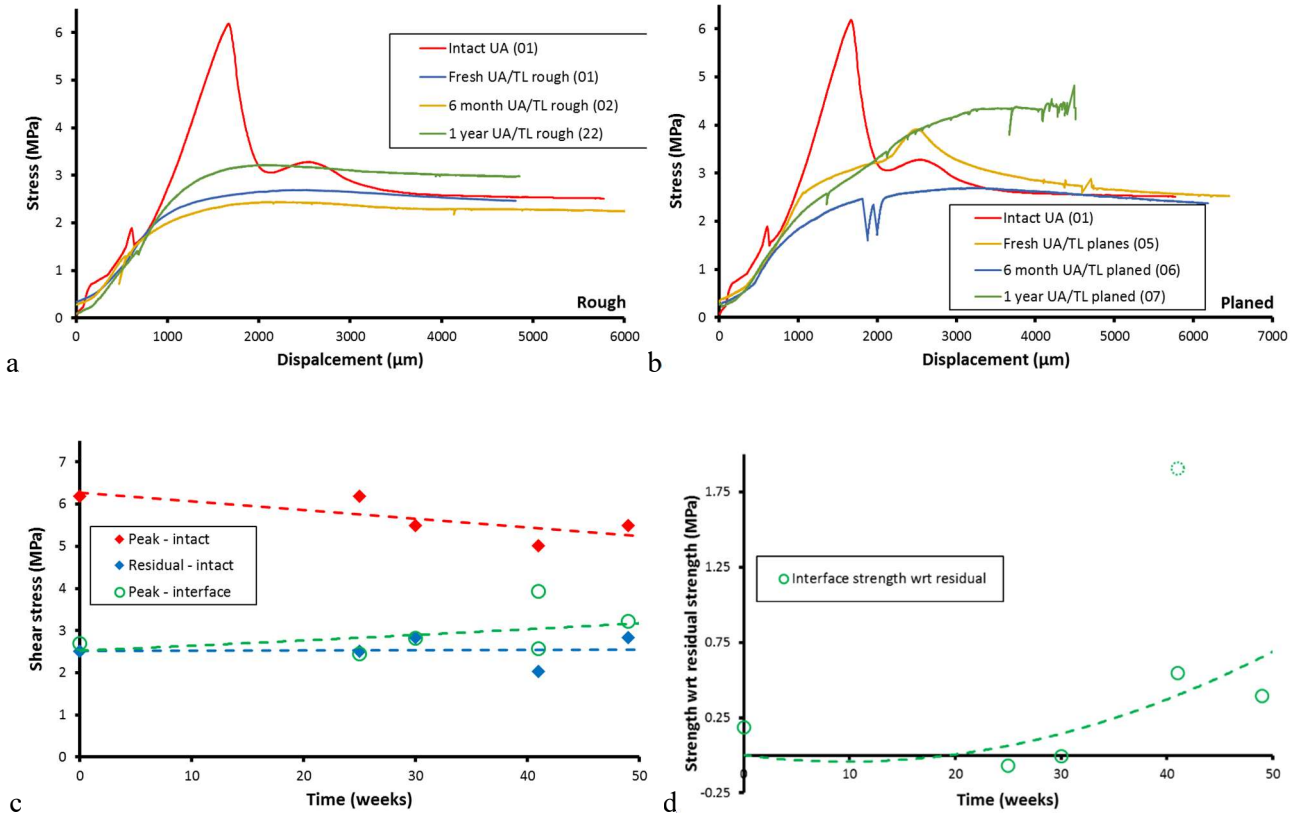

3.5. Modification of flow with shear

Flow during shearing showed two different behaviours. In some tests the flow rate reduced as the shear stress in the sample increased (a). Flow reduced to reach a minimum coinciding with the residual strength sliding of the

interface. However, in a limited number of tests, the flow reduced as shear stress increased, but increased around the peak stress condition (b). This suggests that in (a) the shear movement along the interface acted as an effective self-sealing mechanism, whereas in (b) the formation of a shear zone parallel with the interface has resulted in enhanced flow.

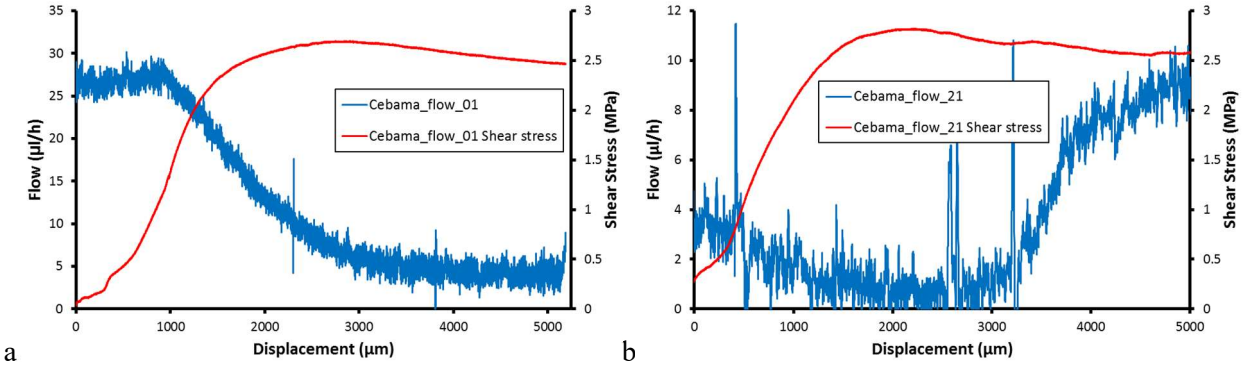

3.6. Shear dependent flow

In general, the reduction of flow as shear stress increased resulted in a near linear relationship. Therefore, the COx/T_L interface displayed stress-dependent flow.

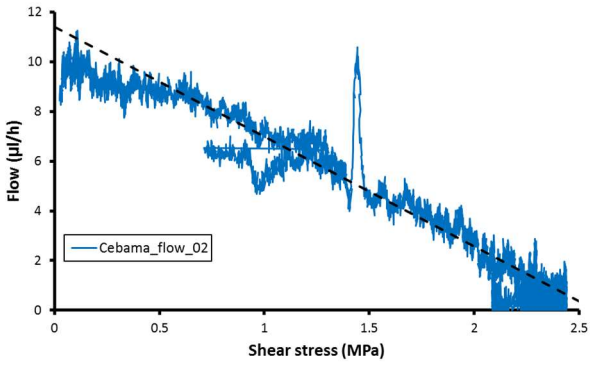

3.7. Changes in flow behaviour with time

A qualitative description can be made about the modification of flow with time. In early tests, the flow decreased about one order of magnitude under a static boundary condition. A further order of magnitude reduction occurred during shearing of the interface. However, as the COx/T_L interface aged, the starting flow of the interface was much lower and quickly reduced to a condition of virtual no flow. Shearing of the interface made no difference to the flow characteristics. Therefore, with time, the flow properties of the interface reduce and the interface does not continue to be a significant region of flow.

3.8. Petrological observations

Despite changes in strength and flow behaviour, no discernible change in geochemistry was seen during petrographic analysis to explain these changes.

Technical Summary – CIEMAT, CSIC, UAM – WP1

1. Introduction & objectives

The evaluation of long-term safety of DGR requires the analyses of the interactions at the EBS. Bentonite and concrete are main components of the EBS. The knowledge of phenomena occurring at their interface with regard the interaction of the near environment, ground waters (GW) is relevant: i) the role of ground waters and EBS pore waters in the stability of the DGR. ii) the bentonite-cementitious materials reactivity at the interface, and 3) the groundwater interaction with cementitious materials in the EBS. Besides, the experimental data used to model the long-term performance of the EBSs are generally based on simulated experiments from short-term test in laboratory. However, the scale up, differences in time and space, of the laboratory experiments respect to real-site was insufficiently supported at the starting of CEBAMA project as it is not an easy task to validate and contrast the information.

Hydrochemical processes at concrete interface: It was accepted as base starting knowledge that the high alkaline Portland concrete pore waters were able to react with the bentonite barrier and as consequence modify the EBS interface due to the impact on physical properties. There was accepted mechanism that the high alkaline pore water ions would be transported first by suction due to its initial unsaturated condition and progress in time interaction by diffusion. In the case of concrete hydro chemical phenomena has been focused in concrete/rock interaction, but less attention has been paid to saturated bentonite pore waters effect on the concrete interface alteration and the consequences at the interfacial EBS and the impact in alteration of physical transport properties.

It was accepted that the presence of cementitious materials in the EBS greatly alter the chemistry of water in the DGR that affects the bentonite barrier stability. It was expected that the cementitious materials provide a large reservoir of unstable Ca-silicate phases that dissolve and precipitate at the rock-water and further also alter the concrete-bentonite interfaces.

There was an enormous concern on determining the concrete behaviour under the long-term action of water, in representative conditions of the real storage scenario. However, at the starting of CEBAMA there was very few published experienced about concrete long-term performance in the conditions of a repository. For high pH OPC concretes the types of reaction mechanism described from laboratory short-term experiments were: 1) Concrete leaching processes that lead the dissolution of cement hydrated phases and the generation of pH gradients, 2) Formation of expansive sulfoaluminate phases on interaction with GW with high sulphate content, 3) Carbonation due to calcium leaching and WG carbonates, and 4) Modification of the CSH structure due to interaction with Mg rich waters. All above processes also promote modifications in the porosity profiles in the concrete at the interface of EBS and affecting in this way the ion transport processes. Regarding low-pH cementitious materials, results are scarce and lab. short-term leaching tests informed on acceptable resistance, although an altered front has been also observed with decalcification of the low Ca/Si CSH, < 1. Also Mg-perturbation of the CSH, identified as a Mg–Si gel-like phases, has been detected placed in rich Mg GW.

The perturbation produced in the EBS caused by cement materials interacting with the clay buffer have to be studied by means of a direct comparison of both materials in contact in a reliable EBS-like configuration. Few studies exists in which a comparison of chemical and physical impacts had been measured under an EBS global conception. The interactions between clay and concrete materials generate an evolutionary system whose reaction pathways lead to a varied mineralogy depending on materials considered. In crystalline rock concrete plugs are used in order to tap the backfill and buffer clay materials. The environmental conditions of concrete-bentonite interaction in granite deposits can be restricted to low-moderate temperatures 15-35ºC.

Local geochemistry in the concrete-bentonite interface surrounded by a granitic environment is driven by granite groundwater chemistry, concrete chemistry (high pH, low pH, mineralogy, ageing), and bentonite chemistry (exchangeable cations, smectite crystal-chemistry, secondary minerals d-p reactions, and porewater chemistry). The groundwater chemistry in the studied case by CIEMAT, CSIC and UAM groups, Grimsel test site (GTS) has very low salinity (TDS < 10 mg/L) and it is composed of Na-Ca-HCO_3-Cl-SO_4; pH near 9. These solutions are going to hydrate concrete and bentonite through the surface galleries contact Then, the major chemical gradients in the EBS system are related to concrete interfaces and bentonite interfaces. In fact, bentonite porewater is saline (~ 0.3 M NaCl; pH ~ 8 type (Na-Mg-Ca-Cl-SO4- HCO_3) in the case of FEBEX, compared to GTS groundwater. Taking in mind the pH gradient (> 13-12 to 11-10 in high pH to low pH concrete) at the concrete-bentonite interface, geochemical processes have been described in several research studies. Among them, the simulation of clay/hydrated concrete interactions performed using $Ca(OH)_2$ (pH 12.5) or C-S-H phases (pH < 12) chemistry, with the concourse of environmentally common salts such as carbonates, sulfates and chlorides, have probe to better focus the EBS performance. A variety of processes can be mentioned for their potential presence in a granitic groundwater bentonite-concrete scenario:

Carbonation of concrete and concrete-bentonite interface: In the initial high pH interface facing the near neutral bentonite porewater the dissolution of CH (portlandite) takes place and precipitation of calcium carbonate rim is produced with the concurrence of dissolved carbonate species coming from bentonite or from concrete matrix when pH is decreasing

Cation exchange in montomorillonite and Mg silicates formation (Mg-Si gels: M-S-H?): high pH cements are initially a source for K and Ca during the migration of concrete porewater. Direct contact of compacted bentonite and OPC concrete at long term is characterised by the decrease of Mg and the increase of Ca concentrations both in pore waters and in the exchangeable cations population. Mg is exchanged and transferred to the alkaline media where it is precipitated as brucite or M-S-H-like phases depending on the availability of silica, released during montmorillonite or amorphous silica dissolution.

Dissolution of CH, development of a Ca-rich front, C-S-H evolution and C-A-S-H formation: Concrete evolution, affected by the low pH environment of bentonite, is driven by portlandite and high Ca/Si C-S-H dissolution and the precipitation of low Ca/Si tobermorite type C-S-H. C-A-S-H have been identified also within the bentonite contact.

Sulfate and chloride reactions in concrete: Cement minerals can react with chloride in different ways to form chloroaluminates, Friedel's salt, Afm-like phases, or being adsorbed in C-S-H minerals, thus, they can retain the chloride, which can be diffused from the compacted bentonite. Dissolved sulfates can react also during CH dissolution from concrete. Al dissolution from montmorillonite favour to form secondary ettringite-like (Aft) needle aggregates.

All these mentioned processes are globally in agreement with the observations regarding realistic conditions of reaction in terms of temperature (low) and transport (mainly diffusive in concrete-clay rock interfaces): carbonation of the interface, CH dissolution, low Ca/Si C-S-H formation, and ettringite precipitation. Low pH and high pH concretes exhibited different reactivity and produce different progress in the formation of secondary phases. Some of these phases (i.e. M-S-H or C-A-S-H minerals) have not a precise chemo-structural basis for characterization, although they are detectable. The proposed experiments or in-situ aged interfaces characterisation have been focused to upgrade our understanding of the concrete-bentonite interface dynamics and to support confidence in the predictive modelling capabilities.

To contextualize and integrate the geochemical processes in large and long time-scales, as well as to analyze transport properties of the concrete, the overall objectives of CIEMAT have been focused to:

1. Analyse the hydro-geo-chemical interactions of high pH concrete and FEBEX bentonite from in-situ (FEBEX) and laboratory (HB6) long-term experiments considering processes at various scales: just at the concrete-bentonite and the concrete-rock (groundwater) interfaces and from mm to several cm.
2. Analyse the porosity and gas and water permeability of concrete from the in-situ, long-term FEBEX experiment. Therefore, quantify porosity changes in OPC associated to chemical perturbations, with special focus on the effects on radionuclide transport.

According the existing knowledge of GW interactions on concrete in EBS, the objectives to be covered by CSIC have been focused on:

1. Evaluation of the aging of high-pH concretes alteration from large-scale and long-term experiments to identify the consequences of mineralogy alteration of hydrated phases on transport properties at the interface due to porosity concrete alterations.
2. Assessment of the short term impact of bentonite pore water (BW) and formation groundwater (GW) salinity content on the transport properties of high-pH (HpH) and low pH (LpH) concretes. Analyses of the effect of chemical modifications of hydrated phases on physical alteration properties affecting porosity.

In order to evaluate the concrete and bentonite within the EBS interface, the objectives targeted by UAM have been:

1. The study of geochemical perturbation regarding high pH concrete/FEBEX-bentonite interface (μm-mm scale) at in-situ and long-term laboratory experiments (HB6 experiment).
2. To determine the early (6-18 months) surface interface reactivity of compacted FEBEX bentonite induced by several types of concrete in order to understand the geochemical perturbation produced in long-term and large scale experiments within mm interface distances.

These objectives have been pursued by integrating efforts with a close collaboration of CSIC, UAM and CIEMAT groups interacting with other partners, as summarised in Table 1.

Table 1: *Objectives in relation to experimental structure and collaboration.*

Objective	***Experimental framework***	***Materials / team / spatial and temporal scale***	***Share (S) results and conceptual feedback (F)***	***Sharing with other groups and WP***
1	**FEBEX-in-situ** (UniBern overcoring) **HB6** (CIEMAT)	**Concrete-bentonite interface** / CIEMAT / mm-cm->cm – 13 and 10 years	CSIC, UAM (S,F)	UDC (WP3)
2	**FEBEX-in-situ** (UniBern overcoring) **Through-diffusion tests** (CIEMAT)	**Concrete** / CIEMAT / mm-cm->cm – 5 months, 1, 5 and 13 years	CSIC, UAM (S,F)	WP2 and WP3
3	**FEBEX-in-situ** (UniBern overcoring) **HB6** (CIEMAT)	**Concrete** / CSIC / µm-mm->cm – 13 and 10 years	CIEMAT, UAM (S,F)	UDC (WP3)
4	**I) BW-HpH concrete interaction**	**13 y FEBEX Concrete** /CSIC /µm-mm->cm – 6, 9 and 12 months	CIEMAT, UAM (F)	UDC (WP3)
	II) GW-HpH & LpH interaction **III) GW- LpH CEBAMA REF mix interaction**	**Concrete** / CSIC / µm->cm – up to 24 months **Concrete** / CSIC / mm-cm->cm – up to 24 months	CIEMAT, UAM (F)	VTT/WP1/ Data freezing
5	**FEBEX-in-situ** (UniBern overcoring) **HB6** (CIEMAT)	**Concrete-bentonite interface /** UAM / µm-mm - 13 and 10 years	CIEMAT, CSIC (S,F)	UDC (WP3) BRGM (WP1)
6	**SERIE experiments** (UAM)	**Mortar-bentonite interface** / UAM / µm-mm – 6 and 18 months	CIEMAT, CSIC (F)	CEBAMA MIX Data Freezing

2. Studied system

2.1. Aged systems from long-term concrete-bentonite interaction

This system was used to cover objectives 1, 3, 5 and part of 2 by a close collaboration of CIEMAT-CSIC-UAM.

ENRESA initiated in 1995 the FEBEX Project to demonstrate the technical feasibility of installing the engineered barriers (EBS) for a high-level waste disposal facility in crystalline rock and to study their behaviour. A part of the project consisted on the FEBEX in-situ experiment at the Grimsel Test Site. It was a full-scale engineered barrier experiment performed under natural conditions and designed for the study of the near field of a repository of high-level waste in crystalline rock following the Spanish reference concept in crystalline rock: canisters are placed horizontally in drifts surrounded by a clay barrier constructed from highly compacted bentonite blocks. Two heaters were used to simulate the thermal effect of the wastes. FEBEX bentonite extracted from the Cortijo de Archidona deposit (Almería, Spain), compacted to 1.69 - 1.70 g/cm^3 dry density, was used as clay barrier. The montmorillonite content of the FEBEX bentonite is above 90 wt.% (92 ± 3%) and contains variable quantities of quartz (2 ± 1 wt.%), plagioclase (3 ± 1 wt.%), K-feldspar (traces), calcite (1 ± 0.5 wt.%), and cristobalite-trydimite (2 ± 1 wt.%). A concrete plug sealed the gallery. Heating started in 1997 and since then

a constant temperature of 100°C was maintained, while the bentonite buffer was slowly hydrating in a natural way. After five years the heater closer to the gallery entrance was switched off. In the following months the concrete plug, heater and all the bentonite and instruments preceding and surrounding it were extracted. The remaining part was sealed with a new concrete plug constructed by the shotcreting technique, whose composition was 430 g/m^3 of CEM II A-L 32,5 R, 30 kg/m^3 of nanosilica MEYCO MS 660; 50 kg/m^3 of steel fibres Dramix ZP 306; 800 g/m^3 of polypropylene fibres; 1.5% of superplasticiser GLENIUM T803; W/C = 0.40; 1700 kg/m^3 of aggregate 0-8 mm; 1% of curing compound MEYCO TCC 735 and 6% accelerant MEYCO SA 160 E. The second operational phase started in 2002 until the definitive dismantling in 2015.

The hydration was natural and some boreholes were drilled radial (before installing the experiment) and parallel (after first dismantling) to the gallery and packed-off to sample and check the evolution of the groundwater. The granite groundwater composition analysed from borehole samples around the FEBEX gallery is Na^+-Ca^{2+}-HCO_3^--type water, with low electric conductivity (76 - 236 µS/cm) and pH neutral to alkaline.

Post-mortem samples of aged bentonite/concrete interface coming from the dismantling of the experiment were studied by CIEMAT, CSIC and UAM in the context of CEBAMA to analyse if materials maintain their technical requirements as barriers after 13 years of interaction. In particular, data and interpretation were based on the investigation of geochemical processes and transport phenomena at the interface and the extent of the altered zone in both the concrete and the bentonite.

Simultaneously, a series of small-scale, long-term laboratory tests currently running at CIEMAT (initiated during EU projects NF-PRO and PEBS) were designed with a dual objective: to complement the information acquired from larger scale in-situ test and to have a temporal up-scaling by sequentially dismantling of a series of six identical experiments, named HB1 to HB6, representing different stages of the re-saturation phase of the repository. The tests consist of a FEBEX bentonite cylinder column (7 cm length) which hydrates through a high pH OPC (CEM I) concrete disc (3 cm). The hydration was made with synthetic clayey (Na^+-Ca^{2+}-SO_4^{2-})-type water. At the opposite side the bentonite face a hot steel plate maintained at 100ºC. The dismantling and analysis of the last of those tests after running during some more than 10 years (HB6), was also a part of the collaborative work CSIC-CIEMAT-UAM in CEBAMA in terms of geochemistry and transport properties. Its modelling will help the temporal up-scaling activities.

CSIC focused on the analysis of concrete alteration from bentonite interface and consequences on transport properties of the aged concrete. CIEMAT-UAM focused on the concrete-bentonite interaction, being the objective of the UAM the reactivity just at the concrete-bentonite interface (µm-mm) and of the CIEMAT the mass transfer at the interface and on a larger scale, as well as the measurement of the porosity and gas permeability properties of the concrete.

2.2. System focused on the impact of bentonite porewater (BW) and formation groundwater (GW) on concrete transport

Three systems were considered from CSIC to cover objective 4 as summarized in Table 1:

2.2.1 Short-term lab-scale interaction of BW in High pH concrete

Concrete samples of 6ϕx10 cm, from cores of 13 years old GRIMSEL FEBEX plug were employed for the interaction with simulated FEBEX bentonite water. The simulated bentonite water was prepared according to a protocol and composition given by CIEMAT. 24 samples were pre-saturated and after unidirectional diffusion

tests were performed, through a ponding of BW on one surface. Changes in BW composition, concrete pore soluble ions, cement paste and pore structure were evaluated periodically up to 12 months exposure.

2.2.1. Short-term lab scale GW (either granite or clayey water) interaction in high and Low-pH concretes

GW infiltration tests, of 2 bars pressure, were carried out with concrete samples of 5ϕx5 cm. The system included the collection of percolation water. GWs of different salinity were used: 1) Granite groundwater from GRIMSEL site, identified as low salinity for the experiment, being the composition Na^{+}-Ca^{2+}-HCO_3^{-} and 2) simulated clayey water with a composition like the one used to hydrate the HB6 cell. Different concrete typologies were employed, varying: concrete age, concrete pore-pH, concrete density and concrete composition. The distribution of the concretes according the GW composition infiltrated was:

Granite water from GRIMSEL site (low salinity):

a) Low density, high pH concrete CEMII+6% SF 13 years old: 6, 12 ,18 M water interaction.
b) Low density Low-pH concrete: OPC + 40% SF, 9 years old: 5, 9, 21 M water interaction.

Clayey simulated water (high salinity):

a) High density, High pH concrete CEM I, 0.5 years old: 9,13, 24 M water interaction.
b) High density Low-pH concrete: OPC + 40% SF, 9 years old: 9, 13, 24 M water interaction.

2.2.2. Short-term lab scale GW interaction in CEBAMA Reference mix Low-pH concretes

GW infiltration tests, of 8 bars pressure, were carried out similarly as described in II). Also GRIMSEL granite and simulated clayey water were employed. Two CEBAMA Low-pH reference concrete mixes were employed varying their density. The CEBAMA Low-PH ref mix was prepared with 37.5% CEM I + 3 9.5% SF + 23% BFS.

a) High density, Low-pH CEBAMA reference concrete, 0.5 years old: 13, 18, 24 M water interaction.
b) Low density, Low-pH CEBAMA reference concrete, 0.5 years old: 7, 11, 18 M water interaction.

2.3. Serie – early surface reactivity experiments

This system was used to cover objective 6 by UAM

Groundwater infiltration experiments through small cement mortar/FEBEX bentonite interface were used to investigate surface interface reactivity.

SurfacE Reactivity Interface Experiments (SERIE) were 12 composite cylinder columns (2 cm diameter) prepared by casting three different types of cement mortars (1 cm length, high pH (CEM-I and CEM-II), and low pH (b in objective 2), which were put in contact with a compacted FEBEX bentonite column (0.8 cm length) at ambient temperature (20 ± 3ºC).

Experiments consisted in replicated systems running during approximately 0.5 years and 1.5 years:

a. CEM-I/bentonite (2 x 0.5 y and 2 x 1.5 y)
b. CEM-II/bentonite (2 x 0.5 y and 2 x 1.5 y)

c. CEM-I/SF low pH/ bentonite (2 x 0.5 y and 2 x 1.5 y)

GTS groundwater was pressurized (1 MPa) through cement mortars to pass across the compacted bentonite. During these periods water was collected at the bentonite end (from 3 to 10 2 cm^3 aliquots). The experiment represents a 5.5 cm^3 0.5-1.5 year experiment (3 cm^3 and 2.5 cm^3 bentonite); bentonite dry density was near 1.6 g/cm^3 in all of the interfaces.

Cement material/bentonite volume ratio increased from macro to micro experiments. Thus, the SERIE laboratory experiments represent more specifically the interface system.

2.4. Through- and in- diffusion tests in concrete and mortar

This system was used to cover a part of the objective 2 by CIEMAT

Experiments were carried out using CEM I 42.5 R/SR to obtain concrete samples with a water/cement ratio of 0.43, and CEM IV B 32.5 for mortars samples with a water/cement relation of 0.4. Three different porewaters were used to perform diffusion experiments on concrete and mortar. All the waters were prepared under anoxic condition in an anoxic glove box with N_2 atmosphere. The first one was a synthetic water simulating a fresh cement porewater, whereas the other two waters were obtained by contacting the solid (concrete or mortar), at a solid to liquid ratio of 10 g/L, to deionised and decarbonated water, and finally filtered by a Millipore membrane of 0.45 μm.

Effective diffusion coefficient is obtained by the Through-Diffusion (TD) and In-Diffusion (ID) methods, fitting the cumulative mass of tracer through the sample vs. the time in the region of constant flux (steady state).

3. Main results – Scientific highlights

3.1. Aged systems from long-term concrete-bentonite interaction

3.1.1. Results from Objective 1

The results achieved from Objective 1 are complementary to those obtained in the rest of the objectives of study system A (objectives 2, 3 and 5). A brief comparative summary of the results of the hydro-geo-chemical interactions at the full-scale FEBEX in-situ test and in the HB6 laboratory test is presented. Heterogeneity of the real system is put in front of well controlled conditions of the lab test and the changes observed are used to compare geochemical processes in both, taking into account the differences in the composition of the water hydrating the system and the thermal and hydraulic gradient.

Soluble salts in aqueous extracts of bentonite in HB6 follow an inverse relationship with water content (Figure 1), being the maximum values of salinity close to the heater, where the lower water content and the higher temperature are measured. Ionic transport occurs driven by the temperature gradient and the evaporation. At the concrete-bentonite interface the water content was around 25% (degree of saturation around 95%) and the temperature ≈ 45ºC.

Water content in the bentonite just contacting the concrete plug in the in-situ test decreases from the gallery granite wall towards the inner part of the barrier whereas the dry density increases. The samples analysed (CC-32-4 to 6) have a water content 26 - 27% (degree of saturation around 100%) and the temperature at the concrete-bentonite interface was ≈ 30ºC.

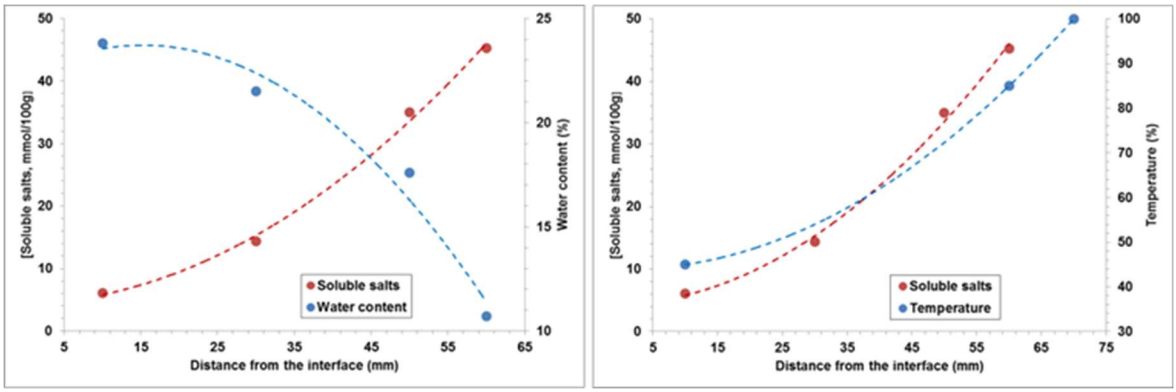

Figure 1: *Variation of total concentration of soluble salts along the bentonite column in HB6 test in relation to water content (left) and temperature (right).*

Progressive hydration of the EBS leads to the dissolution of soluble species and increase of ions in the pore water towards the heater, which is clear in the smaller scale HB6 lab experiment. Close to the interface, which is a colder and saturated zone, the concentration of soluble salts in the bentonite is lower than the original both on the real scale and on the laboratory scale.

The main cation in the aqueous extracts in the bentonite was Na^+ in the two experiments (Figure 2 top) although difference in concentration is notable mainly due to the effect of temperature in the HB6 (Figure 2, top-left), driving the sodium to the heater. Leaching towards the granite (Figure 2, bottom) and homogenization process (Figure 2, top-right) occurred in the in-situ test. A mass transfer from the bentonite to the granite occurred due to the difference in concentration. The last is also observed for the chloride (Figure 2, middle).

The main anion in the bentonite is Cl^- followed by SO_4^{2-}. In the laboratory experiment both ions increase towards the heater. However, the chloride of the in-situ test presents a uniform distribution, being the first 4 cm of the bentonite almost depleted in chloride compared to the original concentration. The reason is that part of the original chloride diffuses to the concrete (Figure 2, middle-right) and part diffuses to the granite (Figure 2, bottom). Na/Cl ratio measured in some points in the granite groundwater (0.93) is higher than in the bentonite porewater (0.81). The source of Na could be: cation exchange of Na^+ for Ca^{2+}, dissolution of plagioclases (albite, feldspars) or mass transfer from the bentonite or the concrete. The release of alkalis from the concrete was shown from the analysis of a sample of water taken at the concrete-bentonite interface. It is worth noting that the analyses carried out in the granite water, once the experiment was dismantled; show a tendency to decrease the concentration of Na and Cl, which demonstrates once again that the source of these ions was bentonite (Figure 2, bottom). The increase in sulphates is very likely due to the oxidation of granite minerals (e.g. pyrites) when the gallery is open.

Differences in the original hydration solution seem not affect the transport and re-distribution of salts, which follows a similar pattern in both experiments in the zone close to the concrete.

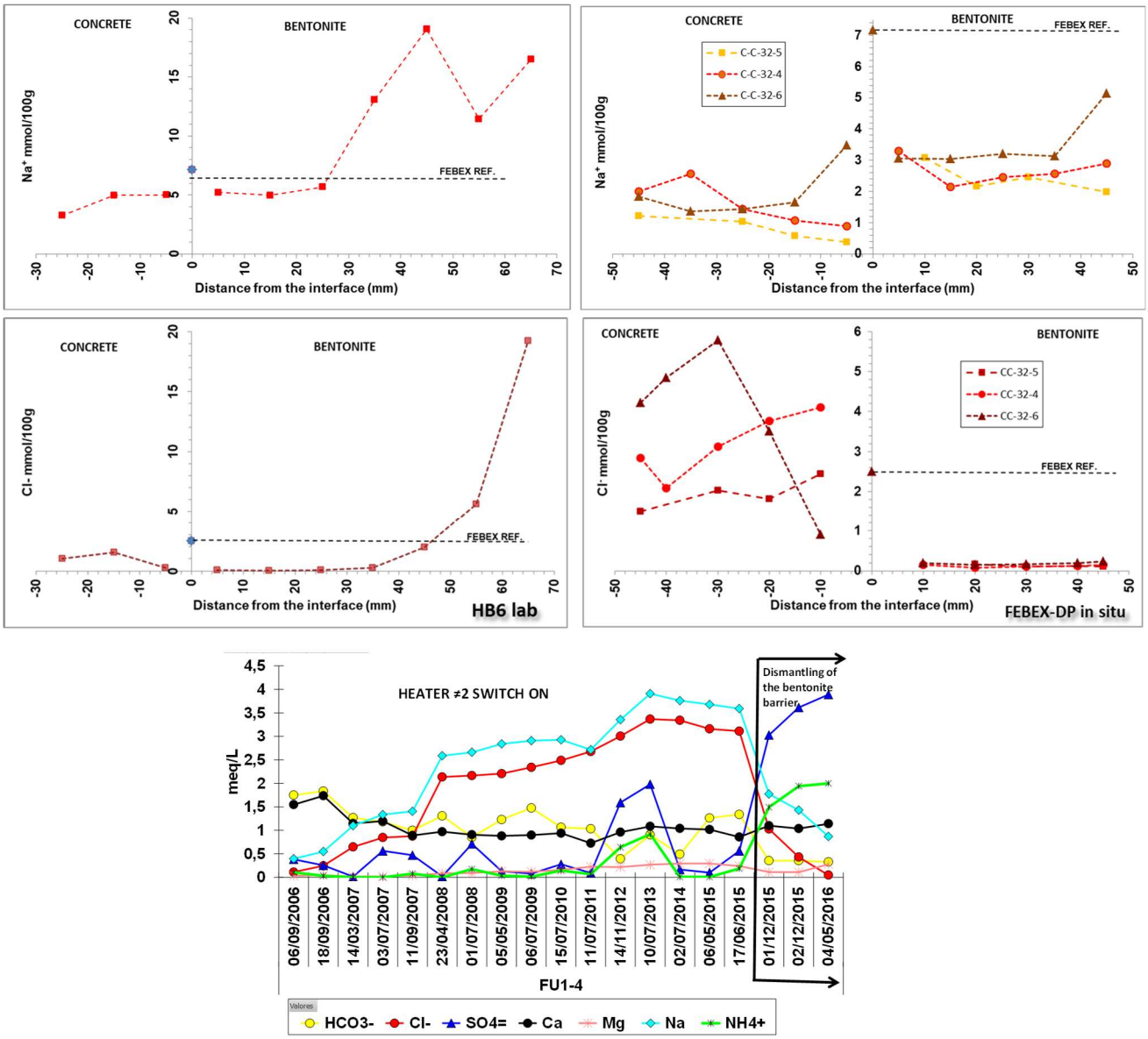

Figure 2: *Distribution of Na and Cl (main ions of the bentonite porewater) in HB6 (left) and in-situ (right) experiments. The figure at the bottom represents the evolution of main anions in the granite groundwater up to dismantling and some months later.*

Related to the exchangeable cations in the bentonite (Figure 3) Na is replaced by Ca and Mg in the hot area of the HB6 test (Figure 3, left), while in the bentonite closest to the interface Mg is replaced by Ca, Na and K both in the in-situ experiment (Figure 3, right) and in the HB6. The pH measured at the interface from a sample of water taken during the dismantling campaign (pH > 10 promoted by the concrete) favours the precipitation of Mg-rich phases. FT-IR results indicate presence of calcite and Mg-rich phase in both experiments just at the interface.

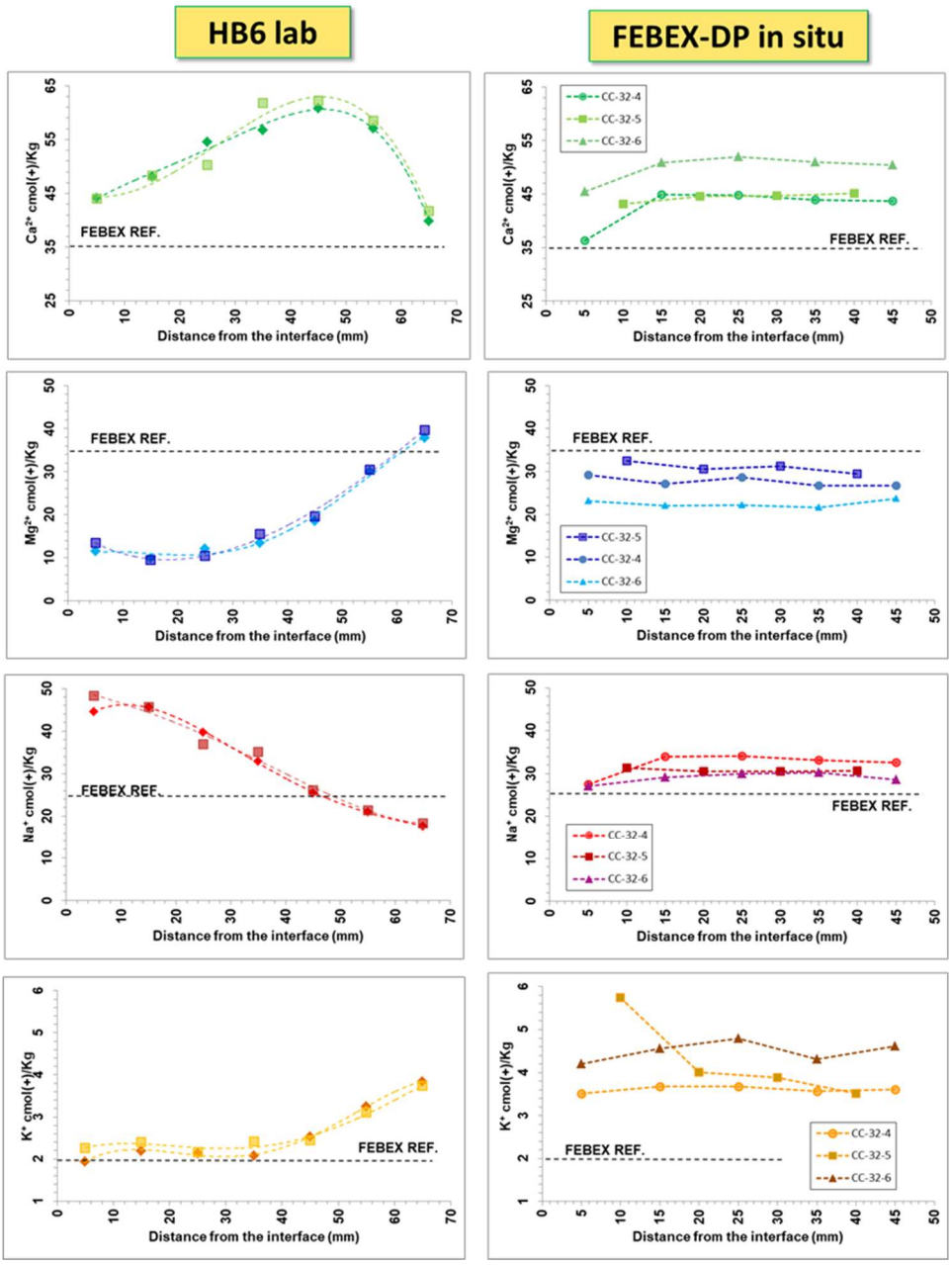

Figure 3: *Exchangeable cations along the bentonite from samples of the HB6 test (left – with the tripled results) and FEBEX in-situ experiment (right). Samples were taken at different distances from the interface with the concrete. Black dashed line FEBEX REF refers to the original material.*

The analysis of stable isotopes to study mass transfer (e.g. carbonates) in the concrete-bentonite interface points to a non-homogeneous chemical environment along the concrete-bentonite interface. The calculated $\delta^{18}O$ value of the solutions in which secondary calcite was formed seem to support significant differences depending on the location of the samples in the plug. Existence of preferential flow areas would be favoured by the proximity of the granite wall and the heterogeneity of the concrete-bentonite interface itself. However, the spatial distribution of $\delta^{13}C$ values along the concrete plug and the first centimetres of the bentonite barrier demonstrate the existence of diffusion front of carbon species from bentonite towards the concrete-bentonite interface that induces the precipitation of calcite at the first millimetres of the concrete.

3.1.2. Results from Objective 2

There is a bimodal distribution of porosity obtained by MIP in the bentonite of the in-situ test. That distribution is quite typical of the FEBEX bentonite and is related to macro- and mesopores. The increase in the MIP intrusion curve in the diameter attributable to the mesopores occurs in all the samples independently of the distance to the concrete or granite interface and has a mode 13 ± 3 nm. The percentage of each type of pores has been calculated: macropores 27 ± 9%, mesopores 21 ± 1%, and micropores 53 ± 8%.

The pore-size distribution of the concrete side of the samples is bimodal as well, with a population of macropores, corresponding to inter-aggregate pores (> 50 nm), and a population of mesopores (2.5 - 50 nm), corresponding to intra-aggregate pores, which would include small (gel) capillaries (2.5 - 10 nm). The samples at distances > 2 cm from the interface with the bentonite has a mode of mesopores 9 ± 3 nm which would correspond to the typical sizes of the space between the C-S-H particles (gel capillaries), while in the rest of samples (< 2 cm) the mode is 43 ± 6 nm, quite close to the mode of the macropores.

The specific surface area (SSA) of the bentonite very close to the concrete in the in-situ test is lower than SSA of the reference material (Figure). Samples with lower water content (HB6 close to the heater) have SSA below the FEBEX reference, decreasing quite sharply when water content decreases.

On the concrete side the minimum SSA values are near 2 mm before the interface and they tend to increase just at the interface. The precipitation of high specific surface minerals could be the cause of the increase of the BET surface towards the interface.

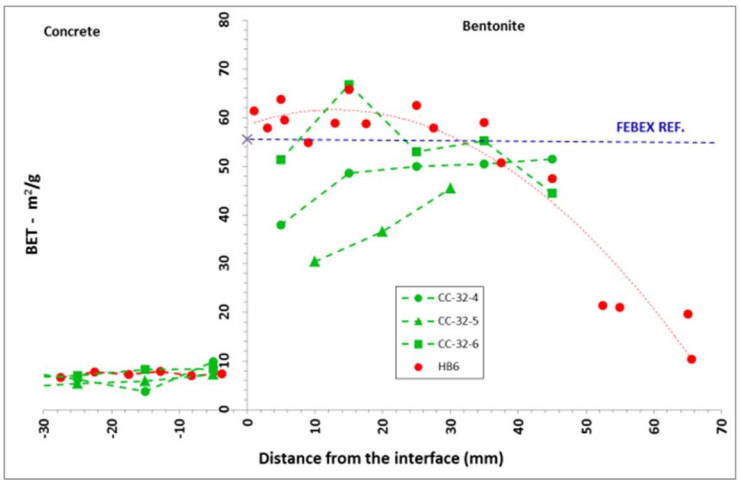

Figure 4: *BET specific surface area measured in concrete and bentonite of the HB6 lab test and the in-situ FEBEX experiment. Blue dashed line FEBEX REF refers to the original material.*

Related to gas transport through the concrete of the in-situ experiment gas permeability and hydraulic conductivity of concrete core samples taken during dismantling at different positions in the first meter of concrete closest to bentonite were tested in custom-built setups, in order to examine the effects of the bentonite pore water or the granite groundwater on the transport properties of the plug. Both were measured in core samples drilled onsite during dismantling and preserved to keep the degree of saturation they had when the plug was demolished. The tests were performed in triaxial cells.

The setup for the gas permeability tests allowed the change of the injection pressure at the upper part of the sample and the control of the confining pressure. The backpressure was kept atmospheric and the gas outflow was

measured by means of different range gas flowmeters. The pressure paths followed consisted in several phases. The maximum confining pressure applied was 3.5 MPa. The results show that the increase in confining pressure did not modify gas permeability, which would be an indication of the absence of microcracking. The gas permeability was higher as the samples had less water content and lower degrees of saturation (Figure 5). The hydraulic conductivity was measured in the core samples after they had been saturated with deionised water.

These tests were carried out in constant head permeameters in which the samples were saturated with an injection pressure of 0.6 MPa under a confining pressure of 0.8 MPa. Once the sample was saturated, a hydraulic head of 0.1 MPa was applied and the outflow was measured. The hydraulic conductivity values obtained were in the order of 10^{-10} m/s, higher than the initial values of the shotcrete plug S1 at 28 days curing (4.3 10^{-11} m/s).

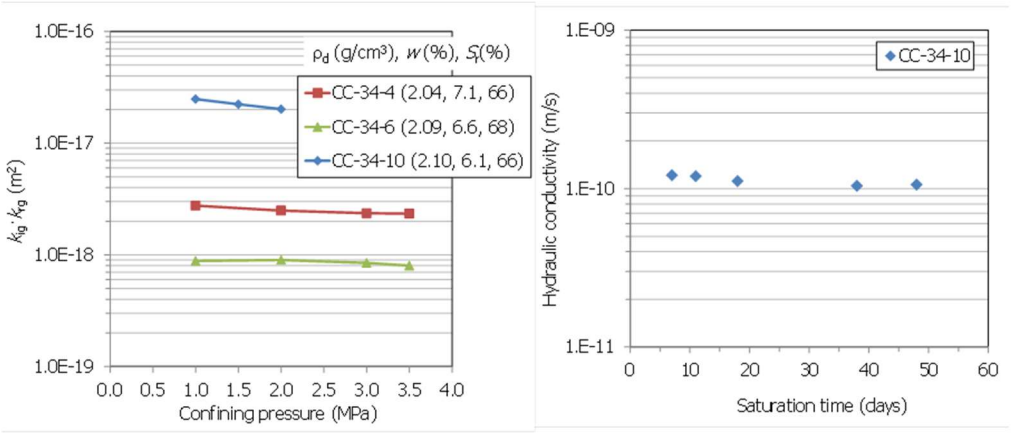

Figure 5: *Effective gas permeability with increasing confining pressure. The values are the average of all steps under the same confining pressure (left). Hydraulic conductivity of sample CC-34-10 over time (right).*

3.1.3. Results from Objective 3

1. Evaluation of the aging of high-pH concretes alteration from large-scale and long-term experiments

Main results from CSIC within objective 3 and systems A, after 13 y concrete FEBEX plug exposure, are summarized. The CSIC studies carried out from the interface of concrete in contact with the bentonite has allowed identifying the modifications generated in the concrete. The study was performed in 4 short cores of 2 x 7 cm and 2 overcoring samples.

- *Changes in the concrete pH and pore water soluble ions*

The most relevant evidence of the study is that the soluble salts from the saturated bentonite have diffused in the concrete inducing a significant damage at the interface of the concrete with the bentonite that extent several centimetres. An increasing pH profile from the concrete interface with the bentonite is measured, contributing to the generation of the alkaline plume of OH^- and alkaline ions, Na, K, transport from concrete towards the bentonite (decreasing profile in concrete). In parallel, but in the opposite direction, from the bentonite to the concrete, sulphates and Chloride are transport inside the concrete generating profiles up to 2 to 6 cm respectively. The kinetic of the process has been evaluated through the estimation of Cl diffusion coefficient. Mean $D_{app} = 1.6 \pm 0.6 \cdot 10^{-12}$ m^2/s have been obtained. Mg and Ca accumulations at the interface are detected, up to 1 and 3 cm inside the concrete respectively, neutralising the entrance of the anions.

- *Changes in cement paste*

The decrease in portlandite is detected up to 2-3 cm, but not evidence of calcite increase at the interface or inside was detected respect the initial content in the FEBEX concrete, already rich in limestone filler. In addition, a clear increase in ettringite is detected (Figure 6, left) up to a similar depth with significant alteration of the cement paste close to the interface with the bentonite. Two phases are clearly distinguished by SEM (Figure 6, middle), the CSH typical of the OPC but with high Al incorporated and other with high Al and low Si content, associated with the massive new ettringite formation. The pore structure at the interface is also altered in two ways, in the first cm the formation of new phases made more compact the system although evidence of microcracking is detected in the cement paste closer to the interface. At longer distance in the concrete pore size increases (Figure 6, right).

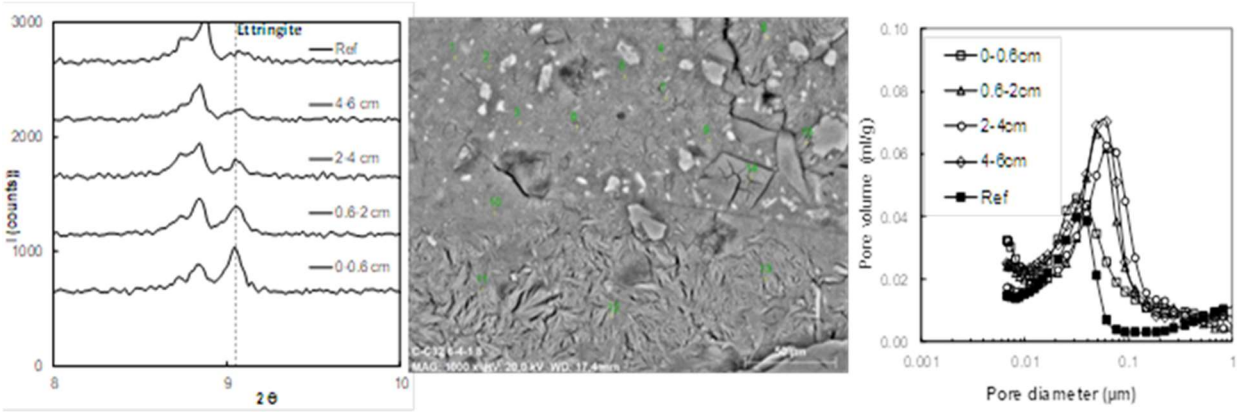

Figure 6: *Changes in cement paste due to bentonite-concrete interaction, left) ettringite increase, middle) altered cement paste and right) pore size changes.*

2. Evaluation of the aging of high-pH concretes alteration from long-term lab experiments

Main results from CSIC study within objective 3 and systems A for HB6 concrete after 10 y exposure are summarized. The CSIC studies carried out from the interfaces of bentonite and clayey water with the high pH concrete. The modifications generated in the concrete have been evaluated. The study was performed in a portion of concrete from the HB6 cell. The main highlights from present study indicate that both interfaces of concrete, one in direct contact with the clayey water and other interacting with the saturated bentonite are altered 6 mm from the bentonite interface, while in the interface with the clayey water inlet, only the 1 mm of the concrete is altered.

Main changes observed from FEBEX in-situ and HB6 long-term concrete-bentonite interaction are:

At both interfaces:

- Significant decrease of the pH at the concrete interface and increase of soluble ions due to diffusion of salts from clayey and bentonite waters. The portlandite has been leached out at both interfaces.

From Clayey water interface

- An external layer, < 100µm, rich in Ca associated to calcite formation. Leaching of Ca-Si as observed in Figure 7, left.

- Accumulation of Al_2O_3, MgO and SO_3 in the first mm,
- Some small nodules of ettringite but with not damage of cement paste.

From bentonite interface:

- The concrete interface in contact with the bentonite is more degraded.
- Formation and accumulation of new calcite. The high Ca content is explained by the increase of formation of calcite accumulated inside the cement paste, differences associated to the aluminates present in cement.
- The cement paste is enriched in Al_2O_3 and MgO. A CaO/SiO_2 increasing profile is detected up to 300 µm, due to decalcification of C-S-H (Figure 7, middle) while incorporates Al to enrich C-A-S-H phases.
- Not ettringite formation is detected, in this high-pH concrete at the interface with the bentonite, as happens in FEBEX concrete plug, indicating the relevance of the concrete composition in the alteration processes at the interface
- A more refined pore structure at the bentonite interface respect to clayey interface (Figure 7, right).

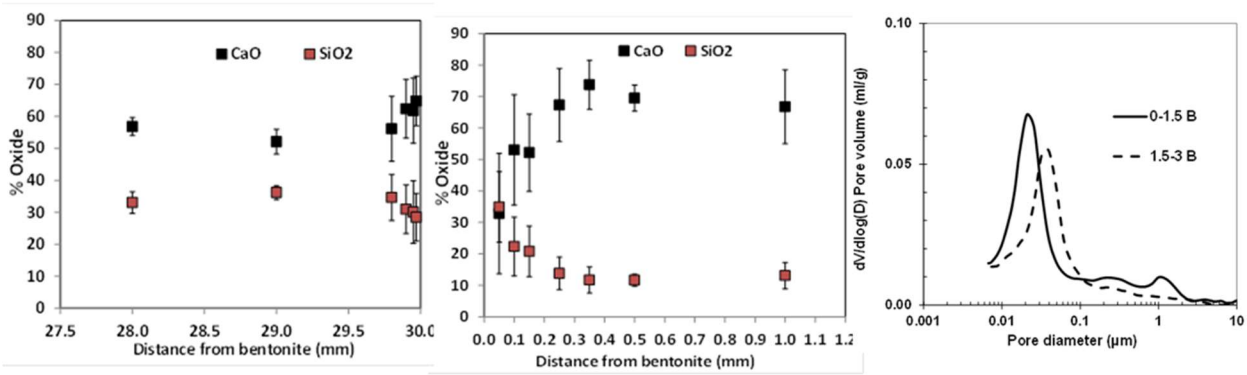

Figure 7: *HB6 concrete alteration 10.5 y exposure. Left) Ca-Si profiles from bentonite interface, middle), C-S profiles from clayey water interface, right) pore structure at the interfaces.*

3.1.4. Results from Objective 5

Mineralogy of geochemical perturbations

Regarding the objective 5, the nature of the geochemical perturbation (µm-mm scale) is characterized by the Mg and Ca anomalies located at in-situ interfaces and long-term laboratory experiments (HB6 experiment).

Both in-situ and the long term HB-6 experiments produced the precipitation of calcium carbonates at the concrete interface (a very thin and heterogeneous rim < 100 µm in the in-situ case); and, at the same time, the formation of a mixture of hydroxide and Mg-silicate phases (without any or very poor in Ca phases) within a sub-millimetre rim in the bentonite interface. These Mg-phases can coexist with CASH or CSH-montmorillonite mixtures at the bentonite side although the identification of their presence, shown in previous research carried out by UAM team, is difficult at low contents due to the presence of calcite and also considering their typical low crystal size domains. Ettringite is also formed in concrete and is relevant in the in-situ experiment within a 2 cm rim behind the contact with bentonite (Figure 8). Conversely, ettringite is absent from the first 5 mm of concrete in contact with bentonite in HB6. The original 14.5 Å basal spacing of montmorillonite is virtually maintained within 1 mm thickness interfaces in both long-term systems so it had minor alteration at 10-13 years scale. Figure 8

illustrate the aspect of the XRD powder patterns of these bentonite interfaces compared with small scale SERIE experiments (C-system studied by UAM) in which the alteration of bentonite is characterized by three broad peaks at near 7.5, 3.65 and 1.53 Å related to Mg anomalies. Their positions evidenced the presence of brucite-montmorillonite chlorite-like complex (serpentine 1:1 sheet silicate mineral cannot be discarded) and the formation a new tri-octahedral smectite phase (estimated by XRD in < 5 wt.%). Complementary, IR and DTG data confirmed the presence of tri-octahedral Mg-OH stretching bands and also brucite layers, respectively.

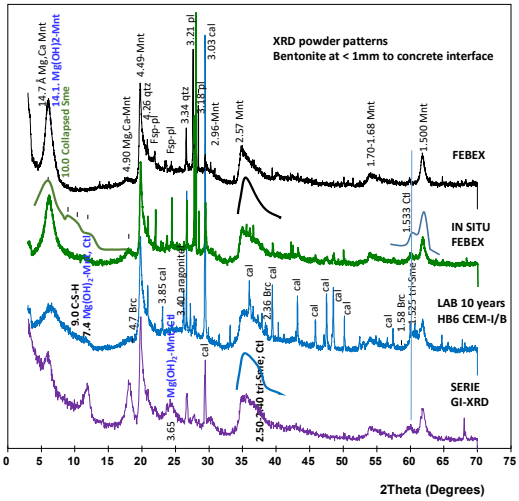

Figure 8: *XRD on randomly oriented powder patterns of interface bentonite samples. Black: reference Mg-FEBEX bentonite sample. Mnt=montmorillonite; tri-Sme= tri-octahedral smectite; C-S-H=calcium silicate hydrates; ctl=serpentine (chrysotile); qtz=quartz; Fsp-pl=feldspar-plagioclase; cal=calcite; Brc=brucite. GI-XRD: grazing incidence-XRD in bentonite interface surface performed in small size UAM Serie experiments.*

A series of photographs (Figure 9) prove the net separation of the materials and the existence of discrete phases with very different chemistry (Mg-silicate separated from calcium phase). The HB6 studied interface show different Mg-silicate phases of columnar (serpentine-like) or lamellar (2:1 or 2:1:1 sheet silicate), and the presumable presence of C-A-S-H phases.

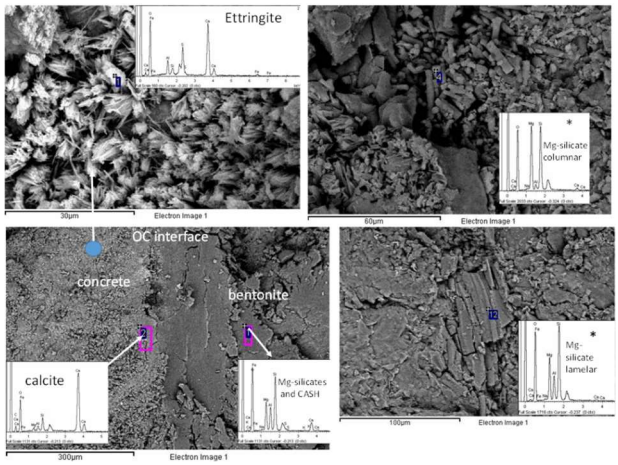

Figure 9: *SEM-EDX phase morphology and chemistry at the concrete-bentonite interface at the in-situ FEBEX and HB6(*) experiment.*

3.2. Impact of bentonite porewater (BW) and formation groundwater (GW) on concrete transport

3.2.1. Results from Objective 4 (and link to Objective 3)

I. Short-term lab-scale interaction of bentonite water in High pH concrete

This piece of research compiles the main results within objective 4 (short term) and compared with objective 3 (long-term) carried by CSIC. The tests were carried out in small samples taken from 13 y undamaged FEBEX concrete plug. Direct interaction of concrete with simulated bentonite water in order to analyse if the processes observed after long-term and in large-scale exposure (objective 3 in A system) are comparable.

Results confirm the formation of a pH profile increase from the BW interface, reaching similar values and depths after 9 to 12 months lab exposure and 13 y large scale and long-term. Also decrease of alkalis, Na, K is detected close to the interface with accumulation in the bentonite water reservoir. Accumulation of Ca is also observed at the interface of the concrete and also Mg. The penetration of Cl (up to 2-3 cm) and sulphates (up to 1-2 cm) is detected with a profile decreasing inside the concrete bulk. The kinetic of this process was evaluated in the Cl profile through fitting to a diffusion transport process, The $D_{app} = 3 \pm 0.8 \cdot 10^{-12}$ m^2/s was of the same order of magnitude that obtained for long-term large-scale test.

In relation to the cement paste changes, although portlandite has not completely disappeared, a reduction in the first cm at the interface is detected. Besides, the increase in ettringite is clearly detected at the interface with simulated bentonite water, as also detected in the objective 1 with concrete FEBEX plug. The C-S-H is altered showing a clear increase of Al incorporation and the new ettringite formation.

These results have allowed us to conclude that the same processes are taking place in the lab short term experiments that in-situ although the level or advance of the damage (kinetics) is accelerated.

II. Short-term lab scale Ground waters interaction in high and Low-pH concretes

Here is compiled the main results within objective 4, related to analyses of system B) interaction of ground waters of different salinity content with high and low-pH concretes, from a) to d) composition. The main aim of this study was to identify and evaluate the modifications that take place in the bulk of the concrete and in the percolated waters due to the interaction of the GW and that could affect the characteristics and properties of the concrete that could compromise its suitability to be used in a DGR for the storage of high-level radioactive wastes, taking into account different variables such as the GW type or the pH and composition of the concrete.

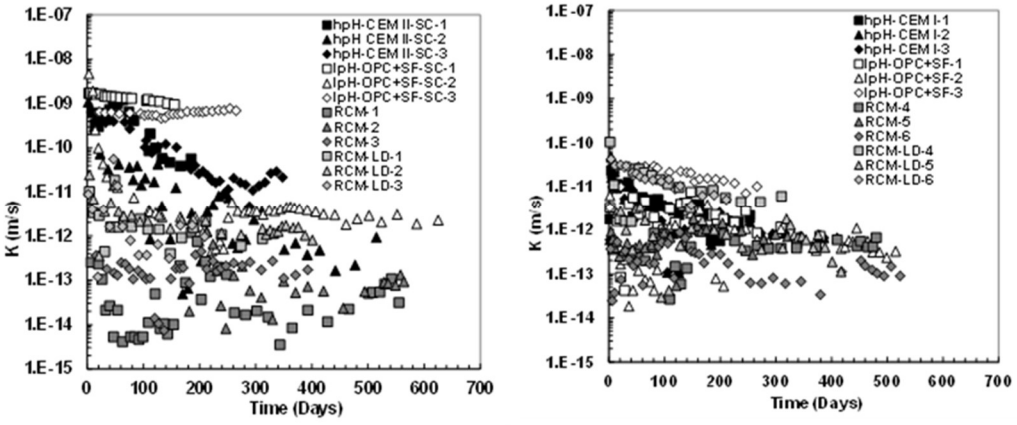

Figure 10: *Hydraulic permeability of concretes with granite (left) and clayey (right) ground water.*

The differences in densities with the different concretes have allowed different volume of water percolated, varying between 3 L with the shotcrete concretes in short times to < 0.1 L after 24 months in the high dense reference concrete mix (RCM). Differences in water transport induce different levels of alteration of concretes from interfaces that vary with residence of GW before being percolated, changing the leaching level and the reaction.

Interaction with granite water (GW): In the high pH concrete, CEM II from FEBEX plug, the alkaline plume was evidenced and its duration (from pH = 12.3 to 9) was independent on the heterogeneity and the amount of water percolated but more related to the time of interaction of the water in the pores of the concrete (11, left). It has been confirmed that the alkalis are the ions first released and are the responsible for the alkaline plume. The decay in the alkaline plume in the percolated water is not an indication that the pH of the bulk of the concrete decays in the same level. The release of Ca has been confirmed as good parameter to identify the alteration of the cement paste and as consequence increase in pore size due to decalcification of CSH. The portlandite is progressively reduced and accumulation of ettringite due to the CEM II composition. In the LpH-OPC+SF, the alkaline plume is not detected even at short ages. The release of alkalis is not significant respect that of HpH-CEM-II, what confirms the reason for the alkaline plume in HpH concretes. On the contrary the Ca released is similar or more significant that in HpH concrete and the process of leaching maintain longer. Progressive increase of calcite is detected after high volumes of water percolated.

Interaction with clayey water (CW): The alkaline plume in the high pH CEM-I is also confirmed with CW but that not occurs from LpH concrete. The LpH concrete is enriched in alkalis that confirm its retention in cement paste. Retention of sulphates is detected with new solid phases formation in the bulk of the concrete (Figure 11, middle), mainly in the LpH, the HpH has low Al_2O_3 content what limits the formation of ettringite or monosulfoaluminate. Retention of Cl is observed in the cement paste. The Ca/Si ratios of cement paste also result altered. A Neo-formation of calcite is detected distributed inside the cement paste increasing the Ca content (Figure 11, right), while with low ionic GWs an additional external layer of calcite is formed but less accumulation in the bulk. Mg $(OH)_2$ is also appreciated in contact with the clayey water, and increase of Mg in cement paste. Pore structure is also altered with clear increase close the CW.

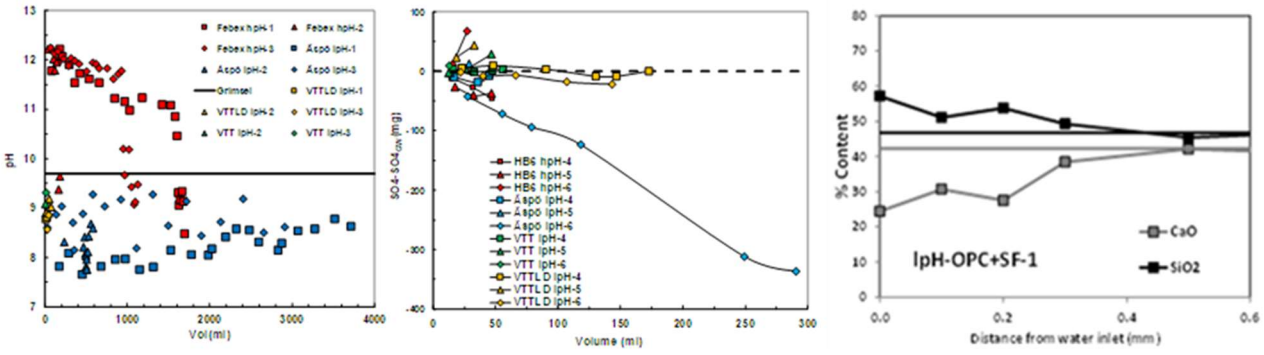

Figure 11: *Left) Alkaline plume with GW, middle) sulphate retention and right) Ca-Si in LpH with CW*

III. Short-term lab scale WGs interaction in CEBAMA Reference mix Low-pH concretes

The CSIC received two RCM concrete types, basically with the same composition and dosages but differentiated in the w/b ratio to allow differences in density that will affect transport properties. The tests carried out by CSIC in both RCM concretes are dealing with three main aims: 1) Analyses of binder hydration advance and effect on microstructure, 2) Cl transport diffusion and 3) Characterisation of alteration of mineralogy and transport properties due to interaction with granite and clayey waters:

1) No portlandite or ettringite is detected after 5 and 15 months of hydration. The Ca/Si ratio is in the order of 0.5. Pore pH = 11.5. Low porosity (2.5% for RCM high density, respect to 12% in Low density)
2) Chloride transport test give values for diffusion coefficient of $0.056 \cdot 10^{-12}$ for RCM and $0.3 \cdot 10^{-12}$ m/s^2 for the low density.
3) The GW percolation tests main results indicate the low hydraulic permeability in both concretes, as shown in Figure 10, from 10^{-13} to 10^{-12}. The low volume of percolated water (up to 50 mL in reference RCM and 200 mL for low density RCM) suggests low alteration microstructure after 24 months test. The interaction with granite water, low salinity. Some alkalis are released. No calcite increase and no external layer of calcite is detected. As for the C-S-H no changes in cement paste Ca/Si is detected at the interface. With CW interaction leaching of Na and K at the water inlet, but retention of sulphates and Cl is detected. Also Mg increase at the interface from 0.3 to 1 mm. Some formation of ettringite nodules at the interface. A thing calcite layer, < 10 μm, but discontinuous is formed in some cases. In low density RCM enrichment of Mg up to 1.5 mm, decrease of Ca/Si ratio to 0.4 up to 0.2 mm and formation of discontinuous external calcite layer.

3.3. SERIE – EARLY SURFACE REACTIVITY EXPERIMENTS

3.3.1. RESULTS FROM OBJECTIVE 6 (AND LINK TO OBJECTIVES 1, 3 AND 5)

Objectives 1, 3, 5 and 6 become interconnected once the several scales of the experimental framework have been analysed. Perturbed bentonite mineralogy at the concrete interface is complex. It has been measured to affect a few mm at long term and a few hundreds of microns in short term 0.5 - 1.5 years surface interface reactivity small SERIE experiments. Three types of cement mortars were examined in the SERIE experiments. Figure 12 compares Mg and Ca profiles determined through bentonite to cement mortars. Mg perturbation affects with more relevance bentonite in the high pH systems showing relative high Mg atoms concentration (25 - 20%) in the first 100 μm. After this maximum, a step with medium concentration in the range of 20-10% from 100 to 750 μm, reaching the bentonite reference concentration (6%) in less than 1 mm. Ca profiles showed a sharp increase in the mortar side in a < 50 μm rim, all the perturbations less developed in the low pH cement mortar. In Table 2, measured distances with details of the mineralogical perturbation at the interfaces, are summarized for long-term to short-term experiments.

The comparison of short-term long-term different spatial scales systems can be used to build the picture of the evolution of the geochemical perturbation. Figure 13 contains the comparison of CEM-II systems in contact with FEBEX bentonite in the different time and scales approach. CEM-II concrete in the FEBEX gallery show heterogeneous chemical profiles according to the centimetres altered rim in which it is possible to detect also the Mg perturbation, which is not observed in the laboratory experiments both at short or long term in high pH cements. Regarding bentonite, we can define the geochemical perturbation in terms of propagation of the Mg-phases. Close to the concrete there are three different regions: a high Mg region (50 - 25 %Mg), a medium Mg region (25 - 10%) and a low Mg region (10 - 6%). They were propagated up to 250, 1000 and 3000 μm respectively in 13 years and up to < 100, 750 and 1250 μm in the SERIE experiments. The volume of bentonite near the cementitious material is proportional to 10^6/1 comparing the gallery to SERIE experiments. This means that there exists a huge source for Mg precipitation in the bentonite potentially extractable from the exchange complex in the in-situ gallery case as can be deduce from Figure 3. In consequence it can be argued the relative impact of this mineralogical perturbation is low in terms of time and spatial evolution.

Ca increases due to calcite precipitation in bentonite are not very significant as far as its semi-quantification by DRX did not reach a > 5% level in the first 5 mm rim of bentonite, which is in agreement with the relative invariance of calcium in the chemical profiles analysed.

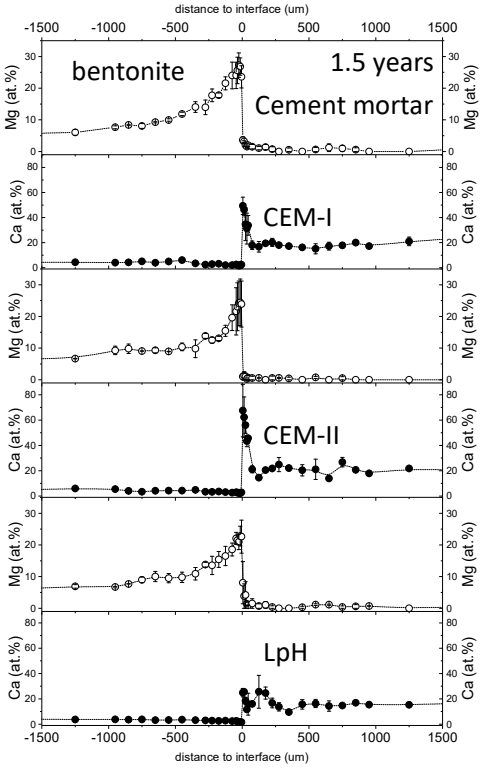

Figure 12: *Mg and Ca (% atoms calculated excluding C and O in SEM-EDX analyses) profiles for SERIE small experiments system C at 1.5 years. Error bars are calculated for replicate experiments.*

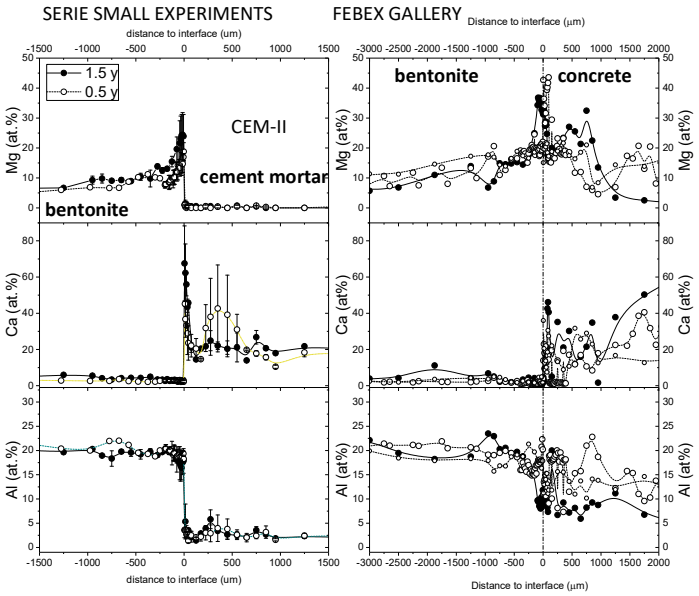

Figure 13: *Mg, Ca and Al (% atoms calculated excluding C and O in SEM-EDX analyses) profiles for SERIE small experiments system C at 0.5 and 1.5 years compared to FEBEX gallery in-situ experiments. Error bars calculated for replicate experiments. FEBEX GALLERY: solid circle: CC-32-4 Overcoring; open circle: 32-5; open small: 32-6.*

Table 2: *Systems comparison for mineralogical alteration thickness.*

System ***time***	***Ca-phase (concrete)***	***Ca thickness***	***Mg-phase Hydroxides, tri-sheet***	***Mg-Thickness***	***#exp***
FEBEX CEM-II **13 years** **granitic water**	Calcite Sharp front	< 250 µm (*)	7 Å (1:1; 2:1:1) 1.53 - 52Å (2:1)	< 250 µm **50 - 25% Mg** < 250 - 1000 µm **25-10% Mg** 1000 - 3000 µm **10 - 6% Mg**	**3(**)**
(HB6) CEM-I **10.5 years** **saline water**	Calcite Aragonite Sharp front	< 100 µm	Brucite complex 7 Å (1:1; 2:1:1) 1.53 Å (2:1)	< 500 µm **25 - 10% Mg** 500 - 1000 µm **10 - 6% Mg**	**1**
SERIE CEM-II **1.5 years**	Calcite Sharp front	< 100 µm	Brucite complex **7 Å (1:1)** 1.53 – 52 Å (2:1)	< 100 µm **25 - 20% Mg** 100 - 750 µm **20 - 10% Mg** 750 - 1250 µm **10 - 6% Mg**	**2**
0.5 years	Difuse front	< 500 µm	Brucite complex 7 Å (1:1) **1.53 – 52 Å (2:1)**	< 50 µm **25 - 20% Mg** 50 - 500 µm **20 - 10% Mg** 500 - 750 µm **10 - 6% Mg**	**2**

(*): Sharp Ca maximum. Calcite is a component of the concrete and it is not possible to distinguish its concentration in the bulk. (**): other additional three in-situ sampled interfaces were studied under FEBEXdp project with similar results.

3.4. Through- and in- diffusion tests in CEM I and CEM IV

System D is covered by objective 2 and results are presented in this part. Table 3 shows the range of effective diffusion coefficients obtained for HTO and ^{36}Cl in concrete and mortar using synthetic water (Na-Cl) and water at equilibrium with the respective solid (CEM I concrete or CEM IV mortar) after Through- Diffusion tests. Conservative elements as HTO and ^{36}Cl are not adsorbed in the solid; therefore, the differences in the diffusion coefficients must be related to changes induced in the solid structure, not to the porewater chemistry itself. The diffusion coefficients obtained with the respective equilibrium porewaters are slightly higher than those determined with the synthetic porewater (factor 1.5 to 2 approximately). As the synthetic water is not necessarily in equilibrium with the system, some mineral precipitation may occur and bias the results of the tests. Although the differences are not extremely large in this case, they must be accounted for.

Table 2: *Effective Diffusion Coefficient (m^2/s).*

Tracer/Material	***Synthetic Porewater****	***Equilibrium with concrete/mortar porewater***
HTO Concrete	$(1.1 – 1.9)\cdot10^{-12}$	$(3.3 – 3.7)\cdot10^{-12}$
HTO Mortar	$(1.4 – 1.6)\cdot10^{-12}$	$(1.1 – 1.3)\cdot10^{-12}$
^{36}Cl Concrete	$(1.6 – 1.9)\cdot10^{-13}$	$(2.4 – 2.8)\cdot10^{-13}$
^{36}Cl Mortar	$(2.2 – 2.6)\cdot10^{-13}$	$(3.4 – 3.9)\cdot10^{-13}$

**Na-Cl water*

To observe the effects caused by changes in the mortar pore structure In-Diffusion experiments were carried out with ^{137}Cs, using experimental times from 150 up to around 1500 days. Figure 14 shows the concentration profiles measured at three different times and the fit obtained to determine the apparent diffusion coefficients. From the fit of the experimental data, it could be observed that the value of the apparent diffusion coefficients (D_a) varied decreasing with the experimental time: after 148 days it was $1.8 \cdot 10^{-14}$ m^2/s; after 380 days, $1.2 \cdot 10^{-14}$ m^2/s and after 1494 days, $0.7 \cdot 10^{-14}$ m^2/s. Apart from this clear variation, it could be pointed out that, in the experiments of less duration, the Cs concentration profiles in mortars could not be adjusted considering a single diffusion coefficient (or a single porosity model). The experimental data were better simulated considering the superposition of two diffusion profiles and assuming that a fraction of Cs (approximately 25%), penetrates more deeply and faster whereas the rest penetrates less. As a general conclusion, it can be stated that the appropriate selection of the experimental time is very important to obtain reliable diffusion coefficients in these materials.

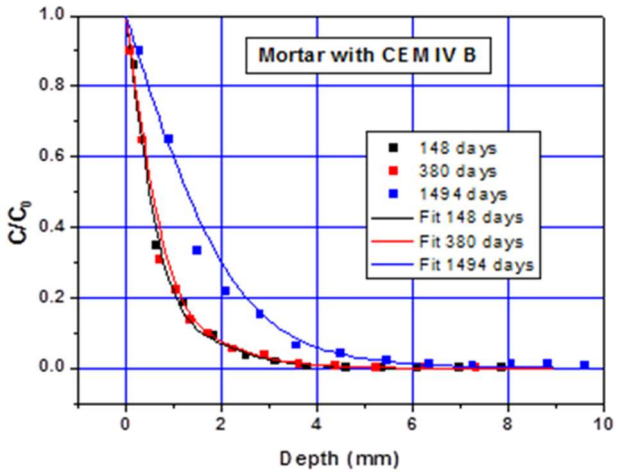

Figure 34: *Concentration profiles of ^{137}Cs in mortar at different times.*

Technical Summary – SCK·CEN & BRGM – WP1

1. Introduction & Objectives

The concrete structures used in nuclear disposal facilities are subjected to complex interactions with the geological matrices (e.g. clay, granite). The interaction processes are very slow but important for the long-term durability assessment (> 1000 years). The interaction disturbs the equilibrium between the pore solution of the cementitious materials and the solid phases of the cement matrix which results in dissolution and/or precipitation of minerals. The alteration is even more pronounced at the clay host rock side. The interaction typically results in alteration of mineralogy and microstructure which are mostly followed by alteration of its transport properties and influences the long-term stability of an engineered structure. In order to understand and predict this alteration over time, comprehensive experimental approaches focusing on the concerned materials are necessary. In case of Belgium, yet, the interface between concrete and Boom Clay has not been fully characterized. Therefore, the present study aims at characterizing and understanding the induced changes at the interfaces (both concrete and clay side) and its transport properties for fluids and solutes. How the ageing processes can affect these interface characteristics will also be assessed with the main focus on:

- Characterization of the mineralogical and microstructural changes at the interface of Boom Clay and concrete using a multi-scale investigation. Join effort between SCK·CEN and BRGM.
- Determine changes in the transport properties at different time scales (short term lab, long-term anthropogenic analogues). SCK·CEN.
- Provide data in order to test/validate the outcome of coupled geochemical-microstructural modeling (WP3). Join effort between SCK·CEN and BRGM.

2. Studied system

The Boom Clay formation, which is a dark organic-rich and poorly indurated argillaceous clay with a high pyrite content, has been considered as a potential host rock for intermediate and high-level radioactive waste in Belgium. This work focuses on the characterizations of more than 13 years concrete-clay interfaces stemming from the underground research laboratory (HADES) located at a depth of 225 m in Mol (below SCK·CEN), which are representative for disposal conditions. The laboratory experiments to mimic the real interaction conditions are also studied in this work.

3. Main results – Scientific highlights

The main objectives of this work is to understand the chemical degradation processes occurring at the interface between cementitious materials and Boom Clay with the focus on leaching and carbonation as the most dominant degradation processes. Therefore, an experimental laboratory program was designed to prepare interfaces under carbonation and leaching by putting backfill concrete (high porosity) and Boom Clay in contact in either accelerated percolation or batch-type experiments. Furthermore, 14 years old in-situ interfaces were investigated.

The main goal of this research is to evaluate whether clogging occurs in the clay and/or concrete side, hence influencing the transport properties for fluids and solutes. The following tasks have been done:

In-situ experiments:

- 2 drilling campaigns to obtain the Concrete-Boom Clay interfaces were done at EURIDICE (done by SCK·CEN).
- Microstructural and mineralogical analysis using µ-tomography, ^{14}C PMMA autoradiography, SEM and FIB-SEM (done by BRGM).
- Permeability and diffusivity measurements of lining concrete (done by SCK·CEN).
- Water sorptivity of interface and lining concrete (done by SCK·CEN).

Lab-made interfaces:

- *Percolation type experiments*
  - Representative for the backfill cementitious materials in the Belgian disposal concept
  - The conditions in the HADES URF are mimicked: Chemical compositions, advective flow
  - Follow-up chemical, pH and transport permeability evolution
- *Batch type experiments*
  - Backfill cementitious material – clay suspension
  - Follow up chemical, pH and transport properties evolution (permeability, diffusion)
- Microstructural and mineralogical analysis on lab made interfaces (using the same techniques for aged interfaces).
- MIP + N_2-adsorption + water porosity (done at SCK•CEN).

Selected results:

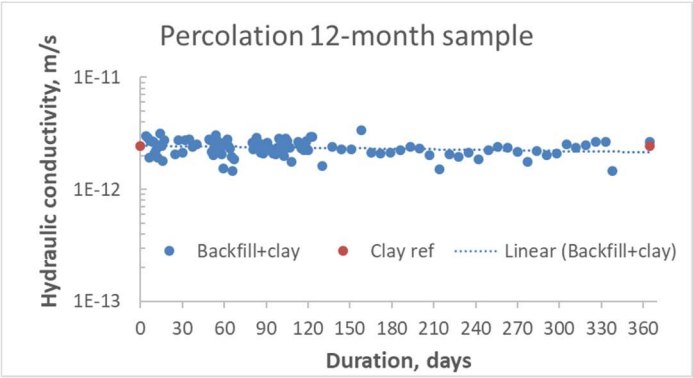

Figure 1: *Permeability evolution during percolation experiment: The composite permeability slightly decreased. However, the change compared to the reference permeability of clay can be negligible taken into account the uncertainty of permeability measurement in the percolation experiment. Both precipitation and dissolution might simultaneously occur at the interface. Some precipitation of calcium carbonate could occur in the clay side due to carbonation resulting in a porosity drop. On the other hand, dissolution of some phases in clay due to advective (and also diffusive) flow could increase the porosity of clay which compensate the porosity decrease due to carbonation. Therefore, a significant change in permeability was not observed. For the backfill side, similar phenomenon could happen. However, these change in microstructure could be too small to interfere with the permeability.*

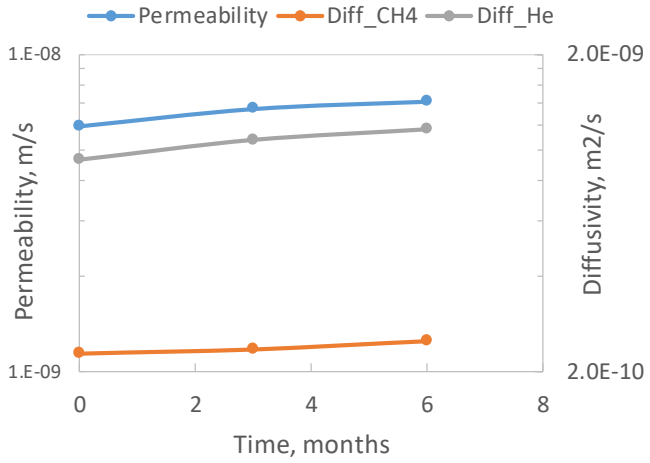

Figure 2: *Increase in transport properties of backfill materials during batch experiment which is due to Ca-leaching.*

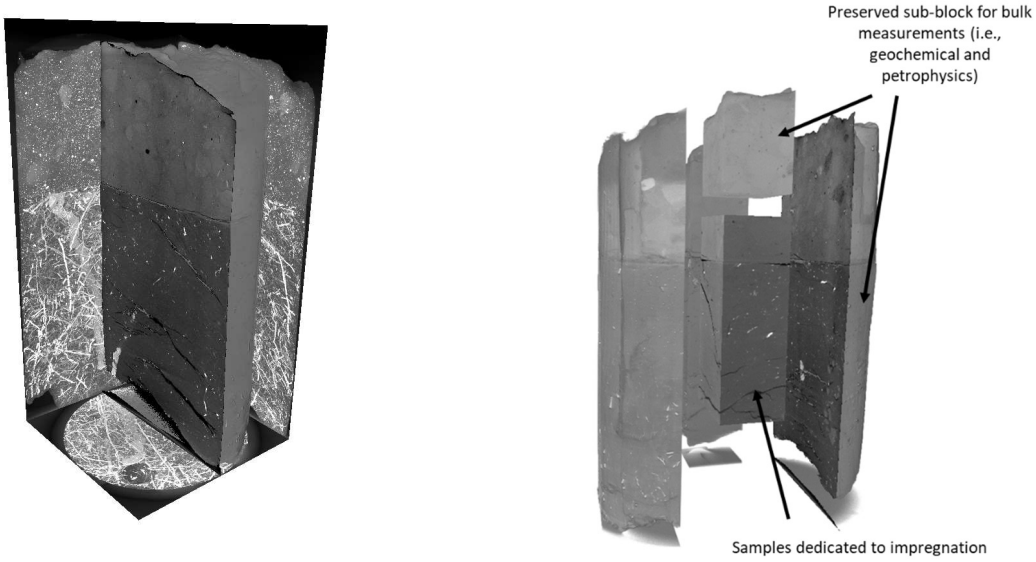

Figure 3: *On the left side µ-tomography visualization (voxel size 61 µm³) of the 13 years old Boom Clay-Concrete interface. On the right-side sampling strategy for the sub sampling spatialization.*

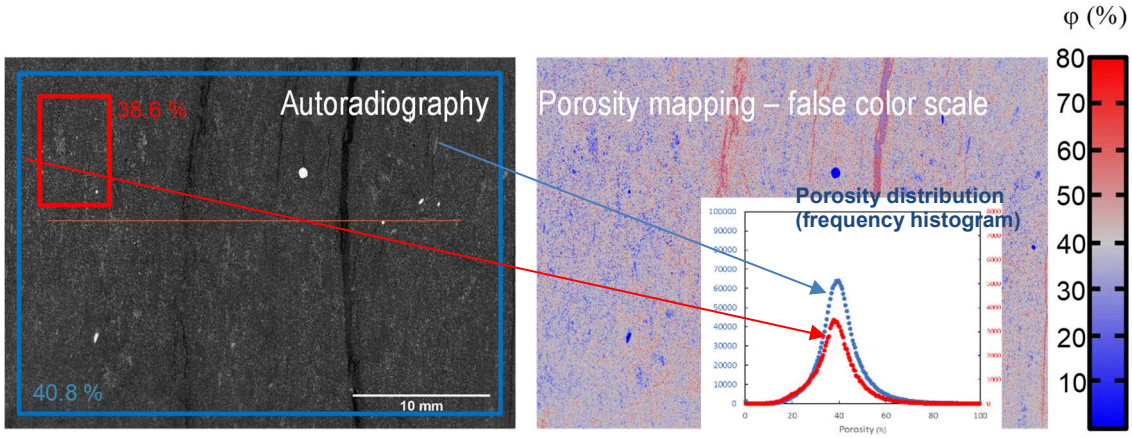

Figure 4: *Porosity maps of Boom clay obtained by autoradiography showing that the total porosities were around 40% (which is close to the typical reported porosity of 37%).*

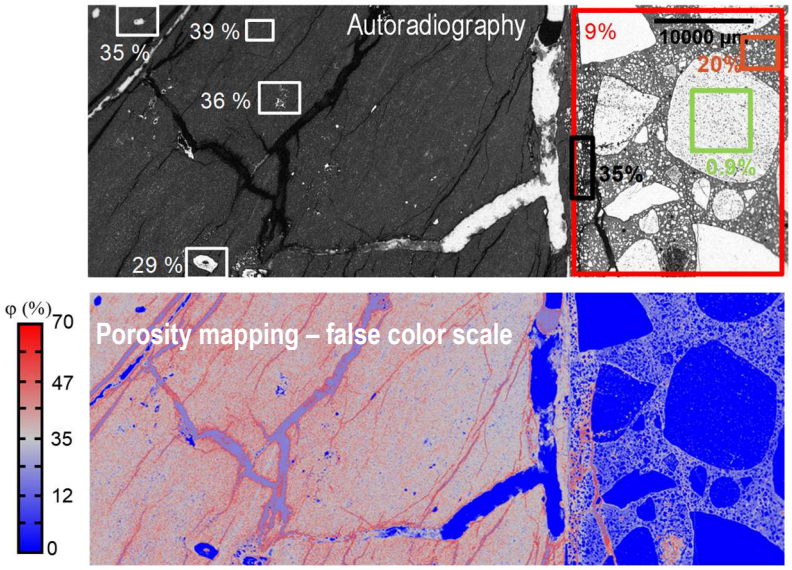

Figure 5: *Spatial distribution of porosity at concrete, clay sides and the interface indicating that the average porosity of the paste (including sand) of concrete was about 20%. A significant increase in porosity at the concrete interface was observed, up to 35%. For clay side, some area had lower porosities then the average due to the presence of some less porous grains.*

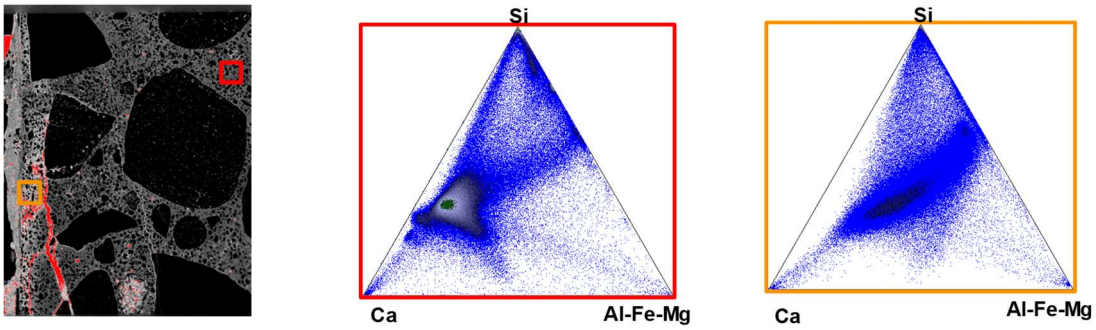

Figure 6: *Chemical evolution of the concrete toward the interface – measured in 2 mm thickness from the interface which proves that the Ca/Si decreased, while the Al-Fe-Mg increased at the concrete interface. This gives an indication that Ca has been leached from the concrete interface because Si as well as Al, Fe, Mg concentration are quite stable (evidenced from batch and percolation experiments).*

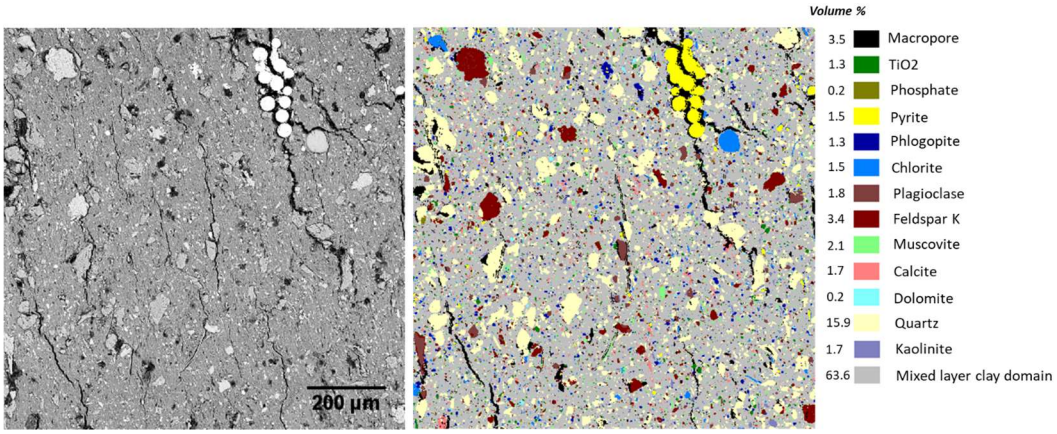

Figure 7: *Example of minerological mapping. On left side SEM backscatter image of the pristine Boom Clay. On right, the mineralogical mapping gather after a segmentation procedure. The formula for the mixed clay domain is* $Na_{0.02}K_{0.32}Ca_{0.04}(Si_{3.68}Al_{0.32})[Al_{1.33}Fe_{0.46}Mg_{0.21}]O_{10}(OH)_2$.

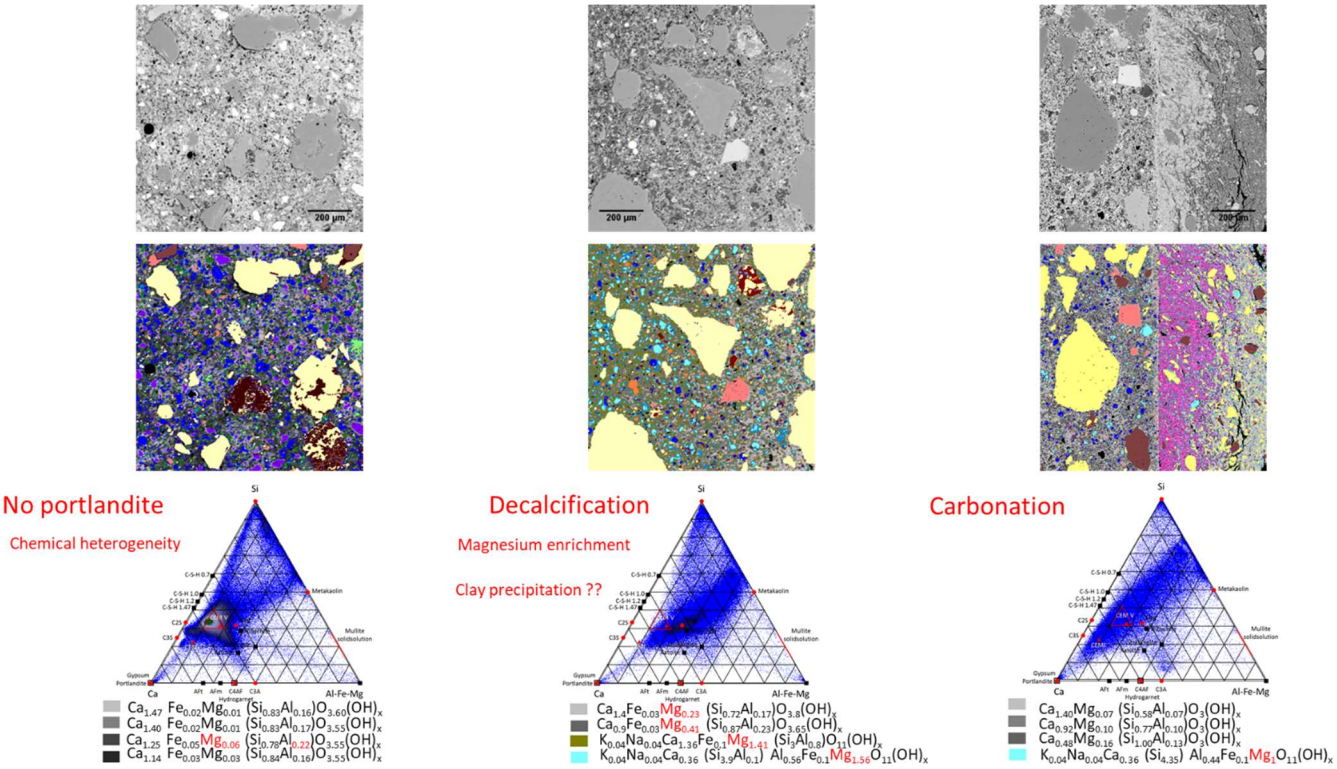

Figure 8: *Summary of the main mineralogical changes that have been observed at the interface.*

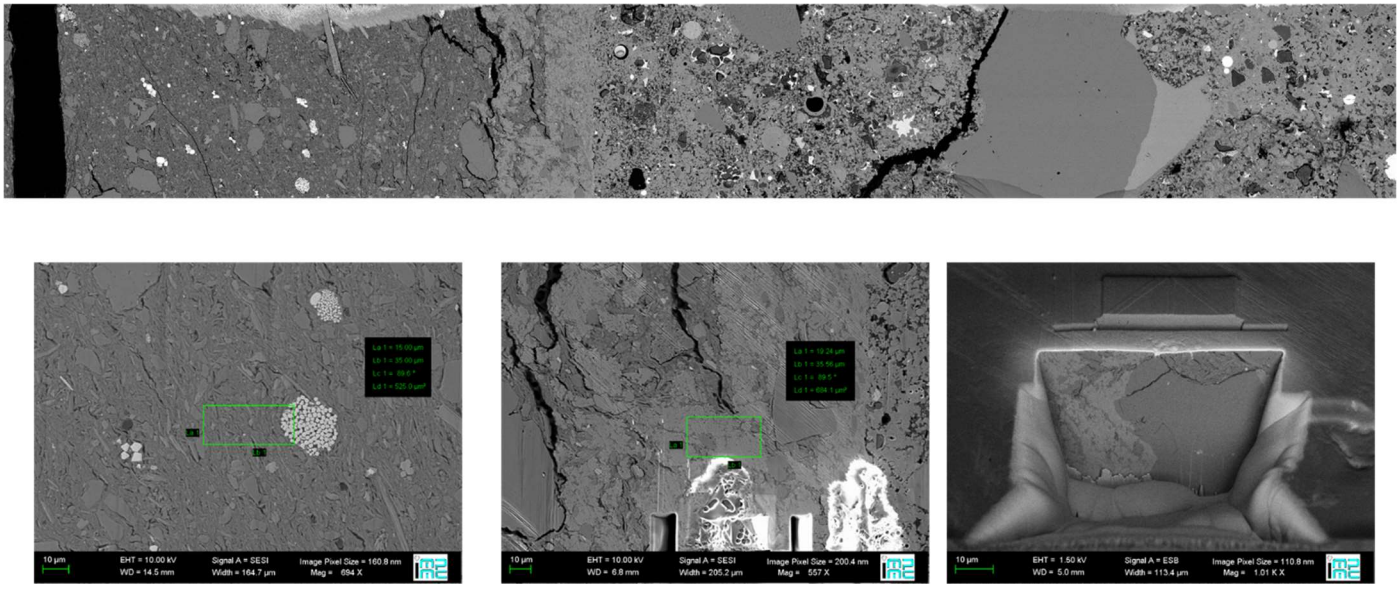

Figure 9: *SEM Imaging, BIB polishing and FIB localization of zone of interest for FIB SEM acquisition.*

Technical Summary – UJV & CTU – WP1

1. Introduction & Objectives

The Czech Deep Geological Repository (DGR) concept assumes that waste packages containing spent nuclear fuel (SNF) assemblies will be enclosed in steel-based canisters placed in vertical or horizontal boreholes at a depth of ~ 500 m below the surface. The void between the canisters and the host crystalline rock will be backfilled with compacted bentonite. Intermediate-level waste (ILW) with long-lived radionuclides, not being allowed to be disposed of in the near-surface repositories, will be disposed in DGR separate section. The ILW will be emplaced in concrete canisters in specially excavated chambers filled by bentonite as a backfill. Concrete will be used in the repository as both barrier material and construction material (e.g. fibre concrete containers for ILW, sealing and separation concrete plugs, floors, walls, supporting construction elements, shotcrete, grouting). The knowledge of cementitious materials behaviour under the DGR conditions is essential for the predictions of EBS evolution.

Generally, the behaviour of cementitious materials under different conditions is predominantly studied due to building and construction reasons. However, the conditions of DGR are specific (e.g. a combination of materials) and the EBS have to fulfil the long-term stability requirements. In the literature related to the use of cementitious materials in radioactive waste repositories, the most studies deal with conventional Portland cement (OPC) but there are also some studies concerning low-pH cementitious materials. The topics cover mainly geochemical and physical evolution of cementitious material under DGR conditions, hydromechanical behaviour or radionuclides sorption and diffusion on these materials. The review of all these topics can be found in Deliverable D 1.03 (WP1 Experimental studies – State of the art literature review).

The objective of both Czech partners (ÚJV Řež, a. s. and CEG CTU) was to contribute to an experimental study on the interaction between cementitious materials (OPC and RPM – low pH reference mix design) and bentonite. Experimental works included long term laboratory and in-situ experiments in the Underground laboratory Josef and subsequent laboratory analyses of cementitious and bentonite samples from these experiments. The effect of cement/bentonite/water interactions under defined temperature load was studied. The main aims were to study the changes in bentonite and cement properties due to mutual interaction under in-situ and laboratory conditions (diffusivity, porosity, mineralogy, fluid composition, uniaxial compressive strength etc.) and also to provide the input experimental data to WP3. The obtained data is partly directly applicable to the long-term performance assessment (e.g. diffusion coefficients) and partly as supporting arguments for material selection (e.g. material compatibility).

2. Studied system

The dismantling of in-situ experiments in the Underground laboratory Josef completed the long-term interaction experiment among Czech bentonite B75, cement material CEM II and groundwater from Underground laboratory Josef lasted 6 years. In general, four perforated stainless steel pipes (cartridges) were filled with B75 compacted to 1600 - 1700 kg/m^3 in a shape of cylinders 7.8 cm long and with cement compacted to 1800 kg/m^3

also in a shape of cylinders but 3.5 - 4.0 cm long. One cartridge (P1) was filled with bentonite only, another one (P3) was filled alternatively by cement/bentonite cylinders. The cartridges were installed into boreholes in the Josef Underground laboratory in September 2010. They were pulled out progressively at four time intervals (after 9, 20, 26 and 72 months).

The laboratory work was based on ageing processes in small pressure vessels with respect to Czech bentonite (B75), cementitious materials (Portland-type, OPC, and a low pH reference mix design, RPM) and groundwater from the Josef Underground Laboratory (GW Josef) under in-situ and high temperature (95°C) load conditions. The overview of the experimental program is in Table 1.

Table 1: *Summary of the experimental program - long-term laboratory experiments and dismantling of the in-situ experiment.*

	Ageing procedures	***Bentonite B75***	***GW Josef***	***CEM II 42.5R***	***RPM***	***Temperature 95 °C***
Laboratory experiments	Bentonite suspension + CEM II (OPC) or RPM + 95 °C	×	×	×	×	×
	Bentonite suspension + CEM II (OPC) or RPM	×	×	×	×	
Sampling intervals 9/18/27 months	GW Josef + CEM II (OPC) or RPM + 95 °C		×	×	×	×
	GW Josef + CEM II (OPC) or RPM		×	×	×	
	Bentonite suspension	×	×			
	CEM II (OPC) or RPM + humid air (10 °C)			×	×	
In-situ test, 72 months	Cartridge (bentonite)	×	×			
	Cartridge (bentonite + CEM II)	×	×	×		

Note: *"Bentonite suspension" is a mixture of Bentonite 75 (B75, 2010y, Keramost, a.s.) and groundwater from Underground laboratory Josef (ratio 1:5), "CEM II" is CEM II A-S 42.5R - Lafarge Cement, a.s., "RPM" is reference paste*

3. Main results – Scientific highlights

A part of the high-level radioactive waste (mainly the waste from nuclear power plant dismantling) is supposed to be emplaced to concrete containers in the separate area of a deep geological repository and one of the potential backfilling materials is bentonite. Assessing the long-term performance of cement material for radionuclide encasement requires knowledge of the radionuclide-cement migration, interaction, and mechanisms of retention.

This understanding will enable accurate prediction of radionuclides fate when the waste forms get in contact with groundwater. The geotechnical and geochemical stability of cementitious materials in contact with backfilling material and groundwater is important for prediction of its long-term evolution in the safety assessment.

3.1. The long-term in-situ interaction experiment (cartridges)

The dismantling of an in-situ experiment after 72 months in the Underground laboratory Josef completed the long-term interaction experiment (four sampling intervals: 9, 20, 26 and 72 months). The experiment confirmed the slow rate of mineralogical changes under in-situ conditions. One remarkable parameter was the replacement of Na cation by Ca and Mg cation in an exchangeable complex of bentonite clay minerals (montmorillonite). In this process, groundwater was dominantly involved, with minor effects of the alkaline front from cement material. The geotechnical parameters such as hydraulic conductivity and swelling pressure were also influenced in a measurable way.

3.2. Laboratory experiments – ageing procedures (small pressure vessels)

As the quality of RPM material is quite sensitive to compliance of mixing procedure, ratio and type of components (plasticizers, silica fume, etc.), the set of tests demonstrating the variation of results was performed before samples for the ageing procedure were manufactured. Two types of plasticizer and various details in the mixing procedure were applied. The microstructure of RPM illustrates Figure 1.

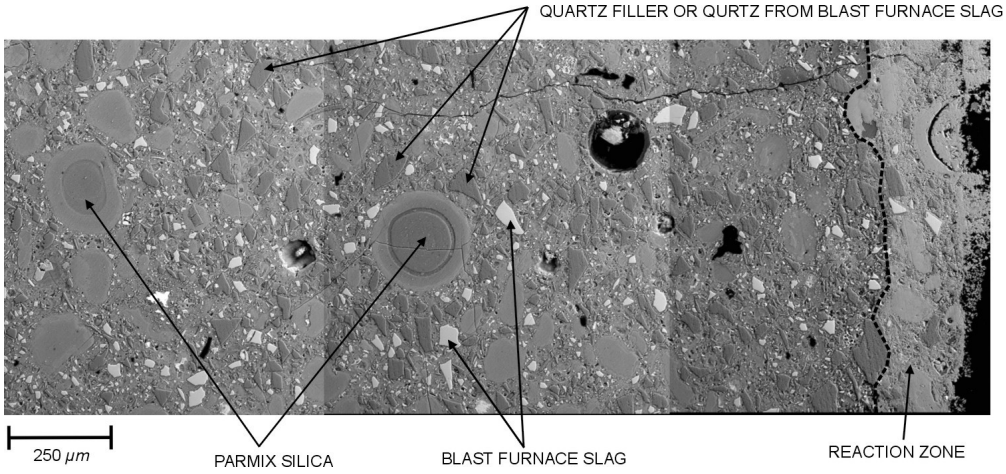

Figure 1: *Scanning electron microphotograph of RPM sample with an identification of individual paste constituents (BSE). The reaction zone highlighted with a dotted line is the result of bentonite suspension interactions.*

Stability of mechanical behaviour of cement samples (OPC or RPM) was determined by compressive strength test before and after ageing periods. The specific shape of the samples was used in order to magnify the interaction effect. The thin plate (cylinders with a diameter of 50.0 mm and thickness of 8.2 mm) and the corresponding non-standard punch test methods were employed (Figure 2, left). It provided results in the form of "load at breakpoint [kN]" which can be subsequently recalculated to "punch compressive strength [MPa]". "Press head displacement - a position [mm]" was also recorded which contributed to the observation of changes of the load-deformation behaviour. The "rigidity" [kN/mm], derived from the linear section of particular strength test records (Figure 2, right) well described changes in elasticity of the samples.

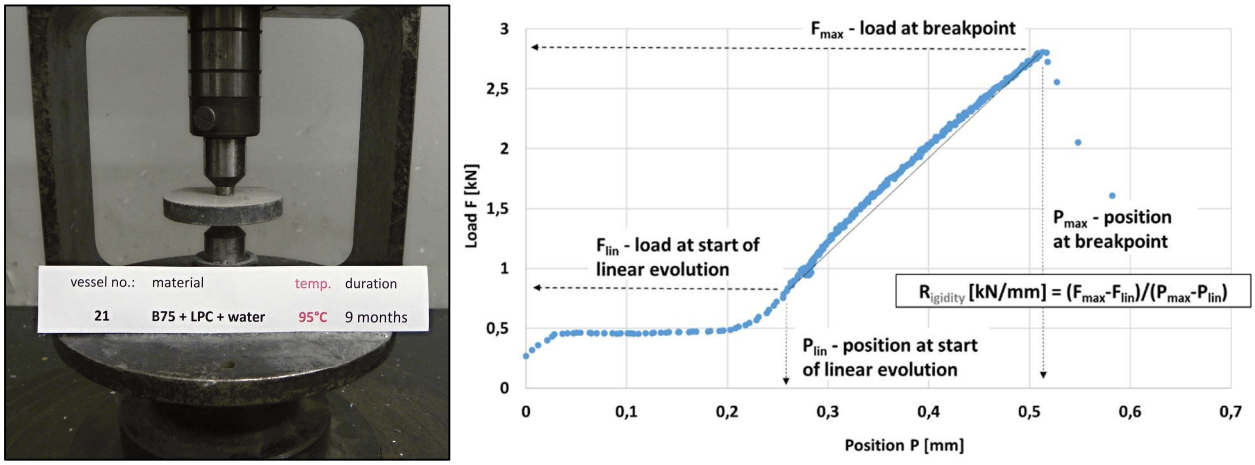

Figure 2: *The punch test setup (left) and test record with derivation of "rigidity" (right).*

The results of mechanical behaviour test revealed changes in both the strength and rigidity (elasticity) of samples of both types of cement paste. The temperature was found to exert a key effect on most of the observations. The compressive strength of OPC decreased with respect to the "heated" (95°C) OPC to 50% of the initial value while the compressive strength of the OPC treated at a temperature of below 10°C increased slightly over time (up to 120% of the initial value). In addition, a significant decrease, down to 30% in rigidity (elasticity) was observed with concern to all the heated OPC samples (see Figure 3).

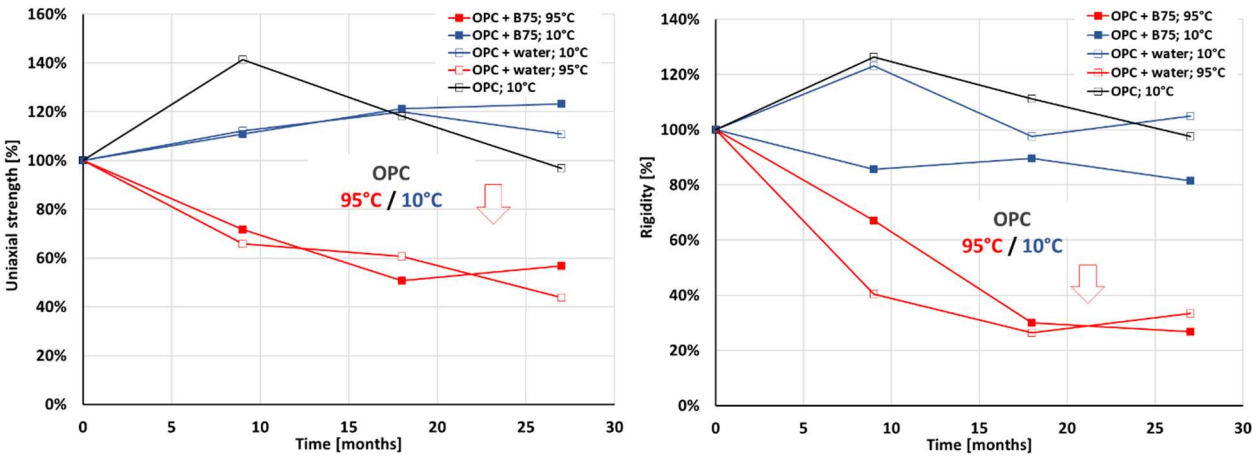

Figure 3: *Time evolution of uniaxial strength (left) and rigidity (right) – OPC.*

All the RPM samples exhibited a significant increase in compressive strength with regard to all the ageing processes (from 140% for reference conditions – humid air under 10°C; up to 180% for samples immersed in the "heated water") over first nine months of the experiment. After 18 months, the values remain almost stable. The temperature of the environment is more significant than the presence of bentonite in the suspension. Contrary to this rigidity (elasticity) of RPM is more sensitive to the absence/ presence of bentonite in the suspension than to the temperature. All the aged RPM samples exhibited similar or higher rigidity values than initial ones (see Figure 4).

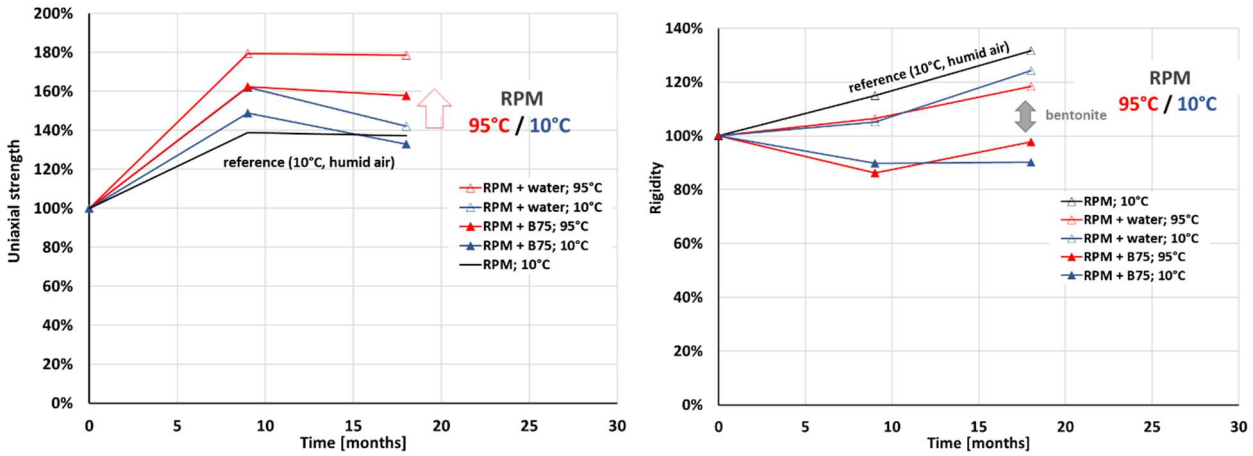

Figure 4: *Time evolution of uniaxial strength (left) and rigidity (right) – RPM.*

The results of the testing of geochemical behaviour confirmed the dominant influence of temperature and the type of material (OPC versus RPM). The chemistry of the GW Josef in contact with the OPC and RPM samples indicated that temperature accelerates mineral dissolution which results in increased concentrations of calcium and sulphates. In the case of the OPC samples, these ion concentrations were found to be approximately seven times higher for the heated than for the non-heated samples. Generally, the pH and total dissolved solids (deduced from conductivity) were much higher for that GW Josef exposed to OPC than that exposed to RPM (Figure 5).

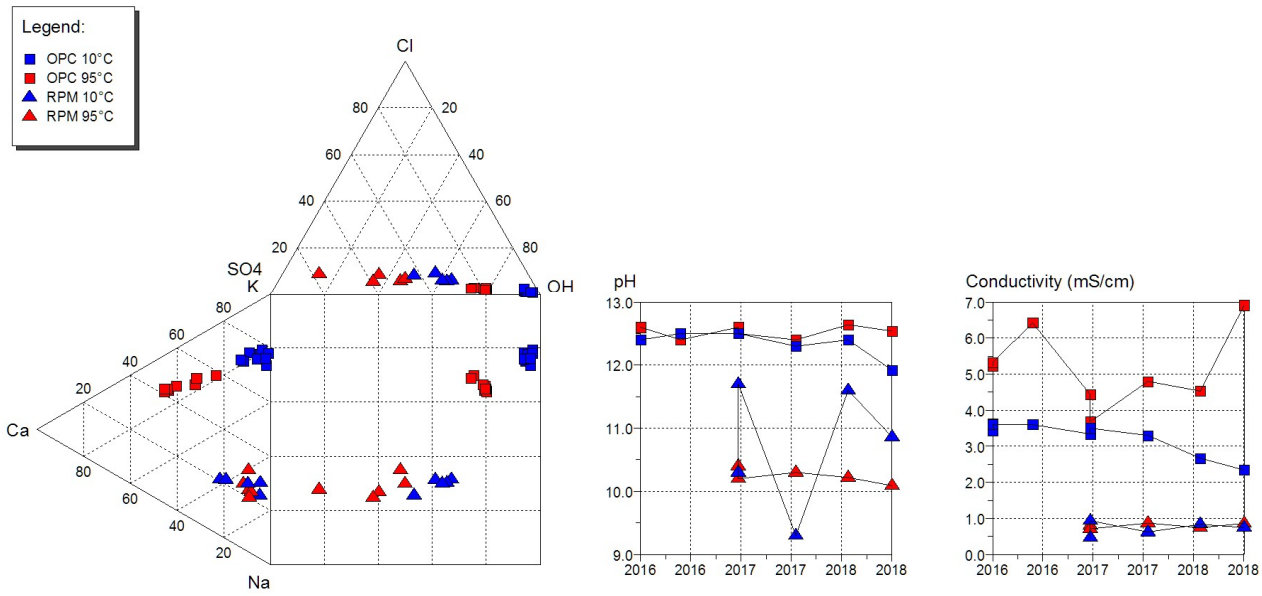

Figure 5: *Chemical composition, pH and conductivity of solutions in small pressure vessels, where OPC or RPM samples were in contact with GW Josef.*

The temperature was mainly responsible for the variation in the pH of the RPM leachate samples, see Figure 6. The pH results of the RPM leachates are gradually approaching those observed for Cebama Reference Paste (VTT). In addition, changes in mineralogy were also influenced by temperature. In a case of RPM samples, the high-temperature completely transformed (dissolved) minerals such as ettringite and C4AF phase.

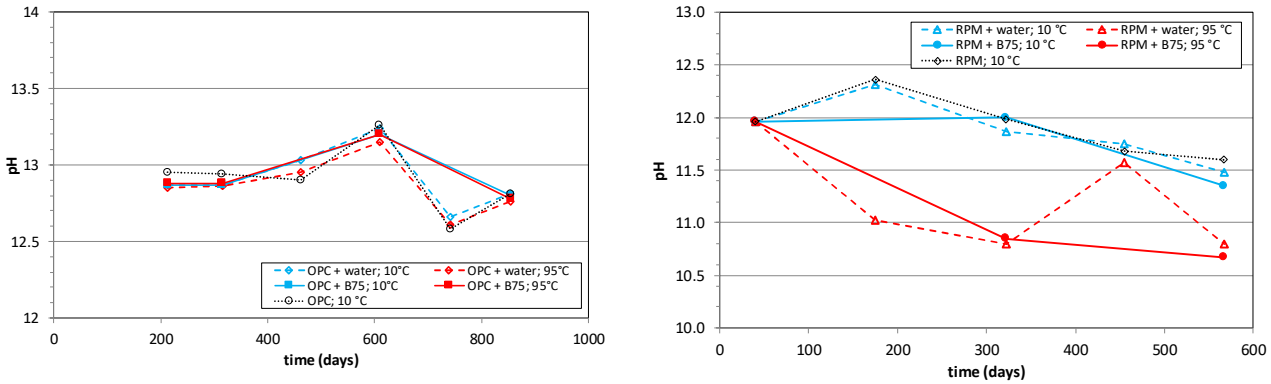

Figure 6: *Time evolution of the leachate pH values of the OPC (left) and RPM (right) samples, time from casting the samples.*

Carbonate precipitates, consisting principally of calcite, were discovered on some of the samples. With respect to both types of samples (OPC and RPM), the precipitates were most significant following ageing in bentonite plus GW Josef suspension at approximately 95°C; they were markedly less significant after ageing in the same suspension at 10°C. Oversaturation to calcite was attributed to the large carbonate pool in the bentonite as well as the calcium present in the cement paste. It is known that the solubility of calcite decreases with increasing temperature. More detailed view with scanning electron microscope equipped with electron probe micro-analyzer showed the calcium enrichment in RPM samples at the boundary with bentonite suspension. The propagation of calcium front increased with the temperature (Figure 7).

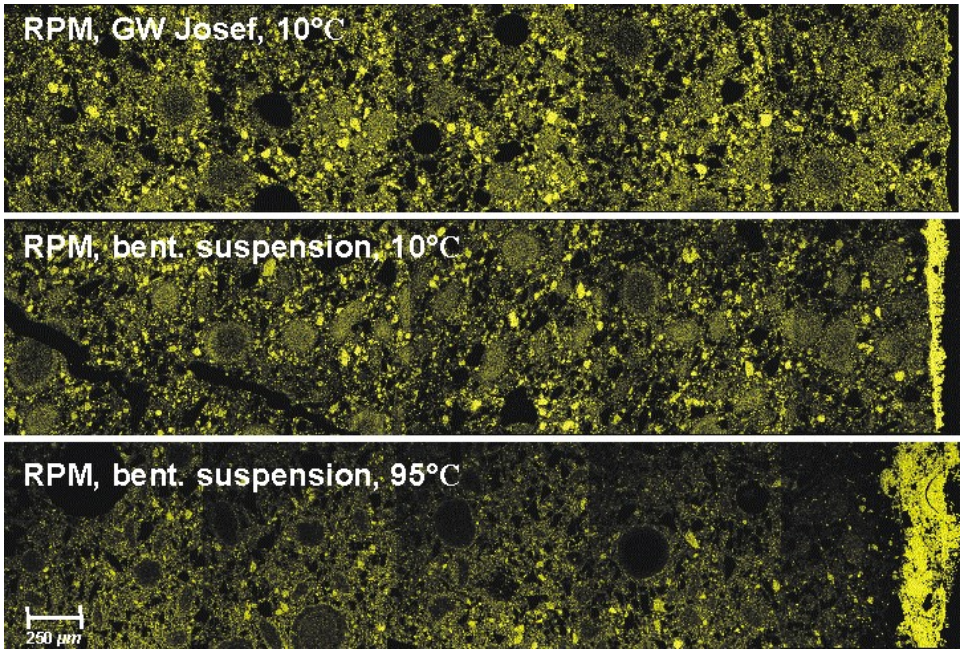

Figure 7: *Scanning electron microphotograph of RPM samples with Ca element map (yellow) showing the calcium enrichment at the interaction boundary with bentonite suspension.*

The through-diffusion (TD) experiments of HTO (^{3}H, ~5 nM) and chloride (~15 - 20 mM, marked by ^{36}Cl of 55 - 60 µM) were performed at laboratory temperature (2 - 25°C) on both samples that were under temperature and ageing load, described in Table 1. At least two parallel experiments in each sampling period per different type of series were made (in total 55 TD experiments of HTO and chloride-36).

TD experiments on OPC samples were performed in the solution that came from vessels in series "OPC+GW Josef at 10°C", while RPM samples in "RPM+GW Josef at 10°C". The HTO effective diffusion coefficients of the OPC samples increased with temperature load (preceding the diffusion experiment itself) by approximately in one order of magnitude which may have been related to the dissolution of the material under higher temperatures as well as a decrease in elasticity (microcracks) which lead to changes of a geometry of a diffusion pathway; on RPM samples, there is no significant difference – all effective diffusivities are in the same order of magnitude. The sample ageing procedure (approx. 9, 18 or 27 months) in pressure vessels did not confirm any dependency on diffusion parameters. Some of the diffusion experiments are still underway (OPC samples after 27 months of interaction with bentonite suspension, RPM samples after 18 months of all type of interactions), but all are evaluated at the end of January 2019 in Figure 8 (without considering retardation processes, i.e. $K_d = 0$). The lower water to binder ratio confirmed lower porosities (capillary + gel porosity) for RPM samples in comparison with OPC; mean values for RPM are from 0.25 to 0.30 which is in an agreement with observations by BRGM reported in 3rd Annual Workshop Proceedings (document available at the project website).

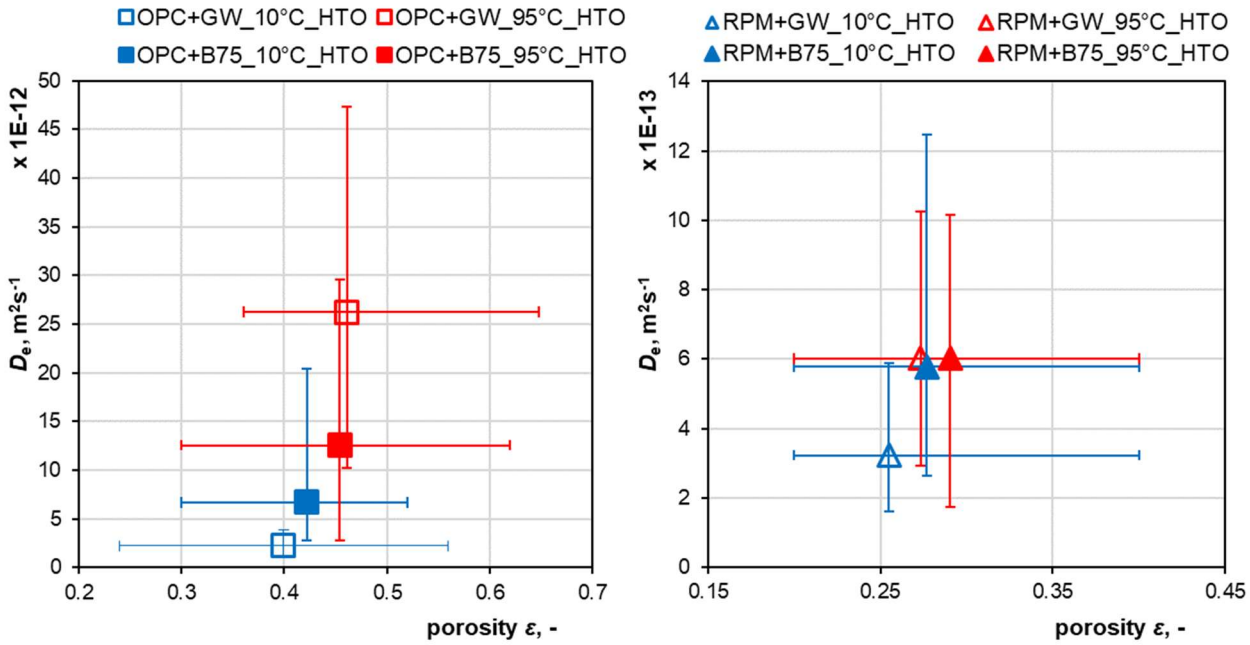

Figure 8: *Effective diffusion coefficient of HTO on OPC and RPM samples: dependency on the porosity of the samples; each series with OPC (RPM): mean value from 7(4) TD experiments.*

The chloride-36 migration was strongly retarded in OPC samples and the evaluation of diffusion coefficients fitting a K_d, porosity "ε" or geometrical factor "G" became challenging. On contrary, the chloride anions were strongly repulsed from RPM samples (no decrease of chloride-36 concentration activity in the inlet reservoir) and no breakthrough (in the outlet reservoir) was observed even after 200 days in all series (except of samples that came from series "RPM+GW Josef at 95°C", where $D_e < 5 \cdot 10^{-13}$). Therefore, we concluded the diffusion process of chloride on RPM samples is very slow (in all remaining series that were under different interactions for approx. 9 months: $D_e < 10^{-13}$ m^2/s) and there are no retardation processes of chloride on RPM samples expected ($K_d = 0$). Nevertheless, for future use of both cement mixtures in the planned DGR, these materials in case of migration of chloride seem to be very effective for retardation or a diffusion resistance.

Technical Summary – University of Sheffield – WP1

1. Introduction & Objectives

The objective of the USFD research was to undertake a detailed physico-chemical characterisation of two cements relevant to international GDF concepts, including those in a UK context, at the cement / groundwater interface. The cements selected for study were the high-pH cement backfill considered for use in the UK geological disposal facility, known as the Nirex Reference Vault Backfill (NRVB), and a low-pH cement used for vault lining, plugs and seals, known as the Cebama reference cement (also used by other partners in the Cebama project). Using three types of groundwater (saline, granite and clay), we aimed to build a mechanistic understanding of how the interaction of cement with groundwater can influence diffusive transport by advancing understanding of such interactions on porosity, permeability and cement mineral phase assemblages. Experiments were conducted in parallel with ULough/USurr. High-resolution datasets generated through these experiments were used to inform cement mineralogy and diffusive transport modelling tasks performed by Juelich and Amphos 21 in WP3.

2. Studied system

The cements studied were:

(1) The Nirex Reference Vault Backfill cement (NRVB), with a w/s ratio of 0.55

(2) The Cebama Reference cement, with a w/s ratio of 0.25

The groundwater solutions investigated were:

(1) Saline

(2) Granite

(3) Clay

Details of the compositions are given in Table1 and Table 2.

Table 1: *Cement formulations utilised in USFD experiments.*

Cement	Component	Content (kg/m^3)
NRVB	CEM I 52 5N	450
	Calcium hydroxide	170
	Calcium carbonate	495
Cebama reference cement	CEM I 42.5 MH/SR/LA	1050

Cement	Component	Content (kg/m^3)
	Silica Fume	1100
	Blast Furnace Slag	650
	Plasticizer	12.6

Table 2: *Groundwater compositions utilised in USFD experiments.*

	Granitic groundwater (mmol/L) (Gascoyne et al. 2002)	**Saline groundwater (mmol/L)** (Gascoyne et al. 2002)	**Clay groundwater (mmol/L)** (Vinsot et al. 2008)
Na	2.8	140	55
K	0.1	2.1	1.1
Ca	0.5	19.9	7.5
Mg	0.2	0.4	5.7
Cl	2.1	172.7	52.5
HCO_3	2.0	2.0	-
SO_4	0.1	4.0	15
pH	8.2	7.7	7

3. Main results – Scientific highlights

3.1. Characterisation of Nirex Reference Vault Backfill material

Prior to undertaking the Cebama project research, there was a limited understanding of the mineralogical and microstructural properties of the Nirex Reference Vault Backfill cement material (NRVB), which has been considered for use as a high pH cement backfill in a UK geological disposal facility within a hard rock environment. During the Cebama project, a state-of-art literature review pertaining to this material was made, and a full characterisation was performed, comparing cement pastes prepared using laboratory reagents or industrial materials. Data obtained included: XRF composition analysis; particle size distribution and XRD of precursor materials; isothermal calorimetry; XRD; TGA-MS; SEM-EDS; ^{29}Si and ^{27}Al NMR; and porosity analysis by XCT and MIP. The literature review and data were published in Vasconcelos et al. (2018).

Further characterisation of the kinetics of hydration of this cement was performed at Diamond Light Source's I11 Long Duration SR-XRD facility (Murray et al. 2017). X-ray diffraction patterns were taken at regular intervals over a four-year period and NMR data were taken on the same material at corresponding time points. Analysis of these data is underway (e.g. see Figure 1 for analysis of the first 48 hours of hydration), including Rietveld refinement of phases present. These data will be used to further underpin leaching experiment observations. The same analysis was performed on the Cebama reference cement, and analysis is currently underway.

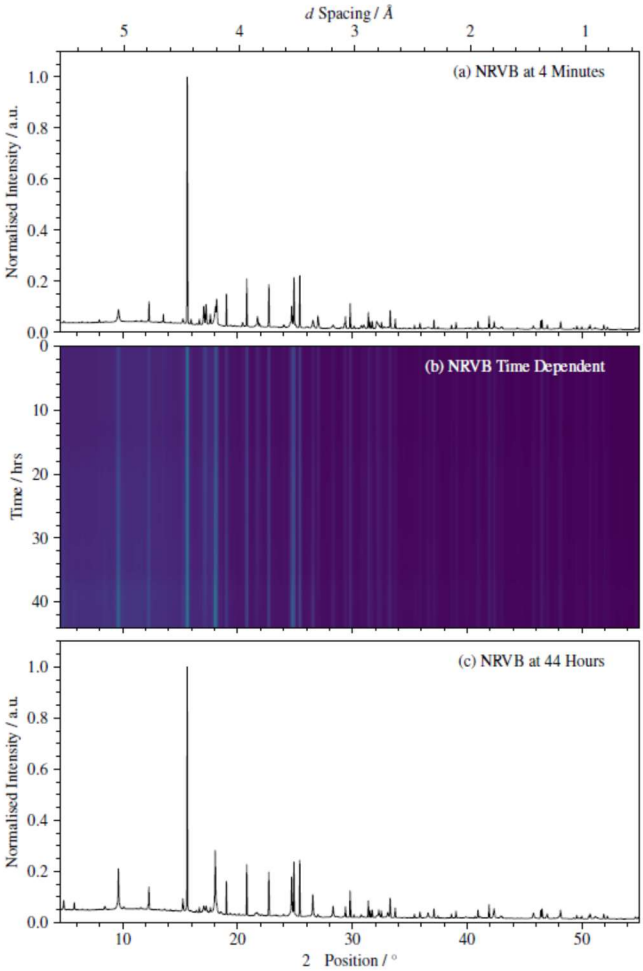

Figure 1: *Initial analysis of SR-XRD patterns of NRVB cement backfill, taken over a 48-hour period.*

3.2. Understanding the influence of groundwater on the mineralogical composition of cement

Cylindrical monoliths of NRVB and Cebama cement paste, 15 mm height x 15 mm diameter, were prepared after 28 d of curing. To allow only radial diffusion of the groundwater, the end of the cylinders was sealed with epoxy resin. Samples were placed in 60 mL vessels (using Teflon baskets) in contact with 50 mL of each of the three groundwaters, to perform a semi-dynamic experiment. The experiment was conducted in an oven at 40°C in a controlled nitrogen environment (i.e. $CO_{2(g)}$ was excluded). Sampling and replacement of the groundwater was performed every two months for a total time of 1.5 years.

The sampling and replacement of the groundwater was performed in a controlled environment ($CO_{2(g)}$ and $O_{2(g)}$-free). The following describes key findings for each of the cement systems studied.

3.2.1. Nirex Reference Vault Backfill cement

The mineralogy of NRVB cement was influenced strongly by both saline and clay groundwater compositions, but was not affected significantly by the granite groundwater, as shown in Figure 2. The presence of sulphur in the groundwater solutions (4 and 15 mmol/L for saline and clay, respectively) was the main source of the mineralogical changes; sulphur was removed from saline and clay solutions by the cement, which promoted the formation of ettringite ($Ca_6Al_2(SO_4)_3(OH)_{12}\cdot 26H_2O$).

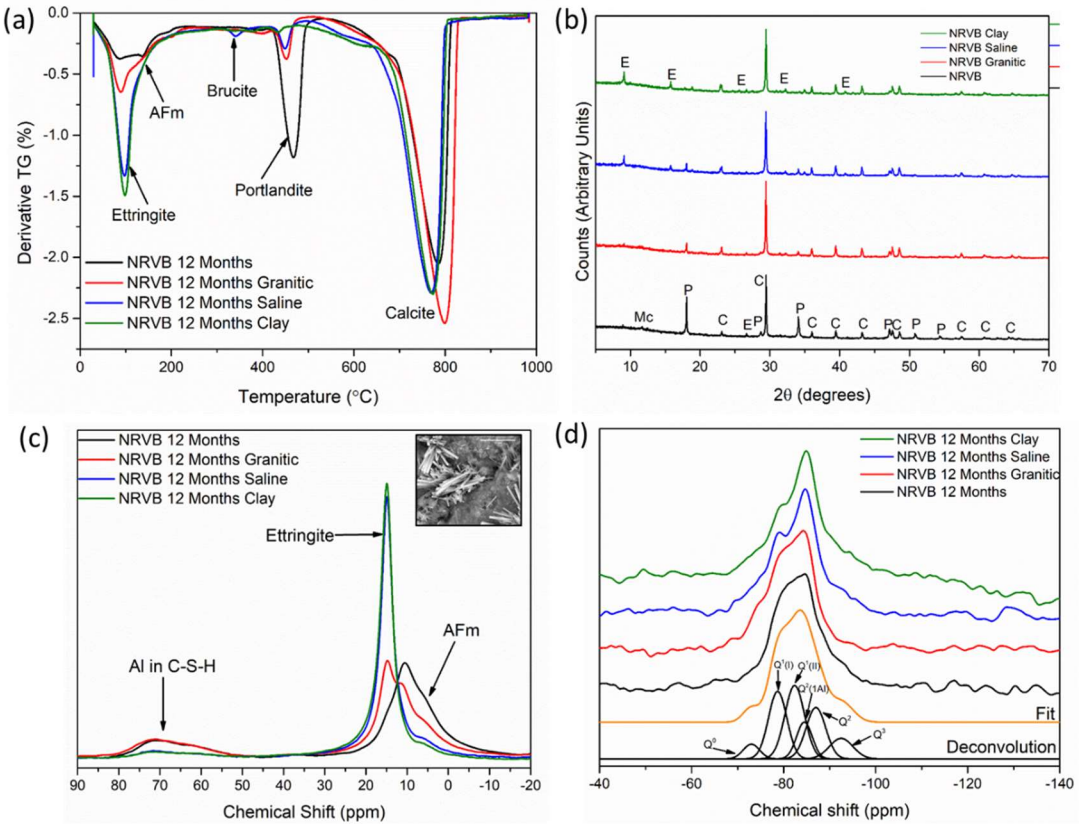

Figure 2: *Comparison of NRVB samples exposed to three different groundwater solutions for 12 months, and comparison to blank (i.e. non-groundwater contacted) material: (a) analysis by TGA; and (b) analysis by XRD. E = ettringite, M = monocarboaluminate, P = portlandite, C = calcite; (c) ^{27}Al NMR analysis; insert in (c) shows SEM images of ettringite needles; and (d) ^{29}Si NMR analysis and deconvolution.*

An increase in DTA peaks and XRD reflections associated with the presence of ettringite was observed for saline and clay solutions (Figures 2a and b, respectively) and there was an increase in the ^{27}Al NMR signal representative of ettringite for these solutions (Figure 2c). The insert in Figure 2c shows an SEM image confirming the presence of ettringite needles. There was a reduction in the Ca/Si ratio of the C-S-H within NRVB in saline and clay groundwaters, as determined by ^{29}Si NMR analysis (Figure 2d), which suggests that C-S-H was decalcified. Since this was not observed in the granite groundwater where no additional ettringite was formed, this suggests that ettringite formation was facilitated by the interaction of sulphur in groundwater with Ca (and Al) in C-S-H.

1.1.1. Cebama Reference cement

Cebama reference cement samples were cured for only 28 days prior to contact with groundwater solutions. At this time, both alite and belite were still present in the cured cement, indicating that cement hydration was not yet complete (which is in contrast with the NRVB material). Figures 3a and b show the ^{29}Si NMR deconvolution for the 28 day cured material and the XRD pattern, confirming that the extent of hydration was low.

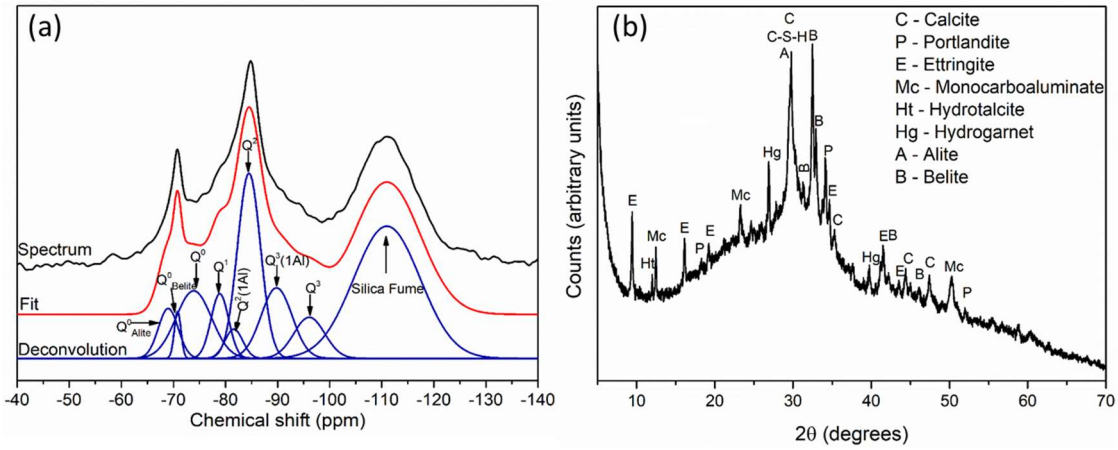

Figure 3: *Analysis of Cebama reference cement after 28 days of curing (no groundwater contact), by (a) ^{29}Si NMR; and (b) XRD.*

Consequently, when the samples were contacted with groundwater, the rate of hydration was faster than under the dry conditions experienced by the control samples. Figure 4a shows the ^{29}Si NMR data for the Cebama reference cement in contact with different groundwaters, compared with the dry-control sample; the peak assigned to the chemical shift of belite was significantly reduced in the samples contacted with groundwater highlighting the greater extent of hydration. In addition, the peaks relating to loosely bound water in analysis of TGA data (Figure 4b) were much greater in samples contacted with groundwater than in the dry-control sample.

There seem to be further differences between the Cebama cements in contact with granitic, saline and clay groundwater. Figure 5 shows EDX analysis of Cebama pellets contacted with each groundwater for 6 months; the left-hand side of the image is the centre of the pellet, and the right hand side is the outer surface in contact with solution. A layer of Ca was observed on the surfaces of cement pellets contacted with granite and saline waters, but not with clay, while Mg precipitation was observed on the outer surface of cement contacted with saline and clay groundwater solutions. Investigation of cements in contact with groundwater solutions for 12 months has been performed, including mineralogical analysis by: XRD; SEM-EDS; cross-sectional SEM-EDS across the diameter of the pellet; and NMR. Corresponding solution chemistry data have been measured, by ICP-OES, IC and pH. These data are currently undergoing analysis and un updated report can be issued in April / May if required.

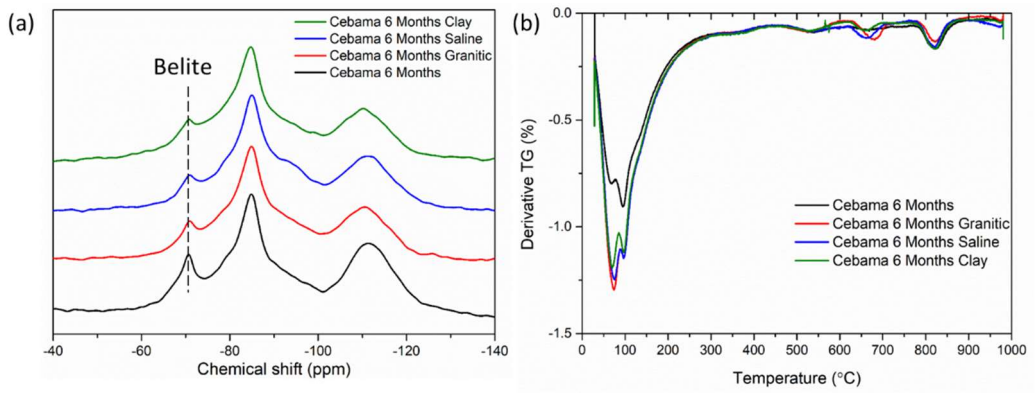

Figure 4: *Analysis of Cebama reference cement by (a) ^{29}Si NMR; and (b) TGA, after 6 months of contact with groundwater compared with dry-control.*

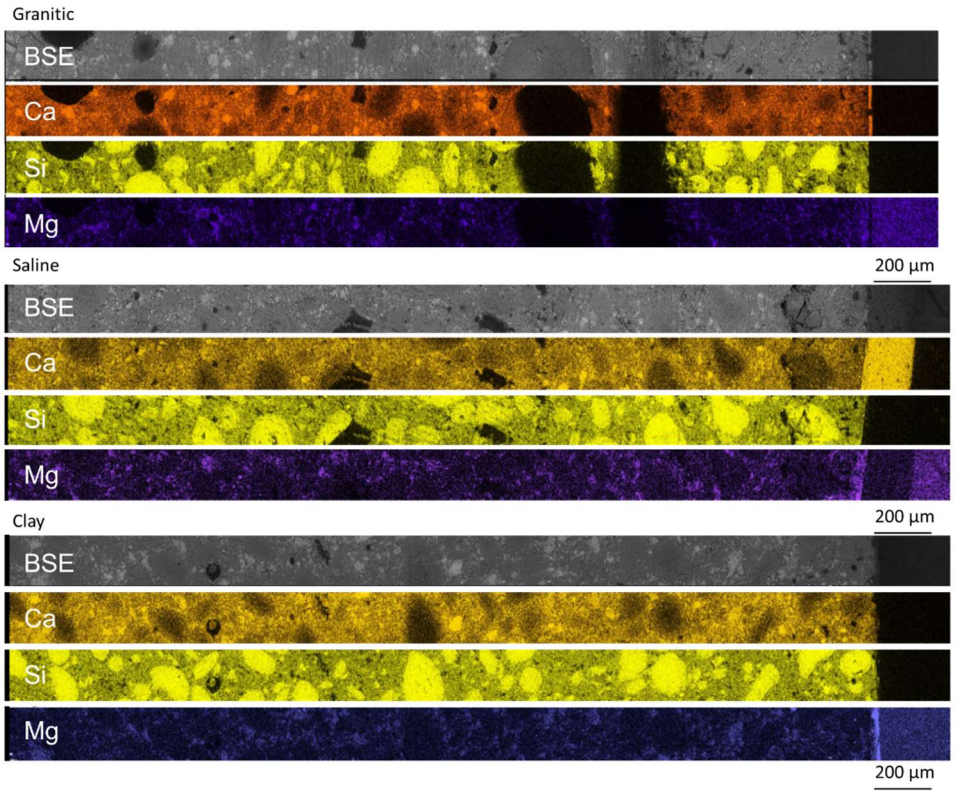

Figure 5: *EDX analysis of Cebama reference cement after 6 months of contact with three different types of groundwater (granitic, saline and clay). The left hand side of the images correspond to the centre of the pellet and the right hand side correspond to the surface in contact with solution.*

References

Gascoyne, M. (2002). Influence of grout and cement on groundwater composition. POSIVA, Working Report 2002-07, Posiva Oy.

Murray, C.A., Potter, J., Day, S.J., Baker, A.R., Thompson, S.P., Kelly, J., Morris, C.G., Yang, S., Tang, C.C. (2017). New synchrotron powder diffraction facility for long-duration experiments. Journal of Applied Crystallography, 50, 172 - 183.

Vasconcelos, R.G.W., Beaudoin, N., Hamilton, A., Hyatt, N.C., Provis, J.L., Corkhill, C.L. (2018). Characterisation of a high pH cement backfill for the geological disposal of nuclear waste: The Nirex Reference Vault Backfill. Applied Geochemistry, 89, 180 – 189.

Vinsot, A., Mettler, S., Wechner, S. (2008). In-situ characterization of the Callovo-Oxfordian pore water composition. Physics and Chemistry of the Earth, 33 (SUPPL. 1), Acknowledgement.

Technical Summary – VTT – WP1

1. Introduction & Objectives

The highest tolerable pH of the leachate is 10 or 11 in the bentonite system. Otherwise the long-term stability of the engineered barrier system is potentially endangered. Mix designs having a leachate lower pH than natural pH of 13-14 have been formulated (Cau Dit Coumes et al 2006; Holt et al. 2014; Vogt et al. 2009; Martino et al. 2011). The low-pH mix designs consist of low alkaline Portland cements mixed with large amounts of pozzolanic materials. Pozzolanic materials are known to react with the hydration products that control the pH of the cementitious materials pore solution. Low-pH materials are still highly basic but the pH value is significantly lower than in traditional Portland cements.

Second process that affects the pH of the cementitious materials in the repository is leaching. Portland cement -based materials will be in contact with the groundwater in the repository. Hardened Portland cement is a soluble material that equilibrates with the pore solution. Solubilities of the hardened Portland cement phases will determine the composition of the pore solution. As pore solution is constantly changing with the external solution, leaching causes degradation of the hardened Portland cement matrix.

The first phases that will dissolve are the alkalis that causes pH values above saturation pH of portlandite (pH > 12.4). Second step is the dissolution of the portlandite, followed by the incongruent dissolution of calcium-silicate-hydrates. When congruently dissolving calcium-silicate-hydrates are formed, the pH will remain constant as long as calcium-silicate-hydrates are present in the Portland cement matrix. High pH leachate region in the groundwater, caused by the degradation of cementitious materials is usually referred as alkaline plume. Figure 1 presents the schematic evolution of the pore solution pH during the leaching pure water of Portland cement paste.

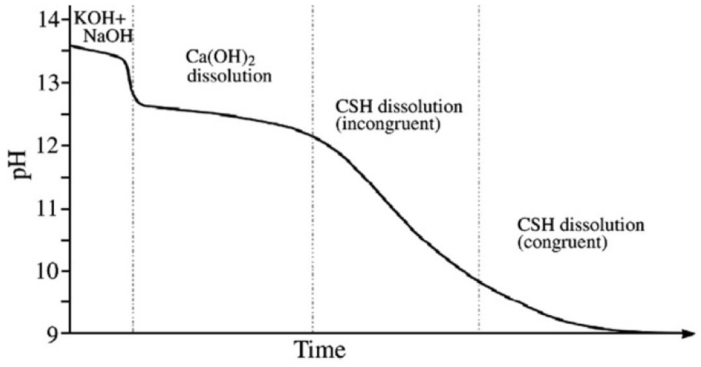

Figure 1: *Schematic evolution of pore solution pH during leaching of pure water of Portland cement (Berner, 1992; Snelman and Vieno, 2005; Cau Dit Coumes et al. 2006).*

The third factor that controls the pH of the alkaline plume is the groundwater composition. Leaching of cementitious materials in distilled water has significantly higher pH than in saline groundwater due the common

ion effects. Ions in groundwater will affect the composition of the alkaline plume and the composition of the hardened Portland cement phases. Groundwater composition might also induce a precipitation of secondary minerals, which is the fourth process that should considered.

As a summary, pH of the alkaline plume of cementitious materials is dependent of four processes:

1. Reaction of pozzolanic materials
2. Leaching of the cementitious materials
3. Common ion effect of groundwater leachate
4. Precipitation of secondary minerals

Above mentioned processes will affect simultaneously in the repository. pH development due to the dissolution of the crystalline phases of cementitious materials is not a major problem as the compositions are known. Largest uncertainties are related to the calcium-silicate-hydrate-phases (CSH, according to cement chemistry nomenclature, C = CaO, S = SiO_2, H = H_2O). Whatever the pH of the alkaline plume is affected by leaching, pozzolanic reaction or common ion effect, CSH phases are responsible of the pH values of alkaline plume in the long-term. The long-term pH values are vital for the integrity of the buffer and backfill materials and therefore the safety of the whole engineered barrier system. The exact nature of the CSH phases in hardened Ordinary Portland cement is not known and uncertainties related incongruent and congruent dissolution regions exists.

The goal of the project is to understand and predict the dissolution of Portland cement based materials in deep geological nuclear waste repository environment. On the basis of increased understanding, the potential effect of cementitious materials to clay-based materials of engineered barrier system is quantified.

2. Studied system

Leaching of cementitious materials with various C/S -ratios were studied in ion exchanged water, saline groundwater and saline bentonite porewater environment. These corresponds to different systems in crystalline bedrock. Fresh water corresponds the effect of freshwater intrusion to system. Saline groundwater corresponds the effect of expected groundwater on concrete structures. Bentonite groundwater corresponds the effect of direct contact of bentonite on concrete structures. In fresh water and saline groundwater cases, the bentonite concrete interaction is through the groundwater diffusion and flow.

Concrete systems studied started from “normal” high pH concrete with C/S-ratio 3.14 to“special” low-pH concrete with the C/S-ratio of 0.2. Both paste, mortar and concrete samples were used in our experimental work.

3. Main results – Scientific highlights

According to results, replacing OPC with pozzolanic materials effectively reduces the pH of the pore solution and leachates. The reduction is substantially higher than simple replacement would induce. In ion exchange water, pore solution pH values under 11 were observed with C/S -ratios below 0.4. In ion exchanged water, pore solution pH under 10 was not observed with any studied composition. Total leached hydroxyl contents were quite similar in stagnant and flowing ion exchanged water, although the pH values in the leachates varied greatly.

Groundwater compositions had significant effect on measured pH values. Generally, the pH values were smaller in groundwaters than in ion exchanged water. Only exception was observed in high C/S -ratio samples in early stages of leaching. Measured pH values were higher in saline bentonite porewater than in ion exchanged water. Phenomenon was observed in experimental samples and modelled samples. According to modelling, the

untypical behaviour originates sulphate content of saline bentonite porewater. Sulphates from the saline bentonite porewater and calcium from the OPC initiated precipitation of gypsum which increased the dissolution of OPC and therefore increased the measured pH values.

In the rest of the studied samples, measured pH values in saline groundwater and saline bentonite porewater were smaller than in ion exchanged water. In experimental samples the decrease in pH values, originated from common ion effect of calcium. Already existing calcium in groundwater reduced dissolution of the binder, causing smaller pH values. In modelled samples, the common ion effect was only observed in small leachate volumes. With larger leachate volumes, the pore solution volume become insignificant respect to leachate volumes and secondary precipitation of Brucite ($Mg(OH_2)$) was observed. Precipitation of brucite effectively reduced the pH, causing differences between measured and modelled samples. Secondary precipitation of Brucite depends on kinetics, which makes difficult to predict the exact behaviour in various scenarios. Large differences in total dissolved hydroxyl contents were not observed between saline groundwater and saline bentonite porewater.

In experimental measurements, salinity of studied groundwaters reduced amount of total dissolved hydroxyls above pH 11 and 10. In studied groundwaters, pore solution pH under 11 was observed with C/S -ratios ≤ 0.8. Pore solution pH under 10 was measured only in saline groundwater with C/S -ratio 0.2. The total release of hydroxyls above pH 11 and 10 were also greatly supressed. In saline groundwater, leaching of pure OPC -samples inflicted only 40% of total hydroxyls above pH 11 (and 10), compared to leaching ion exchanged water. In saline groundwater, binders with C/S -ratio ≤ 0.8 leaching of hydroxyls above pH 11 (and 10) were less than one percent compared to leaching of OPC in ion exchanged water. Example of amount of leached hydroxyls is presented in Figure 1.

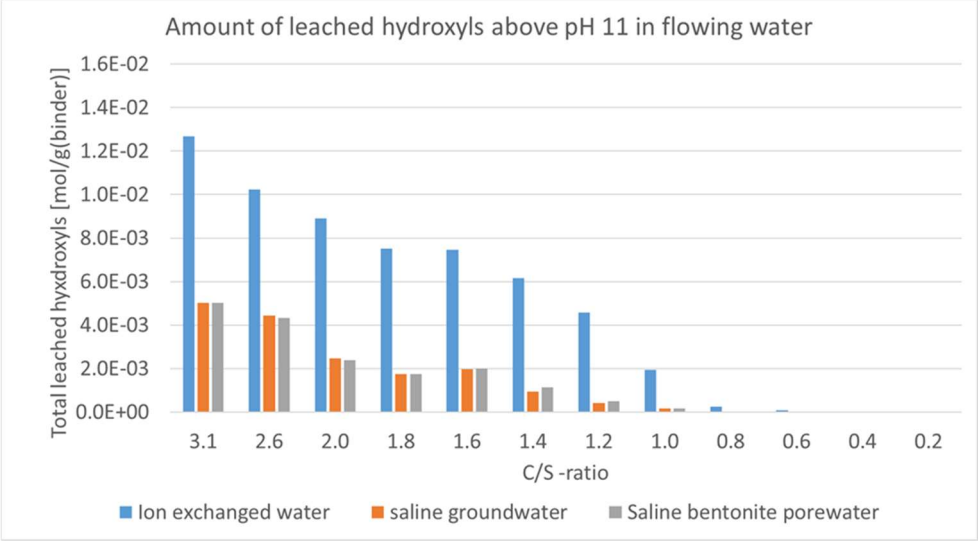

Figure 2: *The amount of dissolved hydroxyl-ions at pH above 11 in flowing water at various water compositions. (x-axis presents the CaO/SiO_2 –ratio in inverse order).*

Leaching was studied in pastes, mortars and concretes. Differences in leaching in different matrixes were not observed. Results obtained from pastes coalesced with mortar and concrete samples.

In laboratory environment, kinetics of the pozzolanic reaction was not a problem. Concrete mix designs with various fineness pozzolans had relatively equal pH development in laboratory conditions. The problems might be encountered in lower temperatures. According to kinetic -studies, activation energy of pozzolanic reaction was double (~ 80 kJ/mol), compared to activation energy of OPC (~ 40 kJ/mol). According to calculations, rate of the

OPC hydration is 1/3 compared to laboratory conditions in 2ºC temperature. Rate of the pozzolanic reaction is only 1/10 in similar scenario. The difference might be even higher if OPC samples are able to heat in the beginning.

Thermodynamically modelling done in WP3 was compared to experimental results. Largest differences between experimental and modelled results were related to precipitation of secondary phases in saline groundwater. In ion-exchanged water, thermodynamic modelling is reliable tool to evaluate the quantity of dissolved hydroxyls

In the studies thermodynamic modelling proved to be a powerful tool to study and understand various phenomena, but for quantity cementitious leachates in saline groundwater, the unreliability related to active phases and kinetics were significant.

The obtained results related to leaching to cementitious materials should be somehow convert to the effect on engineered barrier system. Because the goal is present that the cementitious leachates does not alter the properties of EBS, conservative assumptions are possible to perform.

References

Alonso, M.C., Walker, C., Petterson, S., Cuñado, M.A., Vuorio, M., Weber, H., Ueda, H. (2012). Development of an accurate pH measurement methodology for the pore fluids of low pH cementitious materials. SKB Report, R-12-02.

Berner, U.R. (1992). Evoliution of pore water chemistry during degradation of cement in a radioactive waste repository environment. Pergamon Press. Elsevier, 12, 201–219.

Cau Dit Coumes, C., Courtois, S., Nectoux, D., Leclercq, S., Bourbon, X. (2006). Formulating a low-alkalinity, high-resistance and low-heat concrete for radioactive waste repositories. Cement and Concret Research, 36 (12), 2152–2163.

Holt, E., Leivo, M., Vehmas, T. (2014). Low-pH concrete developed for tunnel end plugs used in nuclear waste containment. In Concrete Innovation Conference (CIC2014).

Martino, J., Dixon, D., Holowick, B., Kim, C.S. (2011). Enhanced sealing project (ESP) Seal Construction and Instrumentation report. Geological Society, Special publications, 400, 63-70.

Snelman, M. and Vieno, T. (2005). Long-term safety aspects of the use of cement in a repository for spent nuclear fuel. In: 2nd Low pH Workshop, 27–40.

Vogt, C., Lagerblad, B., Wallin, K., Baldy, F., Johansson, J.E. (2009). Low pH self compacting concrete for deposition tunnel plugs Stockholm. SKB Report, R-09-07.

Technical Summary – HZDR – WP1

1. Introduction & Objectives

The zone of the host-rock – cement interface is principally highly structured, firstly by the contact itself, but also, because the host-rock in this zone is disturbed by excavation damage, and because the cement is initially a heterogeneous mixture of different components. Therefore, transport and exchange processes are considered as heterogeneous processes with strong spatial variations. Such processes should be characterized with tomographic methods, rather than by conventional determination of physical properties and transport experiments. Input-output experiments, like common permeability measurements and through-diffusion experiments, yield limited information on transport processes along preferential structures, because each single measurement, as well as mean values over a large number of samples, miss the controlling effects of discrete pathways representing the weakest link of barrier integrity. Another frequent issue of such input-output experiment is the limited sample size and the need for intact samples. This could bias the results towards intact homogenous zones, and might miss the effects and properties of disturbed zones.

Microfocus-CT (μCT), which in the past was established as standard tomographic testing method in geosciences, is an excellent method for detection of structural inhomogeneities and for quantitative characterization of pore space geometry. μCT images are the basis for pore scale model simulations with various reactive transport modelling (RTM) codes. The results of these simulations can be cross-checked with input-output experiments. However, a direct alignment of pore-scale RTM with any tomographic experiments was not possible in the past.

This is why we developed the GeoPET-method. It applies positron emission tomography (PET) for extremely sensitive quantitative spatial detection of positron-emitting radiotracers and directly yields spatial concentration distributions during the course of a transport experiment. Initially, before CEBAMA, the method was developed as self-contained imaging modality. Technical issues had to be solved in order to derive quantitative four-dimensional (spatiotemporal) datasets that are applicable for intended alignment with RTM-results.

In contrast to the common method, where RTM is controlled by structural μCT images, the GeoPET-method enables a new approach, where RTM is based on spatially distributed transport parameters, i.e. distributions of the effective volume and flow velocities. This approach required the development of new segmentation methods for extracting these parameters from measured spatiotemporal concentration.

2. Studied system

The present study was at first conducted on samples with well characterized fractures and a salt rock – salt cement contact. The aim was to implement applicable methods and in particular to characterize the properties of the contact zone and to derive diffusion parameters of the materials. The procedure is applicable to clay systems that are in the focus of CEBAMA. Such experiments were prepared in collaboration with the CEBAMA partners, but had to be postponed due to instrumental defects.

3. Main results – Scientific highlights

The benefits of GeoPET as laboratory method for investigating processes at the cement-rock interface were demonstrated. Fluid distribution and diffusional transport at the interface could be parameterized. A new method for deriving the spatial distribution of effective volume and the flow velocity vector field from GeoPET-frames has been implemented. This enables to apply a new principle of core-scale reactive transport modelling with low computational demands and strong experimental bindings.

3.1. Tomography for understanding heterogeneous transport:

From earlier GeoPET-studies it was found that transport processes in barrier materials show a large variety of patterns, from slowly moving homogeneous "plug flow" to fast preferential progression along delimited zones, which could be caused by fractures or material inhomogeneities. One effect of heterogeneous transport is that it could even appear like a hopping process, when the concentration front moves very fast between apparently stable local reservoirs (Figure1).

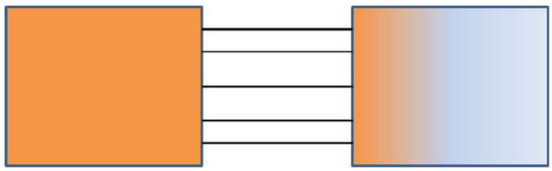

Figure 1: *Schematic of hopping transport: Apparent instantaneous traverse of small links between larger eservoirs.*

The larger reservoirs on both sides should depict larger voids, like air bubbles in the cement or mm-sized fractures in the EDZ. These could be interlinked by a network of narrow pores or micro fractures. The reservoirs can be clearly segmented with µCT, but are frequently below the spatial resolution of GeoPET. The small sizes of the structures of the interlinkage zone may underrun the µm-range, which is the resolution limit of µCT. Then,

the large voids appear unconnected in µCT-images, and transport models that are based on structures segmented from µCT will fail. On the other hand, although both reservoirs and links could be below the spatial resolution of GeoPET, which is 1 mm, the tracer concentration per unit volume will be generally correct, even when the tracer concentration is distributed over a large number of distinct pores within one voxel. Thus, the tracer propagation is also reproduced correctly. Even when the extreme high sensitivity of PET, which is in the order of pico-moles per voxel, is underrun in the interlinkage zone, the transport pathway can be reconstructed from the spatiotemporal correlation of the concentrations in the source and the sink reservoirs. Therefore, RTM simulations based upon GeoPET-images will correctly reflect the connectivity of the pores.

In the first step, the suite of GeoPET-images during transport processes yield the spatiotemporal distribution of tracer concentration. This can be directly compared to the results of pore-scale model simulations. Parameterization of sequences of GeoPET-images during flow experiments yields the distribution of the effective volume and the filtration rate with the resolution of voxel dimensions (millimetres).

Similar acceleration like in heterogeneous flow processes may be present in molecular diffusion in heterogeneous materials, because diffusion could also be confined to preferential zones. Such effects are not observable with common uni-directional through-diffusion experiments in diffusion cells. Presently, PET is the only non-destructive method that enables to visualize the propagation of diffusing species in opaque materials during the course of the process.

This application is under the constraints of a limited number of radiotracers with a suitable decay time and radiation characteristics. The most useful nuclides for diffusion measurements are probably ^{22}Na (decay time 2.602 y) and ^{56}Co or ^{58}Co, both with decay times around two months. In the past, we found indications for preferential diffusion pathways in Opalinus clay by faint deviations of the progress of the diffusion front from clearly homogenous-anisotropic behaviour, probably caused by fine layered more sandy zones. As an outcome of studies on Opalinus clay, anisotropic behaviour should be considered in model parameterization, whereas preferential diffusion pathways appear more like a second-order effect related to the observation scale.

3.2. Improvements of the GeoPET method

In the past, the method was mainly applied as static method for visualizing the tracer distribution at one particular time step, or integrated over a long period. This is adequate for long-term experiments, like diffusion experiments, but had to be modified for faster flow processes. Reconstruction of the velocity field requires a large number of regular time steps (frames), where the propagation distance during one frame length of the tracer front should not exceed the voxel dimensions. Therefore, the original tomographic reconstruction procedure was improved in order to process a large number of tomograms and to produce “3D-movies” of the tracer concentration.

3.3. 4D-movie segmentation

Segmentation is the procedure of feature extraction from grey level images, where different objects are separated by their grey level value. The procedure of feature extraction from spatiotemporal datasets (4D) of tracer transport, which we call in analogy to µCT “4D-segmentation”, is more involved. The target parameters are maximum filling grade with of each voxel during the passage of the tracer cloud, which yields effective porosity, and propagation velocity of the tracer front, which yields the flow density vector or velocity on voxel scale. These target parameters are therefore continuous (float) scalar and vector fields in 3D, in contrast to binary 3D-fields in µCT segmentation. The procedure has to consider a high noise level and hopping transport depicted in Figure 1.

We developed a robust algorithm (“GeoPETFlow”) for deriving these flow process parameters in each voxel from the suite of PET-frames. The effective volume is derived from the measured maximum activity concentration; the flow vector field is computed from its temporal variations and the relation to the nearest neighbours. Apparent spatially intermittent flow, which occurs when the tracer concentration underruns the detection threshold, is cured with a maximum-likelihood algorithm adopted from artificial intelligence. The algorithm was validated on simple synthetic samples and successfully tested on fractured (Figure 2) and intact natural rocks.

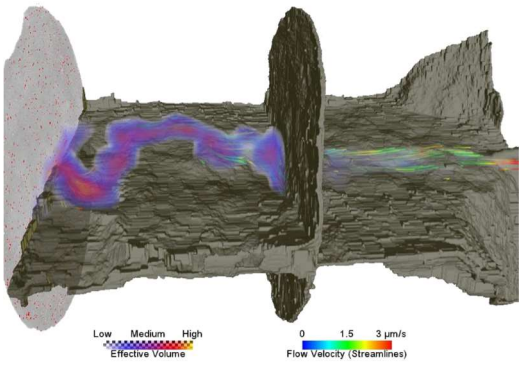

Figure 2: *Results from GeoPETFlow-4D-segmentation of an GeoPET experiment on a fractured sandstone: Effective volume (uncalibrated) as scalar field (cloud) and velocity vector field as streamlines, color-coded with the absolute velocity.*

3.4 A new principle of reactive transport modelling

These resulting data sets can be used as basis for a new principle of RTM computations with comparatively low computing expenses. Common practise is based upon high-resolution µCT-images of the pore space as structural model, typical resolution in the order of 10 µm. Reactive transport is then computed with a variety of codes on this fine-scaled grid. Instead, we start with the volume and velocity distribution resulting from the application of GeoPET-Flow on a suite of PET-frames of a conservative flow experiment and apply iCP (Comsol-PhreeqC-interface) for RTM on this rather course grid with the PET resolution of 1 mm. This strong reduction of computing demands is achieved at the price of uncertainties on the pore scale. For example, the composition and structure of the internal surface is not yet considered. However, the procedure can be further improved, and it is possible to include scalable parameters, like surface density, from co-registrated µCT-images.

The procedure is based on admittedly rather noisy and diffuse information – in contrast to clearly segmentable µCT images. This ambiguity of the PET data is mitigated by the robustness of the segmentation procedure. The focus on maximum resolution in µCT is an essential requirement of common practise in order to avoid the effects of an apparent percolation threshold (Figure 1). Our new procedure is a change of perspective towards highest sensitivity at moderate resolution. The benefits are obvious: The parameterization is based on real flow data, the computing demands are moderate, and the dimensions of the simulated systems are in the order of the representative volume (core scale), which is a significant step for upscaling RTM to the field scale. This opportunity is particularly important in strongly heterogeneous zones, like the cement-rock contact.

3.5. Example: Diffusion at the cement-rock interface

We demonstrate the capabilities of the GeoPET method with a measuring example from an experiment on a rock salt – salt concrete interface, which was conducted together with our partner GRS. The sample was prepared from a mature concrete core that was inserted into a matching salt rock core. The joint was flushed with concentrated salt brine until becoming impermeable by the salt precipitate. After release of the confining pressure, concentrated salt brine, labelled with ^{22}Na was given on the endplate of the sample.

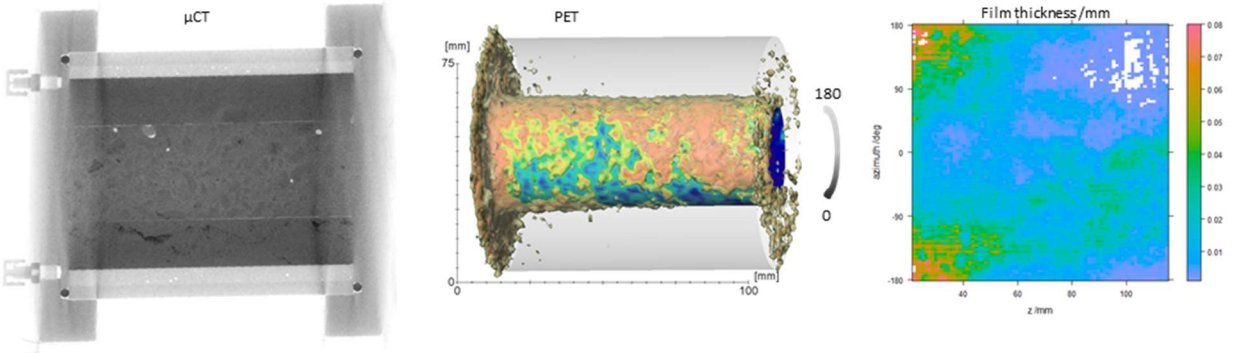

Figure 3: *µCT-image, initial PET-image (15 min after injection at the left endplate) and thickness map of the fluid film derived from PET activity.*

It is obvious from the PET-images (Figure 3) that, driven by capillarity, the brine immediately penetrated into the joint that reopened at pressure release. The fluid film thickness could be derived from the activity measured with PET, whereas the joint is discernible in the µCT-image, but below the µCT-resolution of 70 µm that is a function of the sample size.

The activity distribution was recorded with PET over a period of two years, showing the diffusion of $^{22}Na^{+}$ into the mass (Figure 4). In order to derive diffusion coefficients of the two materials, we simplified the irregularity of the diffusion pattern by radial and axial averaging, which yields the mean concentration as function of the radius. Principally, the solution of the diffusion equation in cylinder coordinates could be fitted to this data set. This solution is represented by a slowly converging infinite series of Bessel functions and therefore inapplicable for non-linear fitting methods. We therefore applied the COMSOL optimization module for parameter finding, yielding diffusion coefficients in the order of 10^{-13} m^2/s for both materials. This - probably first laboratory-derived - estimate of diffusion coefficients in these extremely tight materials has to be interpreted with regard to the experimental conditions: distributed, inhomogeneous source, annular averaging, disturbed material, a situation which is considered to be representative for EDZ-conditions.

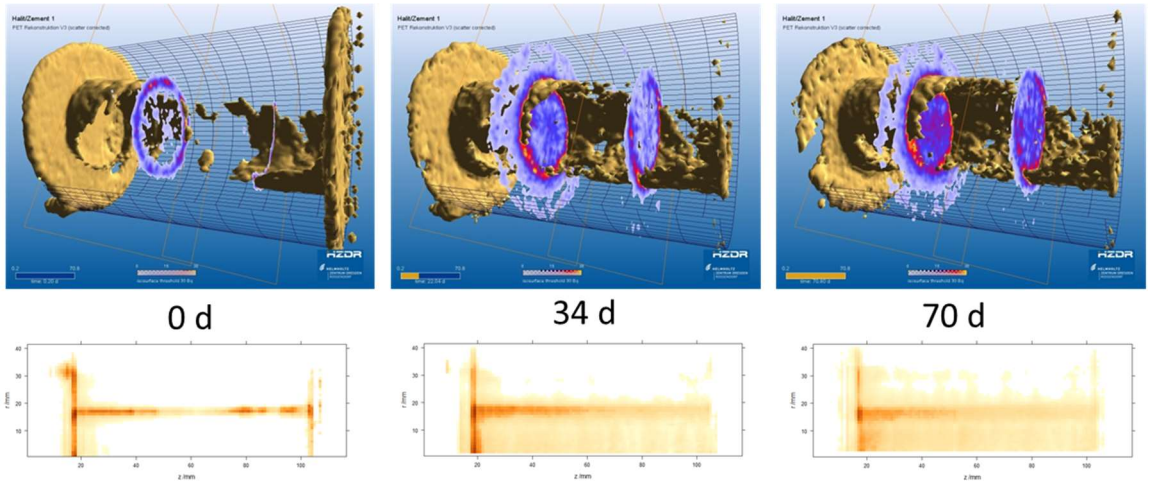

Figure 4: *GeoPET-images (initial, 34, 70 days after injection). Top: Isosurface and two cross sections; bottom: anular average values vs. length.*

Technical Summary – University of Lille – WP1 & WP3

1. Introduction & Objectives

The objective of our work is to investigate mechanical behaviour and permeability of interfaces between claystone and concrete. Very few experimental studies have so far been performed on this topic. In most previous studies, interfaces between clays and concrete have been studied. The morphology of such interfaces is very different with that of interfaces between clayey rocks (claystone) and concrete. In other studies, the claystone sample, for instance a semi-cylinder, is simply put together with the concrete sample, another semi-cylinder. These two samples are not bonded. This type of interfaces is clearly different with the real situation where concrete plugs are directly casted and cured on claystone surfaces.

In WP1, we shall develop a new experimental device to cast high performance concrete directly beside the semi-cylinder claystone sample. We obtain a bonded interface between claystone and concrete. Further an original testing device is designed to conduct direct shear tests and to measure permeability on bonded interfaces under different values of normal stress and pore pressure. A series of laboratory tests are performed under various loading conditions. The obtained results contribute to a deep knowledge of mechanical and hydromechanical properties of claystone-concrete interfaces.

Based on the tests performed in WP1, the objective of the study performed in WP3 is the formulation of a constitutive model in order to describe the hydromechanical properties of interfaces between claystone and concrete.

2. Studied system

The studied system is the interface between the Callovo-Oxfordian (COx) claystone and Low-pH high-performance concrete.

3. Main results – Scientific highlights

3.1. Main results obtained in WP1

Interface bonding feature

Each of the interface samples is composed of two semi-cylinders. One semi-cylinder is made up of the COx claystone and the other is made up of a low pH high performance concrete. The semi-cylinder COx claystone was previously prepared and placed into one side of a cylindrical stainless steel mold. The concrete is then casted into the other side of the cylindrical mold, next to the COx claystone. With the help of the casting procedure proposed in this study, we have obtained good quality cylindrical samples including planar interfaces between the claystone and the concrete, as shown in Figure 1. One can observe that the two materials have an apparent boundary at the interface but they are well bonded together at the interface after concrete hardening and curing.

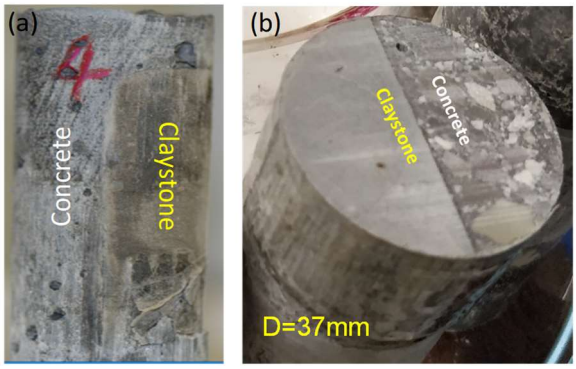

Figure 1: *Image of samples including well-bonded planar interface between COx claystone and concrete: (a) sample during concrete curing; (b) sample before test.*

A detailed characterization of the top surface of an interface sample is shown in Figure 2 with the help of Optical Microscopy. In Figure 2(a), there are clear boundaries at the interface of the sample. It seems that a boundary of a different colour from the two mother materials is formed as shown in Figure 2(b) and Figure 2(c). There is an alteration zone of about 60 µm in width, which bonds the two materials at the interface. In addition, there are no apparent fissures at the newly-formed buffer zone. However, some micro-cracks are observed in the claystone along the bedding planes and adjacent to the interface buffer zone.

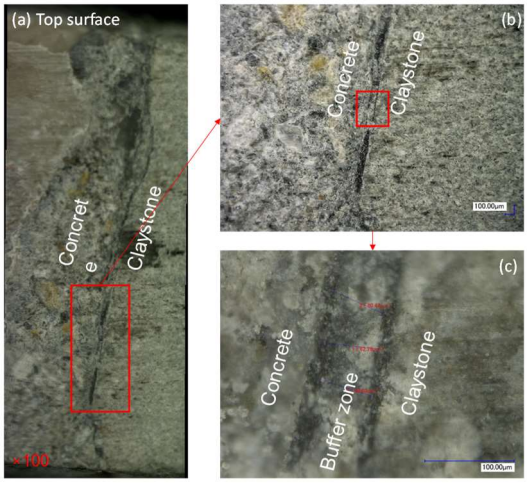

Figure 2: *Optical Microscopic characterization of samples including a well-bonded planar interface between COx claystone-concrete.*

Hydromechanical properties of interface

We have performed a series of triaxial direct shear tests under different values of confining pressure from 2 MPa to 12 MPa and different values of pore pressure from 1 MPa to 4 MPa. The specific values of confining stress and pore pressure are chosen such that their difference is the same between a pair of tests respectively with and without injection water pressure. The objective is to investigate the effect of pore pressure on the shear strength of interface and to check the validity of effective stress concept for interfaces.

The representative stress-strain curves obtained in the test with a confining pressure of 12 MPa, an injection water pressure of 4 MPa are shown in Figure 3. Positive stress denotes compression and negative strain means dilation. In Figure 3(a), there is a nonlinear relation between the shear strain and shear stress even during the first

stage of loading. However, the radial strain or the diameter change (ΔD) remains very small during the first stage of shearing. It means that the shear strain does not induce interface opening or closure when it is less than some critical threshold. After that threshold, we obtain an important negative radial strain. The shear strain induces a significant closure of interface, probably due to the degradation of asperities in the interface zone.

The image of the tested sample is presented in Figure 3(b). One can see that the two semi-cylinders are clearly slipped each to other but the two parts are still hold together due to the compressive normal strain (compaction) of the interface. The two surfaces of the tested sample are shown in Figure 3(c). We can clearly observe frictional traces of shearing at the surface. In addition, the claystone powders are found on the sheared surfaces of both semi-cylinders, due to the fact that the claystone is much weaker and more sheared than the concrete in the two-material system. Some claystone powders can be pushed into concrete pores, leading to a decrease of the permeability of the interface zone.

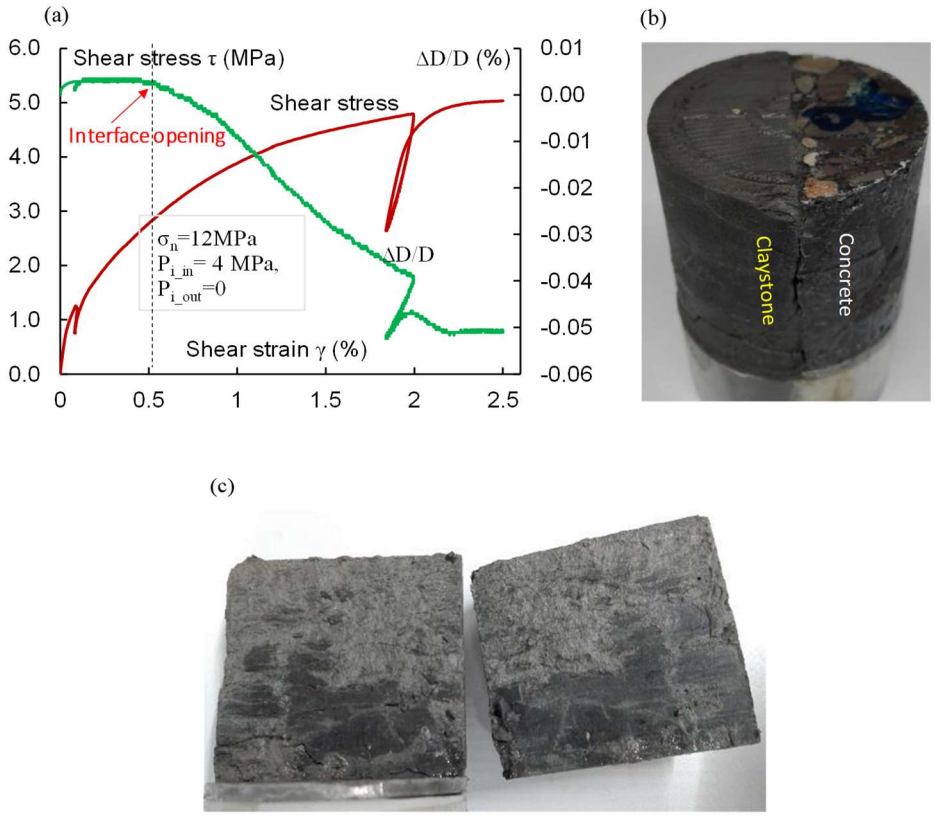

Figure 3: *(a) Mechanical responses of an interface sample during direct shear under confining pressure of 12 MPa with water injection pressure of 4 MPa; (b) Sample overview after test; (c) Sheared interface surface.*

The values of stress at the interface opening onset and of the peak shear stress obtained from the direct shear tests are presented in Figure 4. It is found that a linear Mohr-Coulomb type criterion can be adopted for the description of shear strength of interface, except the test performed without normal stress (simple shear test). For the case of saturated samples with water pressure, it is found that the shear strength of interface can be described by a generalized effective normal stress. The average effective stress coefficient for the studied interfaces is about 0.75. The classical Terzaghi's effective stress is not valid for these interfaces.

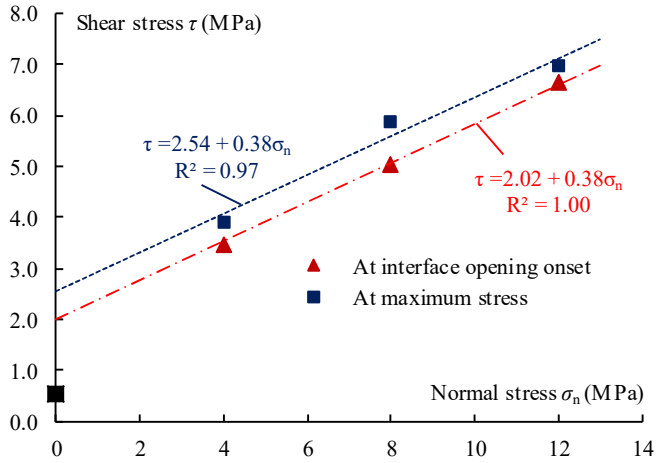

Figure 4: *Interface opening onset surface and peak strength surface of interface samples under direct shear tests.*

The water permeability of the interface samples is also estimated by injection of the synthetic water that has the same composition than that of in-situ ground water of the COx rock formation. Due to the ultra-low permeability of the interface sample, the saturation and permeability measurement lasts several months. It is found that the permeability of the interface sample is at the magnitude of 10^{-20} m^2. This value is similar to the instinct permeability of the COx claystone and of high performance the concrete. This means that the interface does not represent a weak zone of permeability. In addition, the interface permeability increases up to 50% when the normal stress is increased to 12 MPa.

3.2. Main results obtained in WP3

The objective of WP3 is to develop numerical modelling of hydromechanical behaviour of claystone-concrete interfaces. The modelling is therefore inherently related to the experimental study performed in WP1. We have proposed an elastic-plastic model which is able to reproduce both the shear strain and normal strain (dilation or compaction) of the studies interfaces. After calculating the opening or compaction of interface due to shear strain, the variation of permeability can be calculated by using the cubic law. Further, in order to evaluate the modification of mechanical properties of concrete due to chemical degradation, namely leaching and carbonation, we have also developed a micro-mechanics based elastic-plastic model by using nonlinear homogenization techniques. The proposed models have been assessed by comparing model's predictions with experimental data.

Technical Summary – ANDRA – WP1

1. Introduction & Objectives

Nuclear waste disposals will use a significant quantity of cement for the construction of access galleries, disposal cells, plugs and seals, and finally as containment material for some low and intermediate radioactive waste. The understanding of hydraulic, mechanic and chemical evolutions of this type of disposals requires input data on the materials used from their formulation to their long term physical and chemical behaviour.

Low hydration heat/low pH concrete have been designed over the past decade within the context of the nuclear waste disposals. Beyond the formulations, one of the main goals of the surveys was to understand the long term chemical interactions between these cementitious materials with their potential natural environement. Programs dedicated to cement/clay interactions have been conducted to give a quantification of the chemical evolutions at clay hot rocks/ low pH concrete interfaces.

In this context, physical evolutions of the concrete in a short time scale and their chemical/physical evolutions in atmospheric conditions were not a key issue. In parallel, hydration model was developped to understand the physical evolution of classical cements, from pure clinker to blended cement (i.e. CEM V according to european standards).

The present work has two main goals:

1. To assess the short timescale physical behaviour of the low hydration heat/low pH concrete formulations at a large scale to validate a physical model including the hydration of such blended cements;
2. To assess the physical consequences of the evolution at the interface with the host rock and the interface with the atmosphere in the underground facilities:
    a. To evaluate the impact of in-situ casting (contact with a clay host rock) on the hydration and the development of the physical properties;
    b. To quantify the impact of atmospheric carbonation on the concrete based on highly blended cements.

The specification to formulate those cementitious materials are in connection to the physical and chemical evolution of in-situ casted large concrete elements in contact with the clay host rock. Such concretes must have a low hydration heat to prevent temperature increase during setting and a “low pH” (pH of the hydrated cement pore water) to prevent significant chemical evolution of clay materials with time (the Callovo-Oxfordian claystone, as well as the swelling clay of the seal core).

2. Studied system

An in-situ test has been designed and realised in the French Underground Research Laboratory (URL) in Bure (Meuse/Haute-Marne, France), at 500 m depth in the Callovo-Oxfordian claystone layer. It has been designed to be representative of the operating conditions of a geological disposal facility and to assess the evolution of the concrete with two type of boundary conditions (i) the face in contact with ventilation air which evolve under atmospheric conditions and is submitted to drying and atmospheric carbonation; (ii) the concrete/clay interface where hydro-mechanical properties evolve mainly due to geochemical interaction between both materials.

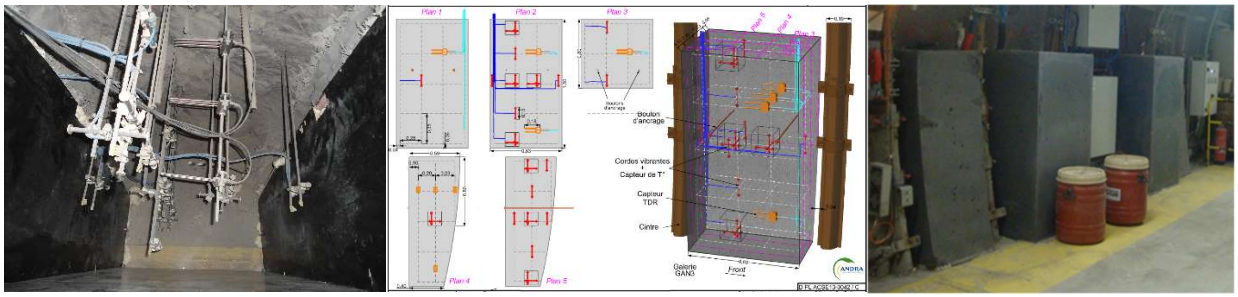

Figure 1: *Views of the in-situ test.*

The studied cementitious materials are “Low Hydration Heat/Low pH concretes”, specifically designed for plugs and seals. Two formulations were studied. Both recipes fulfil the requirements regarding the physical and the chemical expectations. Both are based on a ternary blend with Clinker, Silica Fume and Fly Ash or Blast Furnace Slag.

To follow the evolution of their physical properties with time, the concrete elements are monitored. Temperature and geometrical evolution were followed with time. To assess the chemical behaviour of such cementitious materials, samples have been taken to analyse both interfaces with the atmosphere and the geological medium.

3. Main results – Scientific highlights

Compositions of the two high performance concretes, respectively called T_{CV} and T_L are reported in Table 1. Four walls have been prepared with these two formulations and monitored as soon as they were casted.

Two days after casting the maximum temperature is reached. The Tmax. is close to 37°C at the central point of each element (maximum temperature increase ~ 17°C with a gradient close to 5 to 6 °C/m in the thickness and the height). This confirms the “low hydration heat” property of these concretes. From a kinetic point of view as well as a thermal point of view, these two materials have a similar behaviour. A week is necessary to cool down the concrete and to reach a temperature below 25°C.

Table 1: *Compositions of the ternary blends.*

	T_{CV}	T_L
CEM I 52.5 PM-ES (kg/m^3)	140.6	76
Silica Fume (kg/m^3)	121.9	123.5
Fly Ash (kg/m^3)	112.5	-

	T_{CV}	T_L
Blast Furnace Slag (kg/m^3)	-	180.5
Superplasticizer (Chryso – Optima 175) (kg/m^3)	5.63	5.70
Sand (0/2 mm – 0/4 mm) (kg/m^3)	248.6 – 581.3	253.8 – 593.5
Gravels (5/12 mm) (kg/m^3)	930.5	940.4
Total water (kg/m^3)	150	152
Compressive strength (90 days) (MPa)	71 ± 5	80 ± 2

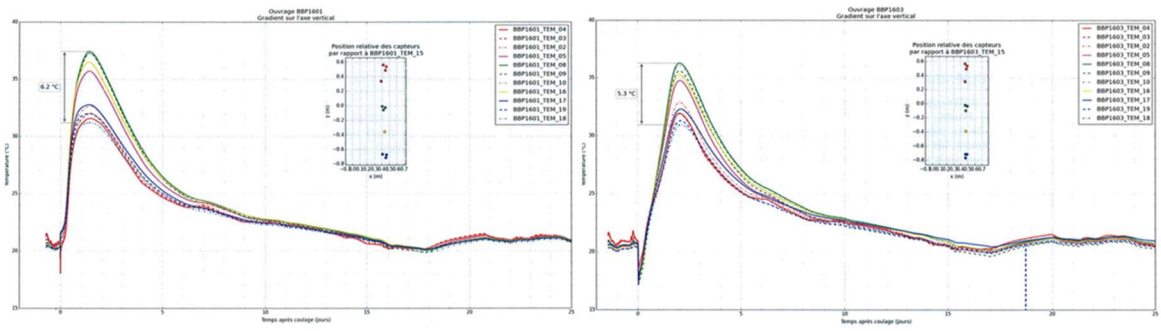

Figure 2: *temperature evolution of the thick walls T_{CV} (left) and T_L (right).*

Measured temperature are in accordance with lab'scale experiments on these two blended cements. There is a small impact on the temperature evolution at the surface considering the boundary conditions (the maximum temperature reached is not more than 10-12°C higher than the ambient temperature at the surface of the walls, compared to the ~ 17°C in the bulk).

The modelled temperature transient in relation to the hydration of the T_{CV} blended cements is correctely reproduced. Due to the very low kinetic of hydration of the slag, some discrepancies are still noticed (temperature maximum reached not as high as measured), leading to differences between measurements and simulations close to 20%. Adiabatic measurements on the slag alone could confirm the accuracy of the fitting.

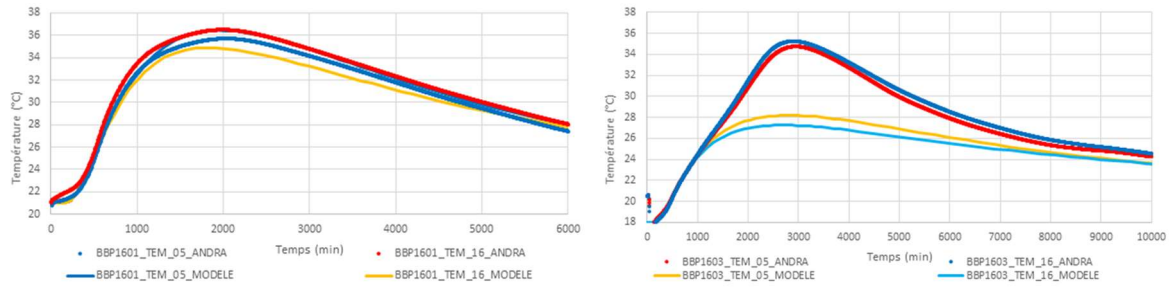

(a) *(b)*

Figure 5: *Kinetic of hydration of (a) "fly ash" ternary blend (T_{CV}) and (b) "slag" ternary blend (T_L).*

To assess the physical behaviour (shrinkage, creep) of the concrete a significant problem to fix is to calibrate and compensate the sensor to separate what is the consequence of the evolution of the boundary conditions (especially temperature variations due to the sensor position in the walls) from the concrete physical evolution. This has been done for the VWS (Vibrating Wire Sensors), assessing the reference VWS kept in adiabatic

conditions. From the raw data, the physical evolution of the concrete have been corrected from temperature variation in the underground facility to give an overview of the physical evolution.

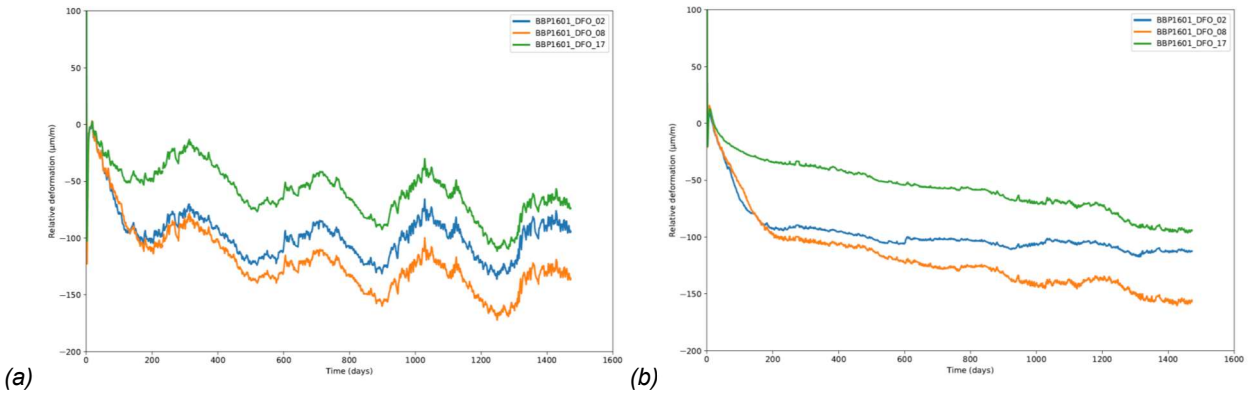

Figure 3: *T_{CV} physical evolution (a) raw data; (b) corrected data.*

The physical evolution of these "low hydration heat" materials highlight another property regarding the hydration. These materials exhibit a long hydration period (up to few years for a total hydration). After a one week thermal transient, few months are still necessary to switch from the hydration period to a "long term" period controlled by the boundary conditions. Such a period could be modelled.

Sensors close to adiabatic conditions, as far as possible from any surface, show physical evolutions in accordance to expected behaviours. On the opposite, some of the sensors too close to the surface give "unexpected" results, strongly influenced by the boundary conditions.

The deformation measured are mainly in relation to the hydric conditions variations and the water saturation of the concrete, controlled by the geological medium and the atmosphere in the gallery. After few years, the global deformations at large scale exhibit small values in a range of 100/150 µm/m. These values are in accordance with the specifications of these materials.

Endogenous shrinkage is in accordance to lab'scale experiments and optimizations realized on the formulation to reach an endogenous shrinkage far bellow 300 µm/m. Considering the main deformation curve in the core of the walls, endogenous shrinkage are close to 150 µm/m. No drying effect of the shrinkage are yet measured, even if the sensors are close to the surface of the walls. The physical behaviour could be then measured at that time scale on the basis of an endogenous behaviour.

Samples have been taken from the thin walls to perform chemical and physical analysis. Visual assessments of the concrete samples give no significant evolution/transformation of both concrete at the interface with the Callovo-Oxfordian argilite. No cracks at a large scale have been detected in both concretes. At the opposite, the clay host rock appears fractured and impossible to remove with the concrete as a single sample.

No particular adherence is noticed between the clay host rock and the cementitious material. The rear of the walls are in contact with the fractured zone surrounding the galleries. Eventhough, prior to casting, the main part of the immediate accessible disturbed host rock has been removed, it remains a significant mechanical disturbed zone which prevent from proper analysis of this zone.

The chemical analysis performed on these samples, give information about the lack of significant chemical of reactivity within the time scale covered, giving information about the very low reactivity of these materials in this context, especially in relation to the lack of availability of water.

Technical Summary – University of Bern – WP1

1. Introduction & Objectives

Cementitious materials used as support and waste matrix in designs of deep geologic repositories of radioactive waste will variably impact interfaces between components of the engineered barrier system and its interface to the confining claystone. Of concern are possible deleterious effects on clay stability, such as diminished retention properties, or enhanced (radionuclides) or diminished transport properties (water saturation of bentonite, gas escape).

A large number of detailed studies on interfaces of claystone (e.g. Opalinus Clay, Callovo-Oxfordian claystone) from laboratory experiments, in-situ tests in URLs and from natural and man-made analogues provided details mainly on mineralogical alteration in the cement matrix and the adjacent claystone. Studies including pore space characterisation are scarce and are limited by the small scale of a large porosity proportion (micro porosity) present in both materials. Direct evidence on the effect of aged interfaces on transport properties (hydraulic conductivity, effective diffusion coefficients) of solutes or water were virtually absent at the onset of CEBAMA.

The objective of our contribution is to perform reactive transport experiments across aged interfaces of ordinary Portland cement (concrete) and a low-alkali cement (mortar) with Opalinus Clay using a new core infiltration apparatus that is X-ray transparent and allows monitoring of long-term experiments over time by repeat CT imaging. Aged interfaces are available from an on-going field experiment carried out at the Mont Terri rock laboratory where sampling had been performed repeatedly. Part of the project includes the development of an X-ray transparent core infiltration device, its testing and implementation. In collaboration with HZDR, the same apparatus will also be used for positron emission tomography (PET) to image the mobile phase during an experiment.

2. Studied system

Two systems are studied, both samples in contact with Opalinus Clay in-situ at the Mont Terri rock laboratory for several years, before sampling, and sealed cold storage until preparation for our experiments.

a) ESDRED mortar, sampled after 3.2 years, and stored 3 more years. Mortar is CEM I 42.5 N Holcim 495 kg/m^3, SF 332 kg/m^3, qz-sand 0.1/0.3, SP and AC.

b) OPC concrete, sampled after 10 years, and stored 1.5 more years. Concrete is CEM I 42.5 R HS Holcim, Protego 4R, sand, gravel, no SP, no AC.

Although samples were well preserved, some partial drying could not be avoided during storage and subsequent sample preparation. After an initial saturation phase, the transport experiments pertain to system behaviour in a pore water saturated state. The fluid used is a synthetic pore water that is a close match of the in-situ pore water in Oaplinus Clay, containing ca. 10 g/L NaCl. Transport direction is from Opalinus Clay across the interface into the cementitious material.

3. Main results – Scientific highlights

3.1. Development of an X-ray transparent core infiltration apparatus

A second-generation of core infiltration equipment (Figure 1) was built and tested to fit into an industrial X-ray tomograph (Bruker SkyScan 2211 Multiscale Nanotomograph) with a high spatial resolution while maintaining a convenient sample diameter of 50 mm. The equipment was shortened compared to previous designs, and small pressure containers (confining pressure, infiltration pressure, sampling syringe) are integrated in a compact unit placed above the sample. A test with a partially saturated compacted sand/bentonite core (50 x 50 mm) showed that it is possible to image the entire sample at 25-35 µm voxel resolution, limited by how close the X-ray source can be moved to the sample (separated by the carbon fibre pressure vessel and confining water). Distinctly higher resolution is possible (at lower contrast) by imaging a sub-volume in focus mode with a different detector but without changing the sample/experiment position. The apparatus is designed to operate autonomously for an entire week, after which it is coupled to a base station with larger containers for maintaining pressures and infiltration, and connected to continuous data acquisition.

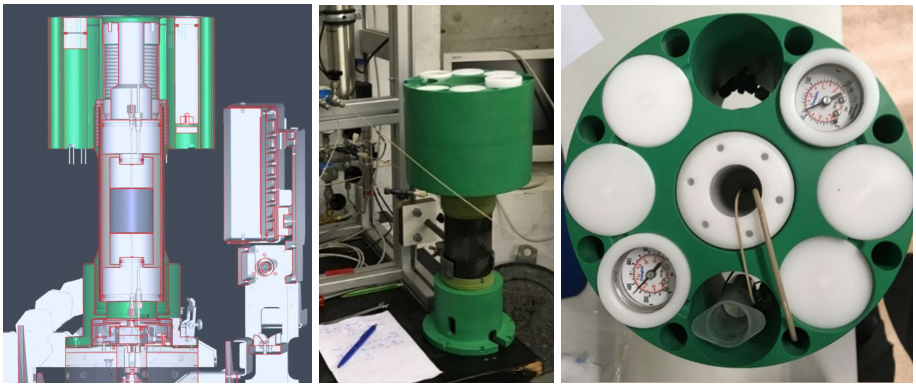

Figure 1: *Technical drawing and images of X-ray transparent core infiltration apparatus built in-house.*

3.2. Characterisation of interfaces between Opalinus Clay and cementitious materials

A 3.2-year-old interface sample of ESDRED mortar and Opalinus Clay was characterised by SEM-EDX element mapping methods (Figure 2a), and by conventional XRD powder diffraction (Figure 3a) on small samples abraded successively parallel to the interface. Micro-XRD mapping (Figure 2b) was performed at two synchrotron facilities (ESRF-SNBL, Swiss Light Source) using different beam sizes and somewhat different techniques, for both quantitative (Rietveld) and qualitative phase characterisation. X-ray CT (Bruker SkyScan 2211) was used for characterisation in 3D (Figure 3b), including the presence of joints in claystone, distribution of aggregate, and changes of X-ray absorbance across the interface region. This sample was used to prepare a core for a first infiltration experiment detailed below.

The overall chemical and mineralogical characteristics of the interface region are:

- Deterioration of cement paste for approximately 1 mm in width, as seen in Ca, Si and S maps, and likewise the distribution of AFm.
- Mg-enrichment at the interface, much better developed in mortar, and essentially absent in OPA except for a narrow band (0.1 - 0.2 mm).
- The mineralogical details are not yet fully characterized, specifically the identity of a possible Mg-rich phase has not been detected (such as for example Mg-Si-hydrate).

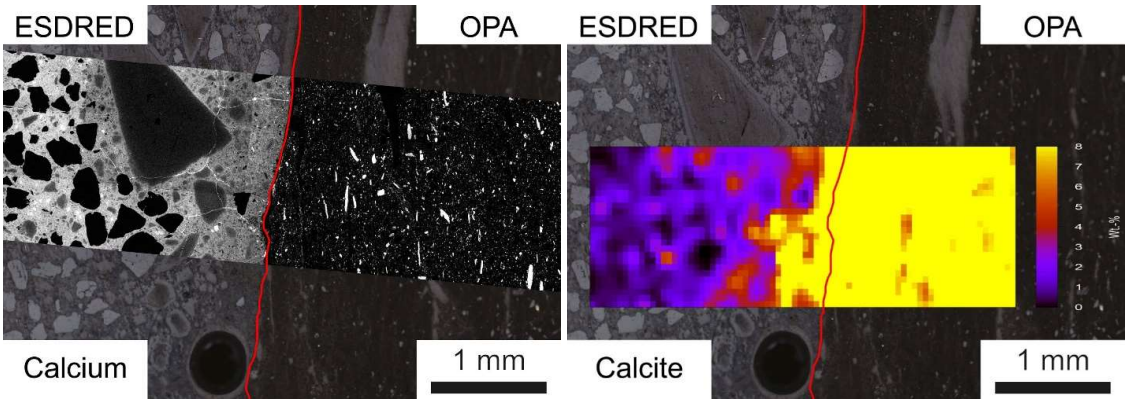

Figure 2: *Left (a), SEM-EDX element map for Ca overlain on back-scattered electron image; right (b), micro-XRD map for quantification of calcite across the interface indicating extent of carbonation in cement.*

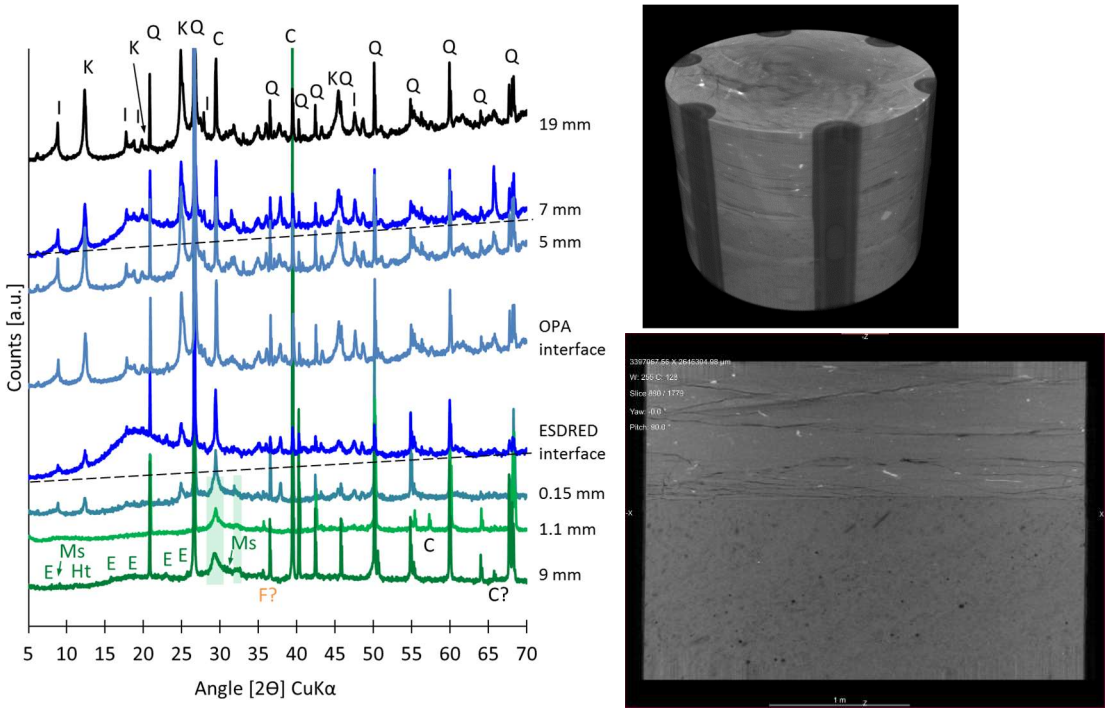

Figure 3: *Left (a), XRD powder patterns from samples abraded parallel to interface, from mortar (lower part) to Opalinus Clay (upper part); right (b) CT images of core sample used for the experiment (above) and section parallel to core axis with mortar (lower part) and jointed Opalinus Clay (upper part).*

The autoradiography results for this interface (Figure 4) were obtained in collaboration with the University of Helsinki using a ^{14}C-MMA (acrylic resin) impregnation technique followed by gamma-activated polymerisation, polishing, radiography and quantification. The claystone (upper part) has a homogenous porosity at this scale, with some joints at about 45° angle to the interface surface (opened during drying). There is some fracturing parallel to the interface reflecting a borehole-disturbed zone. The concrete part is more heterogeneous and there is a notable amount of gas voids in the matrix. There is significant porosity increase in the concrete phase adjacent to the interface area, followed by a denser zone.

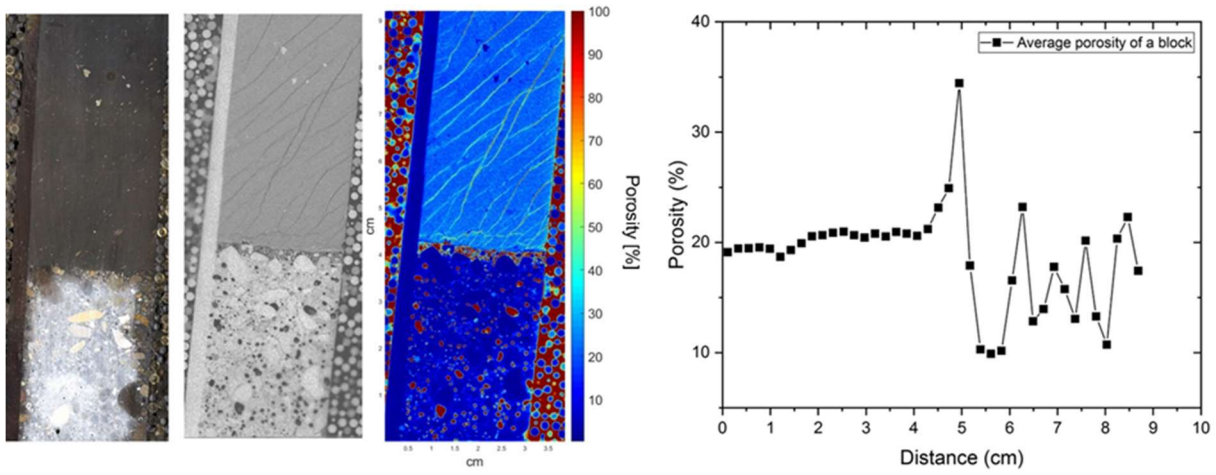

Figure 4: *From left: surface scan, autoradiograph, porosity map, and porosity profile from clay phase (left side) to concrete phase. The interface is located at 5 cm.*

2.3. Reactive transport experiment with "low-pH" mortar and Opalinus Clay

A conventional core infiltration apparatus was used for a first experiment with the ESDRED/Opalinus Clay interface characterized above (Figure 5). The focus was on the hydraulic behaviour to see if a skin effect (thin alteration zone with significantly reduced transmissivity) was present. The chemical-mineralogical characterisation (see above) was summarized and reported for a possible modelling exercise for WP3, amenable for reactive transport simulations covering the 3-4 year evolution of the interface.

The experiment was terminated and the data are presently being interpreted. The evaluation of a potential skin effect is done with Darcy's law formulated for a 3-layer medium (mortar-skin-claystone):

$$q = \frac{\Delta h}{\frac{l_{ESDRED}}{K_{ESDRED}} + \frac{l_{skin}}{K_{skin}} + \frac{l_{OPA}}{K_{OPA}}}$$

where q is the specific discharge ($m^3/m^2/s$), K_i the hydraulic conductivities (m/s), l_i the thicknesses of the layers, and Δh the average hydraulic head difference (m). Because mortar is more transmissive than Opalinus Clay, an effective skin would have to have a much reduced K-value compared to Opalinus Clay. Preliminary data suggest that a skin with a significantly reduced hydraulic conductivity is indicated.

Figure 5: *Sample preparation for core infiltration experiment, from left: layout before drilling and stabilisation, drilled core with 50 mm DM, schematic of core cut to length and placed between filters and adapters to be inserted into a pressure vessel.*

2.4. Reactive transport experiment with OPC concrete and Opalinus Clay

A reactive transport experiment using our newly developed X-ray transparent apparatus (see above) was started in January 2019. The sample is from a 10-year-old interface of OPC concrete and Opalinus Clay, for which also chemical-mineralogical characterisation of the interface is available. The sample core was prepared in similar fashion as shown above, and placed into the apparatus. This experiment can operate autonomously for at least a week maintaining confining pressure, infiltration pressure and sampling in a syringe. The entire apparatus was mounted in an X-ray tomograph (Bruker SkyScan 2211) in Fribourg, CT images recorded, and then the infiltration started. Repeat CT scans were performed over the next 5 days to observe the saturation phase and breakthrough of the synthetic pore water (from Opalinus Clay into concrete). The experiment will continue over the next months, with CT scans performed every 2-4 weeks.

The same experiment is scheduled to be used at the positron emission tomographic facility at HZDR with an anionic active tracer in order to directly observe the migration of the mobile phase across the materials and interface. Details of method and setup are covered in the HZDR project, also part of WP1.

First results from the analysis and processing of CT data document to efficient closure of joints in the Opalinus Clay over few days (a self-sealing effect), the accumulation of pore fluid in the gas pores of the concrete, and possibly also the re-saturation of claystone and cement matrix (work in progress). The final outcome is a comprehensive description of the hydraulic behaviour of this system and its link to the chemical-mineralogical features at the interface region.

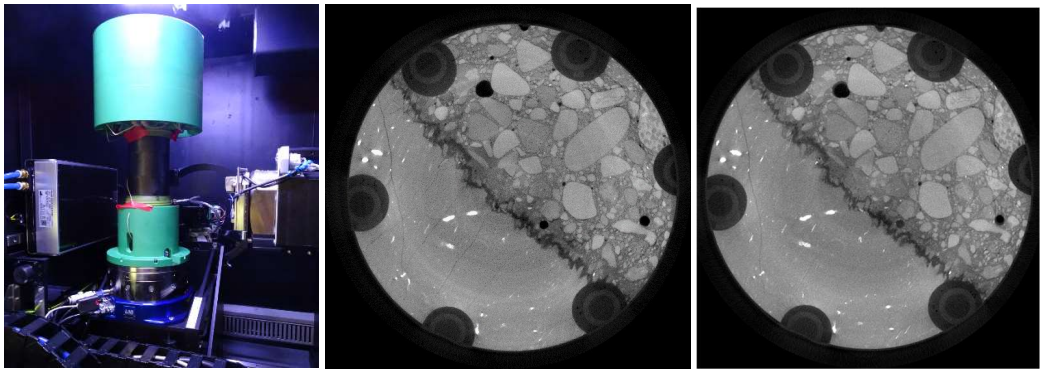

Figure 5: *Experiment in Bruker SkyScan 2211 (left); CT sections across interface with joints seen in Opalinus Clay before fluid infiltration (middle, lower left) that mostly closed within 1-5 days (right).*

Technical Summary – IRSN – WP1

1. Introduction & Objectives

In France, the decision has been taken to design a radioactive waste disposal facility in a natural clayey environment with favourable radionuclide containment properties. However, for stability reasons during the excavation work and for facilitating the installation of radwastes, galleries excavated in clayey rocks must generally be mechanically supported by concrete components. The contact between the clayey rock and the concrete inevitably leads to an alkaline plume spreading from the concrete toward the host rock, while a multi ionic attack occurs from the clayey pore water against the cementitious material side.

Several types of cementitious binders are selected as references today for the design of deep disposal facilities: an ordinary Portland cement and two low-pH binders. The low-pH binders were formulated to induce a less aggressive alkaline plume mainly due to a lower pore water pH. Over the last decades, interest has grown about the geochemical behaviour of cementitious materials in a clayey environment. Studies have focused mainly on the physico-chemical evolution of clay under alkaline conditions and not on the material interface. Only a handful of studies have discussed the interactions at the interface between cement binder and claystone. Such interfaces have been created at ambient temperature by pouring cement mixes into boreholes (Gaboreau et al. 2011; Bartieret al. 2013; Jenni et al. 2014; Dauzeres et al. 2016) or by putting disks of material into contact in transport cells (Dauzeres et al. 2010). In the current design of the French radioactive waste deep disposal facility (ANDRA, 2005), the thermal transient, due to the presence of heat-emitting waste, is expected to entail a temperature increase of up to 70°C in the concrete plugs located in the high-level waste cells and potentially also in the intermediate long-lived waste cells. Based on the existing literature, only a few laboratory studies have focused on the impact of such a temperature level on the evolution of the interface between natural rock and anthropic material, and even fewer in-situ studies have been carried out.

The CEMTEX experiment (CEMent Temperature EXperiment) (Lalan et al. 2014; 2016) aims to fill the lack of knowledge about the geochemical and micro-structural evolutions of these interfaces under representative thermo-hydraulic conditions (i.e. 70°C and full water saturation), which should provide input for future studies on the durability of cementitious materials. Within this framework, six in-situ experiments (three with CEM I and three with a low-pH cement) have been set up in IRSN's Underground Research Laboratory in Tournemire (France) in 2012, before the starting of the CEBAMA project and three other with a second low-pH cement paste were started inside the CEBAMA project in 2016. In paralell, laboratory experiments were started to test the interaction between CEM I and clayey rock in well controlled conditions.

This paper presents quickly the main scientific highlights of the CEMTEX experiments which fill the CEBAMA project.

2. Studied system

2.1. In-situ experimental device

Nine downward vertical boreholes of 1 m depth and 25 cm of diameter were drilled into the argillite in the Tournemire URL (6 in 2012 and 3 in 2016). This depth was chosen to ensure that the devices were located out of the excavation disturbed zone (EDZ) created while the gallery was dug. The bottom of each borehole was polished, the dust cleaned and the rock resaturated to obtain an as perfect as possible contact surface between the rock and the cementitious material To force a one-dimensional mass transport (vertical) across the interface and to protect the borehole sides from hyperalkaline solution, a PVC tube was placed within the borehole with a rubber seal at its bottom. At the same time, four temperature sensors (PT 100) were installed to monitor the temperature during the experiment. Once all these steps had been achieved, the cement paste was poured onto the heater device and the temperature sensors to fill the full inner PVC volume constituting a 30 cm height cement paste plug. One month after the beginning of the cement hydration, heating was started while the device was being maintained under the equilibrium solution at the good pH value with the considered cementitious material in order to ensure water saturation throughout the test.

2.2. Materials

Three types of cementitious binders were placed in the experiments, an Ordinary Portland Cement (OPC) and two low-pH binder (T1 and T3). The OPC formulation was Sulphate Resisting Portland Cement (OPC-SRPC) from Val d'Azergues (Lalan et al. 2016; Dauzères et al. 2017). The first low-pH binder (T1) was made with 37 wt.% of CEM I Le Teil, 32.5 wt.% of silica fume and 30 wt.% of fly ashes (Codina et al., 2008). The second low-pH binder (T3) was a mix of CEM IIIA Rombas at 20 wt.%, silica fume at 20 wt.% and 60 wt.% of calcareous filler (Poyet et al. 2014). The water on binder ratio for the OPC, T1 and T3 was respectively equal to 0.42, 0.4 and 0.6.

2.3.Laboratory experimental device

The laboratory tests were perform with diffusion cells constitutes with the cement and argillite disks in contact with reservoirs filled with alkaline water and argillite pore water respectively. Three diffusion cells were prepared simultaneously with the same cement mix (OPC formulation) and stored at 70°C and 80% of relative humidity in a climatic chamber. The solution was sampled periodically while 76 (cell C), 202 (cell D) and 415 (cell T) days.

3. Main results – Scientific highlights

3.1. In-situ OPC/Argilite interface

The first step of the CEMTEX project concerned the characterization of in-situ CEM I cement paste/clayey rock interface after 1, 2 and 5 year of interaction. The important results in terms of exchange of soluble species, mineralogy changes causing microstructure modifications are summarized in the Figure 1.

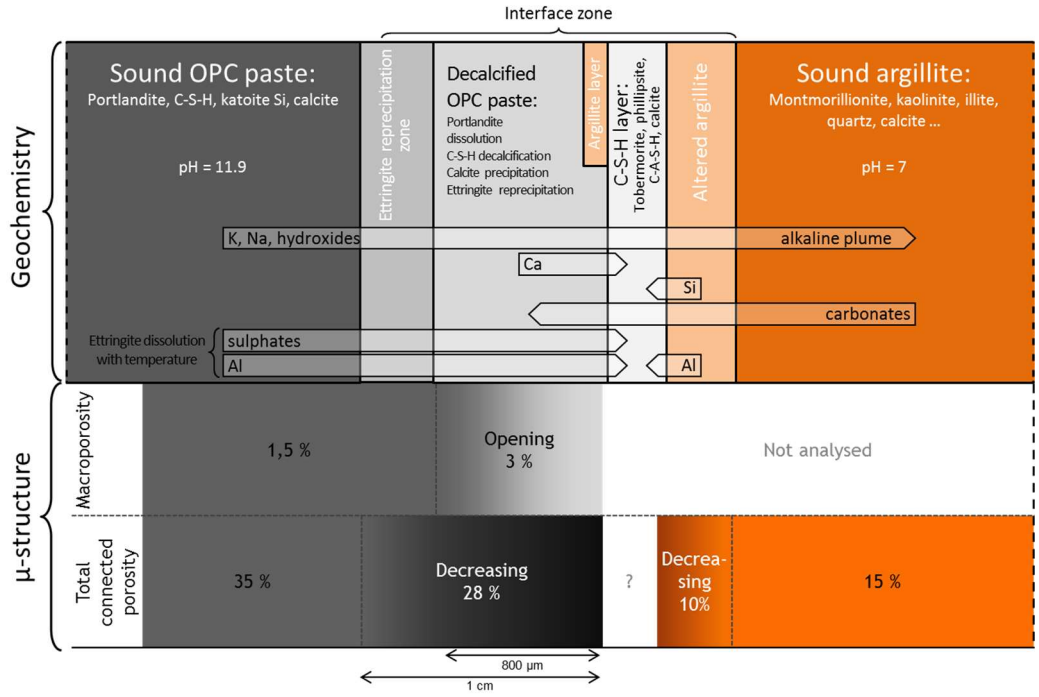

Figure 1: *Summary diagram of the main mechanisms observed at the CEM I cement paste/clayey rock interface at 70°C.*

The important result in term of reactive mechanism is the systematic precipitation of zeolite at 70°C after 1, 2 and 5 years of interaction. This kind of precipitation was never observed in the previous study putting in contact CEM I cementitious material and clayey rock in representative conditions of geological disposal. The second important result is the very low degradation of the CEM I material. The temperature seems favoured the carbonation causing a small decreasing of the total porosity contrary to the results in previous study at 20°C (Dauzeres et al. 2010; Gaboreau et al. 2011).

3.2.Laboratory OPC/Argilite interface

In paralell to in-situ tests, laboratory experiments were started to study the interaction between CEM I and clayey rock in well controlled conditions. The scientist highlights of these tests are related to the kinetics of the differents phenomenon observed in-situ. The carbonation, for instance, was clearly observed in-situ at the interface CEM I/ Argillite. Absent at 76 days, carbonation of the cement paste by calcite precipitation occurred on 150 µm after 202 days and on the same distance at 415 days. The decreasing of the total porosity of the cement matrix related to the precipitation of calcite was also observed in diffusion cells after 202 days (Figure 2).

At 415 days, a layer of C-(A)-S-H, tobermorite and calcite is also clearly visible at the interface. The same kind of homogeneous layer was observed at the interface between clays and CEM I cement pastes after 1, 2 and 5 years in the in-situ experiments. The unique difference is the presence of Phillipsite crystals in addition to the the tobermorite in this layer. Kinetics reasons may explain this difference.

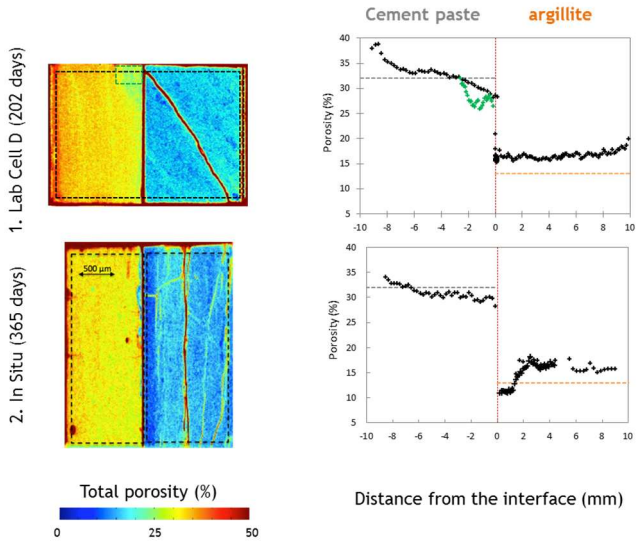

Figure 2: *Total porosity profile measured by autoradiography on doped sample with ^{14}C-PMMA of CEM I / clayey rock interface after 1) 202 days in a diffusion cell and 2) 1 year of interaction in-situ.*

3.3.In-situ T1/Argilite interface

The second step of the CEMTEX project was dedicated to the characterization of in-situ Low-pH cement paste/clayey rock interface after 1, 2 and 5 year of interaction. Only the first Low-pH formulation (T1) was characterised, the analyze of second one (T3) is still in progress. The important results in terms of exchange of soluble species, mineralogy changes causing microstructure modifications are summarized in the Figure 3.

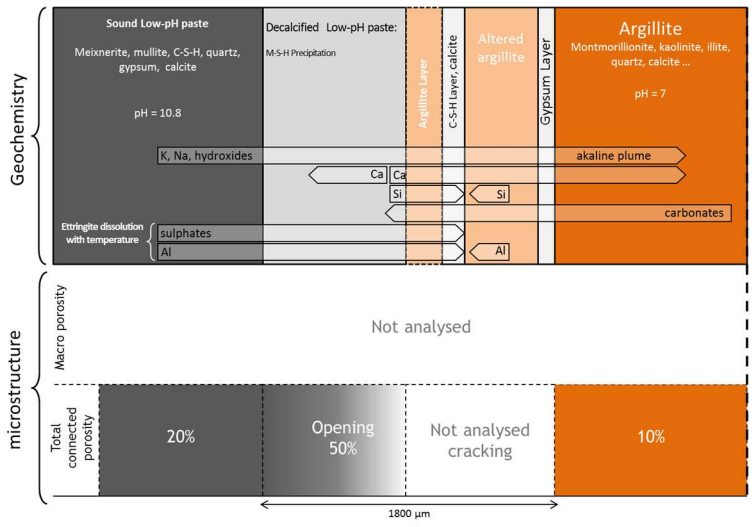

Figure 3: *Summary diagram of the main mechanisms observed at the Low-pH cement paste (T1) /clayey rock interface at 70°C.*

As already observed at 20°C and 50°C (Dauzeres et al. 2010; 2016), the absence of Portlandite in this kind of cement matrix leads to a decalcification of C-S-H close to the interface. This phenomenon is associated in the decalcified zone to the precipitation of M-S-H. This mechanism grew during the first year then stayed constant. No Brucite was observed.

It is interesting to note that the magnesium concentration in the argillite of Tournemire is weak so this enrichment indicates a degradation of the argillite, maybe due to the dissolution of smectite phases. Indeed, an altered zone with cracking and microstructure modifications was remarked in the material close to the cement matrix. As on CEM I cement paste/clayey rock interface, a layer of C-S-H/calcite was observed in the altered zone may be due to the diffusion of the calcium present in the cement matrix. However, a gypsum layer was also noticed few micrometers deeper in the argillite. The sources of these two layers may be come from the cement matrix with the decalcification process and the ettringite dissolution.

Concerning the total connected porosity, autoradiography analysis illustrated the opening in cement matrix due to decalcification process. After a year of interaction, the porosity in the decalcified zone increased from 15 to 50%.

Low-pH binder was initially designed to reduce the impact of cement matrix on the argillite. However, at 70°C, results from the CEMTEX project highlight an argillite degradation (clay-phase dissolution) not clearly observable with the CEMI, certainly linked to the chemical transitory during the cement paste hydration. In addition, the cement alteration is clearly more important for the low-pH material (decalcification, M-S-H precipitation causing porosity opening) compare to the CEM I formulation.

References

ANDRA (2005). Evaluation de la faisabilité du stockage radioactif en formation argileuse. Site de Meuse/Haute-Marne.

Bartier, D., Techer, I., Dauzères, A., Boulvais, P., Blanc-Valleron, M.M., Cabrera, J. (2013). In-situ investigations and reactive transport modelling of cement paste/argillite interactions in a saturated context and outside an excavated disturbed zone. Applied Geochemistry, 31, 94–108.

Codina, M., Cau-dit-Coumes, C., Le Bescop, P., Verdier, J., Ollivier, J.P. (2008). Design and characterization of low-heat and low-alkalinity cements. Cement and Concrete Research, 38, 437–448.

Dauzeres, A., Achiedo, G., Nied, D., Bernard, E., Alahrache, S., Lothenbach, B. (2016). Magnesium perturbation in low-pH concretes placed in clayey environment—solid characterizations and modeling. Cement and Concrete Research, 79, 137 150.

Dauzères, A., De Windt, L., Detilleux, V. (2017). Geochemical evolution of cementitious materials in contact with a clayey rock at 70 C in the Tournemire underground research laboratory.

Dauzeres, A., Le Bescop, P., Sardini, P., Cau Dit Coumes, C., (2010). Physico-chemical investigation of clayey/cement-based materials interaction in the context of geological waste disposal: Experimental approach and results. Cement and Concrete Research, 40, 1327–1340.

Gaboreau, S., Prêt, D., Tinseau, E., Claret, F., Pellegrini, D., Stammose, D., (2011). 15 years of in-situ cement–argillite interaction from Tournemire URL: Characterisation of the multi-scale spatial heterogeneities of pore space evolution. Applied Geochemistry, 26, 2159–2171.

Jenni, A., Mäder, U., Lerouge, C., Gaboreau, S., Schwyn, B. (2014). In-situ interaction between different concretes and Opalinus Clay. Physics and. Chemistry of the Earth, Parts A/B/C 70–71, 71–83.

Lalan, P., Dauzeres, A., Barker, E., De Windt, L., Detilleux, V., Desveaux, P. (2014). Evolution of the argillite / CEM I interface at 70ºC.: in-situ tests and modelling results.

Lalan, P., Dauzères, A., De Windt, L., Bartier, D., Sammaljärvi, J., Barnichon, J.D., Techer, I., Detilleux, V. (2016). Impact of a 70°C temperature on an ordinary Portland cement paste/claystone interface: An in-situ experiment. Cement and Concrete Research, 83, 164–178.

Poyet, S., Le Bescop, P., Touze, G., Moth, J. (2014). Formulating a low-alkalinity and self-consolidating concrete for the DOPASS-FSS experimente. In: NUWCEM. Avignon.

Technical Summary – University of Surrey – WP1

1. Introduction & Objectives

Disposal of low and intermediate level radioactive waste in the UK will involve a geological disposal facility (GDF) where cementitious materials will be used for structural purposes, as waste grout and as backfill material. Cement is intended to provide a high pH environment, which may reduce the solubility and hence migration of certain radionuclides (Young et al. 2013; Felipe-Sotelo et al. 2016a, b; Felipe-Sotelo et al. 2017). Upon closure of the repository, influx of groundwater will alter the cement and could potentially compromise radionuclide containment. The state of the art at the start of this project typically involved the study of individual aqueous ions and their impact on cement mineralogy, often at concentrations that were not representative of those anticipated under in-situ repository conditions (e.g. Thomas et al. 2012). There was clear evidence that chloride and sulphate alter cements over time, affecting the material's physical and chemical properties (Whittaker et al. 2016; Ipavec et al. 2013). Cement – water interactions had also been studied using batch experiments on disaggregated material where the solution was in substantial excess (e.g. Ipavec et al. 2013). This experimental set-up places emphasis on alteration of cement surfaces but is not realistic due to the high surface area being exposed, surface effects with crushed minerals and the large excess of solution in contact with the cement. Recent diffusion experiments completed on intact monoliths (e.g. Felipe-Sotelo et al. 2017) used more realistic solid to solution ratios and highlighted the importance of the evolving cement mineralogy in addition to surface adsorption for radionuclide retention. The aim of work within WP1 is to understand the chemical and mineralogical changes that occur at the interface between different cementitious materials and a wider range of groundwater compositions. The objective is to identify how the groundwater ions interact with the hydrated phases of cement and the effect of this interaction on physical and chemical properties, such as the formation, dissolution and/or modification of cement mineral phases, changes in porosity and permeability. The experimental protocols used assess the effect of solid to liquid (S/L) ratio to aid current understanding of results generated from disaggregated and monolithic materials, respectively.

2. Studied system

The University of Surrey has worked on a range of cements and groundwaters, chosen to cover the compositions being considered within different European repository concepts. The cementitious materials studied were a Portland cement (CEM I), a ground granulated blast furnace slag: ordinary Portland cement blend (GGBS:OPC), Nirex Reference Vault Backfill (NRVB) and a CEBAMA reference blend, chosen to allow cross-comparison between the different research groups working on the project. The synthetic groundwaters were selected to emulate granitic, clay and saline host rock environments. Two experimental protocols were employed to evaluate the effects of solid to liquid ratio. In one, a large excess of groundwater was present relative to the cement to ensure ample opportunity for diffusion of groundwater components into hardened cement paste blocks. In the second, equal volumes of cement and groundwater were employed, through which changes in groundwater composition should be more evident. Finally, advective tests are being performed to simulate groundwater recharge during repository re-saturation.

3. Main results – Scientific highlights

3.1. Groundwater excess experiments

Diffusion experiments comprised the submersion of multiple, small-scale hardened cement paste monoliths, made from the four cement blends described previously, into the different synthetic groundwaters (granitic, clay or saline) at a S/L ratio of 0.1 (Figure 1). Each sampling period involved the removal of a cement block (3 cm^3) and an aliquot of groundwater (3 cm^3) in addition to pH measurement. The ends of the cement blocks were sealed with wax in order to allow diffusion and leaching to occur from one plane; the groundwater was not replaced during the experiment. The experiments were completed in triplicate.

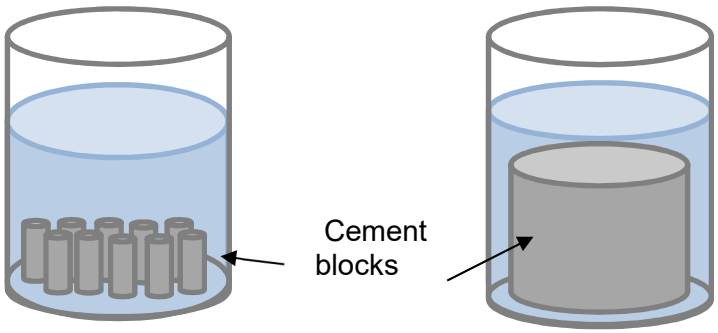

Figure 1: *Set-up for groundwater - cement experiments; L: S/L ratio = 0.1 and R: S/L ratio = 1.*

3.2. Groundwater conditioning experiments

This second set of diffusion experiments involved the use of equal volumes of groundwater (granitic, clay or saline) and cement to represent a more realistic situation. The cement block was submerged in groundwater at a S/L ratio of 1 (Figure 1). Sampling periods were daily for the first five days with this extended to monthly for subsequent samples. An aliquot of groundwater (1 cm^3) in addition to a pH measurement was taken. The experiments were completed in triplicate.

3.3. Materials and Methods

The cements were used in the form of hardened cement pastes (HCP). The mixing proportions for the cement blends are shown in Table 1. After hydrating with tap water, the cement blocks were placed into moulds and cured in tap water for 28 days. After curing, the cement blocks were submerged in the relevant synthetic groundwater.

Table 1: *Powder ratios of cement blends.*

Cement blend	OPC	GGBS	Hydrated Lime	Lime Flour	Quartz	Silica Fume	Water to cement ratio
CEM I	1.00	-	-	-	-	-	0.45
GGBS:OPC	1.00	9.00	-	-	-	-	0.45
NRVB	1.00	-	0.38	1.10	-	-	0.55
CEBAMA Reference mix	1.00	0.62	-	-	1.10	1.05	0.45

The synthetic groundwaters were prepared by dissolution of inorganic salts in deionised water. The compositions of the groundwater were taken from Gascoyne (2002) in the case of granitic and saline groundwater and Vinsot et al. (2008) for clay. The anion content of the solutions was characterised by ion chromatography (Table 2). Cations were measured by flame atomic spectroscopy, ICP-OES and ICP-MS techniques.

Table 2: *Measured anion composition of three synthetic groundwater, determined by ion chromatography (anions) and flame atomic spectroscopy techniques (alkali and alkaline earth metals). All concentrations reported as mg/L.*

Element	Granitic groundwater	Clay groundwater	Saline groundwater
Na	63.2	1118.1	3035.9
K	4.1	52.6	104.7
Mg	16.2	241.4	682.3
Ca	4.7	153.7	8.2
Cl^-	75.2	1901.5	6246.9
SO_4^{2-}	7.4	1434.8	470.1
HCO_3^- [a]	ND	-	ND
pH	8.1	6.3	7.6

ND = Not Determined

[a] *The groundwaters were prepared under ambient atmospheric conditions.*

4. Results and Discussion

4.1. Changes in pH (S/L ratio = 1)

An important property of cement in radioactive waste disposal is its high pH; which can reduce the solubility of some radionuclides and thereby limit their migration (Young et al. 2013; Felipe-Sotelo et al. 2016a, b; Felipe-Sotelo et al. 2017). The pH of the groundwaters following interaction with cement (S/L = 1) increased to > pH 11 after one day (Figure 2 to Figure 4). Thereafter, for GGBS OPC and the CEBAMA reference blend, the pH of the groundwaters appears to decrease after 30 days interaction.

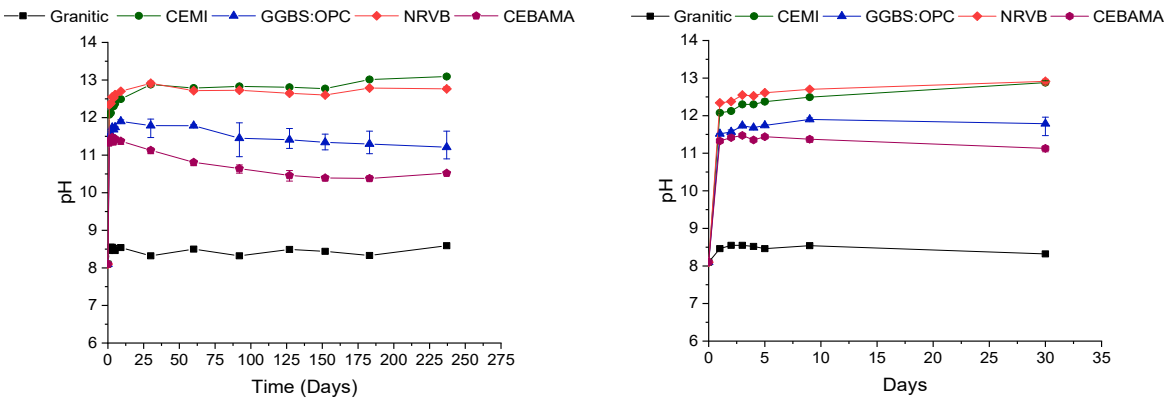

Figure 2: *Changes to granitic groundwater pH following interaction with cementitious materials. Left: 237 days interaction, right: expanded 0-30 day's interaction.*

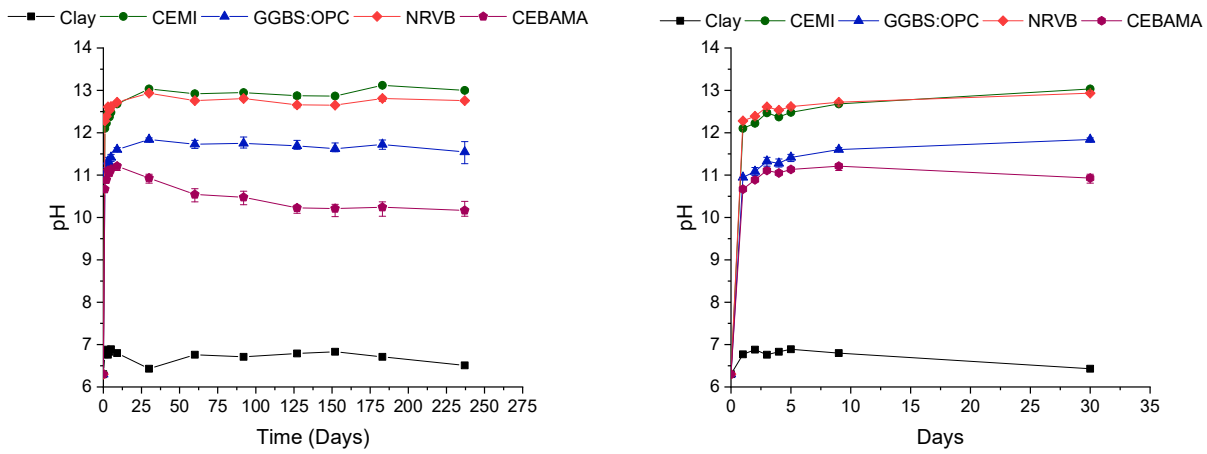

Figure 3: *Changes to clay groundwater pH following interaction with cementitious materials. Left: 237 days interaction, right: expanded 0-30 day's interaction.*

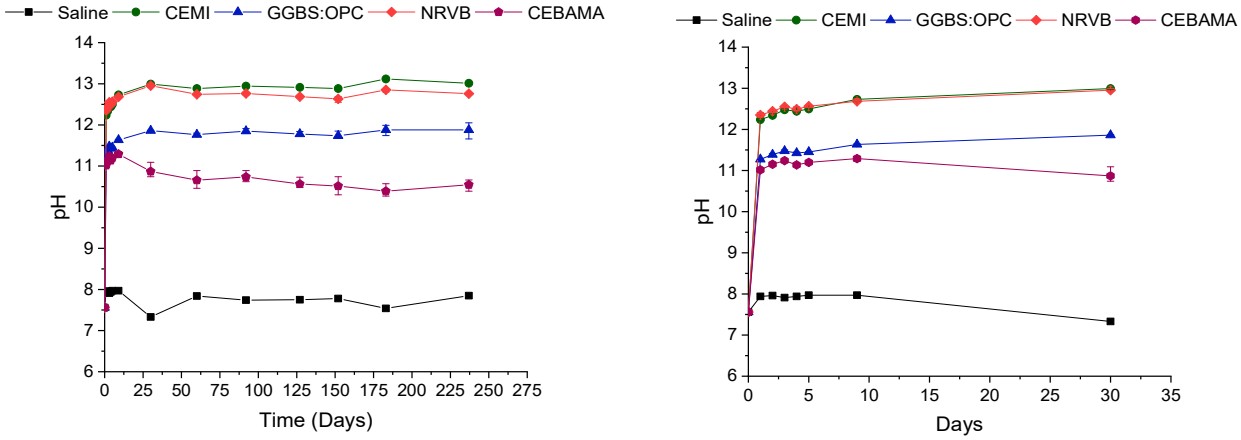

Figure 4: *Changes to saline groundwater pH following interaction with cementitious materials. Left: 237 day's interaction, right: expanded 0-30 day's interaction.*

4.2. Changes in groundwater anion content (solid to liquid ratio = 1)

Changes in groundwater chemistry (S/L = 1) were monitored over a period of five months (Figure 5 to Figure 7). The results are expressed in percentage terms by comparing the cement-groundwater sample composition with the baseline groundwater (no interaction with cement), as shown in Equation 1.

Equation 1:
$$Solution\ chloride\ (\%) = \left(\frac{[anion]\ with\quad cement{-}GW\ sample}{[anion]\ within\ baseline\ GW\ sample)}\right) x\ 100$$

The four cements can be divided into two groups based on trends for uptake or leaching (Figure 5 to Figure 7); CEM I with NRVB and GGBS:OPC with CEBAMA reference blend, respectively. CEM I and NRVB showed the greatest uptake of chloride and sulphate for all the groundwaters. For the granitic groundwater, there was an initial increase in solution sulphate following interaction with GGBS:OPC and CEBAMA reference blend cements. This is believed to be due to the higher sulphate content of the cement compared to the low concentration in the groundwater.

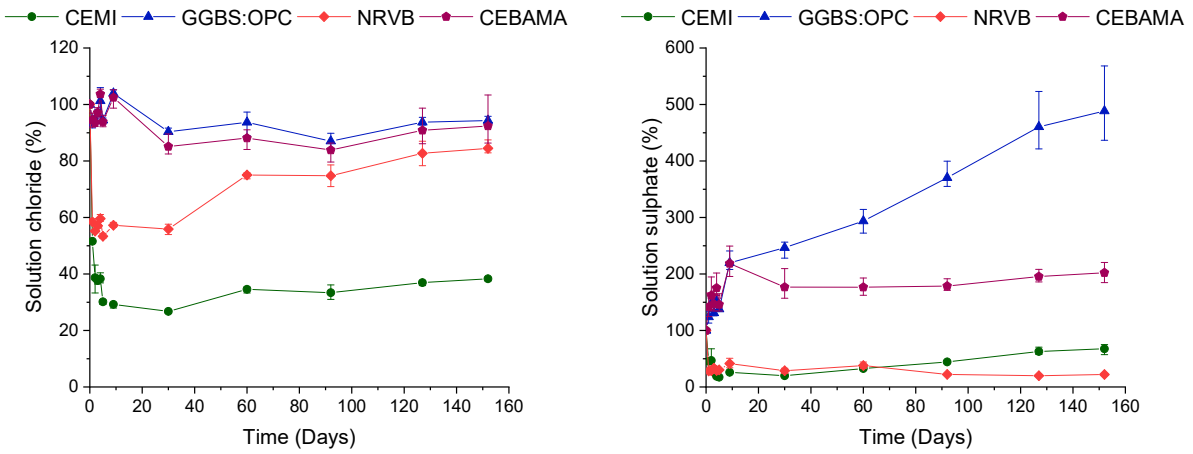

Figure 5: *Changes to solution chloride and sulphate of granitic groundwater following interaction with cementitious materials.*

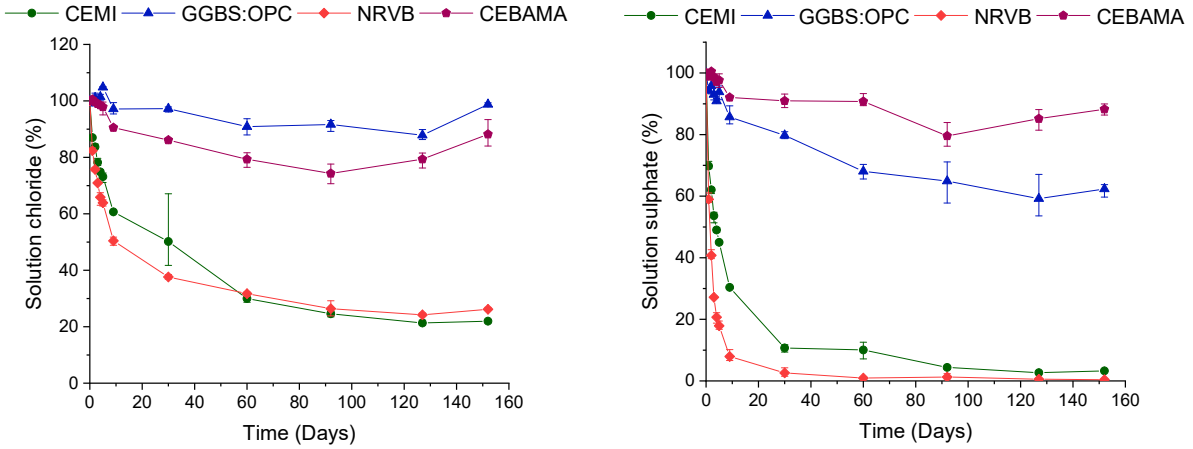

Figure 6: *Changes to solution chloride and sulphate of clay groundwater following interaction with cementitious materials.*

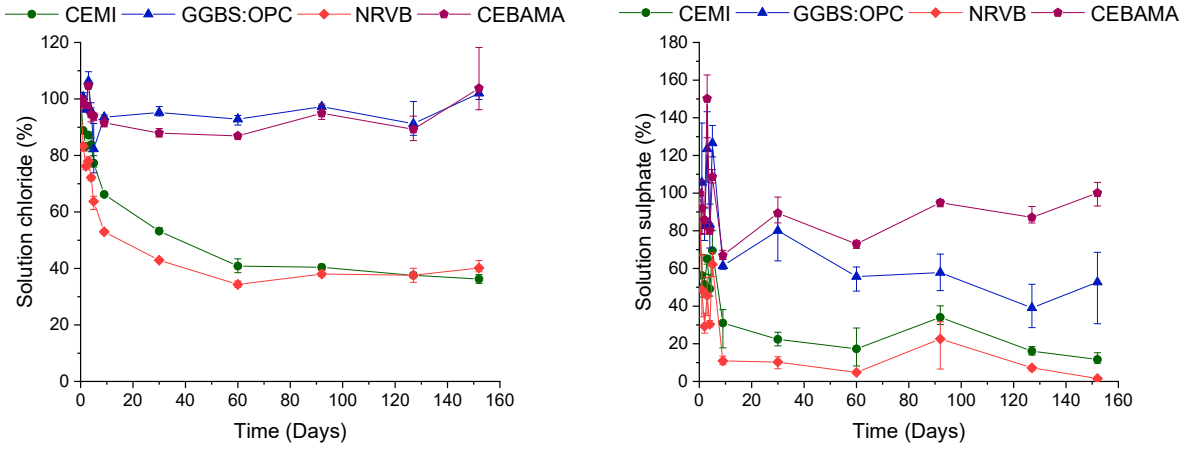

Figure 7: *Changes to solution chloride and sulphate of saline groundwater following interaction with cementitious materials.*

4.3. Solid characterisation (solid to liquid ratio = 0.1)

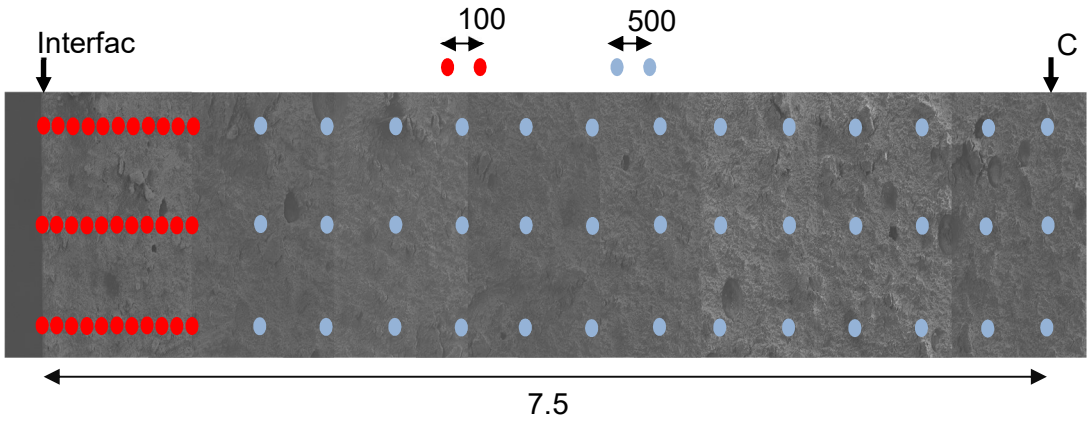

Figure 8: *Example of depth profile protocol using SEM-EDX on NRVB.*

Solid characterisation was completed to determine the fate of the anions within the cement following uptake. Depth profiles were obtained using SEM-EDX, at set intervals along a longitudinal cross section of the cement block. More spectra were gained closest to the interface with the groundwater as the greatest interaction was expected here. Figure 8 shows the protocol for the depth profile.

Examples are shown in Figure 9 and Figure 10. Figure 9 shows the depth profiles gained for NRVB following interaction with clay groundwater. It can be seen that over time there is an increase in the weight percentage of sulphur at the interface. Figure 9 appears to show the percentage of sulphur decreasing upon moving towards the core of the cement block, indicative of a reaction front.

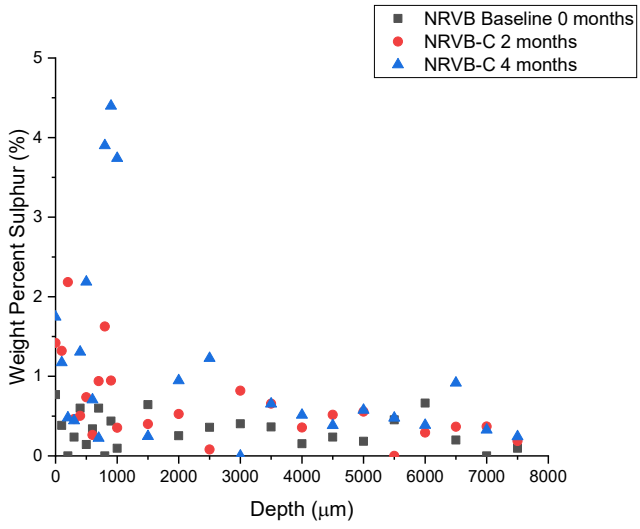

Figure 9: *Depth profile obtained by SEM-EDX analysis for NRVB following interaction with clay groundwater.*

Figure 10 shows chloride uptake by NRVB following four months interaction with saline groundwater. The high porosity of the NRVB matrix allows chloride penetration with groundwater derived Cl^- detected throughout the profile.

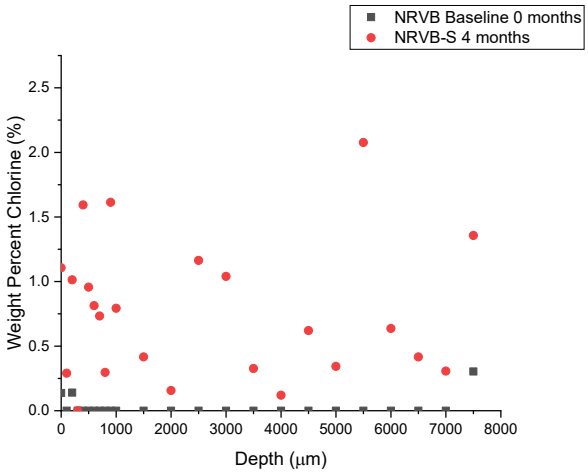

Figure 10: *Depth profile gained from SEM-EDX analysis for NRVB following interaction with saline groundwater.*

5. Conclusion

In summary, there are significant changes in the composition of the groundwaters following interaction with the cement blends owing to both leaching and uptake. There is a substantial decrease in groundwater chloride and sulphate following interaction with CEM I and NRVB cement blends when compared to GGBS:OPC and CEBAMA reference blend. Analysis of both phases within the system, solution (groundwater) and solid (cement) has allowed the outcome of the interaction to be better understood.

References

Felipe-Sotelo, M., Hinchliff, J., Evans, N.D.M., Read, D. (2016a). Solubility constraints affecting the migration of selenium through the cementitious backfill of a geological disposal facility. Journal of Hazardous Materials, 305, 21-29.

Felipe-Sotelo, M. Hinchliff, J., Field, L.P., Milodowski, A.E., Holt, J.D., Taylor, S.E., Read, D. (2016b). The solubility of nickel and its migration through the cementitious backfill of a geological disposal facility for nuclear waste. Journal of Hazardous Materials, 314, 211-219.

Felipe-Sotelo, M., Hinchliff, J., Field, L.P., Milodowski, A.E., Preedy, O., Read, D. (2017). Retardation of uranium and thorium by a cementitious backfill developed for radioactive waste disposal. Chemosphere, 179, 127-138.

Gascoyne, M. (2002). Influence of grout and cement on groundwater composition. Posiva Oy, Working Report 2002-07, 1-44.

Ipavec, A., Vuk, T., Gabrovšek, R., Kaučič, V. (2013). Chloride binding into hydrated blended cements: The influence of limestone and alkalinity. Cement and Concrete Research, 48, 74-85.

Thomas, M.D.A., Hooton, R.D., Scott, A., Zibara, H. (2012). The effect of supplementary cementitious materials on chloride binding in hardened cement paste. Cement and Concrete Research, 42, 1-7.

Vinsot, A., Mettler, S., Wechner, S. (2008). In-situ characterization of the Callovo-Oxfordian pore water composition. Physics and Chemistry of the Earth, 33, S75-S86.

Whittaker, M., Zajac, M., Ben HaHa, M., Black, L. (2016). The impact of alumina availability on sulfate resistance of slag composite cements. Construction and Building Materials, 119, 356-369.

Young, A.J., Warwick, P., Milodowski, A.E., Read, D. (2013). Behaviour of radionuclides in the presence of superplasticiser. Advances in Cement Research, 25, 32-43.

Technical Summary – KIT-INE – WP2

1. Introduction & Objectives

Beryllium is a chemotoxic element used in nuclear reactors as reflector or moderator due to its low thermal neutron absorption cross section and its specific chemical / structural properties. The amphoteric behaviour of Be(II) is widely accepted in the literature, although the number of experimental studies reporting the formation of anionic hydrolysis species ($Be(OH)_3^-$ and $Be(OH)_4^{2-}$) under alkaline to hyperalkaline pH conditions is very limited. The formation of ternary Na/K–Be(II)–OH(s) and Ca–Be(II)–OH(s) solid phases under hyperalkaline pH conditions has been described in the literature. These solid phases may eventually control Be(II) solubility in cementitious environments, but no thermodynamic data are available so far for these systems. Be(II) forms also strong complexes with carbonate, but so far most of the available studies investigating this interaction have focused on acidic to weakly alkaline pH conditions. In spite of the lack of dedicated studies assessing the uptake of Be(II) by cementitious materials, a weak sorption is predicted based on the formation of negatively charged hydrolysis species of Be(II) in the pH conditions relevant in cement systems. In this context, this study focuses on the solubility and hydrolysis of Be(II) under alkaline to hyperalkaline pH conditions, further extending to its sorption behaviour in cementitious systems. The main objectives are the development of comprehensive thermodynamic and activity models for the system Be^{2+}–Na^+–K^+–Ca^{2+}–H^+–Cl^-–OH^-–H_2O(l), the assessment of the impact of carbonate on the solubility, as well as the quantitative evaluation of the uptake of Be(II) by different cementitious materials and model compounds (C-S-H phases).

2. Studied system

2.1. Solubility studies

Solubility experiments were performed under Ar-atmosphere at T = (22 ± 2)ºC. Three different solid phases were investigated: BeO(cr) (commercial), $Be(OH)_2$(am) (synthesized in this work) and β-$Be(OH)_2$(cr) (aged amorphous phase). The following systems were investigated:

Absence of carbonate

- 0.1 – 5.0 M NaCl–NaOH, 5 series, with $5 \leq pH_m \leq 14.5$
- 0.1 – 4.0 M KCl–KOH, 5 series, with $9 \leq pH_m \leq 14.3$
- 0.05 – 3.5 M $CaCl_2$, 4 series, with $9 \leq pH_m \leq 12$
- 4.0 M NaOH
- 4.0 M KOH

Presence of carbonate

- 0.5 M NaCl with C_{tot} = 0.01 and 0.1 M
- 5.0 M NaCl with C_{tot} = 0.1 and 0.4 M

2.2. Sorption studies

- Ordinary Portland cement paste (CEM I 42,5 N BV/SR/LA type), degradation phase I (pH ≈ 13). Batch sorption experiment conducted with 10^{-6} M ≤ $[Be(II)]_0$ ≤ $10^{-2.5}$ M and 2 g/L^{-} ≤ [S/L] ≤ 50 g/L.
- Ordinary Portland cement paste (CEM I 42,5 N BV/SR/LA type), degradation phase II (pH ≈ 12.5). Batch sorption experiment conducted with 10^{-6} M ≤ $[Be(II)]_0$ ≤ 10^{-2} M and [S/L]= 2 g/L.
- Cebama low-pH cement paste (VTT). Batch sorption experiment conducted with 10^{-6} M ≤ $[Be(II)]_0$ ≤ 10^{-3} M and 0.2 g/L ≤ [S/L] ≤ 2 g/L.
- C-S-H Ca:Si = 0.6 (provided by BRGM). Batch sorption experiment conducted with 10^{-6} M ≤ $[Be(II)]_0$ ≤ 10^{-3} M and 0.2 g/L ≤ [S/L] ≤ 2 g/L.
- C-S-H Ca:Si = 1.0 (provided by BRGM). Batch sorption experiment conducted with 10^{-6} M ≤ $[Be(II)]_0$ ≤ $10^{-2.5}$ M and [S/L]= 2 g/L.
- C-S-H Ca:Si = 1.6 (provided by BRGM). Batch sorption experiment conducted with 10^{-6} M ≤ $[Be(II)]_0$ ≤ $10^{-2.5}$ M and [S/L]= 2 g/L.

3. Main results – Scientific highlights

3.1. Solubility of Be(II) in dilute to concentrated NaCl, KCl and $CaCl_2$ solutions

Figure 1 shows the XRD patterns of BeO(cr) and $Be(OH)_2$(am) solid phases used in this study. The patterns of the crystalline phase perfectly match those available in the literature for BeO(cr). The diffractogram of the amorphous phase was taken after 14 days of equilibration, and it is expected to evolve with time towards the formation of β-$Be(OH)_2$(cr). The final characterization of the solid phase in planned for February 2019.

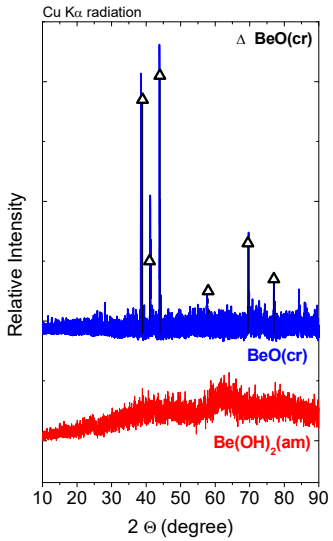

Figure 1: *XRD patterns of BeO(cr) and $Be(OH)_2$(am) solid phases used in this study. BeO(cr) reference patterns as reported in JCPDS database.*

Figure 2 exemplarily show selected Be(II) solubility systems in NaCl, KCl and $CaCl_2$ solutions. Solubility data confirm the amphoteric character of Be(II), with a solubility minimum at $pH_m \approx 9$. At this pH_m value, [Be(II)] in equilibrium with BeO(cr) and $Be(OH)_2$(s) is $\approx 10^{-7.5}$ and $\approx 10^{-7}$ M, respectively. No relevant differences are observed between [Be(II)] quantified in the clear supernatant and after 10 kD ultrafiltration, thus excluding any significant contribution of dissolved colloidal beryllium species to the total solubility. Solubility data obtained in weakly alkaline conditions clearly show that the hydrolysis constant previously reported for $Be(OH)_2$(aq) in potentiometric studies is importantly overestimated. The solubility of $Be(OH)_2$(am) determined in strongly alkaline, dilute NaCl systems is in excellent agreement with the only solubility study available to date in this pH region (Gilbert and Garrett, 1956).

The solubility of Be(II) in dilute, alkaline $CaCl_2$ solutions is very similar to analogous experiments in dilute, alkaline NaCl and KCl solutions. However, Be(II) behaves very differently in concentrated $CaCl_2$ solutions. In these systems, the solubility is significantly enhanced above $pH_m \approx 9$ with a slope ($\log_{10}$ [Be(II)] *vs.* pH_m) of $\approx +2$. These observations point towards an earlier stabilization of the moiety $Be(OH)_4^{2-}$ most likely due to the strong interaction with Ca. Note that under similar conditions, the formation of ternary complexes Ca–M–OH (aq) has been described for M(III) (Nd, Cm), M(IV) (Zr, Tc, Th, Np, Pu) and M(V) (Np) (Neck et al. 2009; Altmaier et al. 2008; Fellhauer et al. 2010; 2016; Yalcintas et al. 2016). This work provides evidence that analogous ternary complexes form for Be(II).

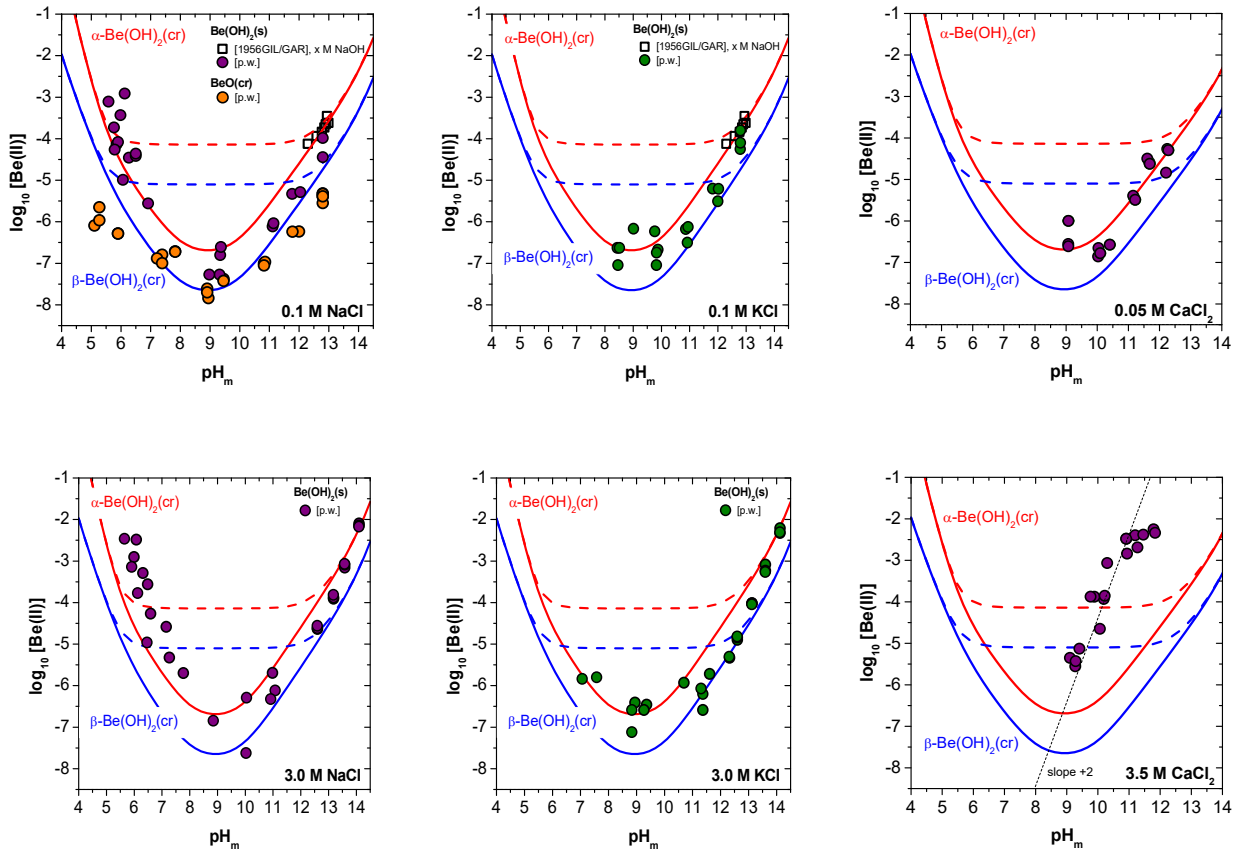

Figure 2: *Solubility of BeO(cr) and $Be(OH)_2$(s) in 0.1 / 3.0 M NaCl solutions ($5 \leq pH_m \leq 14$), 0.1 / 3.0 M KCl solutions ($7 \leq pH_m \leq 14$) and 0.05 / 3.5 M $CaCl_2$ solutions ($9 \leq pH_m \leq 12$). Squares correspond to Be(II) solubility data reported by Gilbert and Garrett (1956) in NaOH solutions. Calculated solubility appended for comparison: using thermodynamic data based upon solubility + potentiometric studies (dashed red/blue lines), and based upon solubility + solvent extraction studies (solid red/blue lines) (see text).*

Solubility data and solid phase characterization conducted in this work do not support the initial hypothesis of the formation of ternary solid phases Na/K/Ca–Be(II)–OH(s) within the investigated boundary conditions. The combination of solubility data determined in this work, solid phase characterization and ^{9}Be NMR (data not shown in this report) allow deriving comprehensive chemical, thermodynamic and (SIT, Pitzer) activity models for the system Be^{2+}–Na^{+}–K^{+}–Ca^{2+}–H^{+}–Cl^{-}–OH^{-}–H_2O(l).

3.2. Impact of carbonate on the solubility of Be(II)

The effect of carbonate on the solubility of Be(II) was investigated in 0.5 M NaCl–$NaHCO_3$–Na_2CO_3 solutions with $9.5 \leq pH_m \leq 13$. Experiments were performed with $C_{tot} = [HCO_3^-] + [CO_3^{2-}] = 0.01$ and 0.1 M. Thermodynamic calculations conducted using thermodynamic data available in the literature predict the predominance of the species $BeCO_3(OH)_2^{2-}$, and accordingly a very significant increase of the solubility. In spite of this, solubility experiments performed in this study show only a marginal effect of carbonate on the solubility of $Be(OH)_2$(s) in alkaline solutions, event for $C_{tot} = 0.1$ M (see Figure 3). The figure shows that the solubility of Be(II) remains unaffected for solutions with $C_{tot} \leq 0.1$ M and $pH_m \geq 11$. A slight increase in the solubility (c.a. 1 $\log_{10}$-units) is only observed at $C_{tot} = 0.1$ M and $pH_m \approx 9.5$. These results highlight that, within the boundary conditions expected in cementitious systems, carbonate cannot outcompete hydrolysis and the aqueous speciation of Be(II) is dominated by the species $Be(OH)_3^-$ and $Be(OH)_4^{2-}$.

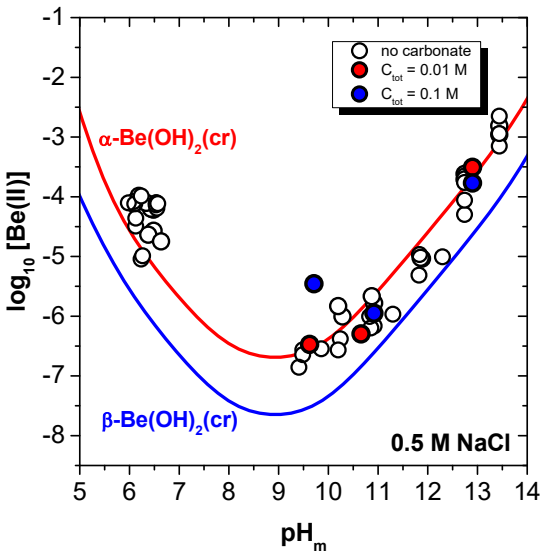

Figure 3: *Solubility of $Be(OH)_2$(s) in 0.5 M NaCl–$NaHCO_3$–Na_2CO_3 solutions with $9.5 \leq pH_m \leq 13$ and $C_{tot} = [HCO_3^-] + [CO_3^{2-}] = 0.01$ and 0.1 M.*

3.3. Uptake of Be(II) by cement and C-S-H phases

Figure 4 shows the main results obtained for the uptake of Be(II) by cement (only CEM I 42.5 N BV/SR/LA type shown in the figure) and C-S-H phases with Ca:Si = 0.6, 1.0 and 1.6. Note that the figure summarizes data collected under various boundary conditions (S/L ratio, $[Be(II)]_0$, time), which partly explain the dispersion in the data plotted – the representation of $\log_{10} R_d$ *vs.* pH has been favoured in this discussion. Note that all data shown in Figure 4 hold concentrations of Be in the aqueous phase below the solubility limit for the corresponding pH (see Section 3.1. of this contribution), and accordingly solubility phenomena are disregarded to play any role in the following discussion of the sorption data.

All investigated systems show a very strong uptake of beryllium by cement and C-S-H phases ($\log_{10} R_d \geq 4$, with R_d in L/kg). The figure shows a trend to decrease $\log_{10} R_d$ with increasing pH, with the highest $\log_{10} R_d$ values observed for C-S-H phases with Ca:Si = 0.6 (pH ≈ 10.2, $\log_{10} R_d \approx 5.5 \pm 0.5$) and the lowest for CEM I in degradation phase I (pH ≈ 13, $\log_{10} R_d \approx 4.4 \pm 0.7$). A good agreement is obtained between $\log_{10} R_d$ values obtained for C-S-H with Ca:Si = 1.6 and CEM I in degradation phase II. Note that C-S-H phases with Ca:Si = 1.6 prevail in the degradation phase II of standard Portland cement (pH ≈ 12.5), and thus these results provide further confidence in the sorption experimental program developed in this study.

The decrease of sorption with increasing pH can be related with the aqueous speciation of beryllium in the investigated pH-region (see Figure 5). The comparison of Figure 4 and Figure 5 suggests that the species $Be(OH)_3^-$ is mostly responsible for the uptake of Be(II), whereas the decrease in sorption is caused by the predominance of $Be(OH)_4^{2-}$ in the more alkaline systems investigated. Note that a very similar behaviour has been previously reported for U(VI) and Np(VI) (Tits et al. 2014). Although at a first sight Be(II) and An(VI) are expectedly very different, their aqueous speciation in hyperalkaline systems shows clear analogies, i.e predominance of $Be(OH)_3^-$ / $Be(OH)_4^{2-}$, $UO_2(OH)_3^-$ / $UO_2(OH)_4^{2-}$ and $NpO_2(OH)_3^-$ / $NpO_2(OH)_4^{2-}$.

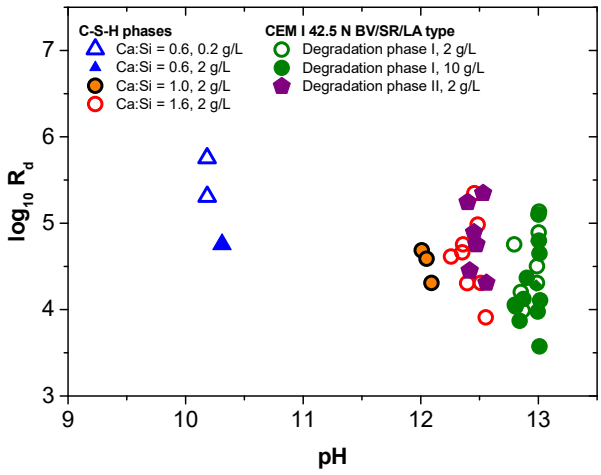

Figure 4: *Uptake of Be(II) by cement (CEM I 42.5 N BV/SR/LA type, degradation phases I and II) and C-S-H phases with Ca:Si = 0.6, 1.0 and 1.6. R_d values provided in L/kg.*

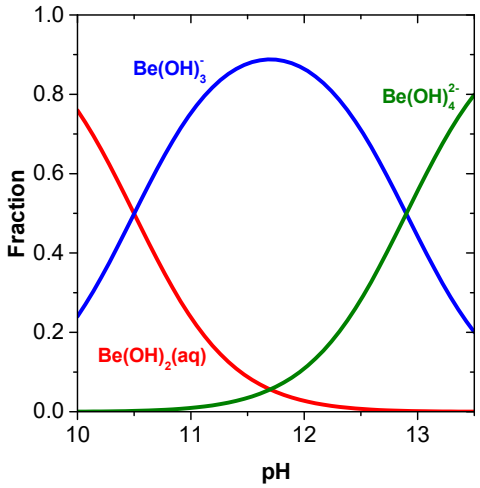

Figure 5: *Aqueous speciation of Be(II) within 10 ≤ pH ≤ 13.3 as calculated with thermodynamic data derived in the present work. Calculations performed at I = 0.*

These results represent the first experimental evidence of the strong uptake of Be(II) by cementitious materials, with clear links to the aqueous speciation and hydrolysis as investigated in the first part of this study.

References

Altmaier, M., Neck, V., Fanghänel, T. (2008). Solubility of Zr(IV), Th(IV) and Pu(IV) hydrous oxides in $CaCl_2$ solutions and the formation of ternary Ca-M(IV)-OH complexes. Radiochimica Acta, 96, 541-550.

Bruno, J. (1987). Beryllium (II) hydrolysis in 3.0 mol dm^{-3} perchlorate. Journal of Chemical Society Dalton Transactions, 2431-2437.

Fellhauer, D., Neck, V., Altmaier, M., Lützenkirchen, J., Fanghänel, T. (2010). Solubility of tetravalent actinides in alkaline $CaCl_2$ solutions and formation of $Ca_4[An(OH)_8]^{4+}$ complexes: A study of Np(IV) and Pu(IV) under reducing conditions and the systematic trend in the An(IV) series. Radiochimica Acta, 98, 9-11.

Fellhauer, D., Rothe, J., Altmaier, M., Neck, V., Runke, J., Wiss, T., Fanghänel, T. (2016). Np(V) solubility, speciation and solid phase formation in alkaline $CaCl_2$ solutions. Part I: Experimental results. Radiochimica Acta, 104, 355-379.

Neck, V., Altmaier, M., Rabung, T., Lützenkirchen, J., Fanghänel, T. (2009). Thermodynamics of trivalent actinides and neodymium in NaCl, $MgCl_2$ and $CaCl_2$ solutions: Solubility, hydrolysis and ternary Ca-M(II)-OH complexes. Macromolecular Science Pure and Applied Chemistry Journal, 81, 1555-1568.

Gilbert, R.A. and Garrett, A.B. (1956). The equilibria of the metastable crystalline form of beryllium hydroxide. $Be(OH)_2$ in hydrochloric acid, perchloric acid and sodium hydroxide solutions at 25°. American Chemical Society Journal, 78, 5501–5505.

Tits, J., Gaona, X., Laube, A., Wieland, E. (2014). Influence of the redox state on the neptunium sorption under alkaline conditions: Batch sorption studies on titanium dioxide and calcium silicate hydrates. Radiochimica Acta, 102(5), 385-400.

Yalcintas, E., Gaona, X., Altmaier, M., Dardenne, K., Polly, R., Geckeis, H. (2016). Thermodynamic description of Tc(IV) and hydrolysis in dilute to concentrated NaCl, $MgCl_2$ and $CaCl_2$ solutions. Dalton Transactions, 45, 8916.

Technical Summary – AMPHOS 21 – WP2

1. Introduction & Objectives

Cement materials have been used on a large scale as immobilization matrices for radioactive wastes as well as in the construction of engineering barriers or waste containers in disposal facilities to minimize release of radionuclides. Literature review performed at the beginning of CEBAMA Project showed that some cement hydrates have sorption and ion-substitution properties. Moreover, cement porewater has a high pH which favours the retention of many nuclear waste derivatives. Among the hydrated phases studied in bibliography which are known to be involved in retention processes, monosulphate (AFm), ettringite (AFt) and C-S-H gels have been reported as the most relevant for substitution or precipitation of many radionuclides in cement environments. Different radionuclides of interest are being studied in the frame of CEBAMA Project (i.e. Be, C, Cl, Ca, Se, I, and Ra), the work developed by Amphos 21 was focused specifically on the study of molybdenum retention onto C-S-H gels (C/S ratio 0.8, 1.2 and 1.4), ettringite and ettringite/monosulphate mixtures (S/Al ratios 0.5, 1, 2 and 2.5). Typical molybdenum radionuclides in low- and intermediate-level waste (LILW) are ^{99}Mo and ^{93}Mo. While the former has a half-life of $4.52 \cdot 10^{-3}$ years, the latter (^{93}Mo) in turn is a synthetic radioisotope with a half-life of 4000 years formed by irradiation with thermal neutrons and fast neutrons (Lindgren et al. 2007). Among other activation products, molybdenum-93 may suppose a threat to LILW disposal safety. Sources for ^{93}Mo are metallic materials (steels and zircaloy in the core region), and activation of molybdenum in dissolved form or as corrosion particles in the coolant. The release of activation products in the core components is controlled by the corrosion of steel and stainless steel.

Literature review also showed a general scarcity of data devoted to molybdenum retention on cementitious materials. This lack of data makes necessary a more extensive experimental work on this topic, as most of the data available are taken from analogies with other anions which have similar chemical behaviour. As mentioned before, the most representative phases responsible for molybdate immobilization in cement environment are AFt and AFm phases. Even though no specific studies have been focused on C-S-H capacities for molybdate immobilization, experimental data obtained with other anions such as CrO_4^{2-} and AsO_4^{3-} suggest that C-S-H gels might also be able to retain MoO_4^{2-}. Initially AFt and AFm phases have been proposed as viable cement constituents for oxyanion retention via sulphate substitution, this substitution is known to be highly dependent on size and charge similarities between sulphate and oxyanions. Concerning C-S-H phases, there are studies showing that these phases can immobilize oxyanions by replacing silicate in its structure, which suggests that C-S-H gels could also be an important sink for molybdate (Grivé and Olmeda, 2016). In this context, zeta potential could be an important factor limiting the mechanism and thus the extent of molybdate retention. Another process for molybdenum immobilization is its precipitation as Powellite ($CaMoO_4$(s)). Under cementitious conditions, $CaMoO_4$(s) becomes the solubility-controlling phase for all the states of cement degradation, and thus molybdenum solubility is very sensitive to differences in calcium concentrations.

Considering the lack of data in bibliography, the main aim of Amphos 21 work focused on contributing to the acquisition of new data and understanding the retention mechanisms of Mo in cement-based materials, the experiments involved the study of (i) the kinetics of molybdenum retention and (ii) the parameters affecting its potential release to solution in contact with pure cementitious phases.

2. Studied system

Mo is a redox-sensitive element with a broad range of oxidation states (form –II to +VI), whose aqueous speciation is dominated by the molybdate anion (MoO_4^{2-}) highly thermodynamically stable even under moderately reducing conditions. The principal Mo species existing at alkaline conditions is the mononuclear molybdate ion MoO_4^{2-}, furthermore, molybdenum has a strong capacity to form complex anions such as heteropoly acids, as well as complexes with organic substances such as oxalic, citric acids, EDTA. Considering molybdenum chemistry, Amphos 21 work has been centred on the study of molybdenum retention as molybdate anion.

With respect to the solid phases, we selected:

- *AFt phases*: The most important AFt phase is ettringite, $[Ca_3Al(OH)_6\ 12H_2O]_2(SO_4)_3\cdot 2H_2O]$ (Taylor, 1997) which forms quite rapidly during cement hydration. The properties of these phases are strongly dependent on their crystallographic structure, including crystal size and nature of the layer charge (e.g. isomorphic substitutions, vacancies).
- *C-S-H gels (Ca/Si = 0.2, 1.2 and 1.4)*: The term C-S-H phase comprises a group of more than 30 identified phases that are poorly ordered (Taylor, 2004). These kinds of phases are characterized by their amorphous nature and the variation on their composition which causes significant changes on their properties as adsorbent depending on the calcium-to-silica ratios (Ca/Si ratios are found to range from 3 to 0.6). Surface charge of a solid phase may influence in a great extent the interactions that occur between the solid surface and the species in solution. In this context, zeta potential measurements are of great importance to study surface properties as adsorption. At Ca/Si ratios higher than 1.2 these gels are positively charged, and thus might have the potential to adsorb oxyanions.
- *AFm/AFt mixtures*: Naturally occurring AFm phases (also known AFm-SO_4) are double-layered hydroxides with variable composition. These phases have been proposed by Kindness et al. (1994) as the controlling mineral phases for molybdate in cements. Considering this, the effect of AFm/AFt ratio on molybdenum adsorption was evaluated starting from the evidences found by Matschei et al. (2007) which indicate that these two phases can coexist over a SO_3/Al_2O_3 ratio ≥ 1.

3. Main results – Scientific highlights

The study of molybdenum adsorption onto hydrated cement phases was carried out by developing a set of consecutive tasks involving from the synthesis and characterization of individual phases to the development of adsorption isotherms, including the study of powellite solubility and adsorption kinetics. The main results extracted from this experimental work can be analysed by means of the hydrated cement phases under study, on one hand C-S-H gels and on the other hand AFt and AFm/AFt phases.

3.1. Molybdenum retention onto C-S-H gels (Ca/Si ratios 0.8, 1.2 and 1.4)

C-S-H gels with three different Ca/Si ratios were individually synthesized using a S/L ratio of 20 g/L with SiO_2 and CaO as starting materials. Once weighted, the solids were mixed with DDW (deionized degassed water) and equilibrated during at least 20 days. The whole synthesis procedure was carried out inside a glovebox filled with N_2 99.99999%. Obtained solids, together with their equilibrated waters were extensively analysed by different techniques to clearly characterize their structural and compositional features. The results obtained from characterization agreed with the expected composition as well as with most of the results reported in bibliography for solids with similar composition. Water content increased with the Ca/Si ratio, surface specific area followed the opposite trend, being higher for lower Ca/Si ratios. The three solids presented similar XRD patterns characterized by the amorphous structure.

Molybdenum adsorption kinetics were evaluated as a first approach to the molybdenum adsorption studies. This kind of experiments allowed not only to stablish the time necessary to attain the equilibrium but also to identify those phases able to retain molybdenum more efficiently. The selection of the three Ca/Si ratio tested in this work was based on literature results. Most studies indicate that surface characteristics as zeta potential of C-S-H gels vary as a function of Ca concentration or pH. In this sense, our selection includes three Ca/Si ratios, covering from negative (C-S-H 0.8) to slightly positive values (C-S-H 1.4) with C-S-H 1.2 in between, which presents near neutral charge. The speciation of molybdenum indicates that the most stable molybdenum species in cement environments is the negatively charged molybdate. This fact, together with the surface characteristics of the selected hydrated phases, led thinking that molybdenum retention may be more favoured when contacting with C-S-H 1.4 phase. Experimental results, shown in Figure , confirmed this hypothesis, R_d values found for C-S-H 1.4 are markedly higher than those obtained for ratios 0.8 and 1.2. Molybdenum retention is a fast process and the distribution constant does not suffer significant variation in the time interval studied, indicating that equilibrium is attained in short time intervals.

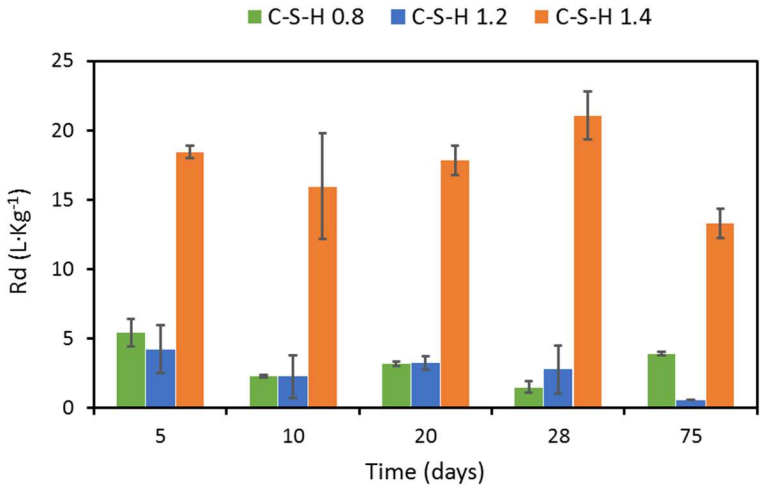

Figure 1: *Molybdenum retention kinetics onto C-S-H gels for Ca/Si ratios 0.8, 1.2 and 1.8. [Mo]i=1·10^{-5} M, S/L= 0.3 g/L at 25 ± 1°C.*

From first kinetic studies, C-S-H gels with low Ca/Si ratios were discarded due to their low molybdenum retention capacity. Lower contact times were tested for C-S-H 1.4 selecting 1 day as optimum for the development of isotherm experiments. R_d values ranging 20 L/kg were obtained from isotherm studies; as far as we know, this value is the first attempt in determining molybdenum distribution ratio for C-S-H gels with high Ca/Si ratio.

3.2. Molybdenum retention onto AFt and AFm/AFt phases:

3.2.1. AFt (ettringite) phase

AFt phase was synthesized from CaO and $Al_2(SO_4)_3 \cdot 18H_2O$ by a hydrothermal procedure at 60°C under N_2 (g) atmosphere to avoid carbonation. AFt corresponding solid and aqueous phases were fully characterized and identified as AFt pure phase. The elemental analysis carried out by EDX confirmed the atomic percentages that match with AFt composition. SEM images showed the presence of only one crystal type on the sample, with typical AFt needle shape. TGA analysis allowed detecting two different types of hydration water, the first one corresponding to water molecules located on the outer surface of AFt, the second one was attributed to the dehydration of aluminium hydroxide. The aqueous fraction was mainly composed by sulphate anions (~ 7 mM) and calcium (~ 4 mM).

Powellite solubility was evaluated using AFt contact waters obtained from the synthesis. These solubility tests allowed confirming that experimental data can be accurately described using the solubility constant reported in bibliography (7.90 ± 0.33 from Thermochimie Database vs 9.b.0 (Giffaut et al. 2014).

Molybdenum retention onto AFt phase was evaluated by analysing the results derived from kinetic studies. The data obtained at different contact times indicated that nearly no molybdenum retention was observed, as happened when analysing C-S-H gels with low Ca/Si ratios. The zeta potential was identified as key parameter to understand molybdenum retention as Ca/Si ratio increases; for AFt phase similar discussion can be done. The surface of AFt solids is expected to have very low zeta potential, which turned negative in the presence of sulphate anions and may hinder the retention of anionic species as molybdate.

Low retention capacity attributed to AFt phases was previously reported in bibliography (Zhang, 2000; Kindness et al. 1994) compared to that observed for AFm phases. Considering this, a new set of experiments consisting on the study of molybdenum retention onto AFm/AFt mixed phases was prepared with the aim analysing the influence of AFm phase on molybdenum retention.

3.2.2. AFm/AFt mixed phases

Several authors indicate that the monosulphate is thermodynamically unstable with respect to Ettringite (AFt) below 40°C (Damidot and Glasser, 1993; Glasser et al. 1999). However, at approximately 20°C, the thermodynamic driving force that stabilizes AFt relative to AFm must be very small, with the result that sulphate AFm is very persistent. Therefore, metastable AFm solid solutions can also occur and persist, being the solid solution between OH- and SO_4-AFm the most relevant to cement chemistry (Glasser et al. 1999). Considering the bibliography review, the synthesis of AFm/AFt mixtures (with S/Al ratios ranging from 0.5 to 2.5) as well as their study on molybdenum retention kinetics was proposed and positively reviewed by the CEBAMA Coordination Team to be granted with a CEBAMA “Mobility Measure”.

AFm/AFt mixtures with variable SO_3/Al_2O_3 ratios (namely S0.5, S1, S2 and S2.5) were synthesized by mixing the appropriate amounts of C_3A, CaO, $CaSO_4$ and $CaCO_3$ and equilibrating the mixtures in DDW for 25 days. The results obtained from the characterization using different analytical techniques were consistent with each other, which suggests the reliability and consistency of the experimental method. AFm and AFt phases precipitated as totally different phases, therefore no solid solution was observed to form between these two phases in the present study. A marked division of the synthesised samples can be observed with a significant different structural composition, i.e. major AFt content in the samples of S(VI)/Al equal to 2 and 2.5, and major AFm content in the samples of ratio 1 and 0.5, as can be drawn from SEM micrographs shown in Figure 2.

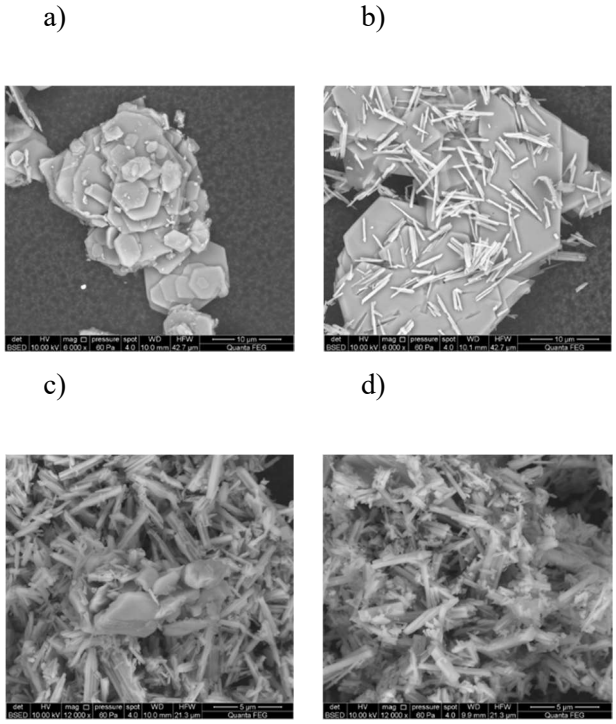

Figure 2: *Micrographs of synthesised mixed samples at 6 kx. S(VI)/Al ratios a) 0.5, b) 1, c) 2, d) 2.5.*

From XRD patterns summarized in Figure 3 the monosulphate precipitation seems to take place in all the synthesised samples regardless the amount of sulphate in the system. In turn, no ettringite was observed in samples of initial ratio S(VI)/Al = 0.5 (Sample S0.5), whereas in the rest of samples, ettringite and monosulphate coexist. Some impurities are also detected in the synthesised samples, such as gypsum in S2 and S2.5 due to the high sulphate content, or hydrogarnet in S0.5. Likewise, although the presence of carbonate has been avoided, some limited monocarbonate and/or hemicarbonate precipitation also occurs in the samples.

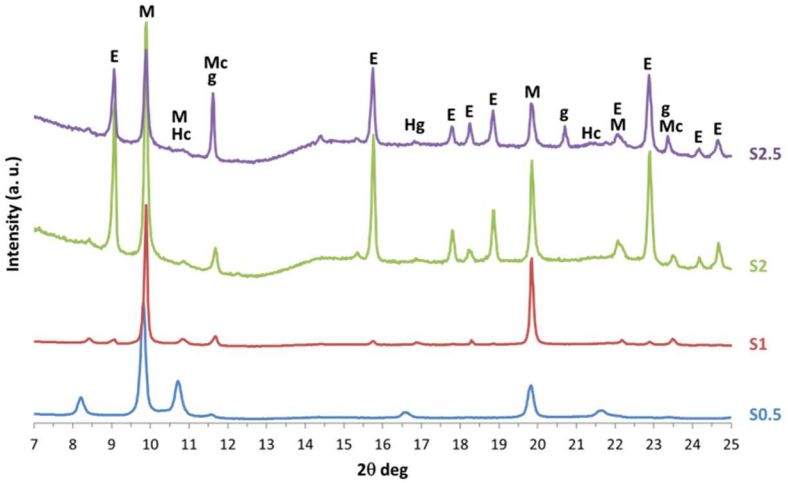

Figure 3: *X-Ray powder diffraction spectra of synthesised mixed phases. M – monosulphoaluminate; E – ettringite; M - monocarbonate; Hc – hemicarbonate; g – gypsum; Hg – Hydrogarnet (C_3AH_6).*

Molybdenum retention onto AFm/AFt mixed phases was also evaluated over the S(VI)/Al ratios tested in this work. As happened when characterizing these phases, two general trends were found. Samples with S(VI)/Al equal to 2 and 2.5 showed very low molybdenum retention while the solids with S(VI)/Al 0.5 and 1 presented not only high Mo affinities but also fast retention kinetics. Isotherm experiments were restricted to the latter, finding extremely high R_d values in the case of S(VI)/Al 0.5 (ranging from 1200 to 46,400 L/kg) and little low Mo retention for S(VI)/Al 1 ($164 < R_d < 693$ L/kg). Our results agree with others found in literature as most of the references pointed out to higher affinities of AFm phase towards anion retention compared to that observed for AFt phases (Keller, 2002; Ma et al. 2017; Zhang, 2000).

Finally, as already suggested in Grivé and Olmeda (2016), these results clearly show that the approach proposed by Ochs et al. (2016b) for molybdate adsorption, which is reported to be strongly related to the presence (and the amount) of ettringite in the system, is not completely correct. Therefore, the best estimates (0.1 – 3 L/kg) and associated upper (0.3 – 33 L/kg) and lower (0.3 – 0.01 L/kg) limits for molybdenum adsorption in cementitious materials proposed by Ochs and co-workers (Ochs et al. 2016b) need to be reviewed and updated with new data.

After analysing the results obtained for each individual hydrated cement phase, some conclusions can be drawn:

1. The main phases involved on molybdenum retention are C-S-H gels with high Ca/Si ratio and AFm phases. Related with this, some data reported in bibliography for molybdenum adsorption by analogy with selenate must be carefully reviewed as they consider molybdenum retention associated to the presence (and the amount) of ettringite.
2. The results indicated that the most probable mechanism involved on molybdenum retention is edge-sorption.

Under selected experimental conditions, adsorption is a fast process which takes place in less than 10 days.

References

Lindgren, M., Pettersson, M., Wiborgh, M., AB, K. (2007). Correlation factors for C-14, Cl-36, Ni-59, Ni-63, Mo-93, Tc-99, I-129 and Cs-135, In operational waste for SFR 1. Swedish Nuclear Fuel and Waste Management Co.

Grivé, M. and Olmeda, J. (2016). Molybdenum behaviour in cementitious materials. State of the art report.

Kindness, A., Lachowski, E.E., Minocha, A.K., Glasser, F.P. (1994). Immobilisation and fixation of molybdenum (VI) by Portland cement. Waste Manag. Jan 1,14(2), 97-102.

Matschei, T., Lothenbach, B., Glasser, F.P. (2007). The AFm phase in Portland cement. Cement and Concrete Research, 37(2), 118–30.

Taylor, H.F.W. (2004) Sulfates in Portland clinker and cement. In K. Scrivener and J. Skalny, p. 3-17.

Giffaut, E., Grivé, M., Blanc, Ph., Vieillard, Ph., Colàs, E., Gailhanou, H., et al. (2014) Andra thermodynamic database for performance assessment: ThermoChimie. Geochem Risk Assess Hazard Waste Geosph, 49, 225-36.

Zhang, M. (2000). Incorporation of oxyanionic B, Cr, Mo and Se into Hydrocalumite and Ettringite: Application to cementitious materials. University of Waterloo.

Damidot, D. and Glasser, F.P. (1993). Thermodynamic investigation of the $CaO-Al_2O_3-CaSO_4-K_2O-H_2O$ system at 25°C. Cement and Concrete Research, 23(5), 1195-204.

Glasser, F.P., Kindness, A., Stronach, S.A. (1999). Stability and solubility relationships in AFm phases: Part I. Chloride, sulfate and hydroxide. Cement and Concrete Research, 29(6), 861-6.

Keller, I.R.B. (2002). The Immobilisation of Heavy Metals and Metalloids in Cement Stabilised Wastes: A Study Focussing on the Selenium Oxyanions SeO_3^{-2} and SeO_4^{-2}. Doctoral dissertation, Universität Zürich.

Ma, B., Fernandez-Martinez, A., Grangeon, S., Tournassat, C., Findling, N., Claret, F., et al. (2017) Evidence of Multiple Sorption Modes in Layered Double Hydroxides Using Mo As Structural Probe. Environmental Science & Technology, 51(10), 5531-40.

Ochs, M., Mallants, D., Wang, L. Cementitious Materials and Their Sorption Properties. In: Ochs M, Mallants D, Wang L, editors. Radionuclide and Metal Sorption on Cement and Concrete.

Technical Summary – BRGM – WP2

1. Introduction & Objectives

AFm are layered double hydroxides found in cementitious environments. They are foreseen to play a pivotal role on the fate of anion, through sorption/incorporation mechanisms. Retention and incorporation capacities are certainly driven by the crystallographic structure of AFm, including crystal size, and nature of the layer charge (e.g. isomorphic substitutions, vacancies).

BRGM contribution to the Work Package 2 (WP2) of the European project Cebama is focused on various aspects of AFm behaviour in cements (Marty et al. 2018; Marty et al. 2017; Grangeon et al. *in prep*), with the global aim of better understanding the role played by this phase in retaining anions from migrating. In this view, exchange constants for a set of anions of interest are to be determined, and the crystal structures of the resulting phased are to be determined. The first point is a prerequisite to the thermodynamic modelling of anion migration in cements, and the second will both allow for a better understanding of the mechanisms of interaction between AFm and anions at the atomic scale, information which is crucial to our capacity to model retention phenomena, and will facilitate further structural studies.

2. Studied system

The general structural formula of an AFm is $[Ca^{2+}_4(Al^{3+}_xFe^{3+}_{(1-x)})_2(OH)_{12}]\cdot A\cdot nH_2O$, where the layered species are between the brackets and $A\cdot nH_2O$ represents the hydrated exchangeable "interlayer anions." These exchangeable interlayer anions compensate for the layer charge induced by the presence of the trivalent cations in the layers, providing AFm with an anion-exchange capacity (AEC). Of all AFm, the most studied is probably the one with the general structural formula $[Ca^{2+}_4Al^{3+}_2(OH)_{12}]\cdot 2Cl^-\cdot nH_2O$. Synthetic samples are often termed AFm-Cl or "Friedel's salt," and natural samples are normally said to belong to the "hydrocalumite" group.

Retention mechanism of Se(VI) and Mo(VI) on AFm-Cl have been investigated. Radionuclides were selected according to priority with focus put on elements and nuclides for which so far insufficient information is available and rather large uncertainties exist (e.g. Cl, Se, Mo). The studies mainly focus on analysing sorption and incorporation processes. Note that molybdenum, whose ^{93}Mo isotope is considered a major steel activation product, will be released mainly under the form of MoO_4^{2-} (i.e. Mo(VI)) in a radioactive waste repository. Understanding its fate is of primary importance in a safety analysis of such disposal. Selenium is present in waste of ^{79}Se coming from fission and have an half-life close to $3.3\ 10^5$ years. Selenium presents four different oxidation states: selenide (Se(-II)), elemental selenium (Se(0)), selenite (Se(IV)) and selenate (Se(VI)). Selenium in oxidation states -II and 0 are poorly soluble whereas oxidation states IV and VI are considered to be soluble and mobile. Regarding the Se(VI), the main species is under the form SeO_4^{2-} for pHs > 2.

3. Main results – Scientific highlights

First part of our contribution was focused on the estimation of reliable weathering/dissolution rates of cement phases that is of fundamental importance for modelling the temporal evolution of radioactive waste repositories. Kinetics of AFm-Cl has been studied with flow-through experiments at pH ranging from 9.2 to 13 (Marty et al. 2017). For pH values ranging from 10 to 13, flow-through experiments indicate congruent dissolutions of AFm-Cl (i.e. Ca/Al ratios close to 2 both for solids and outlet concentrations, Figure 1). In contrast a precipitation of amorphous Al-phases and possibly amorphous mixed Al/Ca phases are observed at pH 9.2 leading to Ca/Al ratios higher than those of the initial solid in the outlet solutions (Figure 1). However, estimated rate in such condition appears to be weakly affected by these secondary-phase formations. Far-from-equilibrium dissolution rates were normalized to the final specific surface areas (ranging from 6.1 to 35.4 m^2/g). None significant effect of pH on dissolution kinetics can be draw and therefore the far-from-equilibrium dissolution kinetics at pH ranging from 9.2 to 13 and room temperature is expressed as Eq 1.

$$\log R\,(mol\,m^{-2}\,s^{-1}) = -9.23 \pm 0.18 \qquad \textit{Eq.1}$$

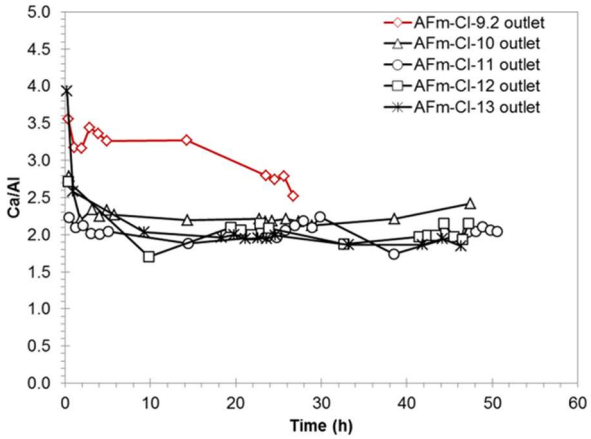

Figure 1: *Ca/Al ratios calculated from outlet concentrations monitored during flow-through experiments (from Marty et al. 2017).*

The second part of our contribution investigated the Cl^-/MoO_4^{2-} exchange processes occurring in an AFm initially containing interlayer Cl using flow-through experiments in alkaline conditions (Marty et al. 2018). The evolution of the solid phase was characterized using an electron probe microanalyzer and synchrotron high-energy X-ray scattering. All data, together with their quantitative modeling, coherently indicated that Mo replaced Cl in the AFm interlayer. The structure of the interlayer is described with unprecedented atomic-scale detail based on a combination of real- and reciprocal-space analyses of total X-ray scattering data. The objective was to describe quantitatively the mechanisms of Mo uptake by AFm, and to provide a geochemical model valid at both macroscopic (chemical) and molecular (crystallographic) scales. It was demonstrated that Mo, under the form of a tetrahedral MoO_4^{2-} complex, binds to AFm by replacing 2 Cl^- in the interlayer mid-plane. The affinity constant was evaluated to $K_{Mo} = 10^{1.3}$. In addition, OH^- competes with MoO_4^{2-} for sorption at the same sorption site, which also prevents MoO_4^{2-} accessing part of the AEC. Both these effects reduce the AFm sorption capacity toward Mo; thus, lowering the capacity of cement-based materials to buffer Mo.

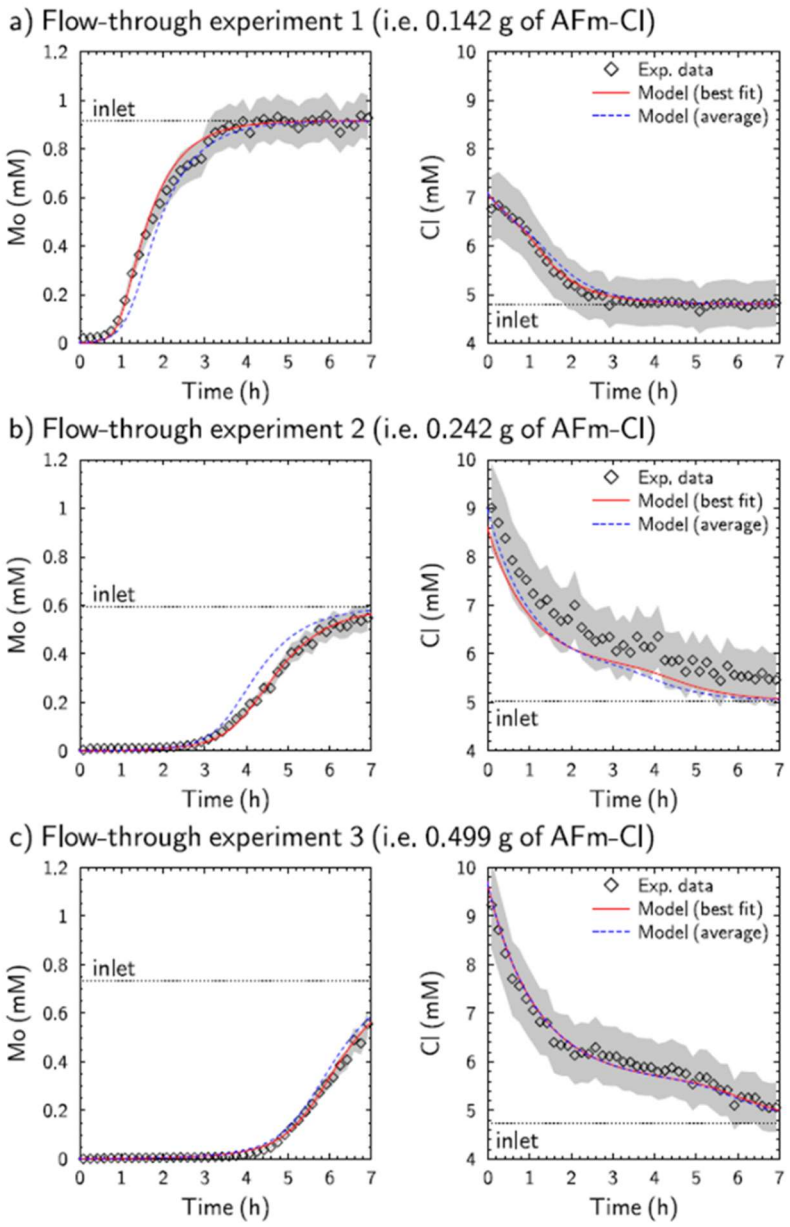

Figure 2: *Evolutions of experimental and modeled Mo and Cl concentrations as a function of time (from Marty et al, 2018). "Best fit" models were obtained using different AEC, while "average" models considered the same* $AEC_{site\ 1}$ *(230 meq/100 g) and* $AEC_{site\ 2}$ *(126.3 meq 100/ g) for all experiments. Gray shading represents estimated error on experimental data (i.e 10%).*

The last part our contribution was dedicated to the study of Se(VI)/Cl (Grangeon et al. *in prep*). Exchange experiments were also carried out using flow-through experiments, in alkaline conditions. The mechanisms of selenate (SeO_4^{2-}) sorption by AFm was studied using a combination of wet chemistry, electron-probe, X-ray scattering and transmission electron microscopy techniques. This study was dedicated to the study of the reversibility of the exchange process (AFm-Cl reacting with Se(VI)-rich solution then Cl-rich solution) as illustrated on Figure 3.

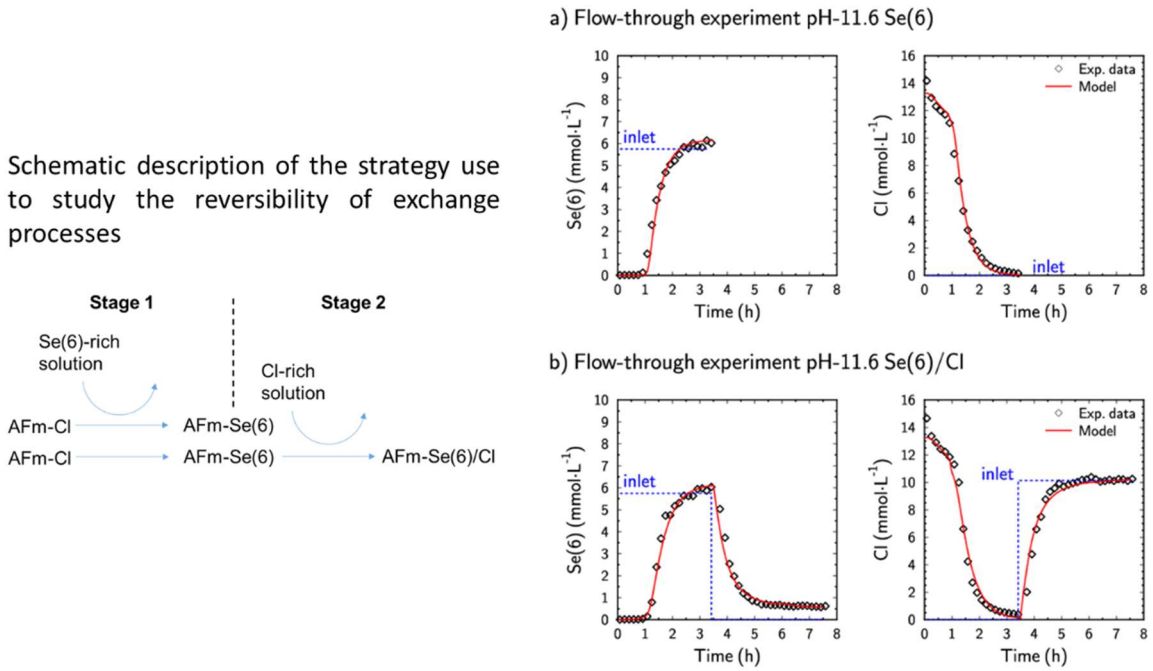

Figure 3: *Evolutions of experimental and modeled Se and Cl concentrations as a function of time (from Grangeon et al. in prep).*

References

Grangeon, S. et al. (*in prep*). Selenate sorption by hydrated calcium aluminate (AFm): evidence for sorption reversibility an implication for the modelling of anion retention

Marty, N.C.M, Grangeon, S., Elkaïm, E., Tournassat, C., Fauchet, C., Claret, F. (2018). Thermodynamic and crystallographic model for anion uptake by hydrated calcium aluminate (AFm): an example of molybdenum. Scientific Reports, 8:7943.

Marty, N.C.M., Grangeon, S., Lerouge, C., Warmont, F., Rozenbaum, O., Conte, T., Claret, C. (2017). Dissolution kinetics of hydrated calcium aluminates (AFm-Cl) as a function of pH and at room temperature. Mineralogical Magazine, 81(5), 1245–1259.

Technical Summary – JUELICH – WP2

1. Introduction & Objectives

Cement-based materials are widely used in nuclear waste management, for example for the solidification of low and intermediate level wastes, as barrier materials in nuclear waste repositories, or in certain waste containers as buffer, for example, in the Belgian Supercontainer. The migration behaviour of radionuclides in cementitious materials is controlled by radionuclide solubility phenomena, diffusion, interface processes such as surface complexation, or incorporation of radionuclides into solid phases, including the formation of solid solutions. The uptake and binding of radionuclides to cementitious materials have been investigated in a large number of studies over the last decades leading also to the development of various sorption coefficient databases. However, the mechanisms governing the immobilization of various safety relevant radionuclides by cementitious materials on the molecular scale are still not completely understood, and detailed knowledge on the behaviour of some radionuclides (e.g. ^{226}Ra, ^{129}I, ^{99}Tc, ^{93}Mo, ^{79}Se), which have high priority from the scientific and applied perspective in cement-based environments, was scarce or lacking.

Thus the aim of our investigations was to enhance the mechanistic understanding of the radionuclide uptake and retention in cementitious materials, and to evaluate the relevance of cement alteration processes, such as carbonation, on the solid speciation of radionuclides in aged concrete, combining experimental and computational approaches. A bottom up approach was used to unravel contributions of individual hydration phases on the radionuclide retention behaviour, studying radionuclide interaction with synthesized cement hydration phases, such as various calcium silicate hydrates (C-S-H), monosulphate (AFm) and ettringite (AFt), in addition to hardened cement pastes. With this approach open questions and uncertainties regarding, e.g. the role of hydration phases other than C-S-H on the retention of ^{226}Ra or the relevance of C-S-H with respect to the retention of anionic radionuclide species of Mo, Se or I were addressed.

2. Studied system

The radionuclide uptake was generally determined in batch experiments performed under anoxic conditions in a CO_2-free atmosphere in a glove box. The systems addressed comprised composite hardened cement pastes prepared from commercially available OPC (CEM I, Heidelberger Zement) as well as the CEBAMA reference low pH cement paste provided by VTT (incl. artificially carbonated cement pastes). The various model phases used in the uptake experiments were synthesized using well established procedures and comprised C-S-H0.9, C-S-H1.4, AFt (ettringite), AFm-SO_4, AFm-CO_3, hydrogarnet (C_3AH_6), calcite and portlandite. To address various stages of cement degradation, sorption/uptake experiments with the single hydration phases were performed using different solution compositions such as equilibrium solutions, artificial young cementitious water (pH ~ 13.5) as well as a portlandite-saturated solution (pH ~ 12.5). The radionuclides/-elements used in these studies included ^{226}Ra, $^{99}TcO_4^-$, I^-/IO_3^-, MoO_4^{-2}, and SeO_3^{-2}/SeO_4^{-2}.

3. Main results – Scientific highlights

The results of the experiments with ^{226}Ra revealed a fast radium uptake by the various hydration phases leading to a sorption equilibrium within 10 to 28 days. C-S-H was the only investigated hydration phase showing a significant uptake of ^{226}Ra, whereas the uptake of ^{226}Ra in systems with AFt and AFm phases was found to be distinctively lower. A distinct dependence of the ^{226}Ra uptake by C-S-H on the Ca/Si ration and solution composition was observed. The uptake of ^{226}Ra by C-S-H was found to decrease significantly with increasing Ca/Si ratios, from about 22,000 L/kg (CSH0.9) to 13,000 L/kg (CSH1.4) in alkali-free systems. This effect is probably due to the negative surface charge at Ca/Si < 1.2, facilitating cation uptake, as well as the higher competition with Ca ions in solution for sorption sites at high Ca/Si ratios. The lower R_d values (about a factor of 2) in systems with artificial young cementitious water are probably due to competition with alkalis for sorption sites, as well as changes in C-S-H surface charge and speciation at higher pH. In general, these results suggest a stronger retention and lower mobility of ^{226}Ra in alkali-poor, aged cementitious systems at stage II (portlandite stage) compared to young cementitious materials in stage I. Moreover, the lower Ca/Si ratios of C-S-H in cementitious materials prepared from low pH cements – as well as partly decalcified C-S-H during stage III – should provide for a higher retention capacity for ^{226}Ra than C-S-H in young OPC based systems.

The uptake of ^{226}Ra by C-S-H is generally explained in terms of cation exchange with calcium and sorption to two silanol-like sites at the C-S-H surface. The selectivity coefficients for the ^{226}Ra uptake on C-S-H were calculated from the R_d-values and Ca-concentrations obtained in the sorption experiments. Based on this, we obtained selectivity coefficients for the Ra/Ca exchange in the alkali free systems of log K_c = 2.2 for C-S-H0.9 and log K_c = 1.8 for C-S-H1.4. The comparison with data for other alkaline-earth elements reveals a decreasing affinity for uptake by C-S-H in the order Ra > Ba > Sr. Hence, Sr seems to be no meaningful analogue for the uptake of ^{226}Ra in cementitious systems due to the significantly lower selectivity coefficient. Ab-initio atomistic simulations to investigate the potential of Ra incorporation into the C-S-H structure, as an additional uptake mechanism to surface sorption, using simplified C-S-H structure models based on the 11 Å tobermorite structure. In a first step, a substitution of Ca coordinated to silanol groups in the interlayer spacing by Ra was compared to a structural Ra uptake into C-S-H due to exchange with Ca in the stable octahedral CaO_2 layers. The differences in the enthalpies (reaction enthalpies) for the two configurations computed using the density functional theory (DFT)-based plane-wave Quantum-ESPRESSO simulation code were found to be rather large (184 KJ/mol for C-S-H0.75), with the lower enthalpy related to the Ra uptake into the interlayer. The enthalpy differences were even more pronounced for C-S-H0.9 and C-S-H1.0. This strongly indicates that Ra substitution for interlayer Ca would be highly preferred over incorporation into the octahedral layer. In order to assess the potential of an exchange reaction of Ra from solution with interlayer Ca in the C-S-H, the ΔG of the exchange reaction was estimated from the DFT-reaction-enthalpy (ΔH), using an estimate of the reaction entropy ΔS. The computed data clearly show that the reaction enthalpy and the free energy of the exchange reaction with Ca in the interlayer increase significantly with increase of Ca/Si, consistent with the observed decrease of the Ra uptake with increasing Ca/Si ratios. The distinctively negative free energy computed of the exchange reaction for C-S-H0.75 suggests that the uptake of Ra in the C-S-H interlayer is a plausible mechanism, in particular at low Ca/Si ratios, i.e. in aged cementitious systems or in materials prepared from low-pH cements.

The uptake of ^{226}Ra by HCP prepared from CEM I reached a steady state after about 10 days with an R_d value of ~ 60 L/kg. In contrast, in the sorption experiments using the HCP prepared from VTT low pH cement mixture, equilibrium conditions were not attained in an experimental time frame of 100 days, which, in combination with the changes in solution pH, suggested an ongoing hydration process in this material and the formation of C-S-H with low Ca/Si-ratios from remaining unreacted clinker phases, silica fume and blast furnace slag (BFS). The R_d value obtained at the end of the experiment (12,300 L/kg) can be attributed to both, the lower system pH and the

lower Ca/Si ratio of the C-S-H compared to CEM I based systems, in qualitative agreement with the uptake behaviour observed for the C-S-H phases as the main hydration phase contributing to Ra retention in cementitious systems.

Experiments addressing the impact of carbonation of cementitious materials on the radionuclide retention behaviour showed that ^{226}Ra previously bound to C-S-H is expected to be predominantly released into the pore solution during carbonation, although some Ra might be retained by newly formed calcite. Sorption by or occlusion in the freshly formed calcite might be plausible uptake mechanisms since an incorporation of Ra into the calcite structure instead of Ca is less likely, due to the large size of the Ra ion. Since other cement hydration phases do not provide for a pronounced retention of radium, this effect has to be considered in particular for disposal environments where carbonate-rich ground waters may affect the properties of the cement-based barrier materials in the long-term due to carbonation.

The uptake mechanism for iodine was found to depend essentially on the aqueous (redox) speciation. Structural incorporation of iodide (I^-) by anion exchange in the interlayer was observed for AFm-SO_4 (R_d ~ 800 L/kg). On the other hand, the uptake of iodate (IO_3^-) by AFt as well as by AFm-SO_4 led to the formation of an iodate-substituted ettringite, formed either by anion exchange or phase transformation. Moreover, we observed that the uptake of iodide by AFm-phases is dependent on the nature of the anion complex, with stronger iodide uptake by AFm-SO_4 compared to AFm-CO_3. The increasing uptake of iodide in C-S-H with increasing the Ca/Si-ratio, and thus increasing positive surface charge, is in good agreement with the assumed electrostatic sorption mechanism for iodide on C-S-H, although the iodide uptake by C-S-H is generally lower (R_d 40 … 80 L/kg) compared to AFm/t or hydrogarnet. In general, all model phases showed a higher uptake for iodide and iodate in artificial young cement water compared to the equilibrium solutions, indicating a higher retention potential for iodine in young cementitious systems. The results of the experiments exploring the iodide and iodate sorption on crushed HCP based on CEM I are shown revealed a fast uptake of both iodine with was observed, with slightly higher sorption of iodate (R_d ~ 25 L/kg) compared to iodide (R_d ~ 140 L/kg), in good agreement with the existing literature data. In general, the results obtained for the uptake of iodide and iodate by HCP systems are in qualitative agreement with the results obtained for the single hydration phases under equilibrium conditions, indicating that the major contribution to iodine uptake can be attributed to the minor cement hydration phases like AFm/AFt that exhibit slightly higher R_d values for IO_3^- than for I^-.

The uptake of pertechnetate (TcO_4^-) by the model phases was found to be generally rather low, suggesting that reductants like Fe(II) and/or Fe(II)-containing phases, which were not studied here, may play a key role in technetium retention in cementitious system. In general, these experiments investigating systematically the pertechnetate uptake by all major hydration phases in cementitious systems for the first time, elucidated the high mobility and low retention of TcO_4^- in cementitious environments in the absence of reductants able to produce the significantly less soluble Tc(IV). The uptake of TcO_4^- by ettringite, which was proposed in the literature as a potential retention mechanisms, was found to be week, i.e. the R_d was generally < 1 L/kg, suggesting practically no uptake due to exchange for SO_4-groups. Batch-uptake experiments on crushed HCP were performed to study the potential accumulation of reduced Tc on reductive sites like Fe(II)-bearing phases originating from iron-containing educts used in the cement formulation, such as blast furnace slags (BFS). The uptake experiments conducted for more than 75 days revealed only a minor uptake of TcO_4^-) by HCP. As expected, the distribution ratios of HCP based on CEM I are lower in general (R_d ~ 2 L/kg) compared to the low-pH paste based on the VTT cement mix (R_d ~ 9 L/kg). This can be explained by the lower Ca/Si ratio of the C-S-H in the VTT cement paste and the higher content of Fe(II) and/or sulphides in this material, due to the BFS used in the cement formulation.

As expected, a pronounced molybdate uptake (R_d ~ 1500 L/kg) by AFm-SO_4 and AFm-CO_3 was observed, indicating no preference of the uptake on the nature of the interlayer anion (i.e. planar CO_3 or tetrahedral SO_4) in this case. XRD studies on the AFm-SO_4 used in the batch sorption experiments showed an increase in the basal spacing compared to pure AFm-SO_4, indicating the structural incorporation of MoO_4-ions in the AFm-structure by anion exchange with the interlayer anion, since the size of the molybdate oxo-anions (Mo-O bond length ~ 1.7 Å) is larger than of SO_4-ions (S-O bond length ~1.47 Å). For C-S-H in equilibrium solutions, a dependency of the molybdate uptake on the Ca/Si ratio was found, with higher distribution ratios for C-S-H1.4 (R_d ~ 750 L/kg) compared to C-S-H0.9 (R_d ~ 420 L/kg). These findings are in agreement with the change in surface charge of C-S-H to positive values at Ca/Si ratios exceeding 1.2, suggesting an electrostatic sorption of the molybdate anion on C-S-H. In alkali-rich young cementitious water, distinctively lower R_d values were observed, which might be due to competition with OH^- ions for sorption sites, suggesting lower molybdate sorption and retention by C-S-H in young alkali-rich cementitious systems. These results show that C-S-H phases in cementitious materials can play an important role with respect to the retention of molybdenum, in particular in aged systems (stage II and III). The high molybdate uptake by hydrogarnet (R_d ~ 3000 L/kg) was found to be due to the neo-formation of a molybdenum bearing AFm-like phase, which can be either a pure AFm-MoO_4 phase or a mixture of this phase with the Mo-analogue of the so called U-phase, depending on pH and alkali concentrations in solution.

The retention of the investigated selenium species ($Se^{IV}O_3^{-2}$/$Se^{VI}O_4^{-2}$) was shown to be particularly due to the well-known uptake by AFm phases and to a lesser degree by AFt, which all showed a tendency for a higher uptake of the more oxidised selenium species. Moreover, a distinctively stronger retention of both Se-species by AFm-SO_4 compared to AFm-CO_3 was observed, indicating a preference of the uptake on the nature of the interlayer anion here. In comparison to the aluminate phases, the uptake of selenium by C-S-H was found to be comparatively low (R_d $Se^{IV}O_3^{-2}$: ~ 100 L/kg; R_d $Se^{VI}O_4^{-2}$: ~ 10 L/kg). Due to the higher amounts of aluminate phases in HCP based on CEM I, the retention capacity for the selenite and selenate is higher in this case compared to the low–pH CEBAMA reference paste; remarkably in all cases the HCP showed higher Rd values for $Se^{IV}O_3^{-2}$ than for $Se^{VI}O_4^{-2}$.

Technical Summary – RATEN – WP2

1. Introduction & Objectives

Before involvement in CEBAMA project, the experience of RATEN ICN on radionuclide sorption on cement based materials was limited at few sorption and diffusion tests for ^{3}H and ^{14}C in cement paste based on CEM II cement, but the influence of cement degradation on sorption properties was not addressed in these studies.

Since the radioactive waste generated from Cernavoda NPP (CANDU 600 type) contain large amounts of ^{14}C- and cement based materials represent an important engineered barrier both for the near surface repository, foreseen to be commenced in the near future for short lived radioactive waste disposal, and for the future geologic disposal for long-lived waste and CANDU spent fuel, it was required to deepen our studies on ^{14}C- sorption on cementitious materials, addressing also the influence of cement degradation on sorption properties. Also, radium-226 was included in this study since it is the major daughter nuclides of the ^{238}U that could be found in the fuel-contact spent ion exchange resins but also in other waste streams.

In its review article (Evans, 2008) it is stated that inorganic ^{14}C ($^{14}CO_3^{2-}$) sorption by cementitious materials can be roughly divided into two reactions: (i) adsorption onto a positive site and (ii) precipitation. Real sorption mechanisms for inorganic carbon ($^{14}CO_3^{2-}$) occur only when carbonate levels are well below the threshold point at which precipitation starts (about $1\text{-}2\cdot10^{-5}$ mol/L carbonate). At higher carbonate concentrations, removal of $^{14}CO_3^{2-}$ is by precipitation and not by sorption. The isotopic exchange with solid $CaCO_3$ in cement paste controls the $^{14}CO_3^{2-}$ retention in HCP (Bradbury and Sarott, 1994) but the extent of removal of $^{14}CO_3^{2-}$ is very dependent on the particular cement/concrete system in question. For CSH phases, the experimental results obtained by batch sorption experiments and zeta potential measurements (Noshita et al. 1995) suggested that the adsorption mechanism for the inorganic carbon-14 ($^{14}CO_3^{2-}$) is electrostatic adsorption onto cationic surfaces of CSH phases at high C/S ratio ($-SiOCa^{+}$).

Experimental data on radium sorption on cementitious materials are scarce. For fresh HCP a two-step process could explain the Ra(II) uptake: fast sorption within one day (with K_d value of $26\cdot10^{-2}$ m^3/kg), followed by a slowly increase of Ra(II) uptake over a period of 60 days (to an K_d value of $40\cdot10^{-2}$ m^3/kg) (Tits et al. 2006). Nevertheless, the slow increase in the K_d value can be questioned due to the high uncertainties on the data (Radium activity measurements by alpha spectrometry, at low activity level). There is good evidence that Ra sorption increases as the C/S ratio decreases on CSH. It is assumed that Ra(II) only sorbs on the C-S-H fraction in HCP and that the aqueous Ra(II) speciation is dominated by the Ra^{2+} species.

2. Studied system

Hardened cement pastes (HCP) based on CEM I 52.5 (Ordinary Portland Cement, LAFARGE, Val d'Azergues factory) and CEM V/A 32.5 (blast furnace slag and fly ash added to OPC, HOLCIM, Heming factory) cement were studied in RATEN ICN in the frame of CEBAMA project. These HCPs were prepared with a water/cement ratio of 0.38 and were received in 2016 from ARMINES, where these pastes were kept for almost 7 years after

setting in saturated portlandite water (pH = 12.4), at 20°C to avoid their carbonation. Between receiving time and using them in degradation and sorption tests, the HCPs were also kept in saturated portlandite water at room temperature (20 ± 3°C).

The slices of the two HCPs were crushed and sieved under nitrogen atmosphere (using nitrogen of 99.99 purity) and the 125 – 250 μm fractions were kept both for sorption tests and to prepare three degraded states of the cement pastes. The first two degradation states (deg_I and deg_II) were obtained by hydrolysis leaching process (15 days) in degassed deionized water (DDW) at two solid to water ratios: ~ 3.7 g/L for the first degradation stateand 0.4 g/L for the second one (Pointeau et al. 2004). A more aggressive degradation protocol was applied to obtain the third degradation state (deg_III). The cement pastes were first mixed with ammonium nitrate solution (S/V ratio of 7.8 g/L) to accelerate the chemical degradation and after that the calcium was leached in DDW, at S/V ratio of 0.01 g/L (after contacting with NH_4NO_3 the cement pastes were washed four times with DDW, until the pH of solution was constant).

A stock solution with ^{14}C in carbonate form ($^{14}CO_3^{2-}$) and a ^{226}Ra standard solution (water solution of barium and radium chlorides in HCl, EUROSTANDARD CZ) were used to prepare de contact solutions for batch sorption tests.

Since the two cement pastes were kept in saturated portlandite water for ~ 9 years, it was considered that this artificial cement pore water (ACW) is most suitable to prepare the contact solutions (spiked with ^{14}C and ^{226}Ra, respectively) for batch sorption on non-degraded HCP, while for degraded pastes, the waters resulted from the degradation tests were used to prepare spiked solutions for sorption tests.

3. Main results – Scientific highlights

The influence of cement degradation on ^{14}C and ^{226}Ra uptake were studied by batch sorption/desorption tests carried on non-degraded cement pastes (based on CEM I and CEM V) and three degraded cement pastes (deg_I, deg_II and deg_III). The batch tests were carried out at asolid to liquid ratio of 2.5 g/L (expressed as dry mass determined by ignition of HCP at 1100°C), at room temperature (23 ± 3°C) in polypropylene centrifuge tubes. Before use, the PP tubes were prewashed in 0.1 M HNO_3 and thoroughly rinsed with deionized water. All experiments were carried out in duplicate samples and cement paste weighting, batch preparation, and supernatant sampling were performed under nitrogen atmosphere. Blank batches were prepared for measuring the ^{14}C and respectively ^{226}Ra content the cement pastes and also the radionuclide sorption on the tubes walls was checked. Desorption tests complemented the sorption ones in order to evaluate the reversibility of ^{14}C and ^{226}Ra on HCPs.

Before adding the ^{14}C and respectively ^{226}Ra spiked solutions, all HCP samples were pre-equilibrated with 8 ml of corresponding ACW for 24 hours, and after this pre-equilibration time, the spiked solutions were added.

During the pre-equilibration and equilibration time, the test tubes were gently shaken (horizontally placed on an orbital shaker), at 100 rpm. After equilibration the test tubes were centrifuged at 11,000 rpm for 40 min. The supernatant was separated and the residual activity of ^{14}C and respectively ^{226}Ra in the batch solutions was measured. These ^{14}C measurements were performed by liquid scintillation counting, using counter model 4910 TRICARB Perkin Elmer. ^{226}Ra measurements were achieved by alpha-LSC method, based on the absorption of the ^{222}Rn resulted by ^{226}Ra decay into an immiscible organic scintillator (UltimaGold F) and counting of the alpha-particles emission of ^{222}Rn and its short-lived daughters (^{218}Po and ^{214}Po) using a liquid scintillation counter with alpha-beta discrimination. For each batch solution, two parallel LSC counting vials were measured with a sample to scintillation cocktail ratio of 1 to 10 and 1 to 1, for ^{14}C and ^{226}Ra, respectively.

3.1. Characterisation of cement pastes used in sorption/desorption tests

To correlate the sorption data with the main phases present in the cement pastes, XRD investigations were carried out. These measurements show that as it was expected, the degraded pastes are indeed free of Portlandite (Figure 1) This was also sustained by the TGA analyses that show that the mass loss between 400 - 600°C, the characteristic range for Portlandite decomposition) is lower in all three degraded phases compared to the no-degraded one.

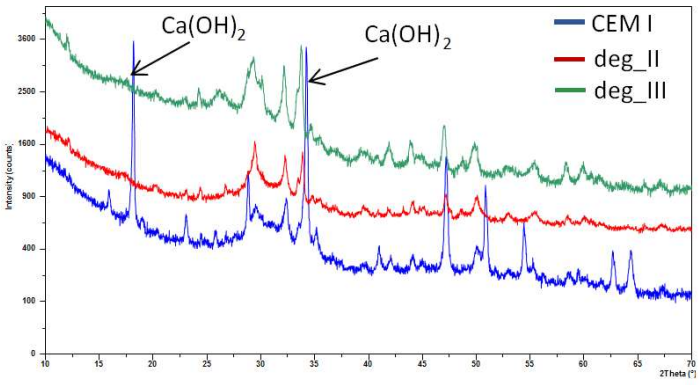

main phase identified, wt %	CEM I			
	non-degraded	deg_I	deg_II	deg_III
Portlandite Ca(O H)2	24	1	1	1
Ettringite Ca6 (Al (O H)6)2 (S O4)3 (H2 O)26	16	18	19	23
Tobermorite Ca3 (Si2O6 (OH)2) (H2O)	8			
Tobermorite13A Ca12 (Si8O28) (H2O)13	8	15	14	24
Tobermorite11A Ca2.25 Si3 O7.5 (O H)1.5 (H2 O)	7			
Tobermorite 9A Ca5 Si6 O16 (O H)2	28	16	19	12
tobermorite 12.5 A Ca7.76 Si6.76 O18.8 (O H)4.88 (H2 O)7.84		9	7	
Clinotobermorite Ca5 Si6 O17 (H2 O)5		16	15	13
Aklimaite Ca4 (Si2O5 (OH)2)(OH)4(H2O)5	8			
Okenite Ca5 Si9 O23 (H2 O)9		24	26	

temperature interval, °C	mass loss, %			
	CEM I			
	non-degraded	deg_I	deg_II	deg_III
22-200 (water)	13.92	10.06	13.13	10.87
200-400 (Ca hydroxy-aluminates)	4.152	5.43	6.99	3.52
400 - 600 Calcium hydroxide	5.83	3.307	2.54	0.739
600-800 (partial carbonation of Ca hydroxy-aluminates)	0.984	1.709	2.815	0.726
800-1000 (cristalyne Ca from admixtures)	0.323	0.054	0.289	0.172
total mass loss	**25.214**	**19.793**	**26.531**	**16.027**

Figure 1: *RD spectra and the main phases identified in non-degraded and degraded CEM I pastes phases (deg_II and deg_III) and the mass loss measured by TGA.*

The extent of Ca content (as it has a strong influence on the uptake of anionic species) in the non-degraded and degraded cement pastes was determined by emission spectrometry carried out on samples resulted by cement pastes dissolution (microwave digestion in HNO_3, HCl and HF). As it was expected, the HCP based on CEM V contain less Ca than the one base on CEM I, mainly due to the lower clinker content of CEM V that has blast furnace slag and fly ash added to the OPC (Table 1). Also, the Ca content in degraded pastes is lower compared with non-degraded ones. These data were also confirmed by EDS investigations, both on non-degraded and degraded cement pastes.

Table 1: *Oxide composition of the cement pastes used in sorption/desorption tests.*

Main oxide content (%)	***CEM I***				***CEM V***			
	non-degraded	***deg_I***	***deg_II***	***deg_III***	***non-degraded***	***deg_I***	***deg_II***	***deg_III***
CaO	49.57	37.26	35.04	22.91	36.52	29.49	26.78	25.31
SiO_2	16.53	16.58	16.54	16.55	22.90	22.90	22.90	22.90

Main oxide content (%)	*CEM I*				*CEM V*			
	non-degraded	*deg_I*	*deg_II*	*deg_III*	*non-degraded*	*deg_I*	*deg_II*	*deg_III*
Al_2O_3	4.13	4.28	4.17	4.55	8.53	8.49	8.63	7.71
C/S ratio	2.99	2.25	2.12	1.38	1.59	1.29	1.17	1.11

3.2.The influence of cement degradation on C-14 uptake

The kinetic tests carried out to evaluate the time needed to attain the sorption equilibrium, showed that after ~ 40 days, for all cement pastes based on CEM I cement, the sorption equilibrium was achieved (Figure 2). Similar time interval is also needed to achieve sorption equilibrium for cement paste based on CEM V cement (Figure 2).

More than 80% from the initial ^{14}C present in contacting solution was sorbed after 40 days on non-degraded CEM I as well as on the first two degraded pastes (deg_I and deg_II), but only ~ 30% was sorbed on the most degraded cement paste used in our experiments (deg_III). $^{14}CO_3^{2-}$ distribution ratio is greatly affected by cement degradation, with values ranging between 1600 ± 268 L/kg for deg_I cement paste, to 120 ± 36 L/kg for deg_III cement paste.

As indicated both EDS and ICP-OES analysis the Ca content in non-degraded CEM I paste is higher than in CEM V cement paste. Nevertheless, sorption data indicate that the $^{14}CO_3^{2-}$ uptake on CEM V cement paste is significant higher compared with CEM I cement paste (3500 ± 275 L/kg).

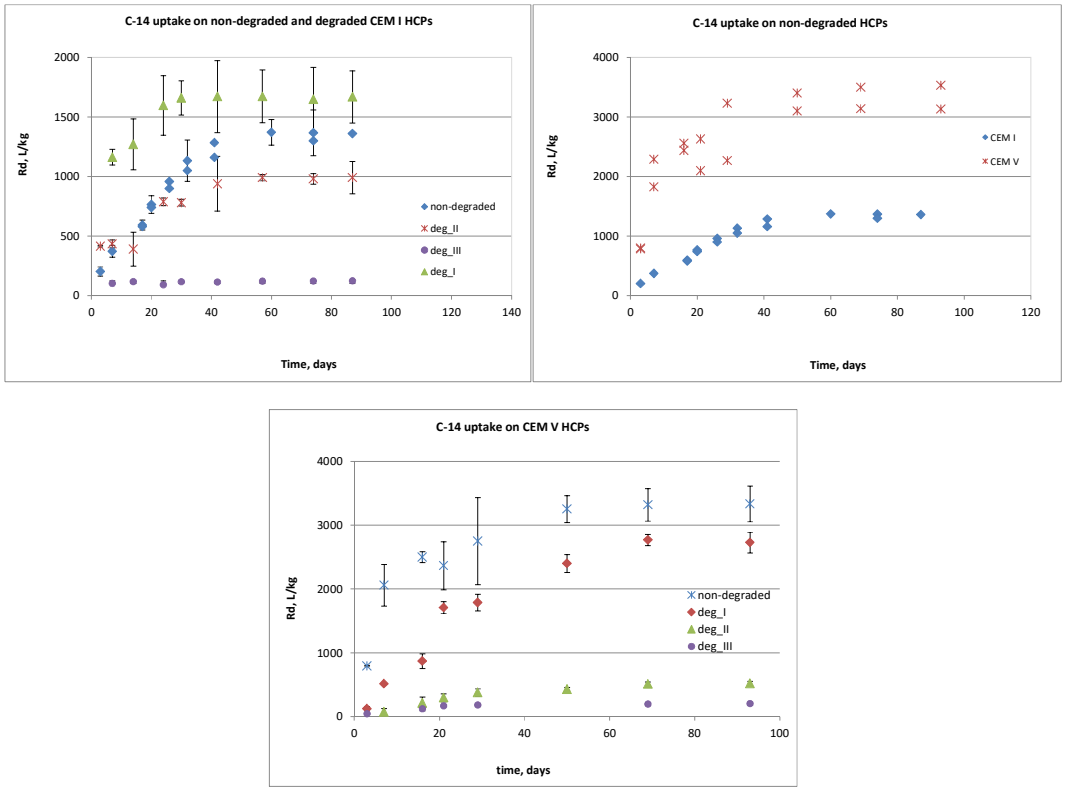

Figure 2: *Evolution of the $^{14}CO_3^{2-}$ distribution ratio on non-degraded and degraded cement pastes.*

In all literature data, isotopic exhange of $^{14}CO_3^{2-}$ with CO_3^{2-} bearing phases (mainly on finely divided calcite) in cement paste is indicated as the main mechanism for $^{14}CO_3^{2-}$ uptake on hydrated cement pastes. Experimental data obtained for ^{14}C uptake on non-degraded and degraded cement pastes indicate that not only isotopic exchange is involved in ^{14}C sorption, but to get insights on the mechanisms involved in ^{14}C uptake, modeling of the sorption experiments have to be carried out. This was identified as the main gap in RATEN ICN regarding studies on radionuclide sorption on cementitious materials that has to be overcome in the near future.

The higher $^{14}CO_3^{2-}$ concentration in the contact solutions was $1.2 \cdot 10^{-7}$ M, and it was assumed it is well below the solubility of carbonate in portlandite saturated water (~ $6 \cdot 10^{-6}$ M). However, since we didn't measure the total C content in the sorption system, precipitation of ^{14}C containing calcite could not be excluded. This could explain the results of desorption tests (carried out for non-degraded CEM I and on most degdaded paste deg_III) that indicated that the desorption equilibrium is attained in slightly longer time than the sorption one (~ 60 days) and around 80% from the ^{14}C sorbed was desorbed in this time.

3.3. The influence of cement degradation on ^{226}Ra uptake

Similar experiments as those performed for ^{14}C sorption on non-degraded and degraded HCPs were also carried out to investigate the influence of cement degradation on ^{226}Ra sorption. For these tests, ^{226}Ra activity in contact solution was 45 Bq/mL.

The results from the kinetic sorption tests indicate that most of the ^{226}Ra was sorbed mostly in the first 2 days of contacting (sorption percentage ~ 33% for CEM I and 35% for CEM V). After two days, radium uptake slowly increase up to 20 days for both cement pastes, up to an distribution ratio of ~ 300 L/kg for CEM I and ~ 400 L/kg for CEM V (Figure 3). No significant increase was observed in radium uptake between 20 and 80 days of contacting, indicating that 20 days of contacting are enough to attain the sorption equilibrium.

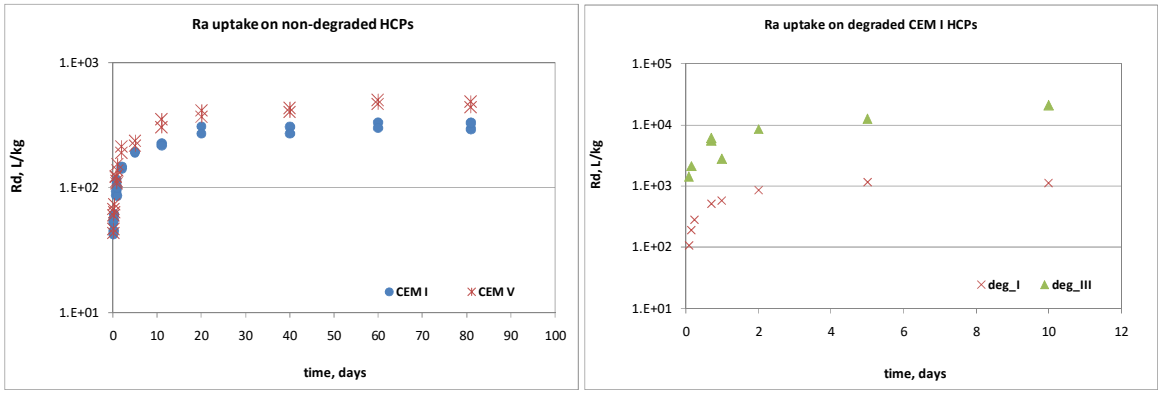

Figure 3: *Evolution of the Ra^{2+} distribution ratio on non-degraded and degraded cement pastes.*

For degraded cement pastes, the kinetic tests were carried out for deg_I and deg_III pastes. These tests showed that for degraded pastes the Ra uptake is faster that for non-degraded pastes, with sorption equilibrium achieved in two days of contacting, and only small increase was found between 2 and 10 days of contacting. The radium uptake on these two degraded pastes is significantly higher than on the non-degraded one (~ 1000 L/kg for deg_I and ~ 20,000 L/kg for deg_III).

Experiments for deriving the sorption isotherms were carried out for ^{226}Ra activity in contacting solution between 45 Bq/mL and 136 Bq/mL, for 20 days of contacting for non-degraded pastes and 10 days for degraded ones. The experimental data were well fitted with linear sorption isotherms (Figure 4). These tests also show that Radium seems to have an higher distribution ratio on CEM V compared to CEM I cement paste.

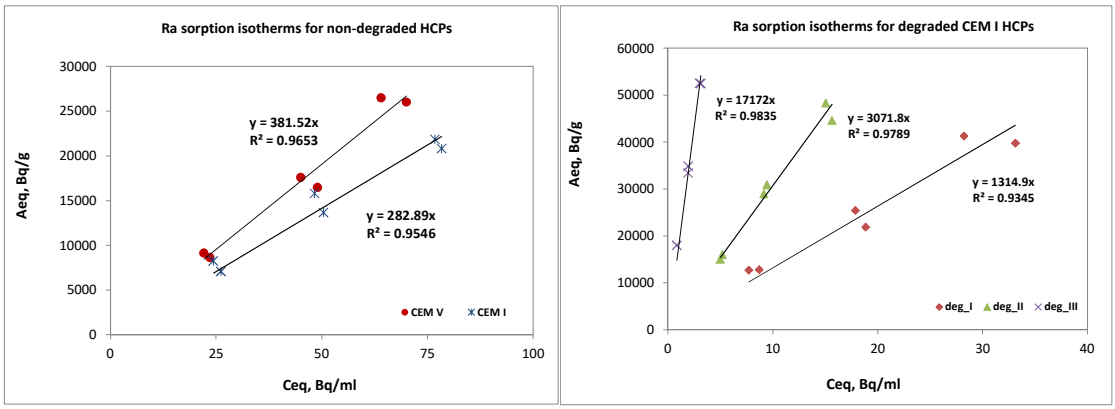

Figure 4: *Ra^{2+}sorption isotherms on non-degraded and degraded HCPs.*

Reversibility of radium sorption on non-degraded cement pastes were assessed by desorption tests. These tests indicated that Radium desorption is much slower that its sorption. Around 40% from radium sorbed on CEM I and ~ 20% from the radium sorbed on CEM V was desorbed after 20 days. Even after 80 days of desorption, the desorption percentage is still slowly increasing.

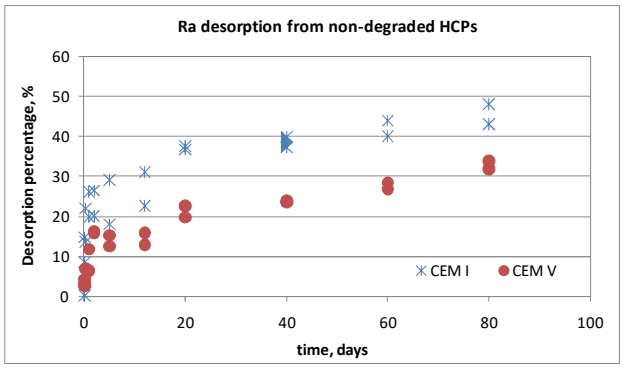

Figure 5: *Evolution of Ra desorption percentage on the non-degraded cement pastes.*

Technical Summary – Armines/Subatech – WP2

1. Introduction & Objectives

In a nuclear waste repository, cement-based materials play an important role either as engineered barriers or as confinement matrices for some Intermediate Level Long-Lived (IL-LL) waste. During the operation period of the facility (ventilation) or after its closure (production of corrosion gas by specific waste), unsaturated conditions may arise and thus induces changes in the environmental conditions of cement-based materials. As an example, the ventilation of underground galleries imposes specific conditions (relative humidity, presence of CO_2) that will modify the hydric state of cement materials (surfacial drying, desaturation) and favour a potential carbonation. These two processes (drying and carbonation) are known to induce changes in the microstructure of cement-based materials (Roosz, 2016; Shah, 2018) and thus may have a potential impact on the diffusion properties of mobile radionuclides (RN) present in waste packages. In recent literature, only few studies exist on the evolution of water (or solutes) diffusion properties in unsaturated conditions (Dridi and Lacour, 2014; Zhang, 2014; Patel, 2016; Savoye, 2018) because of experimental difficulties for acquiring diffusion parameters. Moreover, to our knowledge, none exists on the effect of a drying/rewetting cycle. Concerning carbonation, this process has been intensively studied for decades due to its importance in civil engineering (Auroy et al. 2015; Shah et al. 2018, and references therein). The main consequences of this process are: i) decreasing of pH in the cement pore water, ii) changing cement mineralogy (dissolution of Portlandite, progressive decalcification of C-S-H phases), iii) modifying cement microctructure by precipitation of calcite in the open porosity (clogging) or formation of microcracks depending on the nature of cement. All of these process may have impacts on water and RN diffusion properties.

In literature, very few sorption (and none reversibility) data exists for ^{14}C in fresh non carbonated HCP (pH = 13.5). Pointeau et al. (2008) reported a distribution ratio (R_d) value of 600 L/kg for a CEM I HCP (pH = 13.2). In cement-based materials, ^{14}C may react by isotopic exchange with calcite which is considered as the main phase for ^{14}C uptake in "real" materials (such as mortar or concrete). ^{14}C may also react with Portlandite and C-S-H. For C-S-H, a fast sorption mechanism is suggested with rather low Rd values (40 L/kg) (Henocq et al. 2018).

The objectives of the project are i) to investigate the effect of a drying/rewetting cycle, unsaturated condition (at high water saturation (S_w = 0.85)) and carbonation process on tritiated water (HTO) diffusion properties in fresh and carbonated hardened cement pastes (HCP), ii) to investigate the uptake (and reversibility) and transport properties of ^{14}C (as carbonate ions) on carbonated and non-carbonated (HCP).

2. Studied system

HCP samples used were disks (2 mm thick) of a CEM V/A hardened cement paste (HCP) prepared with a water to cement ratio of 0.43 and cured at least 27 months in an artificial cement pore water (ACW; pH ~ 13.5) (Savoye, 2018). The drying stage consisted of storing HCP samples during several months (20 ± 1°C under Ar atmosphere) at fixed relative humidity (RH) imposed by saturated saline solutions (80%, 70% and 55% RH).

Thus, the initial S_w values were 0.85, 0.72 and 0.63 respectively. Afterward, HCP samples were resaturated with ACW (under vaccum). Additionally, a fully saturated sample was used as a reference. Carbonated samples were prepared in conditions representative of atmospheric carbonation (Auroy, 2015). An accelerated carbonation process was performed in a climatic chamber (P_{CO2} = 3 vol.%, RH = 55% in order to obtain a maximal carbonation rate). Through-diffusion experiments (TD) were performed, in duplicate, using standard two-reservoir set-ups. The effective diffusion coefficient, D_e(HTO) and material capacity factor, α were obtained by modelling the HTO cumulative activity curves (in the downstream reservoir) with a routine based on an analytical solution of Fick laws (with fixed initial and boundary conditions). For TD experiments in unsaturated condition, the osmotic technique was used for imposing a high S_w (0.84). This technique consists of generating a water suction by an osmosis process between cement pore water and a highly concentrated solution of polyethylene glycol PEG (Savoye, 2010). HCP samples are separated from a PEG solution by a semi-permeable membrane (permeable to water molecules and all dissolved species but PEG). The exclusion of PEG from the sample pore water produces a chemical potential imbalance between the pore water and the external solution. This osmotic suction has the effect of keeping the sample partially saturated. A mass concentration of 0.95 kg of PEG/$kg_{solution}$ has been chosen in order to reach a maximal suction potential of 9 MPa leading to a S_w value of 0.84. HCP samples used for these experiments were conditionned beforehand at 55% RH. ^{14}C batch experiments were carried out at ambient temperature (20 ± 1°C) in polypropylene tubes with a solid to liquid ratio of 25 g/L. Samples were pre-equilibrated in ACW pore water during one week before the addition of ^{14}C ($NaH^{14}CO_3$) spike. Tubes were centrifuged (4000 rpm; 30 min) and supernatants aliquots were sampled, weighted and analyzed by beta liquid scintillation counting. Desorption experiments were performed at the end of the sorption step. Supernatants were then replaced by the same volume of ACW (free of ^{14}C). Preparation (except for carbonated HCP) and experiments were performed in a glove box (under Ar) in order to avoid atmospheric carbonation.

3. Main results – Scientific highlights

3.1 HTO transport properties

TD experiments were performed for determining HTO diffusion parameters for three different conditions. The effects of a drying/rewetting cycle and of an unsaturated condition (S_w = 085) were investigated on fresh non-carbonated HCP whereas the effect of carbonation was investigated on fresh carbonated HCP. Transport parameters (effective diffusion coefficient, D_e(HTO) and material capacity factor (α)) are determined by modelling the normalized cumulative activity in the downstream reservoir with a least-square fitting based on Crank analytical solution (Eq.1).

$$Q(t) = \frac{q(t)}{L * S * A_0} = D_e \frac{t}{L^2} - \frac{\alpha}{6} - \frac{2\alpha}{\pi^2} \sum_{n=1}^{\infty} \frac{(-1)^n}{n^2} e^{\left(-\frac{D_e n^2 \pi^2 t}{\alpha L^2}\right)} \qquad \text{Eq. 1}$$

where Q(t) is the normalized total cumulative activity (Bq), q(t) is the normalized cumulative activity in the downstream reservoir (Bq), A_0 the initial activity per volume unit in the upstream reservoir (Bq/m^3); *t*, the time (s); D_e, the effective diffusion coefficient (m^2/s) and α the material capacity factor (-).

In our experimental conditions, the steady-state diffusive flux is achieved after 100 days for most of experiments. As an example, the normalized cumulative activity curve of the reference sample (fully hydrated non-carbonated HCP) is given Figure 1. HTO transport parameters for each experiments are reported in Table 1.

Table 1: *HTO transport parameters values for all experiments.*

Experiments/Effects	*Sample identification*	*D_e(HTO) (m^2/s)*	*α (-)*
Drying/rewetting cycle	Reference (not dried ;fully saturated)	3.9 (0.4)	0.34*
	Dried at 80% RH	3.8 (0.4)	0.34*
	Dried at 70% RH	3.0 (0.6)	0.34*
	Dried at 55% RH	5.1 (0.5)	0.34*
Unsaturation (S_w = 0.85)	Unsaturated	11 (1)	1.7
Carbonation process	Carbonated sample	13 (1)	0.21*

* from water porosity measurement; values into parenthesis indicate uncertainty ranges

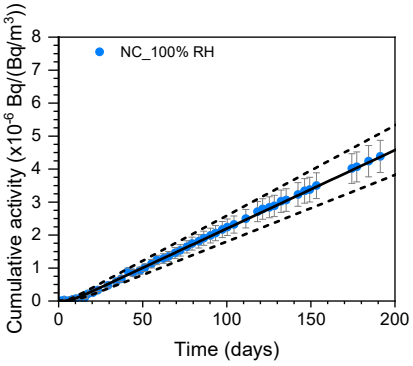

Figure 1: *Normalized cumulative curve for HTO (reference sample). Experimental points (in blue), modelling (black solid line), error ranges (black dotted line).*

D_e^{ref}(HTO), obtained for the reference sample, is 3.94 ± 0.4 10^{-13} m^2/s which is in agreement with literature data for this materials (Savoye, 2018; Landesman, 2018).

For the drying/rewetting cycle, the results show that up to 70% RH, the drying step (before the rewetting step) seems to have no influence on D_e(HTO) since the values are similar to the reference's one. Nevertheless, when samples experienced a stronger drying step (at 55% RH), D_e(HTO) values slightly increase. This behaviour is consistent with the description of the effect of drying on C-S-H (main phases of HCP) given by Roosz (2016). Briefly, in the range 75 - 98% RH, desorbed water molecules come from capillary pores (pores between C-S-H particles) whereas below 75% RH (up to 5% RH), desorbed water molecules come globally from water multilayers adsorbed at the surface of C-S-H particles. As the drying process is not a homogenous process, some C-S-H particles are more dehydrated than others (even if the drying step is moderate). In this case, water molecules are desorbed from the interlayer space of C-S-H particles that may induce a local collapse of the interlayer space and the aperture of new pores (mesoporosity).

This process is a local phenomenon and has generally no impact on the total porosity of the material. Based on the description, the slightly higher value of D_e(HTO) (at 55% RH) is interpreted as due to the presence of a mesoporosity which locally favours the transport of HTO in pore network without modifying the total water accessible porosity.

For unsaturated condition (S_w = 0.85), D_e(HTO) is four times higher than the reference value (S_w = 1) which is the inverse trend of what it is expected (decrease of D_e(HTO) as S_w diminishes). However, as the drying step (at 55% RH) already increases D_e(HTO) by a factor of two, it appears that the unsaturated condition (S_w = 0.85)

acts only by doubling HTO diffusivity. This additional increase of D_e(HTO) is not yet clearly understood. But one hypothesis is that, in our experimental conditions, some changes in HCP microstructure have been produced by the osmosis process (e.g. microcracks due to locally heterogeneous desaturation) and this has induced direct consequences on HTO diffusion parameters (increase of D_e(HTO) and α).

For carbonated HCP samples, the drying/rewetting cycle results in an increasing of D_e(HTO) by a factor of 3 with respect to the reference. This result is consistent with the impact of carbonation on CEM V HCP as recently described by Auroy (2015). In fact, unlike Portland HCP for which porosity clogging, due to the precipitation of $CaCO_3$ (carbonation of Portlandite) in pores is the main consequence of the carbonation process, for composite cement HCP (such as CEM V), carbonation process induces the formation of microcracks (due to C-S-H decalcification, subsequent polymerization which generates shrinkage and eventually cracks). Globally, microcracks act then as a connected porosity network. The increase of D_e(HTO) value supports the conclusion that, for carbonated CEM V HCP, microcracks participate to HTO diffusion pathway. Nevertheless, during through-diffusion experiments with fully saturated samples, conditions (presence of water) are favorable to a self-sealing process to occur in microcracks network, thus reducing D_e(HTO) values.

3.2. ^{14}C (as carbonates) sorption/desorption properties

The aim of this part was to acquired ^{14}C sorption and desorption kinetics data on both carbonated and non-carbonated dispersed HCP samples. ^{14}C concentrations used were well below calcium carbonate solubility limits ($1.6 \cdot 10^{-4}$ mol/L). Desorption experiences started at the end of the sorption step (after 110 days) for a duration of circa 90 days. Results for both sorption and desorption steps are reported in Figure 2a and Figure 2b.

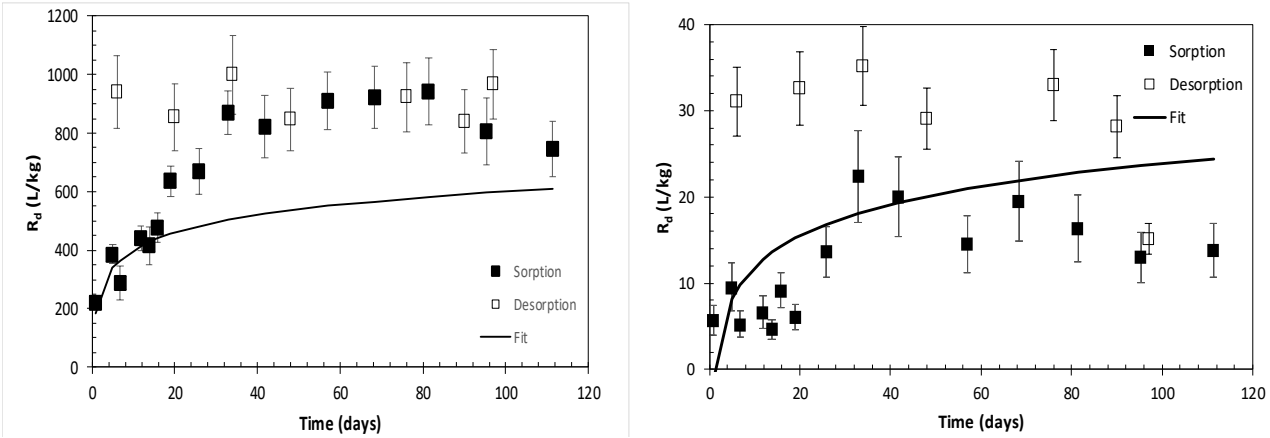

Figure 2: *Evolution of ^{14}C distribution ratios (R_d) vs time on non-carbonated (left) and carbonated HCP (right); solid lines (fit). Initial ^{14}C concentration $6 \cdot 10^{-8}$ mol/L.*

For non-carbonated HCP, the steady-state is reached after around 60 days. The corresponding $R_d(^{14}C)$ value is (750 ± 100) L/kg which is close to data obtained by Pointeau (2018) on CEM I HCP at pH = 13.2 (500 L/kg). Results from desorption experiments show that the uptake process at trace level seems to be reversible. Nevertheless, for higher concentrations ($5 \cdot 10^{-6}$ - $5 \cdot 10^{-4}$ mol/L), sorption/desorption isotherms show that ^{14}C uptake is clearly a non-reversible process ($R_{d,desorption} > R_{d,sorption}$ by on order of magnitude). For non-carbonated HCP, ^{14}C can be either adsorbed on C-S-H or exchanged (isotopically) on the "residual" calcite (always present as dispersed particles in cement paste at ~ 5% in mass).

For carbonated HCP, the steady-state is reached after 40-50 days and the corresponding $R_d(^{14}C)$ value is 20 ± 5 L/kg. In literature, there is no data on $R_d(^{14}C)$ on carbonated HCP at pH = 13.5, but this value is comparable to Pointeau et al's data (cited in Henocq, 2018) obtained on calcite in 0.1 mol/L NaOH solution ($R_d(^{14}C)$ = 10 - 20 L/kg). Results from desorption experiments show $R_{d,desorption}$ values slightly higher (30 ± 5 L/kg) than $R_{d,sorption}$ values. In this case, the non-reversibility is consistent with the uptake of ^{14}C on calcite by a two-step mechanism (isotopic exchange and subsequent incorporation (solid diffusion) in calcite).

In order to go further on the description of ^{14}C uptake by HCP, an attempt of simulation has been performed by applying the very recent modelling approach proposed by Henocq et al. (2018) and developed from ^{13}C isotopic exchange data on nano-calcite. This model interprets kinetics uptake data using a solid 1D-diffusion model with two parameters (solid diffusion coefficient (D) and calcite particles size). It was applied on different types of materials (calcite, calcareous sands, HCP, mortars). For nano-calcite, the value for D was determined as $6.6 \cdot 10^{-25}$ m^2/s. A first attempt for simulating our uptake data was done using this value of D and various granulometry for calcite as no measurement of calcite size was done in this study. The first results are shown in Figure 2 for both materials. It is clear that an improvement of simulations has to be done but these first results are very encouraging.

3.3. Transport properties of ^{14}C in non-carbonated and carbonated HCP

This aim of this part was to test a digital autoradiography technique (Beaver system, AI4R, France) for estimating diffusion coefficients of ^{14}C in non-carbonated and carbonated HCP samples. For those two materials, ^{14}C diffusion experiments were started (at the end of HTO TD experiments) by spiking the upstream reservoir with 2 MBq/L of ^{14}C ($[^{14}C] = 8.6 \cdot 10^{-7}$ mol/L). Experiences lasted 1 year approximatively. ^{14}C diffusion profiles were acquired during 24 h (after cutting samples in two parts and embedding them into resin).

Preliminary results (images and profiles) are reported in Figure 3. On images, the diffusion direction (upstream → downstream reservoir) is indicated by an orange arrow.

For non-carbonated HCP sample, ^{14}C distribution ^{14}C is clearly located in a single zone at 200 - 300 µm depth below the surface (on the upstream side). ^{14}C diffusion seems to have no impact on the rest of the sample (dark zone up to the downstream side at 2.1 mm). The profile, extracted from this image (at each depth, the intensity of pixels is sum over the total width of the sample), gives an estimated diffusion depth for ^{14}C equal to 240 µm.

For carbonated HCP sample, it clearly appears that ^{14}C has penetrated more deeply into the sample. The distribution of ^{14}C shows a 500 µm depth dense zone, below the surface (on the upstream side) followed a more diffuse zone (up to at least half of the sample total depth). Thus, the maximum estimated diffusion depth would be around 1.2 mm.

A routine, based on an analytical solution of Fick laws applied to in-diffusion experiments, was used to calculated ^{14}C diffusion coefficient from profile data (maximum estimated diffusion depth) and $R_{d,sorption}(^{14}C)$ values (estimated from batch experiments). For both HCP samples, the maximum value for ^{14}C diffusion coefficient is below 10^{-13} m^2/s. Nevertheless, more profile data (and so experiments) are necessary for constraining more strongly this estimation. Comparison with other techniques, such as micro-abrasion would surely be very helpful for this purpose.

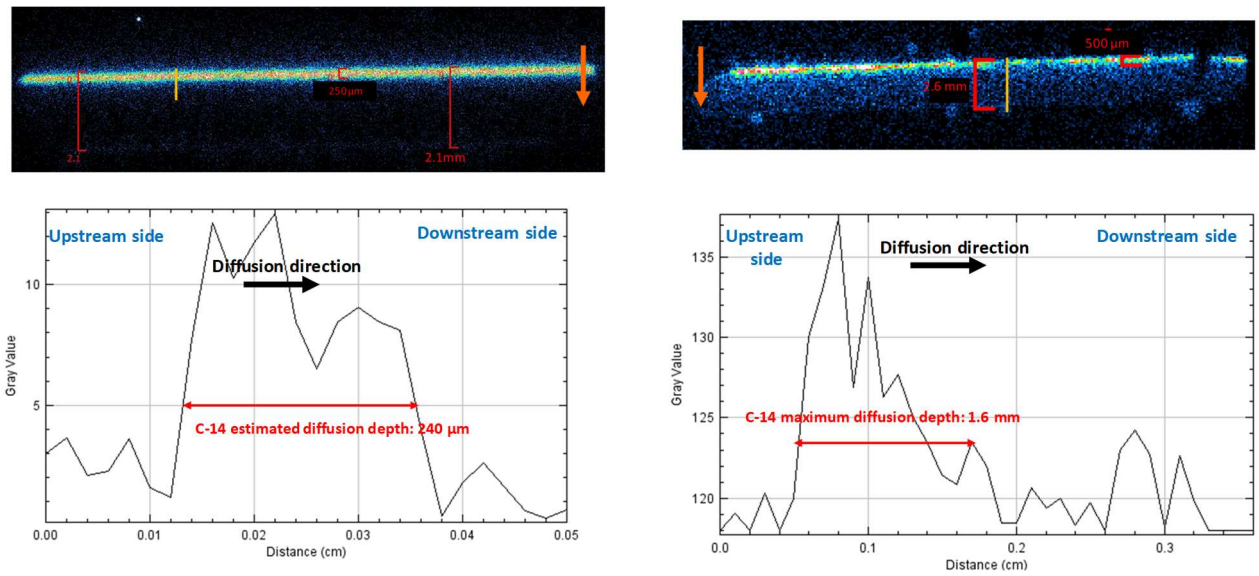

Figure 3: *Image (up) and profile (down) of non-carbonated (left) and carbonated (right) HCP samples at the end of ^{14}C diffusion experiments.*

References

Auroy, M., Poyet, S., Le Bescop, P., Torrenti, J.M., Charpentier, T., Moskura, M., Bourbon, X. (2015). Impact of carbonation on unsaturated water transport properties of cement-based materials. Cement and Concrete Research, 74, 44-58.

Dridi, W. and Lacour, J.L. (2014). Experimental investigation of solute transport in unsaturated cement pastes. Cement and Concrete Research, 63, 46–53.

Henocq, P., Robinet, J.-C., Perraud, D., Munier, I., Wendling, J., Treille, E., Schumacher, S., Hart, J., Dijkstra, J.J., Meeussen, J.C.L., Capouet, M., Meert, K., Vandoorne, T., Gaggiano, R., Dorado, E., Nummi, O., Diaconu, D., Constantin, A., Bucur, C., Grigaliuniene, D., Poskas, P., Narkuniene, A., Vokál, A., Vetešník, A., Ferrucci, B., Levizzari, R., Luce, A., Rübel, A., Gray, L., Carter, A., Mibus, J., Smith, P., Kämpfer, T. (2018). Carbon-14 Source Term (FP 7 European Project CAST). Integration of CAST results to safety assessement D 6.3 report 06/06/2018).

Landesman, C., Macé, N., Radwan, J., Ribet, S., Bessaguet, N., David, K., Page, J., Henocq, P. (2018). Effect of high saline alkaline conditions onto radionuclide transport in a CEM V/A hardened cement paste. 3rd International Symposium on Cement-based Materials for Nuclear Wastes (NUWCEM), October 24-26, (Avignon, France).

Patel, R.V., Phung, Q.T., Seetharam, S.C., Perko, J., Jacques, D., Maes, N., De Schutter, G., Te, G., Van Breugel, K. (2016). Diffusivity of saturated ordinary Portland cement based materials: a critical review of experimental and analytical modelling approaches. Cement and Concrete Research, 90, 52–72.

Pointeau, I., Coreau, N., Reiller, P. (2008). Uptake of anionic radionuclides onto degraded cement pastes and competing effect of organic ligands. Radiochimica Acta, 96, 367-374.

Roosz, C., Gaboreau, S., Grangeon, S., Prêt, D., Montouillout, V., Maubec, N., Ory, S., Blanc, P., Vieillard, P., Henocq, P. (2016). Distribution of Water in Synthetic Calcium Silicate Hydrate. Langmuir, 32, 6794-6805.

Savoye, S., Rajyaguru, A., Macé, N., Lefèvre, S., Spir, G., Robinet, J.C. (2018). How mobile is tritiated water through unsaturated cement-based materials? New insights from two complementary approaches. Applied Radiation and isotopes, 98-106.

Shah, V., Scrivener, K., Bhattacharjee, B., Bishnoi, S. (2018). Changes in microstructure of cement paste on carbonation. Cement and Concrete Research, 109, 184-197.

Zhang, Y. and Zhang, M. (2014). Transport properties in unsaturated cement-based materials– A review. Construction and Building Materials, 72, 367–379.

Technical Summary – CTU – WP2

1. Introduction & Objectives

Originally, in the planned experimental study of behaviour of ^{226}Ra in contact with cementitious materials, data for the development of models of interaction of this radioisotope with cementitious barrier materials should be collected. The preparation of methodology necessary for a case study of LLW-ILW repository Bratrství located in Czech Republic with engineered barriers based on cementitious materials should follow (not as a part of the Cebama project). Since a significant amount of low and intermediate radioactive wastes containing radium is already stored there, the repository will be closed in the near future and the work should be completed in form of a transport model in the near-field region soon. Nevertheless, during the Cebama project, the focus of SURAO (the Czech Radioactive Waste Repository Authority) has moved to the issue of deep geological repository (DGR). In the Czech concept the cementitious materials will be used mainly for construction purposes and also as a barrier material (e.g. fibre concrete containers for ILW, sealing and separation concrete plugs, floors, walls, supporting construction elements, shotcrete, grouting). It is possible that the role of cement as a barrier will deepen due to its influence on corrosion. The content of the ^{226}Ra as a daughter of ^{238}U in spent nuclear fuel will be important in the horizon of at least 10^5 years.

There have not been many studies available at the time the Cebama project started dealing specifically with radium behaviour in contact with cementitious materials. Strontium was usually considered an analogue of radium. An approach utilizing this fact was chosen by CTU DNC for the preliminary methodological sorption study on hydrated cement paste that corresponds with that of other laboratories. Our aim was to gain experience and knowledge about optimal experimental conditions and procedures while working with hydrated cement pastes. The intention was then to utilize isotope ^{226}Ra, which is problematic in terms of the safety of experimental work. Instead of the isotope with relatively long-lived gaseous daughter product ^{222}Rn, ^{223}Ra gained via ^{227}Ac/^{227}Th/^{223}Ra generator was used in the uptake study and diffusion studies eventually.

The description of interaction of radionuclides with cementitious materials, which is necessary in modeling of radium transport in the repository environment, belonged to our intentions too.

2. Studied system

In accordance with the Czech program of radioactive waste disposal with SURAO being the end-user, the methodology of sorption on crushed hydrated cement paste (prepared with water/cement ratio w = 0.667) in our laboratory was implemented via the study of the ^{85}Sr uptake during preliminary sorption experiments on a cement of CEM II grade. CEM II / A-S 42.5 R (produced by Lafarge Cement, a.s.) was chosen for the study of sorption behavior of strontium that served as an analog of radium. As a liquid phase, leachate of the hydrated cement paste (V/m = 5 L/kg, contact time 1 month, pH = 12.8) was then used. Afterwards, first sorption experiments with ^{223}Ra (gained via ^{227}Ac/^{227}Th/^{223}Ra generator) were performed also on another cement of type CEM II (CEM II / B-M (S-LL) 32.5 R - produced by Českomoravský cement, a.s.; Heidelberg Cement Group). This material is Portland composite cement of the strength class made of clinker, granulated blast furnace slag (approx. 15%), of limestone (approx. 12%), and with low TOC content and anhydrite as retarder, and was utilized only in the orientative stage

of the work. On the other hand, the cement CEM II / A-S 42.5 R (hydration for 6 months) was used throughout the project. This cement material is made by grinding together silicate clinker, blast furnace granulated slag (max 20%) and gypsum. Also retardation properties of other cementitious materials were studied – a concrete containing the type of cement CEM I 42.5 (with fine and rough aggregate and fly ash, hydration for 1 month) utilized in ÚJV Řež a.s. to stabilize the solidified solid waste container, and a concrete with the type of cement CEM III B/32.5 (produced by CEMEX Czech Republic, s.r.o., with fine and rough aggregate, hydration for 1 month) used to fill chambers in intermediate radioactive waste repository Richard. All solid materials were prepared in the form of blocks hydrated in a highly humid environment for at least 19 days. For sorption and diffusion experiments these prepared hydrated materials were crushed and sieved for fraction ≤ 0.4 mm and contacted with two types of liquid phases with initial pH around 12.5. It was the filtered saturated $Ca(OH)_2$ (Portlandite water) or the synthetic cement pore water (CPW) with a composition that represents a deeper circulation of groundwater (Table 1) in the fissure environment of the crystalline rocks of the Bohemian Massif mixed with saturated $Ca(OH)_2$.

Table 1: *Composition of synthetic granite groundwater.*

Ion	Na^+	K^+	Mg^{2+}	Ca^{2+}	Cl^-	F^-	HCO_3^-	SO_4^{2-}	NO_3^-	PO_4^{3-}
***c* (mmol/L)**	0.71	0.05	0.35	0.88	0.09	0.02	2.7	0.19	0.03	0.04

3. Main results – Scientific highlights

The experimental work in the Cebama project carried out by CTU DNC focused on Ra interaction with cementitious materials. The aim was to obtain data for the development of models of interaction of Ra with cementitious barrier materials which would eventually lead to the preparation of methodology necessary for a case study of LLW-ILW repository Bratrstvi (Czech Republic), that is of SURAO interest. For this reason, within the project unconventional types of cements were selected. The evaluation of experiment was supported by our activities realized within WP3.

3.1. Characterization of cement materials

Cementitious materials CEM II/A-S 42.5 R and CEM II/B-M (S-LL) 32.5 R were evaluated by pycnometric method, B.E.T., FTIR, and X-ray diffraction. Both materials differ significantly, particularly in the specific surface area and composition. Density of hydrated cement paste made of CEM II/A-S 42.5 R was determined as equal to 2177 ± 44 kg/m^3 by a pycnometric method on crushed material. Specific surface area obtained value by the means of the rapid dynamic flow method for determinations of single-point B.E.T. was 20.1 ± 0.3 m^2/g. The comparison of measured spectrum by X-ray diffraction with database ICDD PDF-2 (version 2013) enabled to identify four mineral phases, namely calcite $CaCO_3$, portlandite $Ca(OH)_2$, hydrotalcite $Mg_6Al_2CO_3(OH)_{16}\cdot 4H_2O$ and ettringite $Ca_6Al_2(SO_4)_3(OH)_{12}\cdot 26H_2O$. FTIR spectra were obtained using the Attenuated Total Reflection (ATR) technique in the scan range of 400 - 4000 cm^{-1}. Leaching of hydrated cement paste to water (V/m = 10 L/kg) for 3 months caused only a very small change in the FTIR spectrum. For the CEM II/B-M (S-LL) 32.5 R hydrated cement paste the results were: density 1998 ± 29 kg/m^3, specific surface area 48.5 ± 0.3 m^2/g, only calcite and portlandite identified by X-ray diffraction. Findings valid for FTIR are the same for both cement materials. Also, characterictics of both concrete materials (Concrete UJV and Concrete Richard) were determined. By means of X-ray diffraction, portlandite $Ca(OH)_2$ and quartz SiO_2 presence was confirmed. Value of specific surface area was 12.65 ± 1.3 m^2/g for Concrete UJV; and 8.37 ± 0.2 m^2/g for Concrete Richard. The mass of solid phase used in the experiments was corrected for the moisture content (determined after 3 days drying at 105°C).

3.2. Study of ^{85}Sr and ^{223}Ra uptake on cement materials relevant for LILW disposal in the Czech Republic

The preliminary study of ^{85}Sr uptake on the cement of CEM II grade (CEM II/A-S 42.5 R) in the form of crushed hydrated cement paste was done. Strontium was used as an analog of radium mainly due to our routine experience with this element. The leachate of the crushed hydrated cement paste of CEM II/A-S 42.5 R contacted with distilled water for 1 month (V/m = 5 L/kg, pH = 12.8) was utilized as a working solution. Important cations were determined by AAS; their concentrations were 5.88 mmol/L Na^+, 23.8 mmol/L K^+, 13.5 mmol/L Ca^{2+}, and 0.35 mmol/L Sr^{2+}. Content of the naturally occuring strontium in the leachate was considered relatively high and therefore, the mean q_0 value of the exchangeable Sr in the solid phase (4.04 ± 0.26 mmol/kg) was determined. $SrCl_2$ was added to the leachate to obtain the desired Sr concentration (0.35 – 2 mmol/L) traced by isotope ^{85}Sr. The observed kinetics of ^{85}Sr uptake, independently of the V/m ratio in the range from 3 to 30 L/kg, was relatively fast reaching equilibrium after 1 day (verified for 4 days).

The uptake experiments were therefore done after 96 hours of contact between liquid and solid phase. The V/m ratios ranged from 3 to 100 L/kg. The equilibrium value of distribution coefficient (K_d) was then determined, based on the activity change corresponding to spikes used (^{85}Sr and subsequently ^{223}Ra). The evaluated distribution coefficient K_d of ^{85}Sr increased with decreasing V/m ratios with the values in the range of 11.4 to 26.5 L/kg, independently of initial Sr concentration in working solution. It turned out that in the transition to other materilas (both concretes), this trend remains. The K_d values are essentially unaffected by the type of the solid material, the presence of the carrier and even with the increasing temperature (Table 2 and Table 4). This finding can be pointed out as evidence that isotopic equilibrium (^{85}Sr – stable isotopes ^{87}Sr and ^{88}Sr) was maintained in experiments performed and that the uptake of Sr was not concentration dependent. The only exception is the behavior of Sr uptake on cementitious materials at the phase ratio V/m = 1000 L/kg where bigger fluctuations of K_d values can be observed (Table 2 and Table 4).

Table 2: *Distribution coefficients K_d (L/kg) for Sr in contact with hydrated cement paste CEM II/A-S 42.5 R in $Ca(OH)_2$ saturated solution; with estimated standard deviations (s).*

V/m (L/kg)	***Hydrated cement paste CEM II/A-S 42.5 R, $Ca(OH)_2$***				
	Sr with carrier (c_0 = 0.35 mmol/L)			**Sr without carrier**	
	22°C	**50°C**	**80°C**	**22°C**	**80°C**
10	12.9 (0.3)	16.1 (0.2)	18.1 (0.4)	14.0 (0.2)	19.3 (0.4)
60	11.4 (0.2)	13.3 (0.2)	12.3 (0.2)	12.4 (0.9)	13.6 (0.2)
100	11.4 (0.4)	14.6 (0.5)	13.0 (0.5)	12.8 (0.3)	13.9 (0.2)
600	18.2 (1.5)	×	24.7 (0.2)	14.2 (0.9)	15.1 (3.2)
1000	48.4 (4.9)	111.5 (3.7)	72.8 (0.2)	20.7 (1.3)	31.6 (1.3)

In the case of Ra, it is not possible to significantly change the concentration of the element in the liquid phase. Concentration of ^{223}Ra in our experiments ranged from $4.7 \cdot 10^{-13}$ to $1.8 \cdot 10^{-12}$ mol/L in the carrier-free configuration. The Ra solubility limit was assessed to be about $1 \cdot 10^{-5}$ mol/L in the cement pore water (pH = 12.55, 25ºC) therefore in our case there is no risk of radium precipitation. On the other hand, the disadvantage of the safe use of the ^{223}Ra isotope is that its concentration is many times smaller than the concentration of Ra assumed in the storage. In addition, the average loss of ^{223}Ra due to sorption to walls of ampules in the absence of solid phase was evaluated, which was about 7.5% (5.8% for Sr). Moreover, the inner area of the walls of one ampoule used in the batch experiments is about 56 cm^2, which corresponds up to 12% of the surface area of the investigated

cement materials at the highest phase ratio V/m. The variable parameters are therefore composition of liquid phase (Portlandite water or the synthetic cement pore water CPW), type of solid phase (hydrated cement paste CEM II/A-S 42.5 R or CEM II / B-M (S-LL) 32.5 R, Concrete UJV, Concrete Richard), V/m ratios that differed in the range from 3 to 1000 L/kg, and temperature (22, 50, 65 and 80°C). The temperature dependence was investigated with respect to the behavior of cement materials; it is assumed that in the DGR the temperature will be initially elevated.

During the kinetic experiments, for all cementitious materials, it was verified that equilibrium occurred within one day (same as in the case of Sr uptake). The equilibrium experiments were therefore done again after 96 hours leading to the equilibrium value of distribution coefficient (K_d).

The influence of increasing temperature was convincingly recorded for radium (Table 3 and Figure 1). The increased value of K_d for the phase ratio V/m = 10 L/kg with increasing temperature occured for the hydrated cement paste CEM II/A-S 42.5 R and to a lesser extent for Concrete UJV. The change of the liquid phase from the saturated $Ca(OH)_2$ to the synthetic cement water CPW resulted in a K_d increase for hydrated cement paste CEM II/A-S 42.5 R (Table 3 and Figure 1). The general K_d increase applied also in order: hydrated cement paste CEM II/A-S 42.5 R, Concrete UJV, Concrete Richard (Table 3 and Table 4), although the content of cement (Concrete Richard contains 19% of cement and Concrete UJV 17%) and, consequently, of the CSH phase responsible for sorption of radium is lower in concretes. Interesting were the resulting K_d for otherwise nearly unused material CEM II / B-M (S-LL) 32.5 R, which approximated the results obtained at temperature 80°C for other CEM II material (Table 3 and Figure 1). Both materials differ mainly in composition and also in the value of specific surface area. It is possible that the specific surface area increases with increasing temperature. The cement material also plays a key role influencing the composition of the leachate – liquid phase used in the experiment with hydrated cement paste CEM II / B-M (S-LL) 32.5 R contained higher concentration of Sr than was naturally present in the hydrated cement paste (preliminary experiment).

Table 3: *Distribution coefficients K_d (L/kg) for Ra in contact with hydrated cement paste CEM II/A-S 42.5 R in solutions saturated with $Ca(OH)_2$ for different temperatures; with estimated standard deviations (s); and for comparison for hydrated cement paste CEM II / B-M (S-LL) 32.5 R in leachate from CEM II/A-S 42.5 R (V/m = 5 L/kg, contact time 1 month).*

V/m (L/kg)	***Hydrated cement paste CEM II/A-S 42.5 R, $Ca(OH)_2$***				***CEM II / B-M (S-LL) 32.5R***
	22°C	**50°C**	**65°C**	**80°C**	**22°C**
10	72.5 (4.5)	128.8 (8.1)	296.1 (9.0)	470.6 (3.0)	529.9
60	91.0 (1.6)	108.2 (0.2)	165.7 (3.7)	176.0 (8.0)	257.2
100	114.8 (6.4)	126.2 (0.6)	177.8 (9.6)	178.2 (0.4)	269.4
600	246.8 (1.8)	×	190.6 (11.9)	174.0 (16.3)	×
1000	477.6 (3.7)	218.6 (10.8)	301.7 (15.0)	265.7 (4.0)	×

Table 4: *Distribution coefficients K_d (L/kg) for Ra and Sr in contact with cementitious materials in $Ca(OH)_2$ saturated solution; with estimated standard deviations (s).*

V/m (L/kg)	*Ca(OH)₂, 22 °C*			
	Ra		Sr with carrier ($c_0 = 3.5 \cdot 10^{-4}$ mol/L)	
	Concrete UJV	Concrete Richard	Concrete UJV	Concrete Richard
10	131.0 (0.2)	95.9 (5.2)	9.0 (0.2)	46.2 (7.6)
60	181.1 (0.9)	179.0 (7.6)	8.9 (0.2)	14.8 (0.5)
100	225.8 (9.4)	224.0 (7.6)	11.0 (0.3)	14.5 (0.2)
600	377.2 (11.1)	495.6 (51.1)	21.0 (3.0)	19.9 (1.0)
1000	403.2 (25.1)	573.6 (24.1)	128.9 (12.5)	39.5 (0.2)

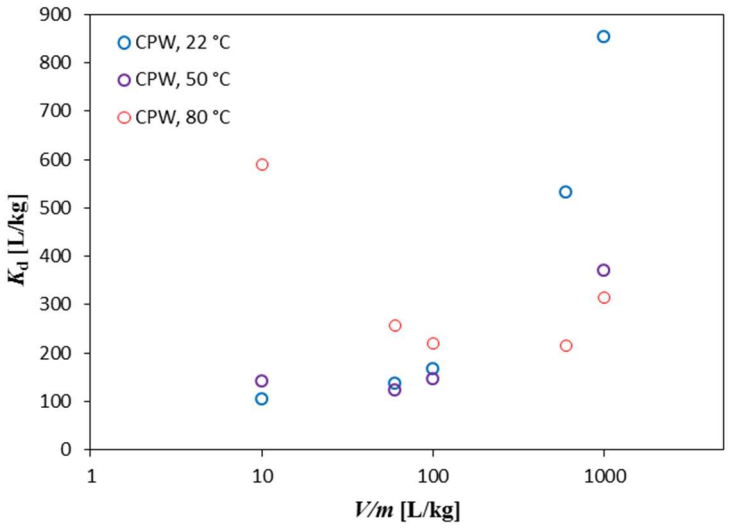

Figure 1: *Dependence of determined K_d values describing ^{223}Ra uptake on hydrated cement paste CEM II/A-S 42.5 R on the phase ratio V/m in CPW at different temperatures.*

3.3. Composition of leachates in sorption experiment

The evaluated K_d for Ra are higher than for Sr. For both elements an increase of K_d was observed with increasing phase ratio V/m that can be explained by the decrease of concentration of competing cations in the working solution. It is not the case of concrete samples (Table 5). The composition of the solution at the time of the sorption experiment sampling was determined for the selected cations (Ca^{2+}, Sr^{2+}, Na^+ and K^+). In general, with a decreasing phase ratio V/m, more K, Na and Sr (Table 5) are leaking from the cement materials into working solution – Portlandite water (prior leaching containing 19.8 mmol/L Ca^{2+}, 0.28 mmol/L Na^+, 0.03 mmol/L K^+ and 0.001 mmol/L Sr^{2+}, with total concentration 20.1 mmol/L). The precipitation of $Ca(OH)_2$ obviously occured, the concentration of which decreases with the decreasing phase ratio. With increasing temperature, the concentration of cations Na, K, and Sr in the solution increases, while the calcium concentration decreases (on averadge 74% in comparison to its concentration at 22°C). It is consistent with the solubility of $Ca(OH)_2$ in water with increasing temperature. The effect of $SrCl_2$ is reflected only in the case of Sr, whose concentration is lower at the lowest phase ratio V/m, otherwise it is limiting to working concentration 0.35 mmol/L. The behavior of

remaining cations is not affected by the presence of $SrCl_2$. Behavior of concretes differ probably because of its different composition.

Table 5: *Total concentration of cations Ca^{2+}, Sr^{2+}, Na^{+} and K^{+} in leachates from cement materials after 96 hours of contact with Portlandite water.*

	Total concentration of cations Ca^{2+}, Sr^{2+}, Na^{+} and K^{+} in leachate (mmol/L) $Ca(OH)_2$, 22°C			
	CEM II/A-S 42.5 R	**CEM II with $SrCl_2$ ($c_0 = 3.5 \cdot 10^{-4}$ mol/L)**	**Concrete UJV**	**Concrete Richard**
10	20.9	20.9	13	8.16
100	20.1	20.5	16.5	14.8
1000	19.1	18.0	19.8	19.2

3.4. Diffusion experiments with ^{223}Ra and Sr

A set of diffusion experiments for ^{223}Ra and ^{85}Sr with a carrier (c_0 = 0.35 mmol/L) was carried out for 3 weeks in Portlandite water or CPW through the CEM II/A-S 42.5 R layer (with a diffusion length of 0.5 cm) that was prepared unconventionally by pressing a crushed hydrated cement paste and saturated with the selected solution prior to the addition of the migrating element. The volume of the inlet and outlet reservoirs was 50 mL. The initial concentrations of both radionuclides were the same as for sorption experiments. The experimental time was limited because of the short half-life of the ^{223}Ra isotope. Consequently, the breakthrough of Ra did not occur.

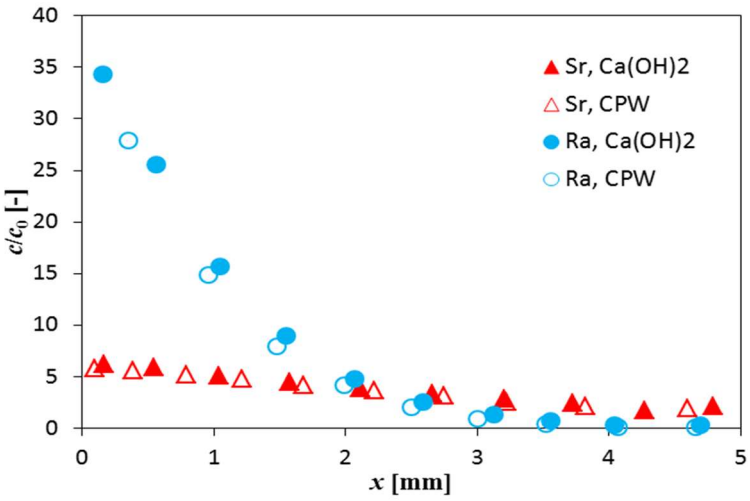

Figure 2: *Concentration profiles of the sorbed elements in hydrated cement paste CEM II/A-S 42.5 R in the environment of Portlandite water ($Ca(OH)_2$ or synthetic cement water (CPW).*

The determined K_d values were around 9 L/kg for Sr for both liquid phases used, 150 L/kg for Ra in the Portlandite water, and 100 L/kg for Ra in CPW. Based on the comparison of the dry sample weight with the sum of the weights of the cut slices generated at the end of the diffusion experiment it can be stated that V/m phase ratio was equal to 0.3 L/kg.

3.5. Conclusions

Sorption experiments under various conditions showed significantly higher retention on cementitious materials for Ra than for Sr. Diffusion experiments confirmed values obtained in sorption experiments. Acquired results are in good agreement with literature. However, it should be noted that the concentrations of the two monitored elements were significantly different in this study.

The results for the phase ratio V/m = 1000 L/kg that shows ambiguous values in several experiments could be affected by large errors due to the use of a very small amount of the solid phase. From a set of data obtained for equilibrated leachates, although they are sufficiently consistent, relevant conclusions can not yet be drawn.

Sr can be use as an analog of Ra with some limitation. The K_d values obtained for Sr are usualy at least 10-times smaller then the K_d for Ra. The “worse case scenario” approach could be applied.

Technical Summary – PSI & EMPA – WP2

1. Introduction & Objectives

Safety assessment studies for low- and intermediate level nuclear waste (L/ILW) repositories have shown that selenium-75 and iodine-129 are important dose-determining radionuclides due to their long half-lives and their presence in the anionic form resulting in weak retention by many common near- and far field minerals (NAGRA, 2002). Such predictions, however, ignore the potential uptake by positively charged anion exchangers present in the cementitious near-field of a L/ILW repository, such as the AFm phases.

The overall objective of the project is to investigate the immobilization of selenium, iodine and sulfur by the AFm phases under the alkaline, reducing conditions existing in a cement-based repository in deep geological formations (-700 mV < E_h < -230 mV (SHE), 10.0 < pH < 13.5) and, based on the acquired knowledge, to develop thermodynamic models that allow the mobility of Se and I in such environments to be predicted. Under the alkaline, reducing conditions in a cementitious near field, Se(IV), Se(-II), I(-I) and S(-II) are the dominating redox states. The aqueous Se speciation is dominated by anionic species SeO_3^{2-}, HSe^- and a series of polyselenides, mainly Se_2^{2-}, Se_3^{2-} and Se_4^{2-} (Olin et al. 2005), whereas the aqueous I speciation is dominated by the anionic species, I^- (Hummel et al. 2002). HS^-, the dominant sulfur species under alkaline, reducing conditions, is considered to compete with these anions in the uptake by AFm phases. There are two types of possible sorption sites in the AFm structure for all these anions: surfaces ion exchange sites and interlayer anion exchange sites. Previous studies on AFm phases have shown that a variety of anions can be intercalated in the AFm interlayers leading to the precipitation of a new AFm phase (e.g. B-AFm, Champenois et al. 2012; NO_3-AFm, Renaudin and François, 1999) or the formation of solid solutions (e.g. (SO_4-CrO_4)-AFm solid solution, Leisinger et al. 2012).

The potential of the AFm phases to incorporate the various Se, S and I anions in their structure has been the subject of several studies before (e.g. Baur and Johnson, 2003; Bonhoure et al. 2006; Mace et al. 2007 for Se; Motzet and Pöllmann, 1999 for S; Aimoz et al. 2012a for I) but only few are dealing with the strongly reduced HSe^- (Rojo et al. 2018) and HS^- (Le Cornec et al. 2017) anions. This is mainly due to the experimental difficulties related to the stabilization of the S(–II) and Se(-II) oxidation state. The binding of S(VI) in AFm phases and its structure are very well investigated. The S(VI)-AFm has a rhombohedral structure belonging to the $R\bar{3}$ space group (Allmann, 1977). The S(IV)-AFm phase has been synthesized and characterized before (Motzet and Pöllmann, 1999) but no solubility measurements or thermodynamic data for it are available. Apart from the precipitation of stable mono-Se and mono-I AFm phases, the formation of AFm solid solutions has also been reported (e.g. (I-SO_4)-AFm solid solution, Aimoz et al. 2012b).

2. Studied system

The systems studied are AFm phases under different redox conditions and pH between ~12 and ~13. AFm (Al_2O_3-Fe_2O_3-mono) phases are positively charged anion exchangers present in the cementitious near-field matrix of low and intermediate level radioactive waste repositories. AFm phases belong to the layered double hydroxides (LDH) and form during the hydration of cement.

They have a lamellar structure with a positively charged main layer, $[Ca_4(Al,Fe)_2(OH)_{12}]^{2+}$, and a negatively charged interlayer, $[X{\cdot}nH_2O]^{2-}$, where X denotes two singly charged or a doubly charged anion. The main layers consist of sheets of $Ca(OH)_6$ octahedra with every third Ca^{2+} site being occupied by Al^{3+} and/or Fe^{3+}, generating thus a positive net charge. Different charge balancing anions and different numbers of water molecules can be present in the interlayer. The anions typically found in AFm phases are OH^-, SO_4^{2-}, Cl^- and CO_3^{2-} forming hydroxyl-AFm, monosulfate, Friedel's salt, hemi- and monocarbonate, respectively.

3. Main results – Scientific highlights

The work performed can be split in three main parts: 1) synthesis and characterization of AFm end members containing one of the various S and Se, as well as I, anions – S(VI)-, S(IV)-, S(II)-, S(-II)-, Se(VI)-, Se(IV)-, Se(-II)- and I(-I)-AFm; 2) synthesis and characterization of binary solid solution series of the type SeO_3^{2-}-X^{n-} and I^--X^{n-} (with $X^{n-} = SO_4^{2-}$, SO_3^{2-}, $S_2O_3^{2-}$, CO_3^{2-}, OH^-) and development of solid solution models; 3) testing the models with the help of sorption experiments.

3.1. Synthesis and characterization of mono-S, mono-Se and mono-I AFm phases

In a first phase of this project pure AFm end members containing one of the following anion species SeO_4^{2-}, SeO_3^{2-}, HSe^-, SO_4^{2-}, SO_3^{2-}, $S_2O_3^{2-}$, HS^-, and I^- were synthesized and characterized by XRD, TGA, DVS, FTIR and Raman spectroscopy. Crystal structure analysis of the synthesized samples revealed the formation of well crystalline AFm phases showing X-ray powder diffraction patterns typical for the AFm family, characterized by strong basal reflections (00l) at low 2Θ values and the (110) diffraction peak at ~31° 2Θ. The S(VI)-AFm and the I-AFm are known to crystallize in the rhombohedral $R\bar{3}$ space group (Allmann, 1977; Rapin et al. 1999) which was also observed in this study. For the S(IV)-AFm the same rhombohedral symmetry consistent with the $R\bar{3}$ space group was determined. These three phases, (I-, S(VI)- and S(IV)-AFm) share a common position of the (110) reflection at about ~31° 2Θ but show differences in the interlayer distances. The corresponding d-spacing are 8.93 Å for the S(VI)-AFm, 8.84 Å for the I-AFm and 8.51 Å for the S(IV)-AFm, respectively. In the Se(IV)-sample the co-existence of two distinct Se(IV)-AFm hydrates with interlayer distances of 11.05 Å and 9.65 Å was found. Different structural organization of the SeO_3^{2-} anion in the interlayer gives rise to two distinct symmetries – a rhombohedral symmetry ($R\bar{3}$) with a larger c axis and Z = 3 for the 11.05 Å hydrate and a trigonal symmetry ($P\bar{3}$) with shorter c axis and Z = 2 for the 9.65 Å hydrate. The Se(VI)-AFm and the S(II)-AFm phases exhibit a lower symmetry, correlating with apparent monoclinic unit cells with the interlayer distances 10.18 Å for the Se(VI)-AFm and 10.33 Å for the S(II)-AFm. Structure refinements for these two phases, however, were only partially successful and the monoclinic structure could not be refined. The observed XRD analysis of the S(-II)-AFm and Se(-II)-AFm, finally, revealed the formation of AFm-like phases with rhombohedral structure. The powder patterns of the samples show the characteristic AFm (110) diffraction peak at about 31° 2Θ as well as the high-intensity basal reflections at low angle. The corresponding interlayer distances are 8.46 Å for the S(-II)-AFm and 8.27 Å for the Se(-II)-AFm.

The hydration states of the samples were determined by TGA analyses. The water removal occurs in several steps which vary in size and range for the different samples. Generally, water loss from the interlayer can be observed in three steps up to a temperature of 250°C; water from the main layer is lost in the temperature region between 250°C and 600°C. A total water content of 10 H_2O for the I-AFm, 11 H_2O for the S(IV)- and Se(IV)-AFm, 12 H_2O for the S(VI)-AFm and 13 H_2O for the S(II)- and Se(VI)-AFm was obtained for samples dried at 8% relative humidity.

The characterization of the AFm end members was completed with a water sorption study by Dynamic Vapour Sorption (DVS) analysis. The highest hydration level of each sample observed by DVS was then used for the determination of its solubility product (log K) using the thermodynamic modelling software GEMS (Kulik et al. 2013) and the NAGRA/PSI database (Hummel et al. 2002). The following mean values were calculated: -26.9 ± 0.9 (S(IV)-AFm), -27.8 ± 0.5 (I-AFm), -28.4 ± 1.4 (Se(IV)-AFm), 28.5 ± 1.4 (S(VI)-AFm), -29.2 ± 0.6 (Se(VI)-AFm) and -30.5 ± 0.8 (S(II)-AFm).

Sample oxidation during TGA and DVS analyses prevented proper determination of the H_2O content and the solubility product of the S(-II)-AFm and Se(-II)-AFm phases.

3.2. Synthesis and characterization of solid solution series

In a second phase of the project, the formation of binary solid solution of the type SeO_3^{2-}—X^{n-} and I^--X^{n-} (with X^{n-} = SO_4^{2-}, SO_3^{2-}, $S_2O_3^{2-}$, CO_3^{2-}, OH^-) as the intercalating anions was examined. Samples with total selenite (or iodide) mole fraction of $x_{Se(IV)}$ = SeO_3^{2-}/(SeO_3^{2-}+X^{n-}) = 0, 0.1, 0.3, 0.5, 0.7, 0.9 and 1 were synthesized and characterized.

Based on XRD observations, solid solutions were found between the following pairs: SeO_3-SO_4, I-CO_3, I-OH_CO_3, and I-OH. A continuous solid solution was found between the end members Se(IV)-AFm and S(VI)-AFm, where the larger ionic radius of the SO_4^{2-} anion (2.58 Å) compared to the SeO_3^{2-} anion (2.39 Å) (Jenkins and Thakur, 1979) results in a continuous peak shift towards higher basal spacing (d-values) with increasing amount of SO_4^{2-} (Figure 1a). Solid solution formation was also observed between the pairs I-OH and I-OH_CO_3, favoured by the rhombohedral structure of all three end members - I-AFm, OH-AFm and hemicarbonate (OH_CO_3-AFm). The increasing substitution of the larger I^- anion (2.10 Å) by the smaller OH^- anion (1.33 Å) is reflected by a gradual decrease of the interlayer distance from 8.84 Å in the I-AFm phase down to 8.44 Å at a total iodide fraction of 0.1 (x_I = 0.1). At this composition two phases exist – a mixed (I-OH)-phase and a OH-AFm with d = 7.92 Å indicating the presence of a miscibility gap at very low I^- contents. Similar evolution of the interlayer distance was found in the I-OH_CO_3 pair where the d value decreases to 8.20 Å moving towards the OH_CO_3-AFm end member. In this case, the solid solution is complete as no miscibility gap is observed.

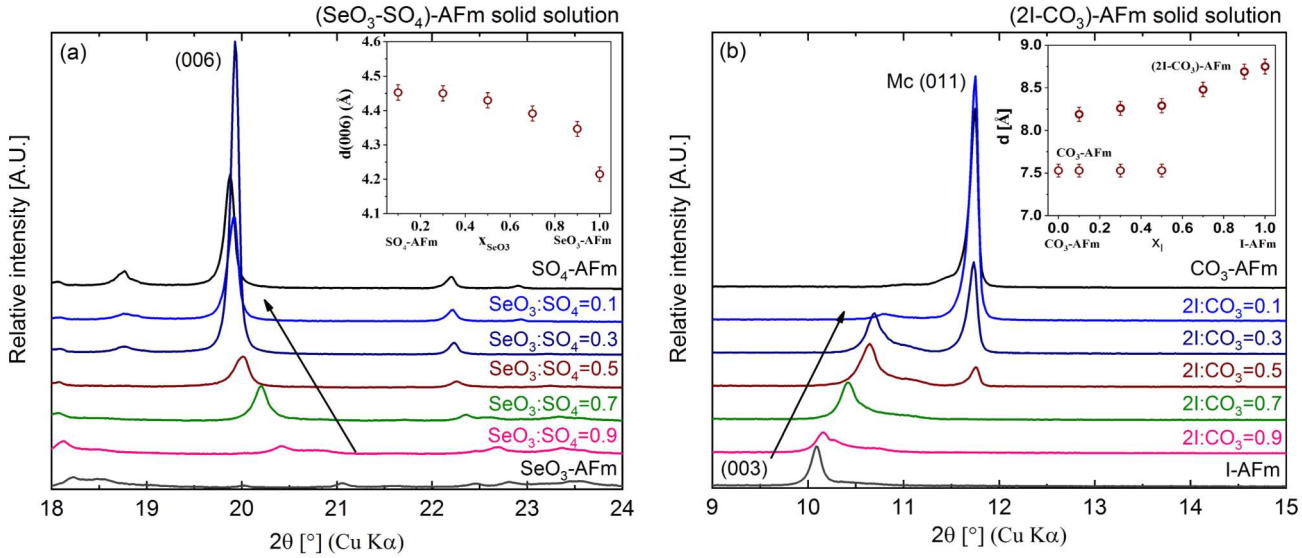

Figure 1: *Evolution of the interlayer distances in the (SeO_3-SO_4)-AFm (a) and the (2I-CO_3)-AFm (b) solid solution series.*

The solid solution formation between the I-AFm and monocarbonate (CO_3-AFm), on the other hand, is incomplete and a miscibility gap with the composition $0.5 \leq CO_3/(2I + CO_3)$ exists (Figure 1b). An initial peak shift up to a composition of $0.3 \leq CO_3/(2I + CO_3)$ is observed, suggesting that small amounts of the CO_3^{2-} anion (ionic radius 1.78 Å; Jenkins and Thakur, 1979) can be well incorporated in the I-AFm structure to form a mixed (2I-CO_3)-AFm phase. The solid solution is limited to compositions $0.5 \leq CO_3/(2I + CO_3)$, where two coexisting phases - an (2I-CO_3)-AFm mixed phase and a CO_3-AFm, indicate the presence of a miscibility gap. This miscibility gap could be related to the differences in the structure as monocarbonate has a triclinic structure, and to the planar arrangement of carbonate in the CO_3-AFm interlayer which prevents the uptake of the larger I^- anion into the structure. A comparable behaviour has been observed for chloride uptake in monocarbonate (Mesbah et al. 2011).

The observations on the solid solution series made in XRD were confirmed by FTIR analyses. The continuous solid solution between the I-AFm and OH_CO_3-AFm end members could also be seen in the FTIR spectra of the samples. The absorption band at ~775 cm^{-1} in the I-AFm is caused by the Al-OH deformation vibration in the rhombohedral structure. With decreasing amount of x_I the band is gradually weakened and shifts continuously towards ~745 cm^{-1}. This shift could be attributed to the different environment Al encounters in the sample as the composition changes. In the FTIR spectra of the I-CO_3 solid solution series the two coexisting phases could be clearly distinguished. For compositions $x_I \geq 0.7$ the Al-OH absorption band shows the same behaviour as observed before and only a single phase is present. At composition $x_I = 0.5$ additional absorption bands at ~948 cm^{-1}, ~875 cm^{-1} and ~667 cm^{-1} appear indicating in addition the presence of triclinic CO_3-AFm.

The obtained data together with bulk chemical analysis of the liquid phases and pH measurements were used for the construction of thermodynamic models describing the above-mentioned solid solutions using GEMS.

3.3. Sorption experiments

The sorption of SeO_3^{2-} and I^- on various AFm phases was investigated in a series of batch sorption experiments at pH ~13. The partitioning of the radionuclides ^{75}Se and ^{125}I, respectively, between the solid and the liquid phase was measured and expressed in terms of the distribution coefficient R_d (L/kg). R_d values for the sorption of Se(IV) on S(VI)-AFm were determined using starting Se(IV) concentrations ($[Se]_{tot}$) between 0.1 M and 10^{-13} M.

The measured R_d values range between ~31 L/kg at high $[Se]_{tot}$ and ~821 L/kg obtained at the lowest $[Se]_{tot}$ (Figure 2a). The same starting concentrations ($[I_{tot}]$: 0.1 M - 10^{-13} M) were used for I sorption tests onto S(VI)-AFm, S(-II)-AFm and OH_CO_3-AFm. The measured R_d values for I are significantly lower than the one observed for Se(IV) for all examined AFm phases. OH_CO_3-AFm shows the highest affinity for I with mean R_d value of 48 ± 10 L/kg. The R_d value for the S(-II)-AFm was determined to be 35 ± 7 L/kg. The weakest sorption is observed for the S(VI)-AFm with a mean R_d value of 27 ± 5 L/kg (Figure 2b). The experimental data suggests that the sorption of I is dependent on the type of the interlayer anion with a stronger sorption displayed by AFm phases with a singly charged anion in the interlayer.

The obtained data from the sorption experiments will be combined with the experimental data from the solid solutions studies for the construction of thermodynamic models describing the Se and I uptake by AFm phases using GEMS. The combination of both data sets would account for sorption on the two types of sorption sites available in the AFm structure: the surface ion exchange sites and the interlayer ion exchange sites.

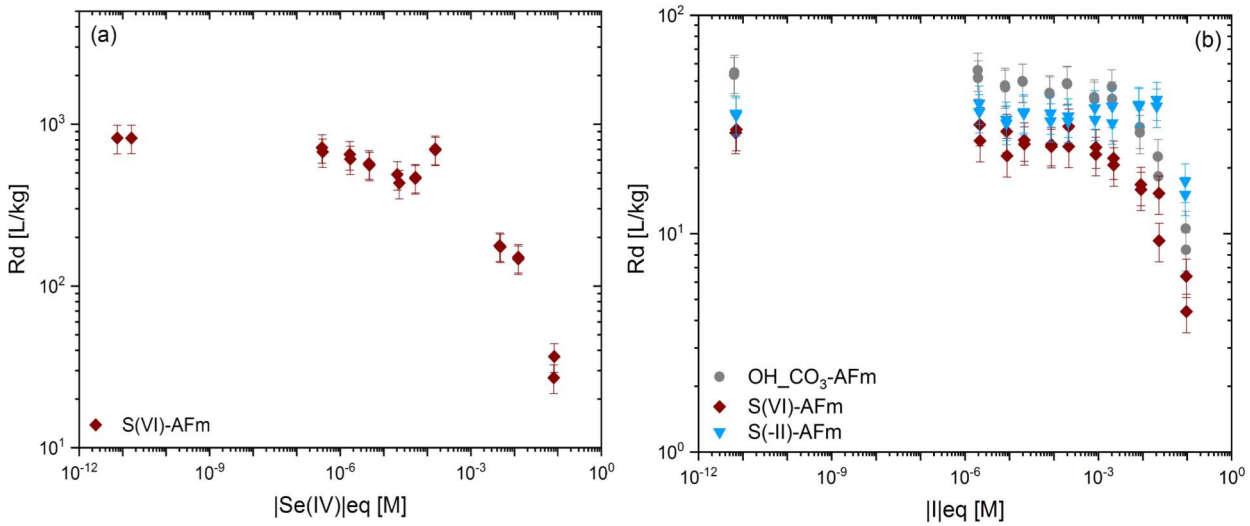

Figure 3: *R_d values for the sorption of SeO_3^{2-} (a) and I^- (b) on different AFm phases at pH ~ 13.*

4. Conclusions

The experimental data provide strong evidence for the intercalation of the sulfur, selenium and iodine anions in the AFm interlayers. The size and the position of the interlayer anion as well as the number of water molecules present give rise to differences in the basal spacing and crystal symmetry. Anion exchange in the interlayer leads to the formation of solid solutions. Limiting factors hereby are crystal symmetry, size of the interlayer anion and hydration state of the phase. Further, it was observed in the case of the monovalent iodide (I^-) that sorption is dependent on the type of competing anion present the interlayer: Stronger sorption is displayed by AFm phases containing a singly charged anion in the interlayer (HS^- in the S(-II)-AFm) than by AFm containing divalent ions (S(VI)-AFm).

References

Allmann, R. (1977). Refinement of the hybrid layer structure. Neues Jahrbuch für Mineralogie-Monatshefte, 3, 136-144.

Aimoz, L., Wieland, E., Taviot-Gueho, C., Dähn, R., Vespa, M., Churakov, S.V. (2012a). Structural insight into iodide uptake by AFm phases. Environmental Science & Technology, 42, 3874-3881.

Aimoz, L., Kulik, D.A., Wieland, E., Curti, E., Lothenbach, B., Mäder, U. (2012b). Thermodynamics of AFm-(I_2-SO_4) solid solution and of its end-members in aqueous media. Applied Geochemistry, 27, 2117-2129.

Baur, I. and Johnson, C.A. (2003). Sorption of selenite and selenate to cement minerals. Environmental Science & Technology, 37, 3442-3447.

Bonhoure, I., Baur, I., Wieland, E., Johnson, C.A., Scheidegger, A.M. (2006). Uptake of Se (IV/VI) oxyanions by hardened cement paste and cement minerals: An X-ray absorption spectroscopy study. Cement and Concrete Research, 36, 91-98.

Champenois, J.B., Mesbah, A., Coumes, C.C.D., Renaudin, G., Leroux, F., Mercier, C., Revel, B., Damidot, D. (2012). Crystal structures of Boro-AFm and Boro-AFt phases. Cement and Concrete Research, 42, 1362-1370.

Hummel, W., Berner, U.R., Curti, E., Pearson Jr, F.J., Thoenen, T. (2002). Nagra-PSI chemical thermodynamic database, version 01/01. Universal Publishers / Upubl.com, New York.

Jenkins, H.D.B. and Thakur, K.P. (1979). Reappraisal of thermochemical radii for complex ions. Journal of Chemical Education, 56, 576-577.

Kulik, D.A., Wagner, T., Dmytrieva, S.V., Kosakowski, G., Hingerl, F.F., Chudnenko, K.V., Berner, U. (2013). GEM-Selektor geochemical modeling package: revised algorithm and GEMS3K numerical kernel for coupled simulation codes. Computational Geosciences, 17, 1-24.

Le Cornec, D., Wang, Q., Galoisy, L., Renaudin, G., Izoret, L., Calas, G. (2017). Greening effect in slag cement materials. Cement and Concrete Research, 84, 93-98.

Leisinger, S.M., Lothenbach, B., Le Saout, G., Johnson, C.A. (2012). Thermodynamic modeling of solid solutions between monosulfate and monochromate $3CaO{\cdot}Al_2O_3{\cdot}Ca[(CrO_4)_x(SO_4)_{1-x}]{\cdot}nH_2O$. Cement and Concrete Research, 42, 158-165.

Mace, N., Landesman, C., Pointeau, I., Grambow, B., Giffaut, E. (2007). Characterisation of thermally altered cement pastes. Influence on selenite sorption. Advances in Cement Research, 19, 157-165.

Mesbah, A., Cau-dit-Coumes, C., Frizon, F., Leroux, F., Ravaux, J., Renaudin, G. (2011). A new investigation of the Cl^--CO_3^{2-} substitution in AFm phases. Journal of the American Ceramic Society, 94, 1901-1910.

Motzet, H. and Pöllmann, H. (1999). Synthesis and characterization of sulfite-containing AFm phases in the system CaO-Al_2O_3-SO_2-H_2O. Cement and Concrete Research, 29, 1005-1011.

NAGRA (2002). Project Opalinus Clay. Safety report. Demonstration of disposal feasibility for spent fuel, vitrified high-level waste and long-lived intermediate level waste, Nagra Technical Report, NTB 02-05, Nagra, Wettingen, Switzerland.

Olin, Å., Noläng, B., Osadchii, E.G., Öhman, L.-O., Rosén, E. (2005). Chemical thermodynamics of Selenium. Elsevier, Amsterdam.

Rapin, J.P., Walcarius, A., Lefevre, G., François, M. (1999). A double-layered hydroxide, $3CaO{\cdot}Al_2O_3{\cdot}CaI_2{\cdot}10H_2O$. Acta Crystallographica, C55, 1957-1959.

Renaudin, G. and François, M. (1999). The lamellar double-hydroxide (LDH) compound with composition $3CaO{\cdot}Al_2O_3{\cdot}Ca(NO_3)_2{\cdot}10H_2O$. Acta Crystallographica, C55, 835-838.

Rojo, H., Scheinost, A.C., Lothenbach, B., Laube, A., Wieland, E., Tits, J. (2018). Retention of selenium by calcium aluminate hydrate (AFm) phases under strongly-reducing radioactive waste repository conditions. Dalton Transactions, 00, 1-10.

Technical Summary – University of Surrey – WP2

1. Introduction & Objectives

Depending on the specific properties of the system and environmental factors, the retention of radionuclides in cements can be governed by solubility phenomena, diffusion, adsorption and/or incorporation into solid phases. Previous studies carried out to investigate the solubility of radionuclides in hyper-alkaline solutions (e.g. Felipe-Sotelo et al. 2017) have tended to focus on cationic species; long-lived anions, such as iodide or chloride isotopes, are typically assumed to be unconstrained by solubility considerations. Batch 'sorption' studies that consider anion uptake by cements (e.g. Tanabe et al. 2010) have yet to fully elucidate the mechanism(s) via which the anion are bound and moreover, utilise crushed or disaggregated materials at unrealistic solution to solid ratios. Finally, radionuclide diffusion studies in cement are difficult to compare as they have been undertaken using very different experimental protocols (e.g. Chida and Sugiyama, 2008; Gilliam et al. 1990; Mattigod et al. 2001; van Es et al. 2015).

Within the framework of CEBAMA WP2, we are investigating whether several safety-critical, anionic radionuclides (Tc, I, Se, Cl) could be mineralised in cements under certain conditions. The research encompasses batch type studies on both hardened cement pastes and individual mineral phases found in Portland cements together with through-diffusion experiments using established and highly reproducible protocols. The primary objective of these investigations is to enhance mechanistic understanding of radionuclide uptake and retention by the cements. A secondary objective is to compare the performance of various cementitious matrices in terms of retarding radionuclide transport.

Several of the radionuclides addressed in this study can exhibit a range of oxidation states under anticipated waste disposal conditions (Se, Tc, I). Therefore, selenium is considered as both selenite and selenite and iodine as iodide and iodate in batch tests. Technetium, introduced as Tc(VII), was added to the original project scope in view of its perceived geochemical mobility.

2. Studied system

Batch experiments were carried out on I, Se and Cl, with radium added at the request of FZ Jülich. The solids used fall into two categories: hardened cement paste (HCP) and single mineral phases. The five cement blends are: CEM I, a ground granulated blast furnace slag: ordinary Portland cement blend (GGBS:OPC), a pulverised fuel ash blend (PFA:OPC), a bespoke backfill material (NRVB, Nirex Reference Vault Backfill) and a CEBAMA reference cement blend, the last used to facilitate benchmarking among the multinational research teams. Sorption experiments were also performed on carbonated samples of the HCP. The individual mineral phases comprise calcium silicate hydrate (CSH), ettringite and monosulphate. These phases were selected as they comprise the major components of a CEM I cement, excluding portlandite as no significant interaction of the latter with radionuclides is expected.

Each HCP above was also employed in the through-diffusion experiments for which solutions pre-equilibrated with the respective cements were prepared. Through-diffusion experiments were performed as described by Hinchliff et al. (2016). 10 kBq of the radionuclide of interest was spiked into the central well with cement equilibrated water, which was then sealed, and the block placed in equilibrated water (120 cm^3). Movement of radionuclides through the block was monitored by taking 1 cm^3 aquilots of the surrounding water and measuring activity using liquid scintillation counting (LSC). After either the concentration of radionuclides reached steady state, or a specified maximum time (owing to the half-life of ^{125}I), the block was removed from the equilibrated water, sawn axially and the distribution of radionuclides measured by digital autoradiography. The isotopes employed were ^{36}Cl and ^{125}I, as originally envisaged. Difficulties were encountered in sourcing ^{75}Se. Given that this had been studied previously by the same authors (Hinchliff et al. 2016) and the acute lack of data for technetium, ^{99}Tc was substituted and the scope extended to include ^{3}H, which was added to emulate a near conservative tracer.

3. Main results – Scientific highlights

Iodine and selenium were taken up rapidly by the single mineral phases and HCP, reaching a stable R_d value within 14 - 28 days. Values obtained for iodate were substantially higher than for iodide in both HCP and individual minerals but the picture for selenite and selenite was less clear. Available evidence suggests that both elements are incorporated into cement mineral phases with the fast kinetics of uptake corresponding to rapid mineralogical changes in the solids. Previous work has shown that selenium forms discrete calcium selenite ($CaSeO_3 \cdot 2H_2O$) in NRVB (Figure 1a), which limits its migration in diffusion tests (Hinchliff et al. 2016). Similarly, SEM analysis in this work revealed needle-like crystals of ettringite (Figure 1b) with varying concentrations of iodine along the main axis. Spot EDX analysis indicates that the crystals incorporate iodine sporadically as they grow. Thus, solubility rather than surface adsorption is expected to govern the behaviour of these elements in Portland cements.

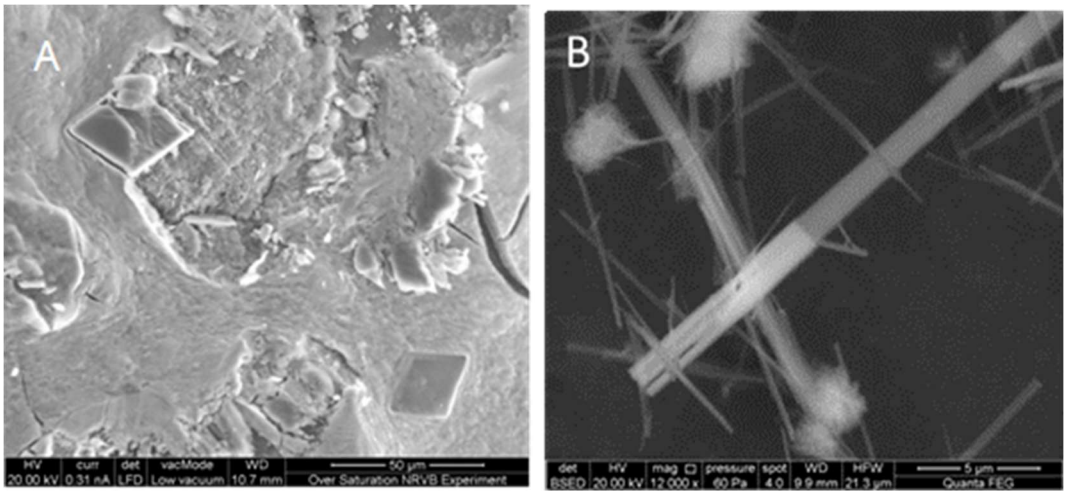

Figure 1: *Precipitation of calcium selenite (A) and incorporation of iodine in ettringite (B).*

Retention of the halogens by cement mineral phases is reflected in the through-diffusion tests where neither iodide nor chloride behaved as a conservative tracer. Breakthrough of chloride occurred within a few days for three of the cements; PFA:OPC, NRVB and the Cebama reference blend. Of these, the PFA mix showed the lowest retention with recovery reaching 90% of the input concentration after 270 days (Figure 2). No breakthrough at all was observed in the case of GGBS:OPC and the CEM1 Portland cement.

Broadly similar results were obtained for iodide, PFA:OPC again showing poor retention (C/C_0 = 84% after 54 days). However, the remaining cements all showed greater capacity to retard iodide migration than chloride (Figure 3).

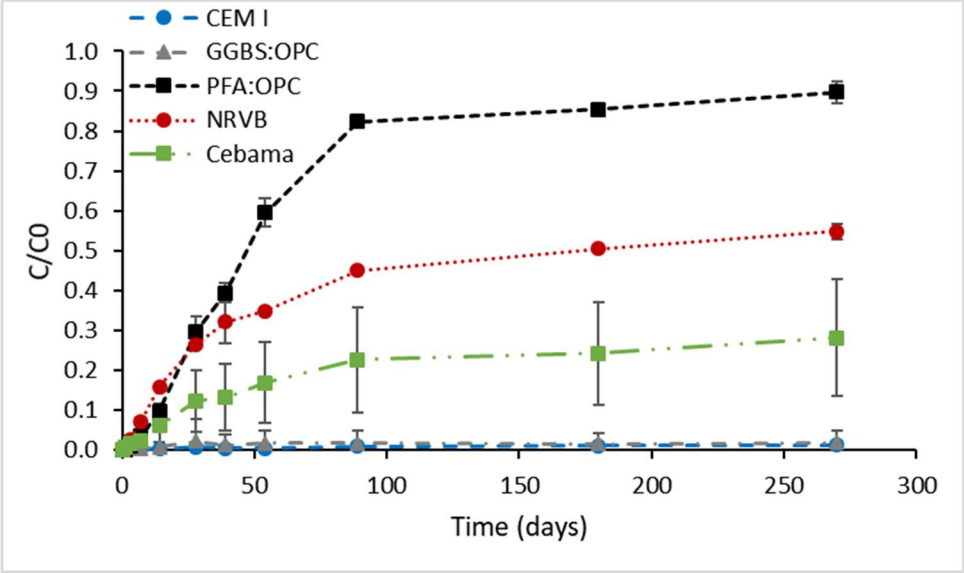

Figure 2: *Breakthrough curves for $^{36}Cl^-$ through five blended cement monoliths.*

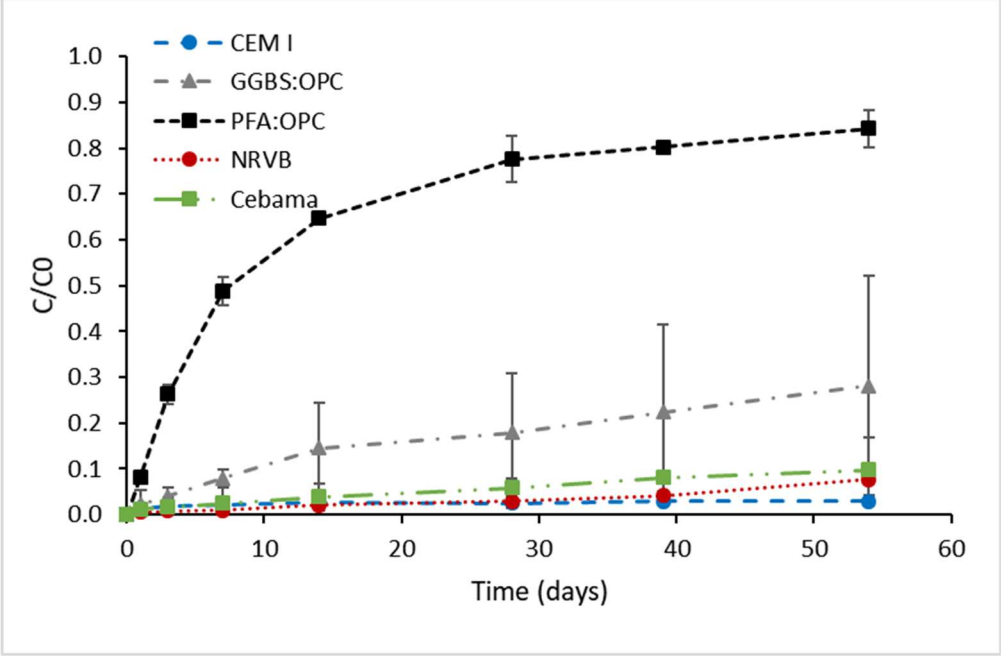

Figure 3: *Breakthrough curves for $^{125}I^-$ through five blended cement monoliths.*

The diffusion data were confirmed by digital autoradiography where the differences in matrix behaviour are stark. Figure 4 compares autoradiographs for chloride diffusion through the PFA and GGBS blends, respectively. The former displays activity throughout the monolithic sample, consistent with breakthrough into the surrounding equilibrated water, whereas in the latter, all activity is concentrated close to the central aperture.

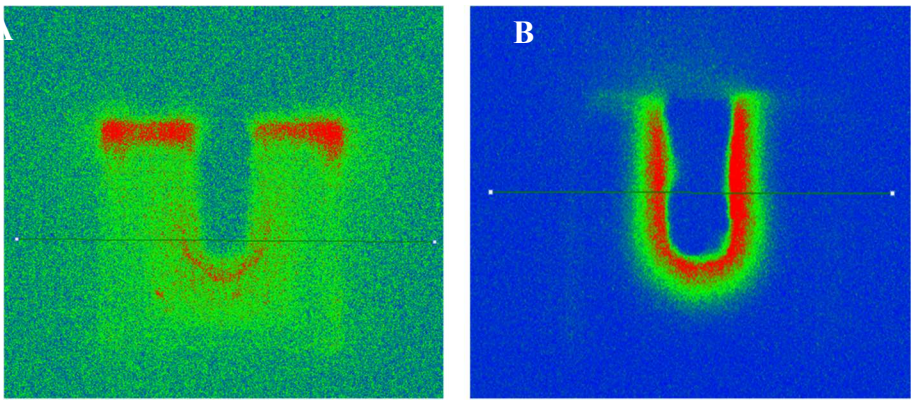

Figure 4: *Digital autoradiographs for $^{36}Cl^-$ diffusion through PFA:OPC (A) and GGBS:OPC (B).*

Through-diffusion results for ^{99}Tc are particularly interesting as they highlight the relative retention capacity of the five cement blends (Figure 5). Four display rapid breakthrough, on the order of one week. The exception is the Cebama reference material, which effectively inhibits migration to the extent that no technetium could be detected in the solution surrounding the monoliths after 270 days. CEM1 and GGBS:OPC show a near linear increase in solution concentration with time to C/C_0 values of 0.2 – 0.3; if the trends could be extrapolated, breakthrough would require around 10 years. NRVB and PFA:OPC perform poorly and produce sub-parallel breakthrough curves during the first month (Figure 5). Thereafter they diverge, with diffusion through NRVB continuing to increase before levelling at $C/C_0 = 0.8$. In contrast, the trend for PFA:OPC reverses after 28 days suggesting that a fraction of the ^{99}Tc that traverses the block is re-adsorbed by the cement matrix.

The markedly contrasting behaviour of the cements is illustrated in the digital autoradiographic images (Figure 6). The NRVB block shows no noticeable enhancement owing to rapid diffusion of technetium into the surrounding solution. Conversely, in the Cebama reference cement, all of the activity is located in or very close to the central well with little evidence of diffusion through the monolith. Technetium was introduced as pertechnetate (TcO_4^-) in each case and physical differences in porosity and microstructure were taken into account by benchmarking with tritium diffusion tests. Therefore, the very obvious differences in behaviour are due to chemical rather than physical effects. The latter could reflect reduction, though this is less likely given data for GGBS, or incorporation of pertechnetate into a specific mineral phase. Work is now underway to characterise the precipitate(s) formed.

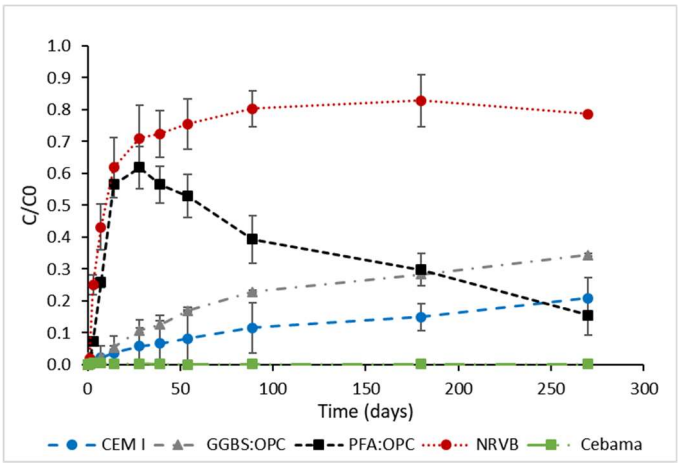

Figure 5: *Breakthrough curves for ^{99}Tc through five blended cement monoliths.*

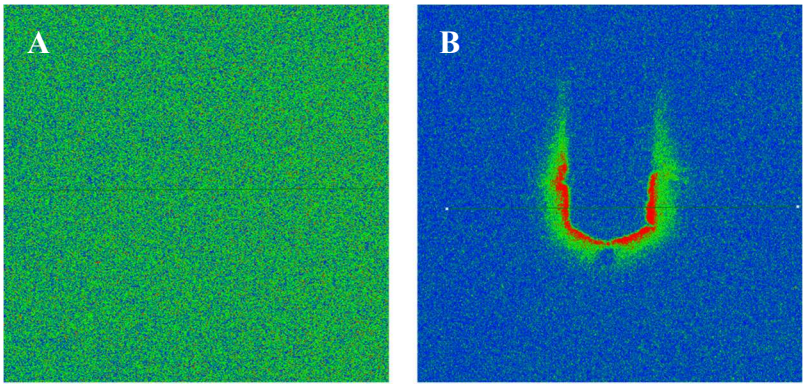

Figure 6: *Digital autoradiographs for ^{99}Tc diffusion through NRVB (A) and Cebama reference (B).*

References

Chida, T. and Sugiyama, D. (2008). Diffusion behavior of organic carbon and iodine in low-heat Portland cement containing fly ash. *In*: Symposium Q – Scientific Basis for Nuclear Waste Management XXXII, 1124, 1124–Q10–15.

Felipe-Sotelo, M., Hinchliff, J., Evans, N., Read, D. (2016). Solubility constraints affecting the migration of selenium through the cementitious backfill of a geological disposal facility. Journal of Hazardous Materials, 305, 21-29.

Felipe-Sotelo, M., Hinchliff, J., Field, L., Milodowski, A., Preedy, O., Read, D. (2017). Retardation of uranium and thorium by a cementitious backfill developed for radioactive waste disposal. Chemosphere, 179, 127-138.

Gilliam, T., Spence, R., Bostick, W., Shoemaker, J.L. (1990). Solidification/stabilization of technetium in cement-based grouts. Journal of Hazardous Materials, 24, 189–197.

Hinchliff, J., Felipe-Sotelo, M., Evans, N., Read, D. (2016). Solubility constraints affecting the migration of selenium through the cementitious backfill of a geological disposal facility. Journal of Hazardous Materials, 305, 21-29.

Mattigod, S., Whyatt, G., Serne, R., Martin, P., Schwab, K., Wood, M. (2001). Diffusion and leaching of selected radionuclides (iodine-129, technetium-99 and uranium) through Category 3 waste encasement concrete and soil fill material. PNNL-13639. Pacific Northwest National Laboratory, Richland, Washington.

Tanabe, H., Sakuragi, T., Yamaguchi, K., Sato, T., Owada, H. (2010). Development of new waste forms to immobilize iodine-129 released from a spent fuel reprocessing plant. Advanced Science Technology, 73, 158–170.

Van Es, E., Hinchliff, J., Felipe-Sotelo, M., Milodowski, A., Field, L., Evans, N., Read, D. (2015). Retention of chlorine-36 by a cementitious backfill. Mining Magazine, 79, 1297–1305.

Technical Summary – KIT-INE – WP3

1. Introduction & Objectives

Cement and clay materials will be used as backfill/ barrier material in deep geological facilities for nuclear waste disposal. During the prolonged period of post disposal, cementitious and clay materials will undergo alterations, possibly changing the chemical and physical (i.e. porosity, permeability) properties of these barriers and developing spatial heterogeneities. One important process that could reduce the durability of the concrete is the leaching/degradation of the solid, especially at the cement/clay interface due to the contact of clay pore water with the cementitious material. In order to minimize the interaction between "classical" ordinary Portland cement (OPC) and the bentonite porewater (pH ~ 7.5), low pH cements were developed within the nuclear waste disposal context in the late 90's. For this reason, the knowledge of low-pH cement systems is much less well advanced that the one of OPC and few studies are available in the literature (Cau Dit Coumes et al. 2006; Codina et al. 2008; García Calvo et al. 2010; Lothenbach et al. 2012; 2014).

In this context, the understanding of the evolution of the interface low pH cement / bentonite over geological time scales and the impact on radionuclide migration requires a detailed knowledge of a series of highly complex coupled Thermo-Hydro-Mechanical-Chemical processes, not investigated in detail in the past. In the last 15 years, a substantial effort has been made in predictive simulations of the long term interactions between different clays (i.e. bentonite and clayrock) and cementitious materials (Savage et al. 2002; 2010a; 2010b; 2011; de Windt et al. 2004; Watson et al. 2007; Berner et al. 2013; Jenni et al. 2017). However, it has to be mentioned that most of these studies are related to the interaction of ordinary Portland cement type with clay (bentonite barrier or clays host rocks), but very few effort has been dedicated to study 'low pH' cements/clay interaction. Only recently, Berner et al. (2013) and Dauzeres et al. (2016) have studied interface processes between low pH cement materials (LAC (Low Alkali Concrete) and ESDRED project concrete) and clay rock at different scales. Berner et al. (2013) investigated by reactive transport modelling the interaction between MX-80 bentonite, Opalinus Clay and low-pH ESDRED concrete materials in a repository scale for 30,000 years of interaction. On the other hand, Dauzères et al. (2016) aimed at reproducing mineral reactions observed at a 5 years old low-pH cement OPA interface during the Mt Terri CI project (Jenni et al. 2014), mainly focusing in the magnesium perturbation in the degraded concrete but not discussing pore clogging.

Therefore, an urgent need to obtain detailed knowledge, process understanding and modelling on the interface low pH cement / clay processes was identified, specially assessing the impact that these processes can have in radionuclide migration which has not been investigated before. For this reason, the specific objectives of KIT in WP3 is to develop comprehensive macroscopic modeling approaches (i.e reactive transport and geochemical modelling) based on experimental observations in the microscale to support interpretation of results and prediction of the long-term evolution of key chemical and transport parameters that could affect radionuclide migration such as mineralogy composition, porosity, permeability and diffusivity especially in the interface between low pH cement and bentonite.

2. Studied system

KIT-INE is mainly involved in 3 different modelling activities (interconnected between them) related with the experiments performed by KIT in WP1 and WP2:

- Hydration modelling of low-pH cements
- Migration of tritiated water (HTO) and $^{36}Cl^-$ through low-pH cement pastes
- Reactive transport modelling of radionuclides migration in the low-pH cement/clay interface

3. Main results – Scientific highlights

3.1. Microstructure and chemical properties of low-pH cements

The hydration model of 3 low-pH cement pastes manufactured at KIT-INE has been performed by using the Gibbs free energy minimization code GEMS (Wagner et al. 2012; Kulik et al. 2013) and the recently updated thermodynamic database CEMDATA18 (Lothenbach et al. 2019).

The solid phases present after 90 days of hydration have been identified experimentally and were described within WP1 (Ait Mouheb et al. 2017; 2018) together with the raw materials characterization which is used as input data. This helps to compare experimental and modelling results. The main hydrated phases identified experimentally are C-S-H and C-A-S-H phases with a Ca:Si ratio between 0.6 - 1.1 and Al:Si ratio of 0.05. Ettringite is present as a minor phase and no portlandite or Friedel's salt are identified. Experimental studies of the iron containing phases is on-going in WP1 and not compared with the model results.

The modelling approach followed is based on coupling a set of kinetic rates (Parrot et al. 1984; Lothenbach et al. 2008) of the dissolution of the raw materials (clinker and silica fume) with thermodynamic calculations between the solution and the hydrates formed (Lothenbach et al. 2014). All other cement constituents, mainly alkali hydroxides and sulphates (gypsum), were not kinetically controlled and therefore assumed to be thermodynamically dissolved.

Although included in the database, kaolinite, gibbsite, quartz, zeolites or crystalline iron phases were not allowed to precipitate in the system. Alkali uptake for Na and K was modelled as ideal solid solutions. Two different C-S-H solid solution models were used and compared: a) the quaternary CSHQ model with 4 different Ca:Si ratio end-members (Kulik et al. 2011) and b) the CNASH_ss model which includes Al and Na in the structure of the C-S-H phases (Myers et al. 2014). Selected results (hydration model of one of the low-pH cement pastes) using both models are presented in Figure 1, showing the volume of solids formed as a function of the hydration time for one of the low-pH cement pastes. The hydrated phases after 90 days predicated from both models are: silica-rich C-S-H, ettringite, gypsum, silica fume not reacted and hydrotalcite, as well as traces of monosulfate and monocarbonate. The main differences between both models, are related to the formation of phases containing aluminium. While the CSHQ model predict the formation of strätlingite and $Al(OH)_3$, the CNASH_ss model predicts the formation of C-A-S-H phases as the only Al-containing phase.

The experimental observations from the solid phase analysis are well reproduced by using the CNASH_ss model. However, the incorporation of the processes controlling the aqueous speciation, especially the potassium concentration is under progress. These results demonstrate that the choice of the appropriate C-S-H model which considers the Al uptake by C-S-H phases is essential to reproduce the hydration phases observed experimentally.

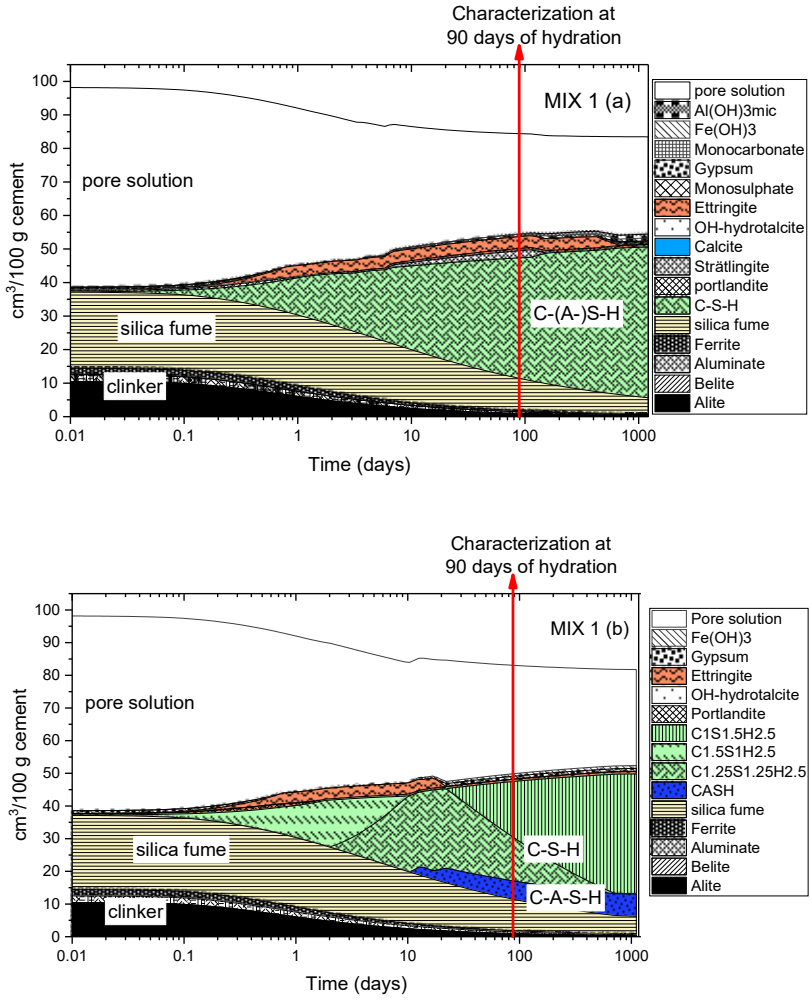

Figure 1: *Modelled changes in volume during the hydration of a low-pH cement using: a) the CSHQ and b) the CNASH_ss model for C-S-H.*

3.2. Migration of tritiated water (HTO) and $^{36}Cl^-$ through low-pH cements

Different numerical approximations are used here to determine the effective diffusion coefficient, D_e, and the accessible porosity of tritiated water (HTO) and $^{36}Cl^-$ in low-pH cement pastes. Through-diffusion experiments were performed in WP1, allowing a direct comparison of model and experimental results. For detailed explanation of the experimental set up please refer to Ait Mouheb et al. (2019) or to WP1 description.

Transport parameters for HTO and $^{36}Cl^-$ were obtained by inverse modelling of the diffusive flux data mol/ (m^2·s) determined at the downstream reservoir by measuring the accumulated activity (in Bq) of both radionuclides (details on flux calculations are given in Tits et al. 2003). Fickian diffusion in a homogeneous isotropic material has been considered as the only transport process. Fick´s first law states that the diffusive flux (J) is proportional to the concentration gradient (see Eq. 1):

$$J = -D\_e \cdot \partial c/\partial x \cdots\cdots \text{(Eq.1)}$$

Where $\partial c/\partial x$ is the concentration gradient [mol/m^4]; and D_e is the effective diffusion coefficient [m^2/s]. The change of concentration with time, t [s], is described by Fick's second law (Eq. 2):

$$\partial c/\partial t = -D\_e \cdot (\partial \hat{} 2\, c)/(\partial x \hat{} 2\,) \quad \cdots\cdots\cdots (Eq.2)$$

The effective diffusion coefficient can be estimated using Archie's law:

$$D\_e \;=\; \varepsilon\_acc \hat{} m \;\; D\_W \quad \cdots\cdots\cdots (Eq.3)$$

with m [-] being an empirical constant, D_w [m^2/s] the diffusion coefficient of the tracer in free water, and ε_{acc} the accessible porosity [-], which is related to the constrictivity (δ) and tortuosity (τ) factors as:

$$\varepsilon\_acc \hat{} m = \;\; \delta/\tau \;\; = \;\; 1/G \quad \cdots\cdots\cdots (Eq.4)$$

Constrictivity (δ) and tortuosity (τ) are assembled together in the geometrical factor (G). The finite element code Comsol Multiphysics 5.3 (Comsol, 2017) has been used to solve the partial differential equations. Based on the experimental setup, a one-dimensional (1D) single porous medium model is considered. Initial and boundary conditions of the tracer concentration are described according to the experimental data:

$$c(x = 0, t > 0) = f\_0\,(t) \text{ and}$$

$$c(x = H, t > 0) = f\_1\,(t)$$

Where H (m) is the thickness of the sample. The initial condition is:

$$c(x, t \leq 0) = 0, \forall\, x \in \text{transport domain}$$

where x [m] is the spatial coordinate, and $f_0(t)$ and $f_1(t)$ are the time-dependent change of the radiotracer concentrations (HTO and $^{36}Cl^-$) in the upstream and downstream reservoir, respectively.

The accumulated amounts (mol) of HTO and $^{36}Cl^-$ in the downstream reservoir of two experiments with the same material are shown in Figure 2. The upstream concentration of HTO and $^{36}Cl^-$ are equal to $1.86 \cdot 10^{-9}$ M and $4.55 \cdot 10^{-6}$ M, respectively, and keep approximately constant during the studied time.

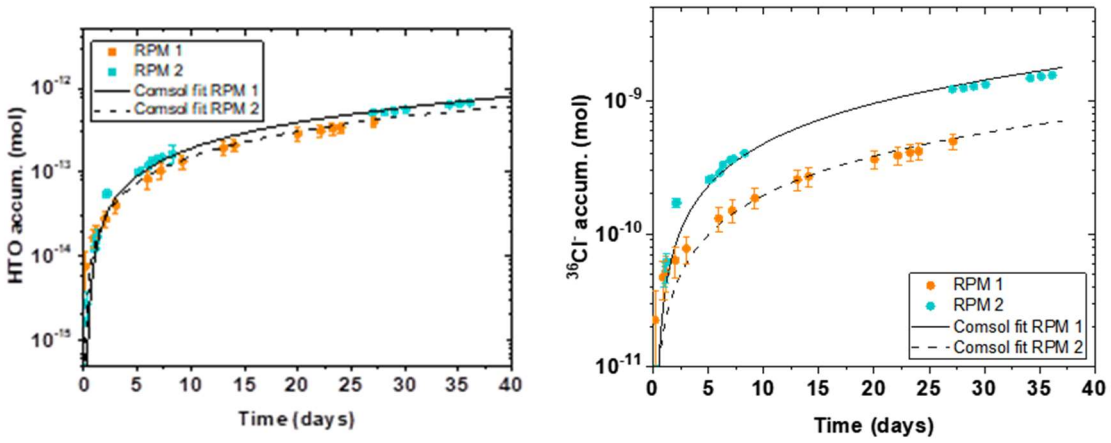

Figure 2: *Accumulated amount of HTO and $^{36}Cl^-$ in the downstream reservoir vs. time during diffusion experiments through two low-pH cement (RPM) samples.*

Experiments are reproducible and within the first hours the fluxes reached a steady state with a value of ~ $5 \cdot 10^{-16}$ mol/($m^2 \cdot s$) for HTO and ~ 10^{-13} mol/$m^2 \cdot s$) for $^{36}Cl^-$. Transport parameters values for HTO and $^{36}Cl^-$ were obtained (average of two samples) with D_e (HTO) = $(2.28 \pm 0.22) \cdot 10^{-12}$ m^2/s, ε_{acc} (HTO) = 0.004 ± 0.009 and D_e ($^{36}Cl^-$) = $(1.55 \pm 6.74) \cdot 10^{-12}$ m^2/s, ε_{acc} ($^{36}Cl^-$) = 0.002 ± 0.009. As observed, to obtain a good fit of the experimental data a very small (unrealistic) accessible porosity was needed. These findings indicate that the porosity-effective diffusion correlation, which is generally described by empirical laws such as the Archie´s law with m values expected for the studied material is not applicable or other transport processes are happening in the system. This could probably be due to the heterogeneous small pore scale (< 10 nm) network. Future work focuses on the fitting of the experimental data with a more complex multiporosity approach model.

3.3. Reactive transport modelling of radionuclides migration in the low-pH cement/clay interface

A predictive reactive transport model consisting of a three-dimensional (3D) fully water saturated isothermal (298.15 K) system has been performed. This modelling work represents laboratory through-diffusion experiments of HTO, Be(II), and $^{36}Cl^-$ across the interface between MX-80 bentonite porewater and low-pH cement (see Figure 3). Coupling between porosity changes due to dissolution/precipitation reactions and transport properties (i.e. effective diffusion coefficient) is also studied.

Diffusion of the selected tracers occurs across the interface between bentonite porewater and different low-pH cements manufactured by KIT-INE within WP1 (Ait Mouheb et al. 2017) or available as reference material in the project. The cylindrical low-pH cement paste has a diameter and thickness of 30 and 10 mm, respectively, and it is surrounded by 2 reservoirs of 50 mL and 4 mL: the upstream and downstream reservoirs, containing bentonite and low-pH cement porewater, respectively. The reactive transport simulations are compared to the mentioned through-diffusion experiments performed in WP1. Considerable effort has been made in both WP1 and WP2 to obtain the required input parameters for the reactive transport model. Among others, the main input parameters that can be obtained from WP1 and WP2 are the pH cement mineralogy, porewater composition, porosity, diffusivity and the aqueous speciation and sorption properties of Be. A large part of the chemical and physical characterization of the cement paste is already documented in Ait Mouheb et al. (2017, 2018) and Gaona et al. (2017, 2019).

The conceptual and numerical model has been set up by using the iCP interface (Nardi et al. 2014). Kinetics and chemical equilibria reactions of the primary and secondary phases precipitating or dissolving in the system are simulated using parameters and data from the appropriate thermodynamic database (i.e. ThermoChimie V.9) and the literature (Giffaut et al. 2014; Gaona et al. 2019). Davies equation is used for the aqueous model and ion exchange reactions for Ca, Mg, Sr, Na and K and radionuclide and iron (III) inner-sphere sorption is considered using a non-electrostatic model. The simulations were carried out for different times of interaction (11 h, 6 months and 1 year) predicting different processes that could affect differently the mobility of the studied radionuclides.

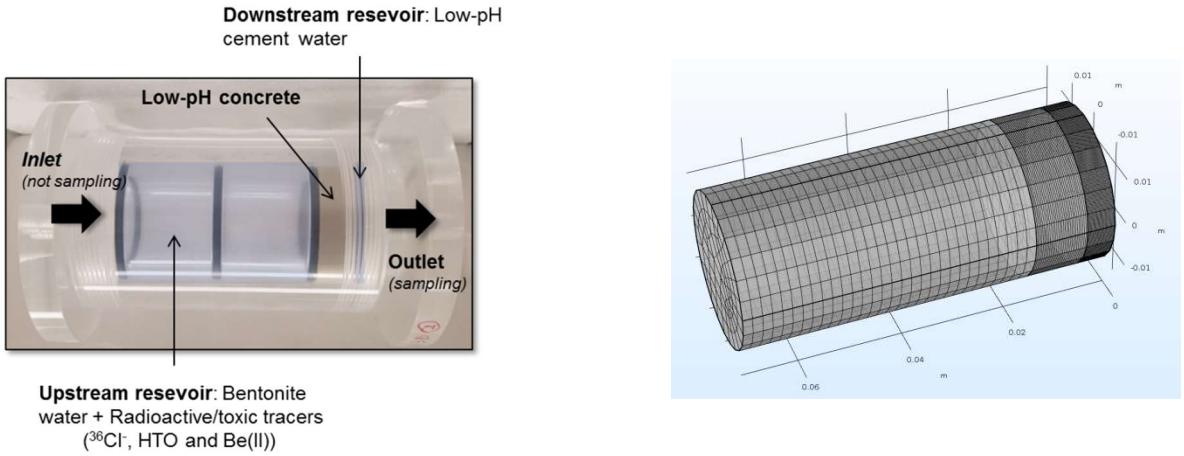

Figure 3: *Cell used in the laboratory through diffusion experiments (left) and the spatial discretization used in the model (right). Domain length 70. 13 / 10 / 5.37 mm in the flow direction.*

Figure 4. shows some of the processes occurring in the system. The alteration on the low-pH cement by the bentonite water is mainly due to the displacement of the Ca^{2+} in the interlayer of the C-(A)-S-H phases by the Na^+ present in the bentonite water. This process release calcium to the solution producing the formation of secondary phases like gypsum in the cement paste which can be observed after 1 year of interaction as reactive front of 1.75 mm. In our system, brucite is undersaturated and attempts to model the magnesium perturbation using available thermodynamic data suggested the formation of hydrotalcite. The partial dissolution of C-(A)-S-H phases results in an increase in porosity at the side of cement close to the outlet, which is produced by the continuous replacement by "fresh water" in the outlet reservoir. On the other hand, in the cement in contact with the bentonite water, no significant changes of porosity are observed and the effective diffusion coefficient remains approximately constant, not affecting the transport of a non-reactive and uncharged tracer like tritiated water (HTO).

Finally, the diffusion of beryllium from the bentonite porewater to the low-pH cement is modelled observing that beryllium will remain close to the inlet even after 1 year of interaction, which is mainly due to the strong sorption of this toxic element in low-pH cements.

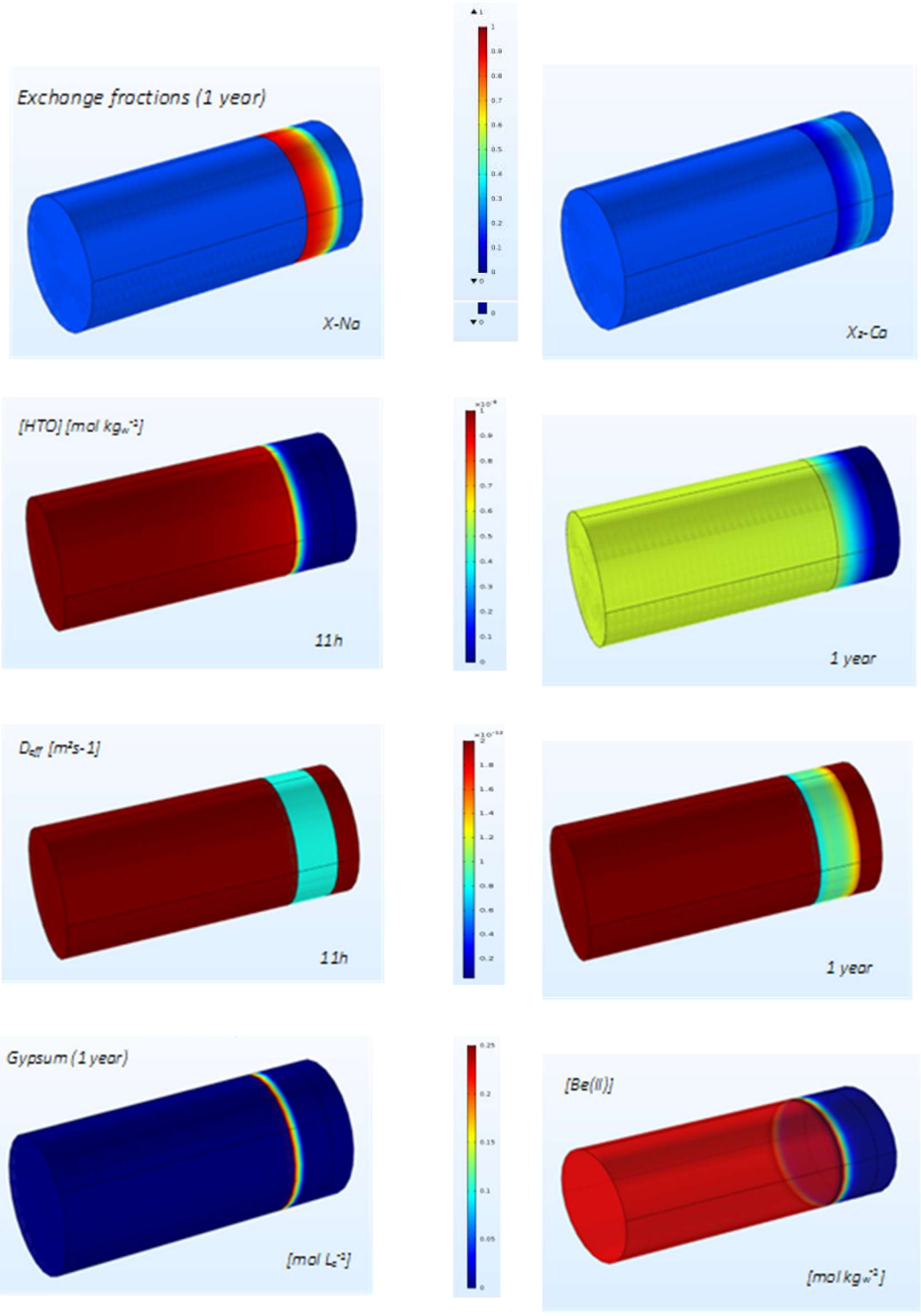

Figure 4: *Selected model results obtained using iCP 1.5 (interface COMSOL 5.3-PHREEQC 3.4).*

References

Ait Mouheb, N., Montoya, V., Borkel, C., Schäfer, T. (2017). Experimental studies on low pH cement / clay interface processes: Characterization of low pH cements. *In*: 1st Annual proceedings of the Cebama project. KIT Scientific report 7734, Karlsruhe, Germany.

Ait Mouheb, N., Montoya, V., Joseph, C., Schäfer, T., Geckeis, H. (2019). 3rd Annual proceedings of the Cebama project. KIT Scientific Report (CEBAMA proceedings *in print*).

Ait Mouheb, N., Montoya, V., Schild, D., Soballa, E., Adam, C., Geyer, F., Schäfer, T. (2018). Characterization and sorption properties of low pH cements. 2nd Annual proceedings of the Cebama project. KIT Scientific report 7734.

Berner, U., Kulik, D.A., Kosakowski, G. (2013). Geochemical impact of a low-pH cement liner on the near field of a repository for spent fuel and high-level radioactive waste. Physics and Chemistry of the Earth, Parts ABC, 64, 46–56.

Cau Dit Coumes, C., Courtois, S., Nectoux, D., Leclercq, S., Bourbon, X. (2006). Formulating a low-alkalinity, high-resistance and low-heat concrete for radioactive waste repositories. Cement and Concrete Research, 36, 2152–2163.

Codina, M., Cau-dit-Coumes, C., Le Bescop, P., Verdier, J., Ollivier, J.P. (2008). Design and characterization of low-heat and low-alkalinity cements. Cement and Concrete Research, 38, 437–448.

COMSOL 5.3. (2017). www.comsol.com.

Dauzères, A., Achiedo, G., Nied, D., Bernard, E., Alahrache, S., Lothenbach, B. (2016). Magnesium perturbation in low-pH concretes placed in clayey environment—solid characterizations and modeling. Cement and Concrete Research, 79, 137-150.

De Windt, L., Pellegrini, D., van der Lee, J. (2004). Coupled modeling of cement/claystone interactions and radionuclide migration. Journal of Contaminant Hydrology, 68(3–4), 165-182.

Gaona, X., Böttle, M., Rabung, T., Altmaier, M. (2017). Solubility, hydrolysis and sorption of beryllium in cementitious systems. 1st Annual proceedings of the Cebama project. KIT scientific report, 7734.

Gaona, X., Cevirim-Papaioannou, N., Böttle, M., Altmaier, M. (2019). Solubility and hydrolysis of Be(II) in dilute to concentrated NaCl and KCl solutions. *In*: Altmaier, M., Montoya, V., Duro, L., Valls, A. (Eds.). Proceedings of the 3rd Annual Workshop of the CEBAMA Project. *In press*.

García Calvo, J.L., Hidalgo, A., Alonso, C., Fernández Luco, L. (2010). Development of low-pH cementitious materials for HLRW repositories: Resistance against ground waters aggression. Cement and Concrete Research, 40, 1290–1297.

Giffaut, E., Grivé, M., Blanc, P., Vieillard, P., Colàs, E., Gailhanou, H., Gaboreauc, S., Marty, N., Madé, B., Duro, L. (2014). Andra thermodynamic database for performance assessment: ThermoChimie. Applied Geochemistry, 49, 225–236.

Jenni, A., Mäder, U., Lerouge, C., Gaboreau, S., Schwyn, B. (2014). In-situ interaction between different concretes and Opalinus Clay. Physics and Chemistry of the Earth, Parts ABC, 70, 71–83.

Jenni, A., Gimmi, T., Alt-Epping, A., Mader, U., Cloet, V. (2017). Interaction of ordinary Portland cement and Opalinus Clay: Dual porosity modelling compared to experimental data. Physics and Chemistry of the Earth, 99, 22-37.

Kulik, D.A. (2011). Improving the structural consistency of C-S-H solid solution thermodynamic models. Cement and Concrete Research, 41, 477-495.

Kulik, D.A., Wagner, T., Dmytrieva, S.V., Kosakowski, G., Hingerl, F.F., Chudnenko, K.V., Berner, U.R. (2013). GEM-Selektor geochemical modeling package: revised algorithm and GEMS3K numerical kernel for coupled simulation codes Computational Geosciences, 17, 1-24.

Lothenbach, B., Kulik, D.A., Matschei, T., Balonis, M., Baquerizo, L., Dilnesa, B., Miron, G.D., Myers, R.J. (2019). Cemdata18: A chemical thermodynamic database for hydrated Portland cements and alkali-activated materials. Cement and Concrete Research, 115, 472–506.

Lothenbach, B., Le Saout, G., Ben Haha, M., Figi, R., Wieland, E. (2012). Hydration of a low-alkali CEM III/B–SiO_2 cement (LAC). Cement and Concrete Research, 42, 410–423.

Lothenbach, B., Rentsch, D., Wieland, E. (2014). Hydration of a silica fume blended low-alkali shotcrete cement. Physics and Chemistry of the Earth, Parts ABC. Mechanisms and Modelling of Waste-Cement and Cement-Host Rock Interactions, 70–71, 3–16.

Lothenbach, B., Le Saout, G., Gallucci, E., Scrivener, K. (2008). Influence of limestone on the hydration of Portland cements. Cement and Concrete Research, 38, 848-860.

Myers, R.J., Bernal, S.A., Provis, J.L. (2014). A thermodynamic model for C-(N-)A-S-H gel: CNASH_ss. Derivation and validation. Cement and Concrete Research, 66, 27–47.

Nardi, A., Idiart, A., Trinchero, P., de Vries, L.M., Molinero, J. (2014). Interface COMSOL-PHREEQC (iCP), an efficient numerical framework for the solution of coupled multiphysics and geochemistry. Computers & Geosciences, 69, 10-21.

Parrot, L.J. and Killoh, D.C. (1984). Prediction of cement hydration. British Ceramic Proceedings, 35, 41–53.

Roosz, C., Vieillard, P., Blanc, P., Gaboreau, S., Gailhanou, H., Braithwaite, D., Montouillout, V., Denoyel, R., Henocq, P., Madé, B. (2018). Thermodynamic properties of C-S-H, C-A-S-H and M-S-H phases: Results from direct measurements and predictive modelling. Applied Geochemistry, 92, 140-156.

Savage, D., Arthur, R., Watson, C., Wilson, J. (2010a). An evaluation of models of bentonite pore water evolution. SSM Technical Report 2010:12. Swedish Radiation Safety Authority, Stockholm, Sweden.

Savage, D., Arthur, R., Watson, C., Wilson, J., Strömberg, B. (2011). Testing geochemical models of bentonite pore water evolution against laboratory experimental data. Physics and Chemistry of the Earth, Parts A/B/C, 36, 1817-1829.

Savage, D., Benbow, S., Watson, C., Takase, H., Ono, K., Oda, C., Honda, A. (2010b). Natural systems evidence for the alteration of clay under alkaline conditions: an example from Searles Lake, California. Applied Clay Science, 47, 72-81.

Savage, D., Noy, D., Mihara, M. (2002). Modelling the interaction of bentonite with hyperalkaline fluids. Applied Geochemistry, 17, 207–223.

Tits, J., Jakob, A., Wieland, E., Spieler, P. (2003). Diffusion of tritiated water and $^{22}Na^{+}$ through non-degraded hardened cement pastes. Journal of Contaminant Hydrology, 61, 45- 62.

Wagner, T., Kulik, D.A., Hingerl, F.F., Dmytrieva, S.V. (2012). GEM Selektor geochemical modeling package: TSolMod library and data interface for multicomponent phase models. Canadian Mineralogist, 50, 1173–1195.

Watson, C., Benbow, S., Savage, D. (2007). Modelling the interaction of low pH cements and bentonite. Issues Affecting the Geochemical Evolution of Repositories for Radioactive Waste. SKI Report 2007:30.

Technical Summary – AMPHOS 21 – WP3

1. Introduction & Objectives

A large body of literature is available about the durability of OPC concrete and several studies have focused on the interaction of 'high-pH' OPC concrete with clayey materials (bentonite, clay host rocks). However, the use of so-called low-pH cements in nuclear waste management is relatively recent. Thus, characterization and understanding of the long-term performance of low-pH concrete barriers and their interaction with other engineered or natural barriers has not received enough attention. Therefore, Amphos 21 has focused on the modelling of experiments with low-pH cement mixes, and on the development of a Common Modelling Task between WP3 partners to simulate and benchmark the interaction of low-pH concrete and Callovo-Oxfordian claystone.

Our goals within WP3 were to:

1) Lead the modelling work package contributions from the different partners.
2) Develop and implement a Modelling Task to integrate efforts within WP3, focusing on low-pH concrete/clay interfaces.
3) Develop numerical hydro-mechanical-chemical (HMC) models with a level of interpretation that covers the gap between a description of microstructural processes and the laboratory experiments. These models covered degradation processes studied experimentally in WP1, at the interface between low-pH cement paste and synthetic groundwaters (saline/clay/granitic). The experimental datasets used also included existing laboratory experiments developed at Chalmers University, in collaboration with SKB.
4) Co-supervise a PhD student (Stephan Rohmen) together with JUELICH on pore-scale reactive transport modelling of low-pH cement paste leaching.

2. Studied system

During the CEBAMA project, Amphos 21 has been involved in several modelling activities, studying different systems. These systems can be summarized as:

- Chemo-mechanical modelling of accelerated leaching experiments using OPC cement paste and concrete specimens performed by Chalmers University, in collaboration with SKB.
- Modelling of the hydration of the low-pH cement paste and concrete mixes developed within WP1 and referred to as CEBAMA reference mixes.
- Reactive transport modelling at 40ºC coupled to cement hydration modelling of low water-to-binder ratio and low-pH cement paste specimens tested under laboratory conditions at USFD; these experiments consisted of leaching tests using different synthetic groundwaters (granitic/clay/saline).

- Pore-scale reactive transport models were developed in collaboration with JUELICH to study the diffusive properties of the low-pH cement paste corresponding to the CEBAMA reference mix and assess the leaching under experimental conditions as defined by USFD.

3. Main results – Scientific highlights

3.1. Chemo-mechanical modelling of accelerated leaching experiments in OPC samples

A multi-scale chemo-mechanical model for cementitious materials has been implemented in iCP to simulate the degradation of transport and mechanical properties of cement paste and concrete as a function of the degree of calcium leaching from the samples. Recent experimental data of accelerated calcium leaching tests have been modelled. Comparison of the model with experimental data shows a relatively good agreement. The results of the multi-scale chemo-mechanical model show the impact of long-term interaction with groundwater on the physical properties.

3.2. Modelling of USFD experiments on low-pH cement paste

The leaching experiments of the low-pH cement paste samples by USFD were modelled using a coupled hydration-degradation model. The cement hydration model includes thermodynamic calculations coupled to a set of kinetic equations for the dissolution of the cement mix components. Degradation is modelled using traditional reactive transport models. Given the mix design of the reference CEBAMA cement paste, it is expected that hydration will continue to a significant degree for a much longer period than 28 days, which has been considered as curing time in USFD experiments. As a result, modelling of the leaching experiments require to simultaneously consider hydration and reactive transport in the simulations. In addition, due to the low water-to-solid ratio and the small dimensions of the samples, it is expected that during the curing period, moisture transfer from the exterior can play a non-negligible role in maintaining an internal relative humidity close to saturation. Thus, moisture transport inside the samples has also been considered. The model developed in the present work couples the three processes (i.e. hydration, reactive transport, and moisture transport). The results show the impact of long-term hydration and the differences between the leaching experiments using diverse groundwater compositions. Further comparison to experimental data will be attempted once these become available.

Technical Summary – BRGM – WP3

1. Introduction & Objectives

Since the mid-19th century, the building industry mostly uses Portland cement concrete, which is a composite material made of fine and coarse aggregates embedded in a Portland cement paste containing calcium-silicate-hydrate (C-S-H). Low-pH cement is a mixture of ordinary Portland cement (OPC), pozzolans (such as silica fume, fly ash, and metakaolin) and blast furnace slag. In addition to having a low water permeability and long-term durability, other properties of low-pH cement are of particular interest for the storage of high-level and long-lived radioactive wastes in deep geological formations. The presence of silica-rich pozzolans decreases pore water pH to values around 11 and hydration heat, limiting the alkaline attack on the surrounding clayey environment and thermal micro-cracking, respectively. It also increases compressional strength as well as the retention of alkali cations.

However, mineralogical and microstructural changes have been observed in laboratory when low-pH concrete was brought in contact with steel reinforcement or other materials (such as bentonite, clay rock or granite) of the geological nuclear waste repository. These changes were due to dissolution and precipitation reactions, such as C-S-H dissolution, calcium leaching, and carbonate precipitation, leading to the evolution of the pore space. By changing the surface binding and petrophysical properties of low-pH concrete, mineralogical and microstructural changes can potentially affect its performance, long-term durability, and confining properties.

In-situ monitoring methods that are fast, non-destructive, and can scan large material volumes are needed to control concrete stability. In the last two decades, the spectral induced polarization (SIP) method has gained popularity in hydrogeophysics to monitor hydraulic properties and biogeochemical changes of soils and rocks for environmental purposes. SIP is an impedance spectroscopy (IS) technique where the complex resistivity of the medium is measured with a four-electrode set-up: two electrodes to inject a sinusoidal current in the mHz to kHz frequency range and two electrodes to measure the resulting voltage in the medium. Resistivity magnitude and phase shift between measured voltage and injected sinusoidal current are very sensitive to conduction and polarization currents occurring in the bulk aqueous electrolyte and on the wetted surfaces of the pores, hence to the microstructure of the material. Compared to impedance spectroscopy with a two-electrode set-up, separation of potential from current electrodes in SIP reduces polarization of potential electrodes, which improves measurement accuracy for frequencies below 1 kHz.

Previous studies focused on the impedance of cementitious materials have mostly used a two-electrode set-up as typically done in impedance spectroscopy studies. Their measurement accuracy at low frequencies (typically < 1 kHz) was limited due to electrode polarization. In our study, the ZEL SIP system was used to measure the impedance of these materials in the low-frequency range (100 mHz - 45 kHz) with a phase shift accuracy of 1 mrad for frequencies below 1 kHz. Our SIP measurements were interpreted using the extended membrane polarization model to consider Maxwell-Wagner (MW) polarization and the interlayer spaces of C-S-H. The SIP measurements and their interpretation were also interpreted in terms of mean pore radius and length, pore radius and length distributions, and connected porosity.

2. Studied system

Samples are a mixture of CEM I Portland cement with silica fume, blast furnace slag, quartz sand, and added quartz-rich aggregates (granites) for concrete. CEM I mostly contains CaO (~ 67.5 weight %) and SiO_2 (~22.5 wt.%), hence has three CaO for one SiO_2 compound ($3CaO•SiO_2$), and C-S-H with a Ca/Si ratio of 1.7. Silica fume and quartz contain at least 95 wt.% of SiO_2, and blast furnace slag contains 42 wt.% of CaO, 36 wt.% of SiO_2, 11 wt.% of Al_2O_3, and 8 wt.% of MgO. The water-to-binder ratio, that is the ratio of the weight of water to the weight of cement, is 0.25 for HCP and 0.43 for concrete.

3. Main results – Scientific highlights

The measured HCP and concrete resistivity magnitudes are extremely high with values above 1 kΩ·m and decrease when frequency increases due to polarization mechanisms such as membrane and MW polarization increasing conductivity (Figure 1a). However, these resistivity magnitudes are surprising at first glance because the bulk pore water resistivity may be relatively low (the measured resistivity of the water surrounding the samples in the storage box was 11.6 Ω·m) and the measured sample porosities are relatively high (~ 25% for HCP and ~ 12.5% for concrete). Interestingly, for frequencies below 1 kHz, the HCP resistivity magnitude is ~ 1.7 times the concrete resistivity magnitude despite the fact that the HCP porosity is about twice as high. The observed resistivity difference can be explained by the difference in the binder content of the two samples. HCP and concrete have a binder-to-water ratio of 4.0 and 2.3, respectively, hence their binder ratio is ~ 1.7, the same ratio than for resistivity. C-S-H has a high specific surface area (between ~125 and 500 m^2/g) and occupies most of the volume of hydrated low-pH cement. Therefore, the extremely high HCP and concrete resistivities can be explained by their C-S-H content. Because the sample resistivity is controlled by the C-S-H content, it seems reasonable to suppose that the lamellar shape of C-S-H particles (explaining their high cementation exponent and resulting long current paths) and their very resistive interlayer spaces (explaining their low electrically connected porosity) are responsible for the extremely high resistivity of HCP and concrete.

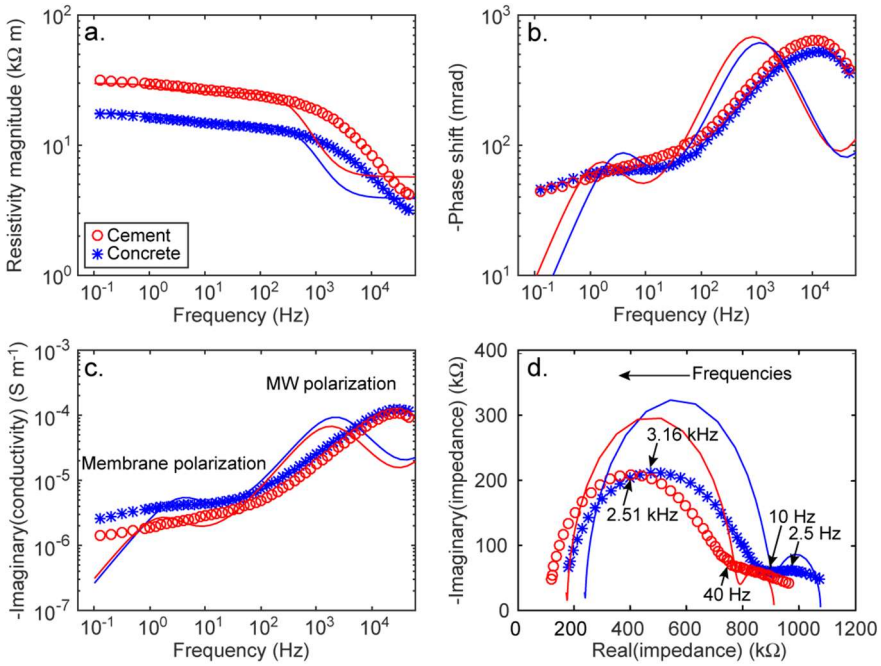

Figure 1: *Measured HCP and concrete SIP spectra (symbols) and simulation results using one bi-tube system (red line for HCP and blue line for concrete).*

The measured phase shifts of our cementitious materials are relatively similar, very high (magnitude above 40 mrad and 100 mrad for frequencies > 100 Hz), and increase when frequency increases up to a frequency of around 10 kHz (Figure 1b). Observed phase shifts are very high because of the very high resistivities of the materials. Indeed, the phase shift depends on the ratio between the imaginary and real conductivity. A very resistive sample has a very low real conductivity and therefore may exhibit a very high phase shift. Because HCP has a higher resistivity than concrete, it has a higher phase shift for frequencies above 1 Hz. However, HCP has a slightly lower phase shift than concrete for frequencies below 1 Hz because HCP has a lower imaginary conductivity than concrete, especially for frequencies below 10 Hz (Figure 1c). Imaginary (or quadrature) conductivity is very sensitive to polarization. Concrete polarizes more than HCP because concrete contains less pore volume occupied by the interlayer spaces of C-S-H, which are "dead" from the perspective of electrical conduction and do not participate in current transport. The presence of additional large granite grains in concrete may induce pore polarization over large (μm to mm) scales and may explain why concrete polarizes more than HCP for low frequencies.

Both the phase shift and the imaginary conductivity increase with frequency because of polarization processes such as membrane and MW polarization (Figure 1b and Figure 1c). From the measured phase shift spectra, membrane polarization alone may also not be able to explain the SIP measurements over the entire frequency range, especially for frequencies above 100 Hz. Negative imaginary impedance versus real impedance measurements (Nyquist plots) also exhibit two semi-circular shapes (better seen for concrete at low frequencies) that may indicate two different polarization processes such as membrane and MW polarization (Figure 1d). Frequencies corresponding to the maxima and minima of the spectra are indicated in Figure 1d. It should be noted that the phenomenon of electrode polarization occurring for low frequencies (typically < 1 kHz) is minimized in our SIP measurements. Therefore, SIP measurements below 100 Hz are particularly interesting in our study.

2D network models where each single impedance corresponds to that of a bi-tube pore system (Figure 2) were used to compute the resistivity of the cement-based materials (Figure 2). Kirchhoff's law leads to a system of equations that can be solved numerically to obtain the impedance of the entire network. Each bi-tube pore system considers membrane polarization as discussed in the previous section. Compared to the computations of the bi-tube pore system, the modelled phase shift spectrum is smoother over the entire low-frequency range, and its shape as well as the imaginary conductivity and Nyquist plots for frequencies below 50 Hz are in better agreement with the measured data. Pore radii inferred from the pore network models are smaller than the values inferred from MIP (Figure 3 for HCP). Only electrically connected pores were included in the models. The connected porosity is still very low and in the percent range. The two bi-tube systems in parallel give the best agreement with the experimental SIP data for frequencies above 100 Hz. The parameter values after manual calibration to the measured SIP data are given in Table 1. Compared to the previous simulations, the mean pore radii (0.2 – 0.25 μm for the wide pore and 5 nm for the narrow pore) are in closer agreement with the measured ones (~ 0.5 μm and 6.5 nm). In addition, the model porosities, ~ 23.8% and 12.8% for HCP and concrete, respectively, better match the measured values (~ 25% and 12.5%).

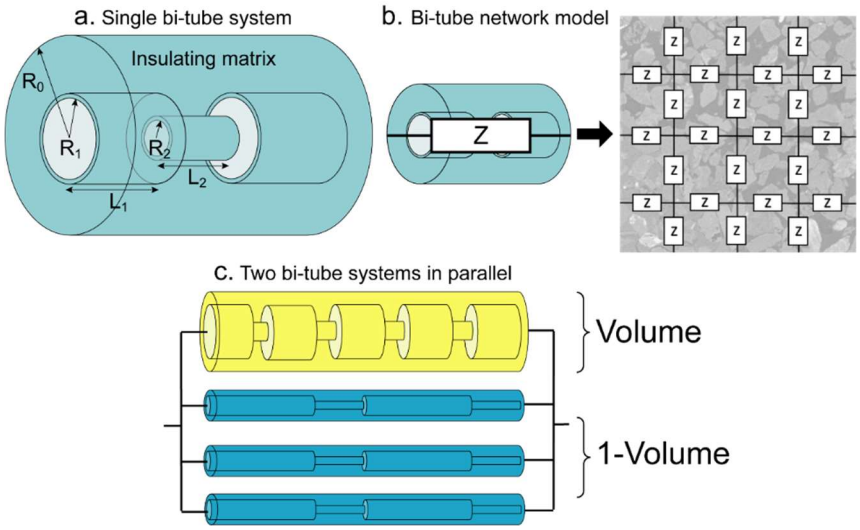

Figure 2: *Impedance models to interpret HCP and concrete SIP spectra.*

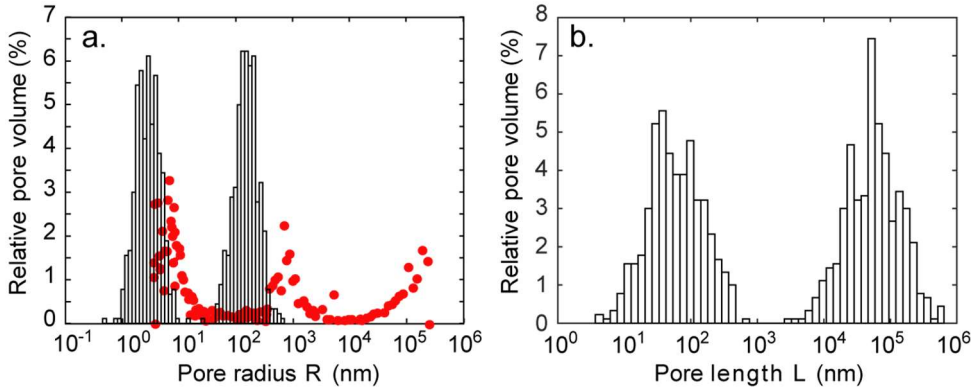

Figure 3: *a. Pore radius distribution and b. pore length distribution used in the network model to match the SIP measurements on HCP. Filled red circles are the pore radii measurements from MIP. The distributions used in the network model to match the SIP measurements on concrete look similar and are not shown for brevity.*

Table 1: *Geometrical parameters of the two bi-tube systems in parallel.*

Property	Symbol	Cement (1)	Cement (2)	Concrete (1)	Concrete (2)
Pore 1 radius	R_1	0.25 µm	1 µm	0.2 µm	1 µm
Pore 2 radius	R_2	5 nm	0.13 nm	5 nm	0.13 nm
Pore 1 length	L_1	42 µm	10 µm	42 µm	10 µm
Pore 2 length	L_2	80 nm	800 nm	80 nm	800 nm
Matrix radius	R_0	4.5 µm	1.4 µm	3.1 µm	1.92 µm
Volume fraction	w	0.5	0.5	0.5	0.5

Technical Summary – JUELICH – WP3

1. Introduction & Objectives

Physical and chemical heterogeneities exist in a range of length scales (nm to cm) in cementitious materials. The macroscale physical and chemical properties of concretes and mortars, etc. strongly depend on the pore structure evolution during hydration and long-term degradation processes. Therefore, pore-scale models can be regarded as an appealing tool to describe the pore space structure and non-uniform distribution of chemical species in a realistic manner. The use of pore-scale models in other disciplines, such as in oil and gas production industry, is relatively well established for natural rocks. However, pore-scale models of cement-based materials are only starting to be developed and the coupling to geochemical codes to perform reactive transport calculations of the evolution of cementitious materials on the pore scale is challenging, due to high computational demands. However, the advantage of these pore-scale models over traditional meso- and macro-scale models is that they allow to explicitly capturing microscopic effects of chemical reactions on the physical properties in a mechanistic way. Thus the focus of this work, which is in line with the objectives of the CEBAMA project, was to develop and validate a pore-scale reactive transport model in order to study the mass transport behaviour and the impact of the chemical degradation of cement pastes (e.g. due to calcium leaching and/or carbonation) on its transport properties, such as diffusivity, permeability, porosity, and pore size distribution. For this purpose, a three dimensional (3D) advection-diffusion solver based on the Lattice Boltzmann Method (LBM) was coupled to a geochemical software.

2. Studied system

The pore-scale reactive transport code *iPP* developed within CEBAMA WP3 is applicable to address (reactive) transport processes in cementitious materials in general, as well as in other natural or synthetic porous media, and is not limited to specific systems. However, within the CEBAMA project, for code testing and validation in particular leaching of the VTT CEBAMA low-pH reference paste was addressed, using selected leaching experiments performed by USFD with various groundwater types (granitic water, clay water, saline water) as application case.

3. Main results – Scientific highlights

In the frame of the CEBAMA project, a coupled code named *iPP* (**i**nterface **P**alabos **P**hreeqC) was developed. *iPP* is able to calculate reactive transport processes in porous media on the pore scale using the operator splitting technique (Sequential-Non-Iterative-Approach, SNIA) to distribute the task of transport to the dedicated advective-diffusive transport code, while a chemical simulator solves the chemical system subsequently. For this, a code based on the Lattice Boltzmann method (Palabos) was used in combination with a geochemical solver based on the law of mass action (PhreeqcRM). Promising benefits of using a Lattice Boltzmann based technique compared to finite element methods (FEM) are straight forward obtainable computational parallelization, due to localized calculation of transport properties and simple and flexible implementations for updating pore geometries.

Cementitious materials are consisting of different phases with different diffusive properties, e.g. C-S-H, as diffusive phase while other hydration phases are deemed to be essentially non-diffusive. C-S-H by itself is a nano-porous material and its diffusivity is determined by various factors including its gel porosity. This gel porosity was not resolved in the pore-scale model developed here, which deals with the micrometre scale rather than the nanometre scale, thus assuming C-S-H as continuous diffusive phase. Following this, the contrasts in diffusion coefficients between sound C-S-H and the solute diffusivity in free water (as in the capillary porosity domains) are about 3 to 4 orders of magnitude. This required using a more sophisticated collision operation in the Lattice-Boltzmann transport simulation than the common Single-Relaxation-Time (SRT; i.e. Bhatnagar–Gross–Krook (BGK) model), since the simple SRT technique is prone for numerical oscillations and errors under the conditions mentioned above. Subsequently, the Two-Relaxation-Time (TRT) collision operation was implemented in the framework of Palabos which overcomes the numerical issues of the ordinary SRT/BGK scheme.

One major focus during the development was the application of *iPP* on high-performance computing (HPC) facilities. Thus, *iPP* exploits MPI parallelization and C++ template meta-programming techniques, allowing usage of a distributed memory computational model and optimizations by modern compiler features. During the course of developing the coupling code, performance measurements revealed major bottlenecks in terms of parallelization overhead due to MPI communication in the PhreeqcRM module. Several optimizations were implemented inside and on top of PhreeqcRM for improving performance scalability on cluster computers.

To validate the coupling between the Lattice Boltzmann transport code and the geochemical solver, 1D diffusion problems were addressed and the results of the numerical simulations were compared to respective analytical solutions. The results determined by the numerical Lattice Boltzmann scheme and those from the analytical solutions were in very good agreement, minor variations were thought to result from the spatial discretization in the numerical simulations.

For benchmarking and validation of *iPP*, leaching experiments performed at the University of Sheffield (USFD) within CEBAMA WP1 were used. Within CEBAMA WP1, USFD conducted experiments that are dedicated to quantify compositional and microstructural changes in low-pH cement pastes due to leaching with different types of groundwaters. The mixture of the cement paste is similar to the one provided by VTT within the CEBAMA project, with the exception that quartz filler is not added to the mix. For selected samples of the hardened cement paste, micro-X-ray computer tomography (μXCT) imaging data were obtained. Due to the common artefact called “partial volume effect” these data could not be segmented by a simple threshold algorithm. Therefore, these volume data were treated by a newly developed segmentation technique which mitigates this effect. Using this algorithm, a three-dimensional (3D) phase distribution in the cement paste specimens was derived, in which air, silica fume, calcium silicate clinker, blast furnace slag, aluminate/ferrite clinker and hydration products could be distinguished (see Figure 1). However, a further separation of different hydration phases was not possible, due to very similar grey values. In order to overcome the gap of information regarding the abundance and distribution of the various hydration products, results of a PhreeqC hydration model of the same cement paste were used, to assign the composition of this mixture of hydration phases.

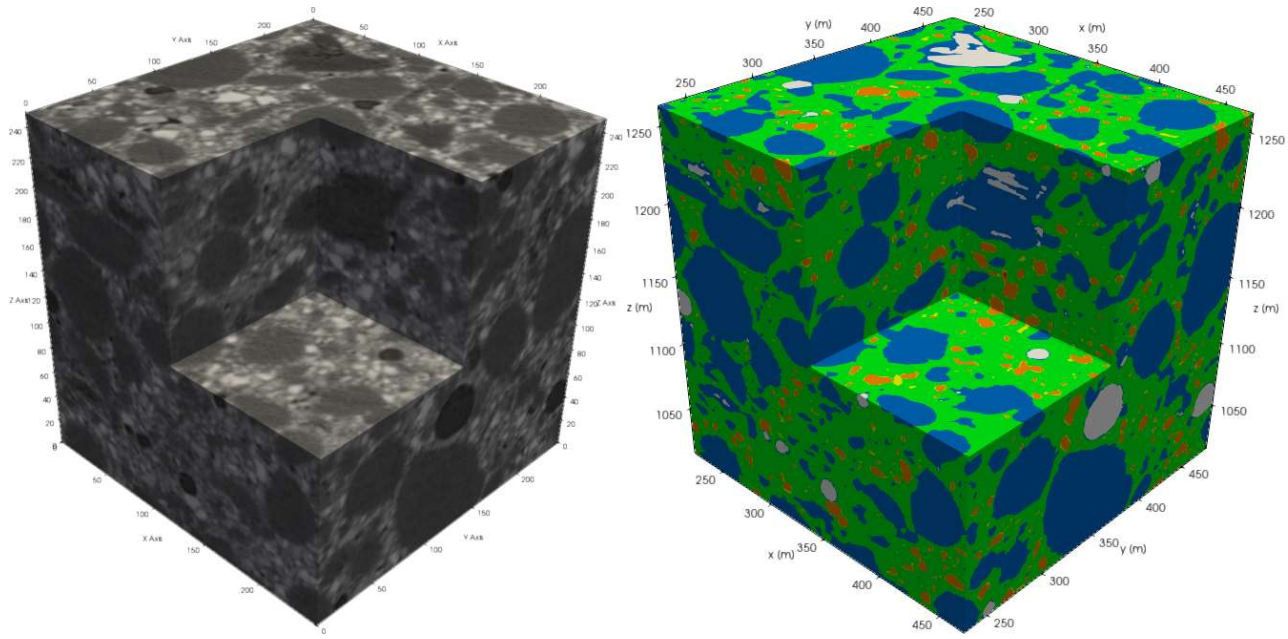

Figure 1: *Original µXCT raw grey image data corresponding to the extracted cube (left) and microstructure of CEBAMA reference paste from segmented µXCT data used as input geometry for the calculation of effective diffusion coefficients (right). A box was clipped from the cube for illustrative purposes. Phases: Air (white), silica fume (blue), alite/belite (yellow), blast furnace slag (orange), aluminate/ferrite (red) and hydration products (green). Total model size is 750 x 750 x 750 µm with a resolution of 3 µm.*

As earlier mentioned, the C-S-H phase was assumed to be diffusive, due to its nano-porous structure. Due to the assumed homogeneous mixture of hydration phases within the hydration products, a corresponding diffusion coefficient had to be estimated. For this, a diffusivity relationship was applied which was based on micromechanical homogenization approaches as Mori-Tanaka (MT) and differential effective media techniques.

Different modelling tasks were conducted which included all the previously mentioned techniques, derivations and assumptions. One modelling application was a 3D simulation of the effective diffusion coefficient of the low pH paste (due to a lack of experimental data at that time), using a linear diffusion setup with constant boundary conditions. For this purpose, a representative cube with dimensions of 750 x 750 µm was extracted from the microstructural model and the effective diffusion coefficients in the x, y and z directions were determined from steady-state diffusive fluxes to check for possible anisotropic diffusivity, applying constant concentration gradients (see Figure 2). The resulting average effective diffusion coefficient was estimated at $3.47 \cdot 10^{-12}$ m^2/s. However, one has to emphasize here that this value corresponds to a low-pH cement paste which did not include the quartz filler and experienced a limited curing time of only 28 days. Effective diffusion coefficients for aged CEBAMA reference cement pastes are likely to be lower, due to further hydration of clinker, slag and silica fume.

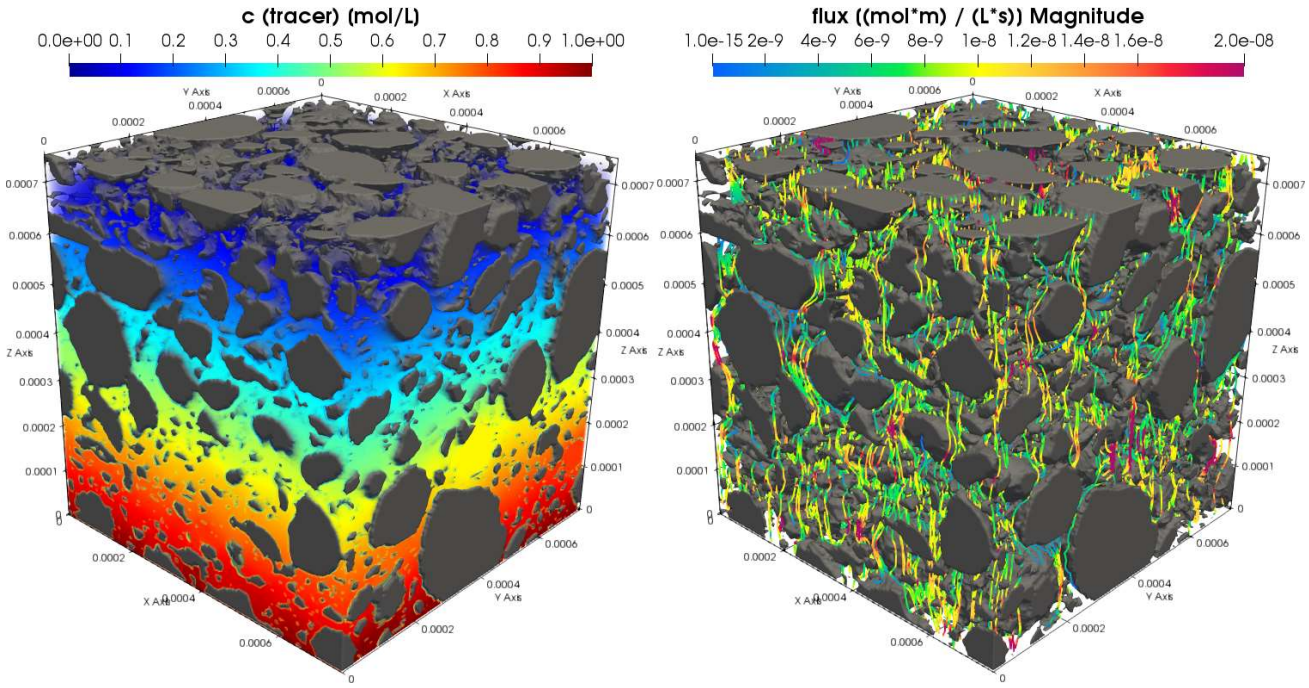

Figure 2: *Tracer concentration profile (left) and diffusive flux streamlines (right) of inert tracer after convergence of diffusion coefficient simulation in z-direction. Non-diffusive phases are indicated in grey while hydration products and voids are transparent.*

To simulate the leaching experiments performed by USFD, a 2D slice of the microstructure was extracted and combined with a constant concentration boundary condition on the left side as inlet. The solute concentrations applied at this boundary referred to the granite water composition, equilibrated with respect to calcite. The simulation was run for 40 minutes physical time. The results show that there is a rather quick clogging effect at the cement-water interface due to calcite and hydrotalcite precipitation (see Figure 3 and Figure 4, left). At the same time calcium is leached from the C-S-H phase reducing its Ca/Si ratio and leading to an increased porosity in the leached zone, while the porosity decreases in the carbonated zone (see Figure 4, right).

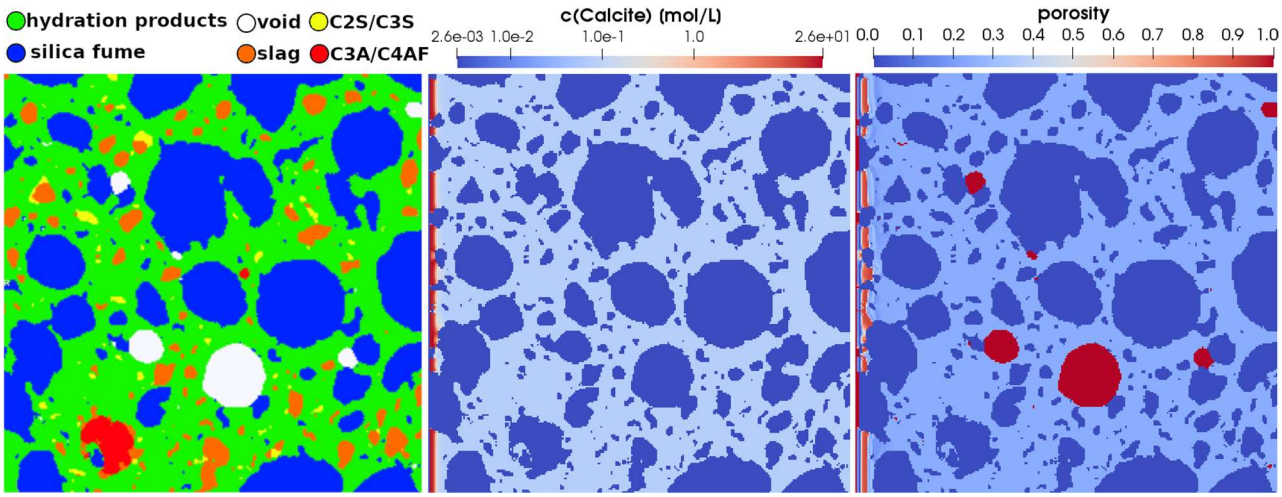

Figure 3: *Initial microstructure (left), calcite concentration in mol/L (center) and porosity (right) after leaching of the cement paste with granite water for 40 minutes. The size of the model domains is 750 x 750 µm.*

Although the simulation time was only 40 minutes compared to the several month of leaching time in the experiments, this outcome is qualitatively in line with the results of USFD, which also suggest a passivation effect at the beginning of the experiments. In order to predict the leaching process over the experimental time scales an appropriate upscaling technique must be applied, i.e. by deriving constitutive relationships between leaching water composition and resulting time dependent leaching rates. Finally, the time dependent leaching rates have to be normalized to the surface area of the simulated interface to be able to simulate this type of leaching experiments over the time scale of several months.

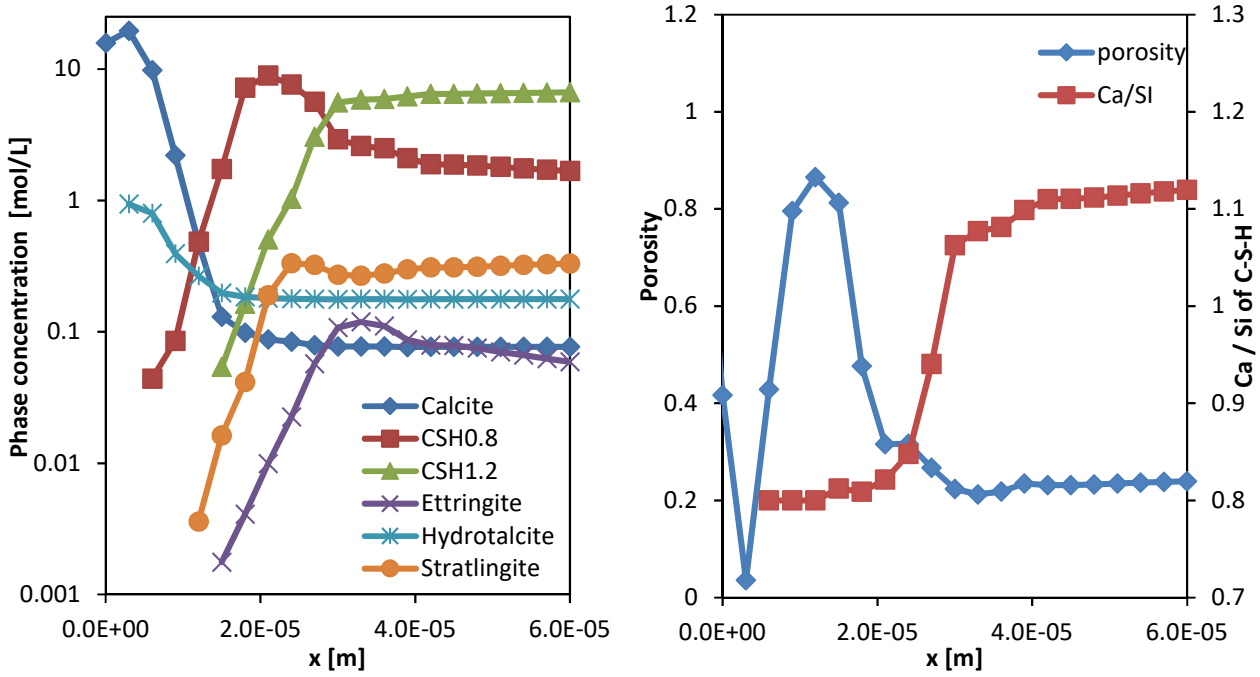

Figure 4: *Average solid phase concentrations (left) and average porosity (right, blue, left axis) and Ca/Si ratio of C-S-H phase (right, orange, right axis) at the cement paste interface after leaching with granite water for 40 minutes.*

Another point of uncertainties affecting the simulation results is the expected heterogeneity of the hydration product phase. Due to the lack of resolution in the imaging technique used, it was not possible to distinguish between the different hydration phases like C-S-H, ettringite, hydrotalcite or calcite in the hydration products. This required to homogenize all hydration products in the simulation and to use additional information from non-spatially resolved hydration modelling to derive the input for the simulation. In particular the composition of hydration poducts located close to clinker grains is expected to be different than hydrates forming in the pore spaces. To solve this issue, further investigations with higher resolving imaging techniques in particular focused on hydration products in this type of cementitious materials are necessary.

Technical Summary – NRG – WP3

1. Introduction & Objectives

The main objective of our contribution was to collaborate with the TU-Delft on increasing the understanding of electromigration multic-component diffusion processes in clay-cement systems, by carrying out electromigration experiments (TU-Delft) and implementing electromigration in a reactive transport model ORCHESTRA (NRG).

2. Studied system

The systems worked with within the CEBAMA project where first the experimental Boom clay and bentonite systems, spiked with Se under controlled potential gradients.

Furthermore, the cement – clay model systems as described in the WP3 benchmark exercise were used.

3. Main results – Scientific highlights

In summary we have:

- Implemented an efficient multicomponent-diffusion module in the ORCHESTRA framework.
- We have carried out simple benchmark calculations to verify the correctness of the implementation.
- We have carried out scoping calculations for the experimental system of the TU-Delft.
- We have verified our calculations against experimental results for electromigration of Se in bentonite and boom clay by the TU-Delft.
- We have taken part in the WP3 benchmark exercise.

Technical Summary – SKC·CEN – WP3

1. Introduction & Objectives

Coupled reactive transport codes are potential helpful in understanding coupled chemical-transport processes on the evolution of a material. These codes starts from an explicit representation of the microstructure; for cement systems, this could be liquid, portlandite, calcium-hydrates silicates, and clinkers. A first challenge is to obtain representative reconstructions of the microstructure that can be based, for cement systems, on hydration modelling, SEM images or FIB-SEM images. A second challenge is to simulate the chemical complex process of combined dissolution and precipitation in a microsystem in which not all pores can be resolved explicitly. The so-called gel pores of a cement system are typically smaller than the spatial resolution of the pore scale model but can form important connected transport paths in cement systems. In addition, dissolution is straightforward to implement in a pore scale model; however, there are conceptual challenges for the precipitation process: where does precipitation happens? Will it occupy completely the pore spaces and are the underlying solid phases still accessible.

The objectives are:

- To improve the representation of cement alteration due to dissolution and precipitation (leaching and carbonation) in a coupled reactive pore scale reactive transport model.
- To evaluate the prediction of macroscopic variables from microstructural information.
- To apply a reactive coupled micro-scale model for simulating the spatial-temporal evolution of geochemical changes in a cement matrix.

2. Studied system

The interaction between a high pH cementitious material with a clayey host rock (Boom Clay).

The conceptual approach development is done for cement materials.

3. Main results – Scientific highlights

3.1. Conceptual framework for precipitation-dissolution modelling in a cement microstructure

In a pore scale model, nodes are often described as either solid or pores. However, at the micrometer scale, a precipitating phase does not always fill the complete pore space, some residual pore space may remain in a precipitated layer covering the rock material. Consequently, mass exchange between the fluids in the pores and the underlying rock material is still possible. Within a multilevel pore-scale model, both resolved pores (solid/pore nodes explicitly represented in the model) and unresolved pores (porous system within a computational node) are present which enables to account for the incomplete filling of nodes during precipitation. Similarly, it is used for nodes in which the solid phase is dissolving or to represent gel pores (size much smaller than the resolution of the pore-scale model). The last aspect of our concept is the mechanism to control the amount of precipitation in a node.

The solubility of solid phases increases with decreasing pore radius. Thus, precipitation will stop before all (unresolved) pores are filled and complete clogging of a node is avoided.The concept of the pore-size dependent solubility will control the residual pore space in a precipitating layer. The implementation was done in the Lattice-Boltzmann solver YANTRA (Patel et al. 2014). The solver is coupled with PHREEQC (Parkhurst et al. 2013) for geochemical calculations including precipitation and dissolution.

3.2. Numerical accelerated procedure for modelling dissolution at the pore scale

To decrease the calculation time of a pore scale modelling study involving only dissolution processes, decreasing the number of time steps. The idea is that the number of iterations can be reduced if the chemical buffering is sufficient to bring transport to a steady state. The criteria is defined by a dimensionless number, introduced as the buffering number Bu. If this condition is satisfied, then it is possible to reduce physical (and thus also computational) time by adjusting the chemical system appropriately (e.g. decreasing the amount of solids, or increasing the equilibrium concentrations). Using appropriate relations, the accelerated simulations can be transformed back to time-scales for the real system.

An illustration of the method uses the simulation described in Seetharam et al. (2018) concerning leaching . The acceleration solved the problem in a few hours which is significantly faster than without acceleration that needed about one month of calculation. This enables analysis of larger systems or to perform a parameter sensitivity or uncertainty analysis in the same time. The figure below shows that the dissolution front (white represents portlandite) obtained with the proposed approach is virtually the same at the original system and at 50 times accelerated system (right).

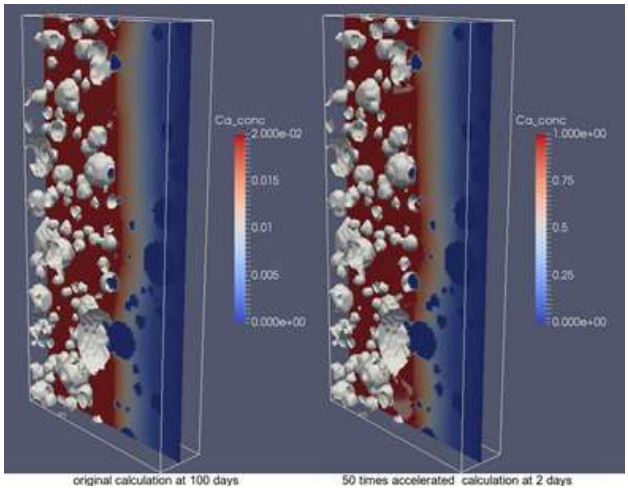

Figure 3: *Dissolution front in mortar at 100 days for the original system (left and at 2 days for system with 50 times higher Bu number (right). Dissolved Ca concentration is given in mol/dm^3. Dark blue spots are aggregates (zero concentration).*

3.3. Reconstruction of 3D microstructures from 2D SEM images

To reconstruct the cement paste with 4 phases, a hierarchal porous media reconstruction algorithm based on simulated annealing was developed. The reconstruction algorithm simulates one phase after each other. To initialize the reconstruction process the training image is therefore transformed into a binary image i.e. the first phase to simulate (e.g. clinker phase) and the background of the phases not simulated yet. In the next step the algorithm determines the histogram of this binary image and initializes a reconstruction with the desired shape and the same histogram as the training image (Ti).

Next the Ti and the reconstruction grid (Rg) are scanned in various direction and two spatial two- points correlation functions. Subsequently the misfit between the individual structural descriptors in Ti and the Rg is determined. In the so-called pixel switching phase, the algorithm will minimize the misfit between the structural descriptors. In this phase, always a pixel from currently simulated phase and the background in the Rg are exchanged. The results of such cement past reconstructions in 2D can be seen in the figure below. We assumed an isotropic material for the 3D simulation. Accordingly, the structural descriptors for the third dimension could be predicted and used for the misfit determination. Figure 1 shows the reconstruction of an isotropic medium in 3 directions, where the continuity between the different slices is ensured.

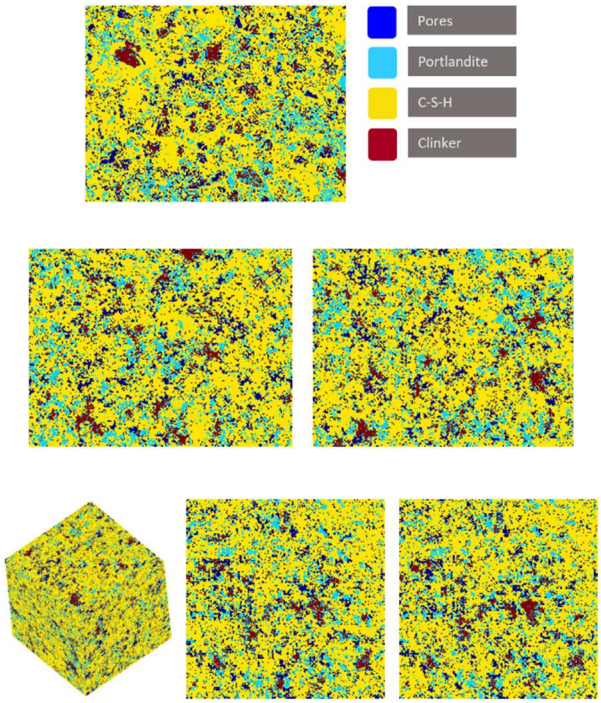

Figure 1: *(Top) Schematic SEM image used as a training image in the algorithm. (Middle) Two independent 2D reconstructions of the training image. (Bottom) 3D view of a reconstructed block using the 2D training image plus two consecutive slices of the Block in z direction to show that the continuity of the particles is also ensured in the z direction.*

3.4. Prediction of effective diffusion coefficient from microstructural information

Three different methods are used to reconstruct the microstructure: (i) simulated microstructure using a cement hydration model (CEMHYD3), (ii) reconstructured using 2D images (see above), and (iii) measured using FIB-SEM with a resolution of 5 nm (data from BRGM collected during CEBAMA project). Using YANTRA, Effective diffusivity along a certain direction can be obtained by applying a fixed concentration gradient over the domain. Taking x direction for instance:

$$D\_ex/D\_0 = Fx/\nabla c$$

where Fx is the average flux in x direction at the steady state; ∇c is the concentration gradient applied at left and right boundaries and equal to 1/L; D_0 is molecular diffusion coefficient in pure water.

The second method (reconstructed) was applied to existing experimental data and predicted D_{ex}/D_0 was close to experimental data (0.0028 versus 0.0032). Differences were larger between WP1 results and predictions with a cement hydration model. FIB-SEM data (obtained from BRGM, WP1)

3.5. Simulation of leaching of hardened cement paste

Simulation of leaching/carbonation of cement during interaction with other materials will be done by the geochemical solvers in YANTRA. The approach was tested by simulating leaching of a hardened cement paste using a microstructure obtained from hydration models. Calculations are shown below for a 3D microstructure (see Figure 2). Leaching rate is directly linked to the ability of ions to transport through the cement paste (thus, higher w/c leads to larger leaching rates). Portlandite dissolution influences capillary pore connectivity in different ways depending on w/c: (i) improved connectivity perpendicular to leaching at low w/c, (ii) first fast improved connectivity perpendicular to leaching followed by improved connectivity in the direction of leaching at intermediate w/c, and (iii) uniform increas in degree of percolation at high w/c. There is a transition zone where portlandite dissolution and C-S-H decalcification occur simultaneously.

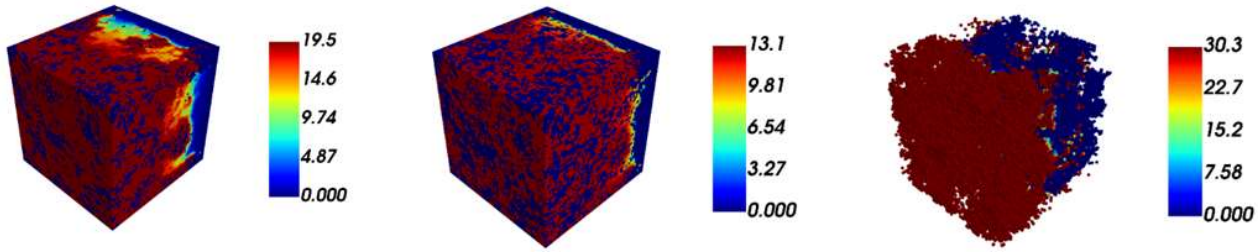

Figure 2: *Simulation of leaching of a hardened cement paste (w/c 0.4) using a microstructure generated with CEMHYD3. (left) Ca concentration in aqueous phase (mol/l), (middle) C-S-H phase (mol), (right) portlandite phase (mol).*

3.6. Simulation of leaching-carbonation of hardened cement paste

A 2D simulation (microstructure from SEM images) was performed for combined leaching – carbonation with a $NaHCO_3$ boundary conditions as a proxy for Boom Clay pore water. Figure 3 below show spatial distribution of portlandite (40% dissolution), calcite and C-S-h at the end of the simulation period (10 s), together with some integrated variables. The developed framework enables to trace the change of effective parameters (porosity, effective diffusion coefficient) during leaching and carbonation. As expected for the boundary condition (only clay water, no clay), a increase in porosity (and thus effective diffusion) is observed.

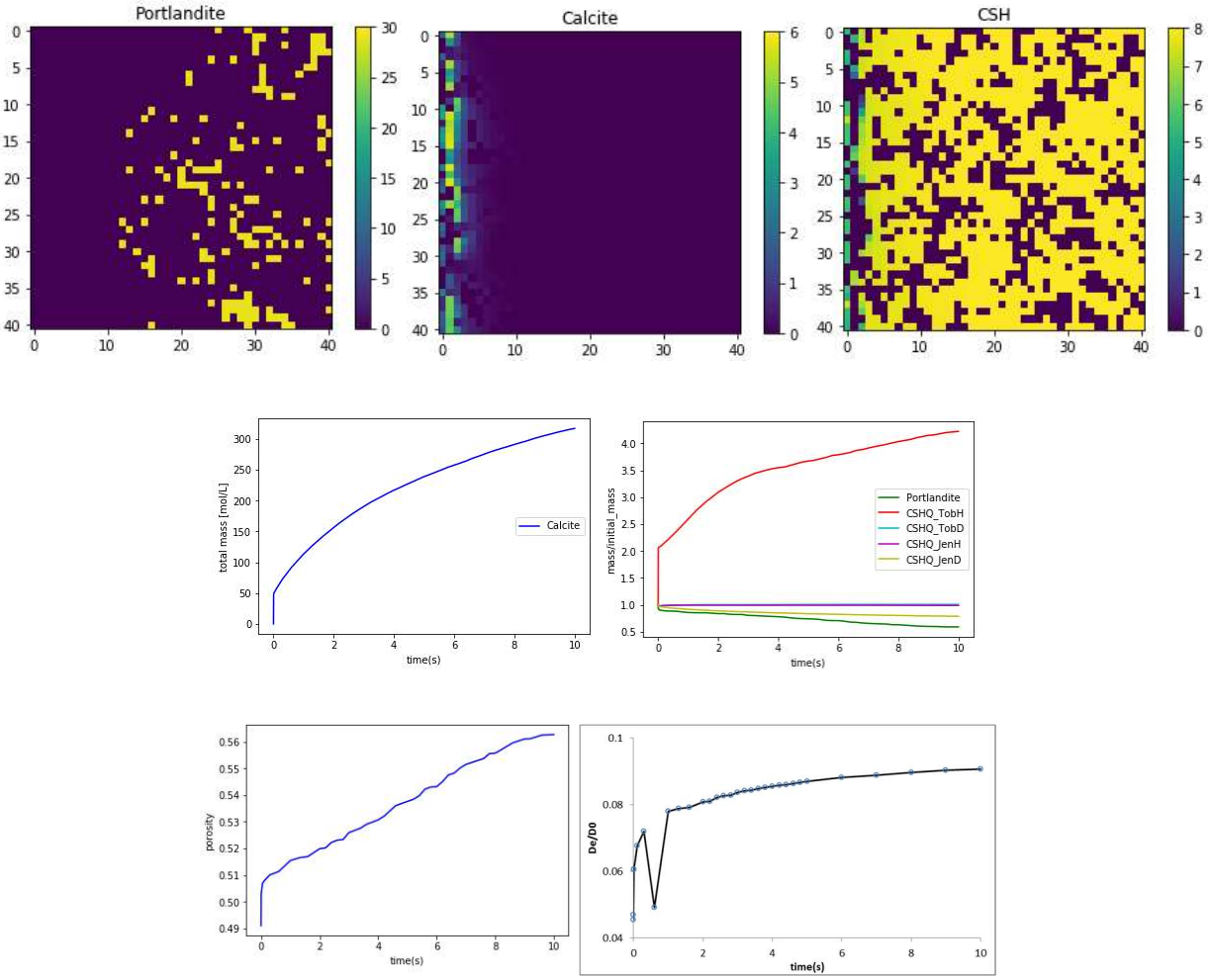

Figure 3: *Leaching-carbonation of cement in contact with $NaHCO_3$ (Boom Clay water). (Top) Spatial distribution of cement phases after 10 s of leaching. (Middle) Change of cement minerals in the whole cell. (Bottom) Effective properties (porosity and D_e/D_0).*

Technical Summary – UDC – WP3

1. Introduction & Objectives

The geochemical evolution of the bentonite and concrete interface during the initial stages of the hydration and heating of the repository depends on the thermal, hydrodynamic and mechanical processes. Coupled THCM numerical models are required to quantify such couplings. For that purpose, UDC has developed coupled THCM computer codes. These codes have been tested and calibrated first with experimental laboratory data on the interactions of concrete and clay.

- Objectives:
  - Improve the reactive transport models and codes for modelling the cement-clay interactions and the chemical, mechanical and hydrodynamic couplings.
  - Perform numerical models of the heating and hydration laboratory experiments already carried out by Ciemat on concrete and compacted bentonite (HB tests) to study the interactions of concrete and bentonite under repository conditions.
  - Perform long-term reactive transport modeling of the concrete and bentonite barrier system of a high-level radioactive waste repository in a clay formation (performance assessment).
- Work within CEBAMA:
  - We have improved the UDC reactive transport codes (CORE2D V5 and INVERSE-FADES-CORE) for modelling the time evolution of porosity, permeability and diffusion coefficient due to changes in mineral precipitation/dissolution. The improvements have been verified.
  - We have performed numerical models of the heating and hydration laboratory experiments on compacted bentonite and concrete (HB tests). We have performed a sensitivity analysis of the numerical models of the heating and hydration laboratory experiments on compacted bentonite and concrete (HB tests). The sensitivity analysis included: 1) thermal field, 2) mineral phases and 3) grid size. The results obtained were presented in the 1st and 3rd Annual Workshops and the S+T Contributions and Deliverables D3.01, D3.04, D3.05 and D3.06. and also published on a paper in Applied Geochemistry in 2018 (Samper et al. 2018).
  - We have performed the long-term reactive transport numerical model of the interactions of concrete, compacted bentonite and clay in a HLW repository in clay. We have analyzed the effect of the grid size on the numerical solution and the effect of porosity feedback. The results obtained were presented in the CEBAMA 2nd Annual Workshop and S+T Contribution.
  - We also participated in the CEBAMA Common Modeling Task and have colaborated with other members of the work package 3.

2. Studied system

Our group has performed coupled thermo-hydro-mechanical and chemical numerical models of bentonite and concrete interfaces. These models have been tested with lab tests performed within the CEBAMA project on OPC concrete samples.

3. Main results – Scientific highlights

3.1. Modelling of experiments performed within CEBAMA

Several tests were performed to study the interactions of concrete and bentonite pore water at the conditions prevailing in the EBS during the early hydration stage (Turrero et al. 2011; Torres et al. 2013). The tests, denoted as HB tests were performed on medium-size cells containing a 7.15 cm thick bentonite sample in contact with a 3 cm thick concrete sample. The cells were hydrated at a constant pressure and at a temperature of 25ºC at the top of the cell through the concrete, while the temperature was maintained constant at 100ºC at the bottom of the cell (Figure 1). The HB column tests provide data on the nonisothermal interactions of concrete and bentonite after 6, 12, 18, 54 and 80 months (HB1 to HB5 tests) and 104 months (HB6 test). The later was dismantled within the CEBAMA Project.

HB1 to HB6 tests were modelled with a 1D grid by assuming that the main direction of the water flow, heat transfer and solute transport is parallel to the axis of the column. Grid size is uniform and equal to 0.9 mm. The model domain includes the concrete ($0 < x < 3$ cm) and the compacted bentonite (3 cm $< x < 10.15$ cm). Bentonite and concrete parameters were taken from the model of the HB4 test in Samper et al. (2013; 2018). The concrete has a porosity of 0.125 and an initial gravimetric water content of 2.2%. The initial temperature is 22ºC along the cell. The prescribed temperature at the bottom of the column, where the heater is located, is 90°C. This temperature is lower than the heater temperature due to lateral heat losses. Similar to the THCM models of the FEBEX bentonite (Zheng et al. 2010; 2011), the initial total stress was assumed uniform, isotropic and equal to 250 kPa. The liquid pressure in the injection tank was initially equal to 500 kPa. It decreased after 400 days due to problems in the water injection system. The liquid pressure at the injection boundary was assumed equal to 500 kPa for $t < 400$ days and 100 kPa afterwards.

The initial mineral volume fractions in the concrete are: 7.4% for portlandite, 2.2% for ettringite, 14.6% for C1.8SH, 1% for brucite, 0.1% for calcite and 62.2% for quartz. Quartz is assumed to be nonreactive. The initial mineral volume fractions in the bentonite are: 0.36% for calcite, 0.08% for gypsum and 1.192% for cristobalite. The smectite was assumed to be not reactive. The model allows for the precipitation of the following secondary minerals: sepiolite, C0.8SH, anorthite and anhydrite. The dissolution/precipitation of portlandite, ettringite, C1.8SH, C0.8SH, quartz and cristobalite was simulated with the kinetic rate laws of Fernández et al. (2009). The specific surfaces of some minerals were calibrated to reproduce the experimental mineralogical observations. Cation exchange and proton surface complexation reactions were assumed to take place only in the bentonite. The current model accounts for the changes in porosity caused by solid deformation and swelling, but disregards the changes in porosity due to mineral dissolution/precipitation because the mechanical changes in porosity for bentonite were generally larger than the chemical changes in porosity. More details can be found in Mon (2017) and Samper et al. (2018).

Model results reproduce the general trends of the measured water content, porosity, and temperature and the observed patterns of mineral phases for the HB1 to HB4 tests. The predictions of the HB5 and HB6 tests show similar trends to those of the rest of the tests (Figure 1). The thickness of the bentonite zone where calcite and brucite precipitate in the constant temperature run is larger than that of the base run. While brucite precipitates in

the concrete and in the bentonite in the base run, this mineral precipitates only in the bentonite in the constant temperature run. The reduction in porosity in the concrete near the bentonite interface and in the bentonite in the constant temperature run is smaller than that of the base run. These results in the constant temperature run attest the conclusions of Lalan et al. (2016) who concluded that the temperature plays an important role in the degradation of C-S-H and the precipitation of mineral phases. The intricate interplays of thermal and chemical processes in this complex chemical system prevent a simple explanation for the results of the sensitivity run to temperature.

Model results are sensitive to the increase of the specific surfaces of portlandite and ettringite. On the other hand, model results are not sensitive to kinetic Mg-saponite precipitation. Mineral precipitation increases at both sides of the concrete/bentonite interface when the grid size is reduced. The calculated porosity in the concrete near the bentonite interface decreases drastically, reaching pore clogging for grid sizes smaller than 0.18 mm.

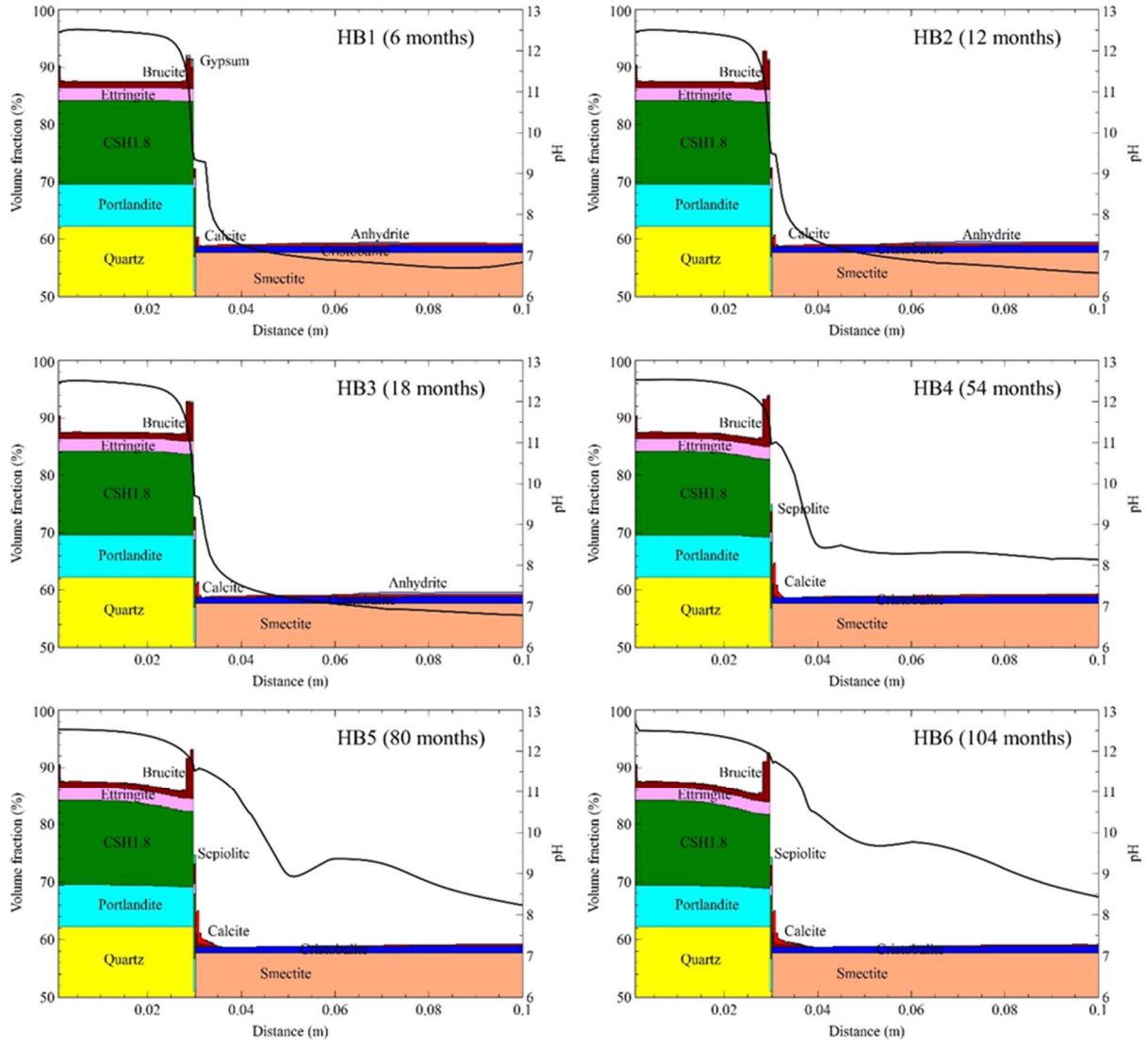

Figure 1: *Computed pH and mineral volume fractions for the HB1, HB2, HB3, HB4, HB5 and HB6 tests.*

3.2. Modelling of long-term transport model of the interaction of concrete, compacted bentonite and clay in a HLW repository in clay.

A non-isothermal multicomponent reactive transport model of the long-term (1 My) interactions of compacted bentonite with the corrosion products of a carbon-steel canister and the concrete liner of the engineered barrier of a high-level radioactive waste repository in clay has been performed. The model corresponds to a radioactive waste repository in clay according to the Spanish Reference Concept (ENRESA, 2004). The details of the conceptual numerical model are presented in Mon et al. (2017).

Concrete degradation leads to the precipitation of secondary minerals and the reduction of the porosity of the bentonite and the clay formation at their interfaces with the concrete liner (Figure 2). The decrease of the porosity is especially important for $t > 10^4$ years. The numerical results show that magnetite is the main corrosion product. Its precipitation reduces the bentonite porosity near the canister. The zones affected by pore clogging at the canister-bentonite, and concrete-clay interfaces at 1 My are equal to 1 and 3.3 cm thick, respectively. The pH in the bentonite after 1 My is uniform and equal to 9.42. At that time, the hyper-alkaline front (pH > 8.5) migrates 2.5 cm into the clay formation. The pH and the porosities computed with fine and coarse grids show similar trend but the zones of concrete, bentonite and clay affected by a reduction of porosity and the spreading of the high pH front in the clay computed with coarse grids are significantly wider than those computed with finer grids are. The major differences of the porosity computed with and without the porosity feedback are located in the concrete, and at the concrete-clay and canister-bentonite interfaces. The thickness of pore clogging in the concrete and in the concrete-clay interface computed with the model with the porosity feedback is smaller than that computed without the porosity feedback. The numerical results show that the porosity feedback starts to be relevant after $t > 10^4$ years. By neglecting the porosity feedback one may overestimate the thickness of the pore clogging zones for $t = 2.5 \cdot 10^4$ years. The relevance of porosity feedback could increase for larger times.

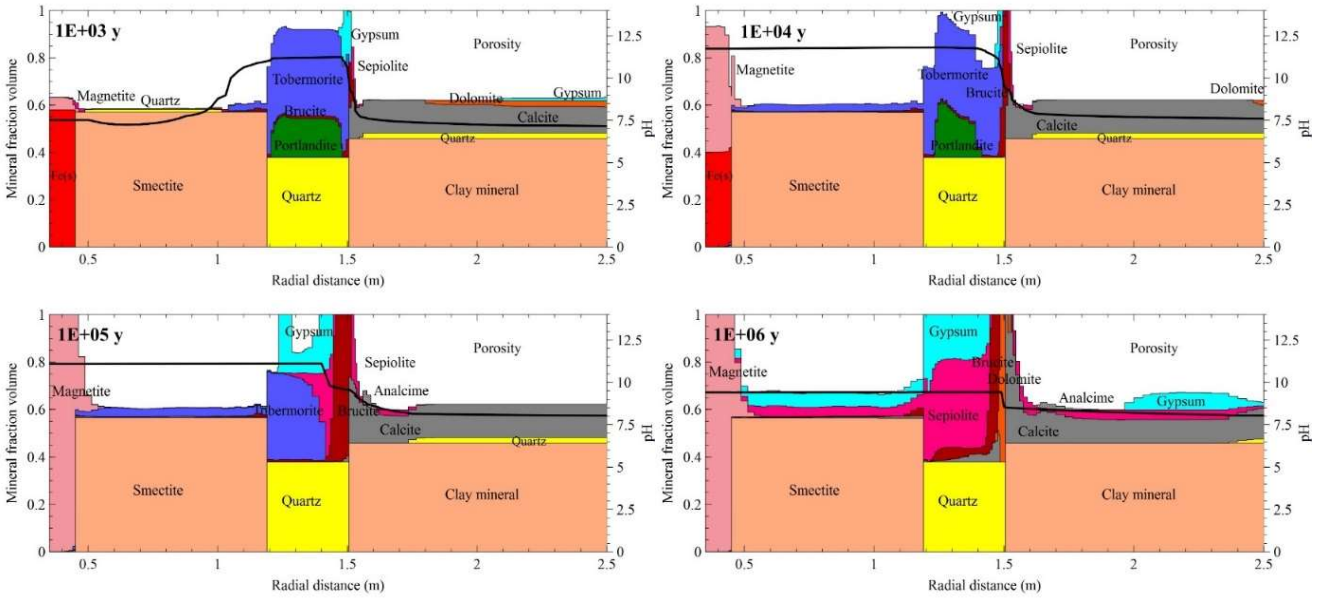

Figure 2: *Computed pH and mineral volume fractions at selected times.*

References

ENRESA (2004). Evaluación del comportamiento y de la seguridad de un almacén geológico profundo de residuos radiactivos en arcilla. Informe ENRESA 49-1PP-M-A1-01 (*In Spanish*).

Fernández, R., Cuevas, J., Mäder, U.K. (2009). Modelling concrete interaction with a bentonite barrier. European Journal of Mineralogy, 21, 177-191.

Lalan, P., Dauzères, A., DeWindt, L., Bartier, D., Sammaljärvi, J., Barnichon, J.D., Techer, I., Detilleux, V. (2016). Impact of a 70°C temperature on an ordinary Portland cement paste/claystone interface: An in-situ experiment. Cement and Concrete Research, 83, 164-178.

Mon, A. (2017). Coupled Thermo-hydro-chemical-mechanical Models for the Bentonite Barrier in a Radioactive Waste Repository. Ph.D. Dissertation. Universidad de A Coruña, Spain.

Mon, A., Samper, J., Montenegro, L., Naves, A., Fernández, J. (2017). Long-term non-isothermal reactive transport model of compacted bentonite, concrete and corrosion products in a HLW repository in clay. Journal of Contaminant Hydrology, 197, 1-16.

Samper, J., Mon, A., Montenegro, L., Pisani, B., Naves, A. (2013). Report on testing multiple-continua THCM models with laboratory and large-scale tests. Deliverable 3.4-1 of the PEBS Project.

Samper, J., Mon, A., Montenegro, L., Cuevas, J., Turrero, M.J., Naves, A., Fernández, R., Torres, E. (2018). Coupled THCM model of a heating and hydration concrete-bentonite column test. Applied Geochemistry, 94, 67-81.

Torres, E., Turrero, M.J., Escribano, A., Martín, P.L. (2013). Geochemical interactions at the concrete-bentonite interface of column experiments. Deliverable 2.3-6-1 of PEBS Project.

Turrero, M.J., Villar, M.V., Torres, E., Escribano, A., Cuevas, J., Fernández, R., Ruiz, A.I., Vigil de la Villa, R., Del Soto, I. (2011). Laboratory tests at the interfaces. Final results of the dismantling of the tests FB3 and HB4. Deliverable 2.3-3-1 of PEBS Project.

Technical Summary – CTU –WP3

1. Introduction & Objectives

The Czech Deep Geological Repository (DGR) concept assumes that waste packages containing spent nuclear fuel (SNF) assemblies will be enclosed in steel-based canisters placed in vertical or horizontal boreholes at a depth of ~ 500 m below the surface. The void between the canisters and the host crystalline rock will be backfilled with compacted bentonite. Intermediate-level waste (ILW) with long-lived radionuclides, not being allowed to be disposed of in the near-surface repositories, will be disposed in DGR separate section. The ILW will be emplaced in concrete canisters in specially excavated chambers filled by bentonite as a backfill. Concrete will be used in the repository as both barrier material and construction material (e.g. fibre concrete containers for ILW, sealing and separation concrete plugs, floors, walls, supporting construction elements, shotcrete, grouting). The knowledge of cementitious materials behaviour under the DGR conditions is essential for the predictions of EBS evolution.

Generally, the behaviour of cementitious materials under different conditions is predominantly studied due to building and construction reasons. However, the conditions of DGR are specific (e.g. a combination of materials) and the EBS have to fulfil the long-term stability requirements. In the literature related to the use of cementitious materials in radioactive waste repositories, the most studies deal with conventional Portland concretes but there are also some studies concerning low-pH cementitious materials. The topics cover mainly cementitious material under DGR conditions on radionuclides sorption and diffusion.

The objective of CTU-DNC in the WP3 was to contribute with modelling of migration processes of radionuclide (through diffusion and sorption) performed on cementitious materials in the WP1 (RPM – reference Cebama mix paste, OPC – "HCP-CEM II") and WP2 (HCP-CEM_II and concretes based on CEM I and CEM III). Experimental works within WP1, performed od co-operating laboratories in CTU CEG and UJV, included long term interactions between cement/bentonite/water under two temperatures (10 and 95°C) in three periods – 9, 18 and 27 and subsequent widespread analyses for characterization of ageing and heat load on durability of cementitious materials (mechanical behaviour, mineralogy, leachates – chemical analysis, ^{3}H and ^{36}Cl through diffusion experiments under laboratory temperature etc.) The main aim was to enhance advanced models for better evaluation of laboratory through-diffusion experiments (using three datasets: concentration profile in the samples, time evolution in the inlet and outlet reservoirs and to help with a better interpretation of observed phenomena.

Works within WP2 (performed in our laboratory – CTU DNC): In accordance with the Czech program of radioactive waste disposal with SURAO being the end-user, the methodology of sorption on crushed hydrated cement paste in our laboratory was implemented via the study of the ^{85}Sr uptake during preliminary sorption experiments on a cement of CEM II grade. CEM II / A-S 42.5 R (produced by Lafarge Cement, a.s.) was chosen for the study of sorption behavior of strontium that served as an analogue of radium. The evaluation of experiments and possible development of Ra interaction with cementitious materials were addressed to our work within WP3.

The obtained data from WP1 and WP2, supported by the evaluation and modelling performed within WP3, are partly directly applicable to the long-term performance assessment (e.g. diffusion coefficients, distribution ratios) and partly as supporting arguments for material selection.

2. Studied system

The laboratory work in the WP1 was based on ageing processes in small pressure vessels with respect to Czech bentonite (Bentonit 75, B75), cementitious materials (Portland-type, OPC, and a low pH reference mix design, RPM) and groundwater from the Josef Underground Laboratory (GW Josef) under in-situ and high temperature (95°C) load conditions. The overview of the experimental program is in Table 1. Afterwards, the effects of the thermal load and time-length of the ageing procedure on the durability of the cementitious samples were studied in the next laboratory analyses (e.g. diffusion behaviour of ^{3}H and ^{36}Cl).

Table 1: *Summary of the experimental program - long-term laboratory experiments, geochemical and thermal interaction in the system with cementitious samples (ca 50 mm in diameter, 8 mm in thickness).*

	Ageing procedures	B75 suspension	GW Josef	Temperature
Sampling Periods 9/18/27 months	Bentonite suspension + OPC / RPM	×	×	10 / 95°C
	GW Josef + OPC / RPM	×	×	10 / 95°C
	CEM II or RPM + humid air (in-situ)			10°C

Note: "B75 suspension" is a mixture of Bentonite 75 (Keramost, a.s.), "GW Josef" groundwater from Underground laboratory Josef (ratio 1:5), "OPC" is CEM II A-S 42.5R - Lafarge Cement, a.s. hardened cement paste (w/c = 0.45) "RPM" is reference Cebama paste mixture.

Laboratory works within WP2, in addition to material OPC, was also focused on another cement of type CEM II (CEM II / B-M (S-LL) 32.5 R - produced by Českomoravský cement, a.s.; Heidelberg Cement Group) and retardation properties of other cementitious materials were also studied - concrete containing the type of cement CEM I 42.5 (with fine and rough aggregate and fly ash, hydration for 1 month) utilized in ÚJV Řež a.s. to stabilize the solidified solid waste container, and concrete with the type of cement CEM III B/32.5 (produced by CEMEX Czech Republic, s.r.o., with fine and rough aggregate, hydration for 1 month) used to fill chambers in intermediate radioactive waste repository Richard.

3. Main results – Scientific highlights

3.1. Methods of evaluation of through-diffusion experiments on sandwich bentonite-cement layers and advanced models of sorption kinetics

- Model of through diffusion experiments implemented in the GoldSim environment

The commonly used methods of evaluation of diffusion experiments are based on analytical solutions of the diffusion equation for idealized initial and boundary conditions (e.g. Shackelford and Moore, 2012). In order to evaluate the experiments performed with diffusion cells that use small volumes of working reservoirs, numerical methods are needed, as the boundary conditions, for which analytical solutions were derived, are not fulfilled. For the evaluation of such experiments in blocks of compacted bentonite, we developed a tool using the software GoldSim (GoldSim Technology Group, 2002). This tool enables to model diffusion through the sandwich layers

consisted of layers of different nature, e.g. separating filters and the studied layer in case of compacted bentonite (Vopalka et al. 2006) or two barrier materials (Rosendorf et al. 2018). This model was thoroughly tested in numerous studies that showed for simple initial and boundary conditions good agreement between modelled solutions of the 1D diffusion equation and corresponding analytical solutions. The model also proved to be consistent with the theory in case of retardation due to the sorption described by different types of interaction isotherm and is able to model and evaluate numerous types of diffusion experiments. The characteristic diffusion coefficients, D_e and D_a, could be obtained with the use of the model not only for experiments at stationary state, characterized by a constant mass flow going into and out of the studied layer, but also for experiments terminated sooner – i.e. in transient, or non-stationary, state. This feature enables to shorten the duration of diffusion experiments. Recently, we extended this model with the aim to prepare methods for evaluation of diffusion experiments within CEBAMA project, namely the Box's method (Box 1965) implemented in GoldSim software is used for fitting the experimental results with the model – i.e. for determination of model parameters. The innovation performed enables to determine the unknown parameters of the studied system (diffusion coefficients, parameters of sorption isotherm, porosity) more rigorously. Three sets of data could be taken into consideration: concentration changes in both input and output containers and concentration profile at the time of termination of the diffusion experiment. The application of the χ^2 test to the comparison of experimental and modelled results enables to assess the goodness-of-fit and helps to determine, which set of fitted parameters is optimal, e.g. by choosing between linear and non-linear interaction model.

- A simple method for the evaluation of diffusion experiments in the stationary state

The numerous simulation studies with the developed model of the through-diffusion experiment helped us to develop a simple tool for the determination of both diffusion coefficients for structured layers. This tool, that can be called method-of-lines, is intended for the determination of diffusion coefficients in cases where all individual parallel layers in the sandwich structure are homogeneous and fully saturated by water and the stationary state is attained. This method is only applicable for materials in which sorption can be described by the linear isotherm. The tool is based on the application of Fick's first law and reflects the knowledge of mass transfer resistance r (equal to the reciprocal value of the equivalent flux $Q_{eq} = D_eS/L$, where S and L are areas of the cross-section and width of the block in which diffusion is studied, respectively, see e.g. Neretnieks et al. 2010) that is expressed, for two layers of porous materials characterized by respective effective diffusion coefficients and widths, as:

$$r\_(x+y) = r\_(x) + r\_(y) \quad \Rightarrow \quad (x+y)/D\_(\text{e\_tot}) = x/D\_(\text{e\_}x) + y/D\_(\text{e\_}y) \qquad \textbf{Eq.1}$$

This evaluation of diffusion experiments was implemented using Excel. We recommend using relations (Eq.1) for the determination of D_e corresponding to the layer of hydrated cement for the description of diffusion through cement-bentonite-filter sandwich layers in experiments, in which the concentration profile in the layer of hydrated cement is not determined.

- Kinetic models for two-phase (liquid-solid) systems

The kinetic models summarized in Table 2 reflect the following different rate-controlling processes: mass transfer (DM), film diffusion (FD), diffusion in inert layer (ID), diffusion in reacted layer (RLD), chemical reaction (CR) and gel diffusion (GD) (Beneš et al. 1994).

Table 2: *Kinetic models of sorption checked in two-phase system crushed cementitious material – alkaline working solutions.*

Control process	Model notation	Kinetic equation
mass transfer	DM	$\frac{dq}{dt} = K_{\mathrm{DM}}(q^* - q)$
film diffusion	FD	$\frac{dq}{dt} = K_{\mathrm{FD}}(C^* - C); K_{\mathrm{FD}} = \frac{3D}{\delta R\rho}$
diffusion in an inert layer	ID	$\frac{dq}{dt} = K_{\mathrm{ID}} \frac{C^* - C}{(1 - \frac{q}{q^*})^{-\frac{1}{3}} - 1}; K_{\mathrm{ID}} = \frac{3D}{R^2\rho}$
diffusion in a reacted layer	RLD	$\frac{dq}{dt} = K_{\mathrm{RLD}} \frac{q^* - q}{(1 - \frac{q}{q^*})^{-\frac{1}{3}} - 1}; K_{\mathrm{RLD}} = \frac{3D}{R^2\rho}$
chemical reaction (taking place in the reaction zone, here for the first order reversible reaction)	CR	$\frac{dq}{dt} = K_{\mathrm{CR}} \frac{C - C^*}{(1 - \frac{q}{q^*})^{-\frac{2}{3}}}; K_{\mathrm{CR}} = \frac{3r_{\mathrm{CR}}}{R\rho}$
gel diffusion	GD	$\frac{dq}{dt} = K_{\mathrm{GD}} \frac{(q^* - q_0)^2 - (q^* - q_0)^2}{q - q_0}; K_{\mathrm{GD}} = \frac{D\pi^2}{2R^2}$

In Table 2, concentrations in liquid (C) and solid phases (q) meet at each time the balance relationship, = V/m (C_0-C)+q_0), where C_0 and q_0 are initial concentrations in the system, and q^* and C^* represent equilibrium concentrations connected with the corresponding concentrations in opposite phases by an equilibrium model (e.g. linear, Langmuir or Freundlich) applied. From this relation implies the form of the rate equation for the concentration in the liquid phase. Other symbols: V/m – phase ratio of aqueous and solid phases, K_{DM}, K_{FD}, K_{ID}, K_{RLD}, K_{CR}, K_{GD} – over-all kinetic coefficients; r_{CR} – rate of the chemical reaction; R - mean radius of the solid phase particle; ρ – specific mass of the solid sorbent; δ - thickness of the "liquid film" on the surface of the solid particle, D – diffusion coefficient of the component in the material of solid particles.

In the case of evaluation of the concentration decrease in the liquid phase the experimental data are compared with the computed concentrations corresponding to individual models (after each time of the concentration measurement). The fourth-order Runge-Kutta method was used for the numerical solution of differential equations. The Newton-Raphson non-linear regression method was used for the determination of desired parameters of kinetic models, minimizing the value of a criterion of the goodness-of-fit. The quantity *χ2/v (or WSOS/DF*, (see Eq. 2) is believed to be the appropriate criterion of the goodness-of-fit, it holds that the fit is acceptable if 0.1 < WSOS/DF < 10 (Herbelin and Westall, 1996).

$$\chi 2 = \sum\_i \hat{}\, n \blacksquare \; [\![SSx]\!]\_i / (s\_i \hat{}\, 2) \qquad \text{(Eq.2)}$$

Here $(SSx)_i$ is the square of the *i*-th deviation of corresponding experimental value from the calculated one, s_i is an estimate of standard deviation of the *i*-th experimental point, and degree of freedom, ν (or *DF*) is the number of experimental points (n) reduced by the number of independent parameters (n_p). Within the evaluation of real kinetic experiments, it was assumed that the relative standard deviations of all experimental uptake data are 0.1 and that the results of long term experiments determine the shape of equilibrium isotherm.

The presented method of evaluation of kinetic experiments was applied to 15 sets of kinetic experiments of Ra on three types of cementitious materials with various conditions of experiments. A thorough analysis of the results is being prepared for a separate publication. The best agreement of model data with the experiment, so the lowest value of the criterion, $\chi 2/\nu$ was achieved, on average, for models of mass transfer (DM), film diffusion (FM) and diffusion in an inert layer (ID). No significant difference between the studied materials was observed. The evaluation of kinetic experiments revealed that the choice of the ideal medium was not unique. However, we assume that this type of quantitative evaluation will help us to describe the sorption properties of cement materials and eventually to prepare the transport model of the radium in the cementitious barrier.

3.2. Modelling and interpretation of diffusion experiments of selected radionuclides through cementitious samples

- Evaluation of diffusion of HTO and chloride through cement samples (for WP1)

The through-diffusion (TD) experiments of HTO (^{3}H) and chloride (^{36}Cl) were performed at laboratory temperature (21–25°C) on both samples that were under temperature and ageing load, the evaluation was performed using GoldSim program developed. The HTO effective diffusion coefficients of the OPC samples increased with temperature load (preceding the diffusion experiment itself) by approximately in one order of magnitude which may have been related to the dissolution of the material under higher temperatures as well as a decrease in elasticity (micro-cracks) which lead to changes of a geometry of a diffusion pathway (higher porosity or geometrical factor of a diffusion pathway). On contrary, on RPM samples, there is no significant difference – all effective diffusivities are in the same order of magnitude. The sample ageing procedures in pressure vessels did not confirm any period-sampling (approx. 9, 18 or 27 months) dependency on diffusion parameters. Some of the diffusion experiments are still underway (OPC samples after 27 months of interaction with bentonite suspension, RPM samples after 18 months of all type of interactions), but all are evaluated up to the end of January 2019. The evaluated results are in Figure 1. The lower water to binder ratio in RPM confirmed lower diffusivities (even more than order of magnitude) and porosities (capillary + gel porosity) in comparison with OPC; mean values for RPM are from 0.25 to 0.30 which is in an agreement with BRGM observations reported in 3rd Annual Workshop proceedings.

The ^{36}Cl migration was strongly retarded in OPC samples and the evaluation of diffusion coefficients by fitting distribution coefficient K_d, porosity ε (or effective porosity ε_{eff}) or geometrical factor G was not successful. On contrary, the chloride anions were strongly repulsed from RPM samples (no decrease of ^{36}Cl concentration activity in the inlet reservoir) and no breakthrough (in the outlet reservoir) was observed even after 200 days in most series. Therefore, we concluded that the diffusion process of chloride on RPM samples is very slow ($D < 10^{-3}$ m^2/s) and there are no retardation processes of chloride on RPM samples expected ($K_d = 0$). Nevertheless, for future use of both cement mixtures in the planned DGR, these materials in case of migration of chloride seem to be very effective for retardation or as a diffusion resistance.

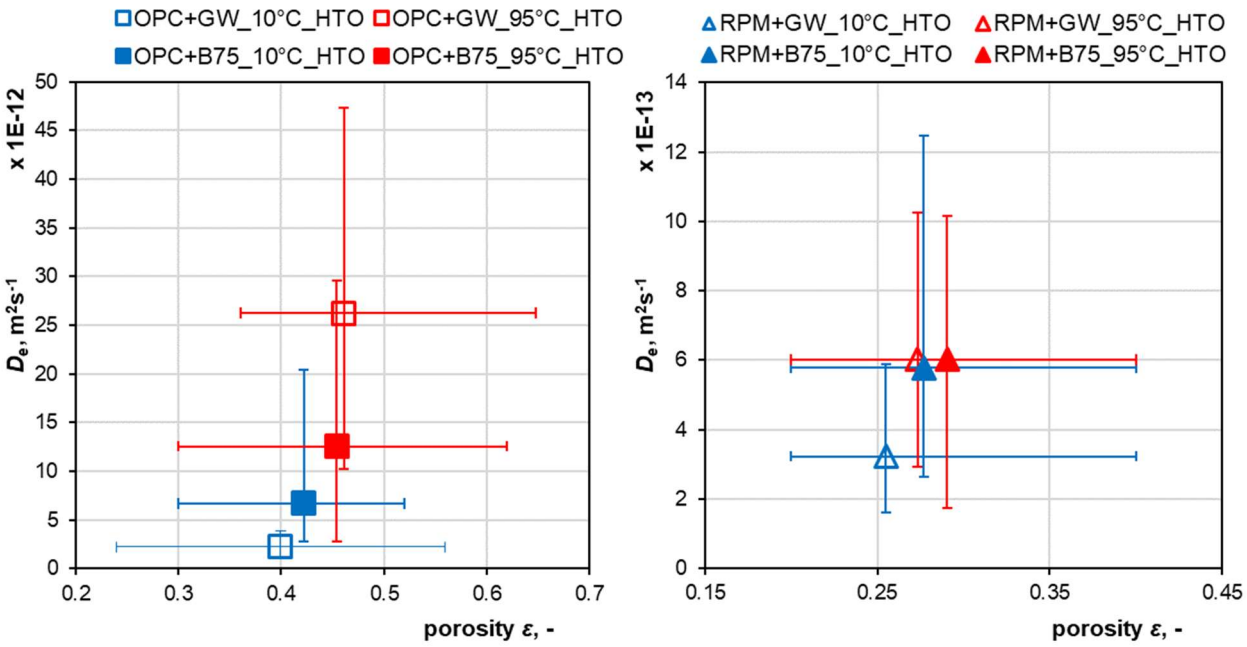

Figure 1: *Effective diffusion coefficient of HTO on OPC (left) and RPM (right) samples: dependency on the fitted porosity of the samples; each series with OPC (RPM): mean value from 7(4) TD experiments.*

- Diffusion of Ra through the pressed layer of crushed hydrated cement paste (for WP2)

Two diffusion experiments with ^{223}Ra were carried out in saturated $Ca(OH)_2$ solution (portlandite water) or synthetic cement water (CPW) through the HCP CEM II layers (CEM II A-S 42.5R), which were formed by pressing a crushed cementitious material. The aims of these experiments were the continuation in the study of the influence of phase ratio V/m on the value of distribution coefficient K_d. The solid material layer of 0.5 cm width was saturated with the appropriate solution prior to the addition of the migrating ^{223}Ra. The volumes of the inlet and outlet containers were 50 mL, separating filters of 0.08 cm width were used for the separation of cementitious material from containers with working solutions. Radium used for the diffusion study was the isotope ^{233}Ra, with a concentration approx. 10^{-12} mol/L. The duration of the experiments was 22 days.

For the evaluation of the experiments, it was necessary to use the multicomponent fitting procedure prepared in GoldSim environment, as the stationary state was not reached. Figure 3 shows the experimental results of Ra diffusion in portlandite water and model curves corresponding to the optimal fits. The quality of fits demonstrates that the model description assuming the linearity of the sorption model and reversibility of the sorption process might be valid for the retarded diffusion transport of and Ra.

The results of diffusion experiments are in agreement with results of batch experiments, as the K_d values for ^{223}Ra computed on the basis of evaluation of diffusion experiments gives similar values as the extrapolation of K_d dependence on phase ratio V/m to lower values, in both cases about 100 L/kg.

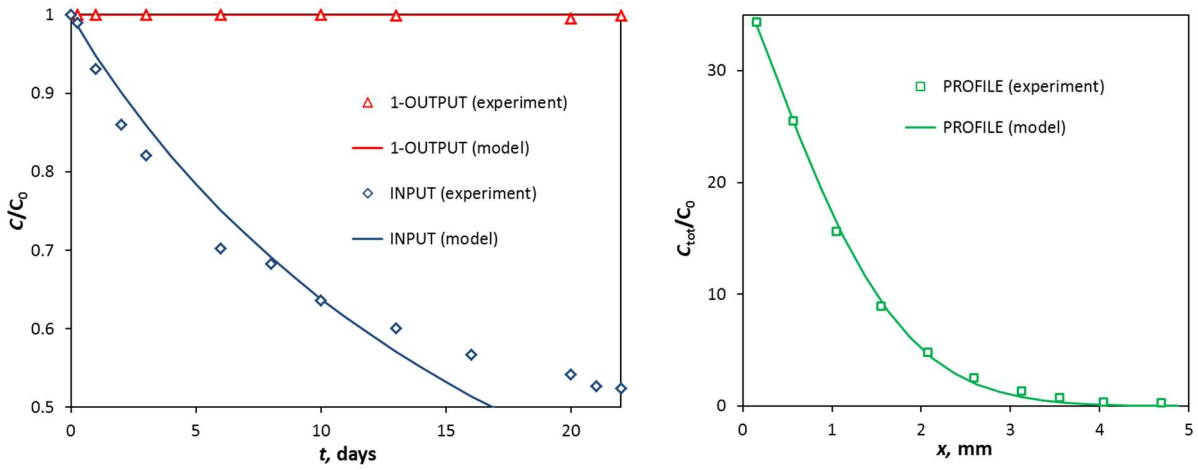

Figure 3: *Results of ^{223}Ra through-diffusion experiment of, which lasted 22 days, in portlandite equilibrated water and its optimal fit.*

References

Box, M.J. (1965). A new method of constrained optimization and a comparison with other methods. Computer Journal, 8, 42-52.

GoldSim Technology Group (2002). GoldSim Contaminant Transport Module, Manual, Version 1.30.

Neretnieks, I., Liu, L., Moreno, L. (2010). Mass transfer between waste canister and water seeping in rock fractures. Revisiting the Q-equivalent model. Technical Report TR-10-42, SKB, Stockholm.

Rosendorf, T., Hofmanová, E., Vopálka, D., Vetešník, A., Červinka, R. (2018). Comparative study of HTO diffusion on individual and coupled systems of compacted bentonite and fresh ordinary Portland cement paste. Applied Geochemistry, 97, 102-108.

Shackelford, Ch.D. and Moore, S.M. (2012). Fickian diffusion of radionuclides for engineered containment barriers. Engineering Geology, 152, 133-147.

Vopálka, D., Filipská, H., Vokál, A. (2006). Some methodological modifications of determination of diffusion coefficients in compacted bentonite. Materials Research Society Symposium Proceedings, 932, 983–990.

Technical Summary – VTT – WP3

1. Introduction & Objectives

The use of cementitious materials is difficult to avoid in modern construction. Concrete and other cementitious materials have optimal properties in terms of strength and durability. Behaviour of concrete structures are also well known and predictable. Concrete has naturally good compatibility with other construction materials due to its inorganic nature. In the Finnish deep geological nuclear waste repository, ONKALO, concrete and cementitious materials are used for structural and isolation purposes during the operational phase of the repository.

In KBS3-V and KBS3-H repository concepts, cementitious materials are not a part of engineered barrier system that ensures the stability of deposited nuclear waste and immobilizes the potentially released radionuclides. The engineered barrier system in KBS3-H and KBS3-V concepts consists of solidified high-level nuclear waste, embedded in copper canisters with cast iron inserts, compacted bentonite clay that surrounds the copper canisters, and then the surrounding bedrock. Bentonite clay consist mainly of montmorillonite -mineral that causes the swelling of bentonite clay. Compacted bentonite clay protects the copper canisters from bedrock movement and absorbs the potentially released radionuclides. Excavated deposition tunnels are further backfilled with bentonite to restore the bedrock close to its natural conditions and prevent the potential changes in groundwater movement.

Although bentonite clay is an optimal solution to protect the copper canisters from bedrock movement and prevent changes in groundwater movement, bentonite is not a stable material in high pH-conditions. Cementitious materials that are used in the operational phase of the repository possess a threat to bentonite stability over the long-term due to groundwater infusion. Groundwater infusion will cause the dissolution of cementitious materials that will induce high-pH leachates that will interact with bentonite clay.

Prediction of the high-pH leachate compositions during the lifetime of the repository is a difficult task. Thermodynamic modelling is a powerful tool to predict the leachate compositions in various conditions. Cementitious systems, experimentally studied in WP1, were modelled in WP3. Modelled and measured leachate compositions of the samples was compared, reliability of the modelling was evaluated and potential sources of error were identified. Compositional model for calcium-silicate-hydrates was derived and the model was compared with existing models.

2. Studied system

Leaching of cementitious materials with various C/S -ratios were modelled in ion exchanged water, saline groundwater and saline bentonite porewater environment. These corresponds to different systems in crystalline bedrock. Fresh water corresponds the effect of freshwater intrusion to system. Saline groundwater corresponds the effect of expected groundwater on concrete structures. Bentonite groundwater corresponds the effect of direct contact of bentonite on concrete structures.

Modelled cementitious systems C/S-ratio ranged from 3.14 (pristine OPC) to highly blended C/S-ratio of 0.2. Elemental composition of the modelled OPC was low alkali CEM I combined with colloidal silica.

Compositional model was derived from the information available in the literature.

3. Main results – Scientific highlights

3.1. Comparison between modelled and measured samples

Comparison between modelled and measured results were two-folded. The measured pore solution pH values and the modelled pH values had good correspondence in the high C/S-ratios. In low C/S-ratios, the modelled pH were lower than the measured pH values. A potential explanation is that the initial C/S-ratio does not present the real C/S-ratio of the samples. The samples might not have reached the thermodynamic equilibrium, or the used model is not accurate in low C/S-ratio samples.

Modelled iron concentrations were decades smaller, compared to the measured concentrations in ion exchanged water. Some of the magnesium results were also decades smaller in modelling. Also silicon concentration was smaller in the modelling compared to the measurements. This difference is probably related to the crystallization of secondary phases. The modelling assumes formation of Goethite (iron hydroxide), a ferrous mineral with low solubility. It is likely that precipitation rate of Goethite is very slow and the kinetics cause the difference between the modelled and measured iron concentrations. Modelling also assumes precipitation of Brucite (magnesium hydroxide). Probably, this phase does not exist in the measured samples. Same behaviour might be related to siliceous phases to explain the difference is silicon results. The modelling accuracy could be increased by excluding the precipitating phases that are known to have extremely low formation rate.

Potassium was only element which modelled concentrations were higher than the measured. This behaviour originates from absorption of potassium to CSH, which is not included in the modelling. Other measured elements had relatively good correspondence between the modelled and measured results in ion exchanged water.

In saline groundwater, modelling predicted lower elemental concentrations than measured. The explanation for this is similar as for iron, magnesium and silicon in ion exchanged water. The salinity of the groundwater probably induces precipitation of secondary minerals in the modelling. In reality, this kind of interaction might be very slow and does not affect in the measured samples. It seems that the modelling accuracy could increase if the secondary precipitation is excluded but the effect of dissolved ions is maintained. On the other hand, thermodynamic modelling presents the situation after infinite long time period. The situation in the repository conditions and timelines is probably something between experimentally studied and modelled samples.

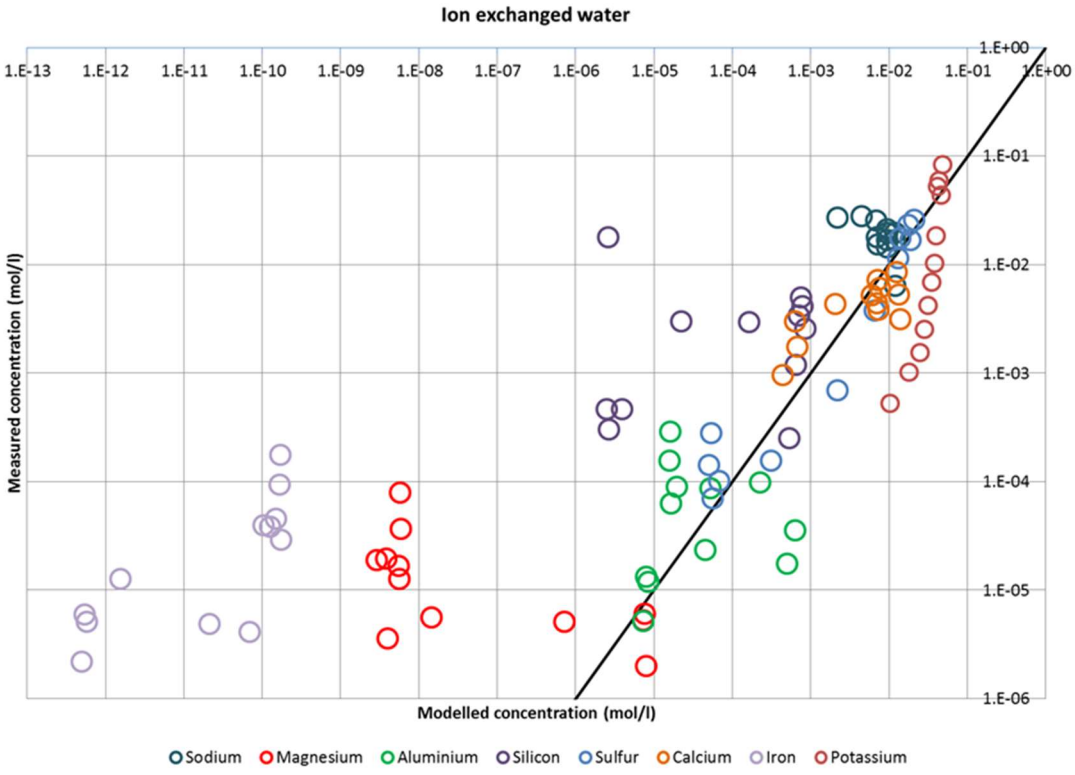

Figure 1: *Comparison of modelled and measured elemental concentrations in ion exchanged water.*

Thermodynamic modelling values and measured pH values have good correspondence in ion exchanged water. In Saline groundwater and Saline bentonite porewater, measured and modelled pH values differed. Measured values were systematically lower than modelled values.

Theoretical calculations have demonstrated that dissolved calcium is the most significant ion in solution that affects the solution pH. Calcium contributes to pH due common ion effect. Already dissolved calcium depress the solubility of calcium containing phases that controls the pH of the solution. Calcium is also able to react with the silicate containing hydrated phases. Reaction between the calcium in the solution and silicate containing hydrated phases will increase the calcium/silicon-ratio of the hydrated phases and decrease the solution calcium concentration.

The reaction between the dissolved calcium and hydrated phases is likely a very slow process. On the other hand, the decrease of pH due common ion effect happens instantly. It is likely that the solution pH is controlled by common ion effect in the experimental samples and the reaction between the dissolved calcium and hydrated phases in modelled samples. Therefore the measured and modelled pH had good correspondence in ion-exchanged water and in calcium containing groundwater the measured values were lower than the modelled.

This difference can be avoided if the thermodynamic modelling is performed in ion-exchanged water and the common ion effect is manually calculated from the modelling results.

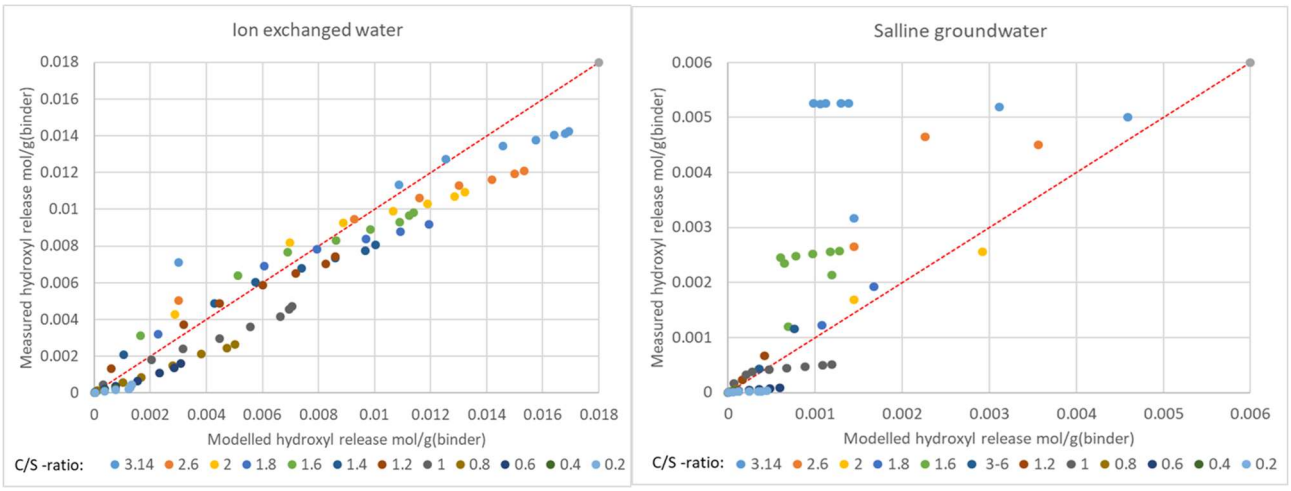

Figure 2: *Comparison of modelled and measured hydroxyl release in ion exchanged water and saline groundwater. Red line presents unison results.*

3.2. Thermodynamic compositional model for solid solution calcium-silicate-hydrate

Leaching is an essential mechanism in the degradation of calcium-silicate-hydrates in crystalline rock repository. Thermodynamic data should describe the leaching process accurately when the cementitious materials behaviour in the repository environment is studied. Another important factor is the low CaO/SiO_2 –ratio of the cementitious materials used in the repository. Cementitious materials having low CaO/SiO_2 –ratio are typically used in repositories where the engineered barrier system consists of bentonite based buffer and backfill. As the leaching and low CaO/SiO_2 –ratio cementitious materials have not been in the focus of interest in traditional concrete technology, these aspects should be carefully evaluated when the system is subjected to thermodynamic modelling.

Thermodynamic modelling that is used to estimate the long-term behaviour of cementitious materials in nuclear waste repository should be also very transparent and credible. The goal of the thermodynamic modelling of solid solution calcium-silicate-hydrate was to derive thermodynamic parameters for calcium-silicate-hydrates which are accurate respect to incongruent dissolution behaviour and able to describe calcium-silicate-hydrates behaviour in various CaO/SiO_2 –ratios. The method used to derive the thermodynamic parameter should be also highly transparent and credible. Also the magnitude of errors, originating from the calcium-silicate-hydrate model should be predictable.

General formulation of compositional model for CSH is presented in Equation 1. In Equation 1, a parameter is the molar fraction of $H_3SiO_4^-$ of total dissolved Si content in the solution, b presents the molar fraction of $H_2SiO_4^{2-}$ and y presents the molar fraction of $CaOH^+$.

$$(CaO)_x(SiO_2)_n(H_2O)_{(x+2n)} \rightleftharpoons (x-xy)Ca^{2+} + xyCaOH^+ + (n-an-bn)H_4SiO_4$$

$$+anH_3SiO_4^{1-} + bnH_2SiO_4^{2-} + (2x-xy-an-2bn)OH^- + (an+2bn)H_2O \quad \textbf{Eq. 1}$$

On the basis of Equation 1, Gibbs energy of formation was calculated to various chain lengths and C/S -ratios from the equilibrium data available in the litterature. Results are presented in Figure 3. By selecting approriate compositions, modelling of calcium-silicate-hydrate is posible to perform by using geochemical modelling code. pH values of the modelling, using dimeric silicate chain length and CaO/SiO_2 -ratios of 0.66, 0.81, 0.84, 1.26, 1.33 and 2.42 are presented in Figure 4.

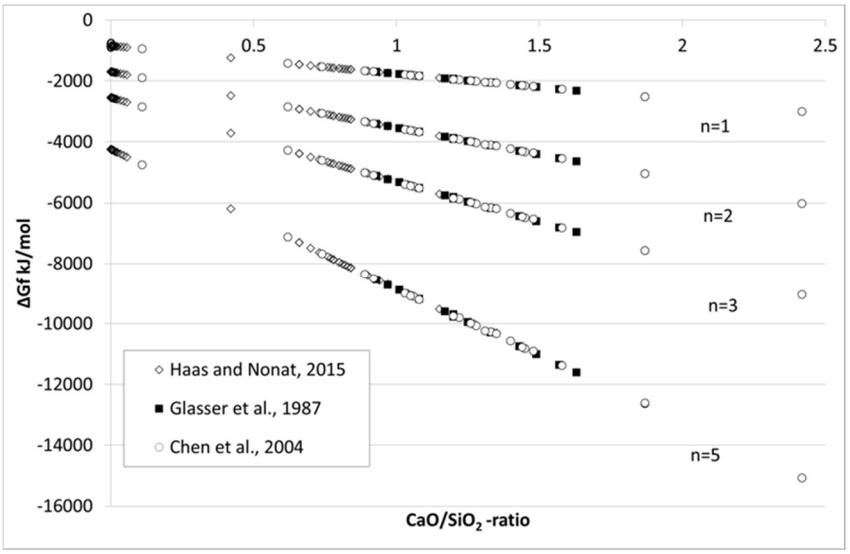

Figure 3: *Calculated Gibbs energy of formation from the datasets available in the litterature.*

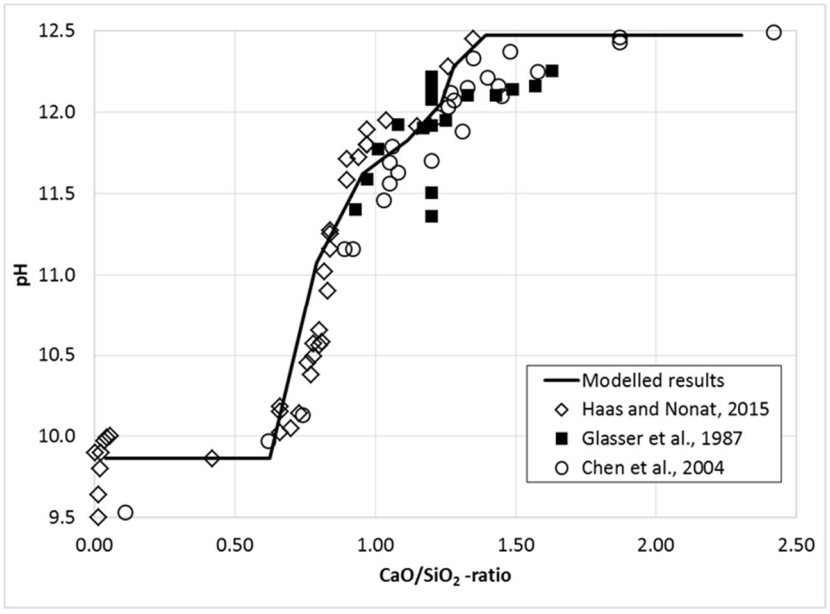

Figure 4: *Modelled pH values and experimental pH values available in the litterature.*

Technical Summary – ANDRA– WP3

1. Introduction & Objectives

Nuclear waste disposals will use a significant quantity of cement for the construction of access galleries, storage cells, concrete plugs and as containment material for low to intermediate radioactive waste. The understanding of hydraulic, mechanic and chemical evolutions of this type of disposals requires approaches, which can integrate time and space variation scales varying respectively from meters to kilometres and from years to hundreds of thousands of years.

Modelling approach helps to fulfil these requirements and till now numerous studies have been done concerning the description of the different phenomenological processes this type of disposal components and their evolutions. Many of these studies were dedicated to only one of these processes (mechanics, hydraulics or chemical). However, these processes are coupled: chemical degradation needs hydraulics and has effect on mechanical behaviour of concrete.

Thus, at the kick-off of Cebama, Andra aims to represent the hydraulic, mechanical, chemical and radionuclide (HMCR) evolution of seals and the intermediate-level long-lived (ILL) waste cells. This was expected to be achieved thanks to a methodology of up-scalling the data/models obtained in experiments developed in WP1 and WP2 (scale effect, etc.).

The work would have thus consisted in the HMCR modelling of seals and ILL cells evolution over a large scale of time and space. Concerning the ILL cells, improvement should have been provided by taking into account the chemical evolution of the cementitious materials in consistency with the related up-take processes of radionuclides. The unsaturated transient period should have also been considered as well as its consequences on chemical evolution of concrete and on some radionuclide retention. This part of the project was abandoned.

Concerning the study of seal evolution, the modelling has been intended to focus on interface between low pH concrete and clay materials (host rock). Definition of levels of coupling has depended on results from WP1 to WP2, and capabilities of the numeric tools (Crunchflow, Min3P, etc.). This part is the centre of all the work done by Andra in the WP3 of Cebama.

2. Studied system

The work of Andra is part of the modelling benchmark of WP3. Thus, the studied system represents the interface between a low-pH concrete and Callovo-Oxfordian argilites (cf. delivrable n°D3.03).

3. Main results – Scientific highlights

Andra's main contribution finally concerns the common modelling task dedicated to the inter-comparison of numerical results from various reactive transport models. Andra contributes to this task with the MIN3P model

developed by the University of Bristish Columbia (Mayer, K.U., PhD. Thesis, 1999. Andra wants to thank the UBC for its help as technical support.

Technical Summary – PSI – WP3

1. Introduction & Objectives

Reactive transport modeling is widely applied to study the temporal and special evolution of geochemical conditions in natural system in various geoscientific fields. In the framework of the CEBAMA project modeling the temporal and spatial evolution of alterations near interfaces between clay and cement based materials is important for the performance assessment of deep geological repositories for radioactive waste. Considering the chemical nature of the involved major materials, the interaction can be generally described as an acid–base reaction (aggregate/clays–alkaline cement). All chemical reactions solely proceed if a stagnant or mobile aqueous phase is present in sufficient quantity. Chemical gradients, here in particular emanating from the strongly alkaline cementitious materials, dictate the reaction courses, and the principles of chemical thermodynamics determine the fundamental reaction products of the interactions. Reaction times are strongly influenced by (often very slow) reaction kinetics and by transport of solutes. Due to the very low permeability of the clay host rocks the transport in these rocks and across interfaces to these rocks is very much dominated by diffusion. The most common approach to model diffusive transport of dissolved species in a liquid or gas phase is to use a common diffusion coefficient for all species and approximate all the water in one liquid phase. Dissolved charged species (ions/cations/complexes) that are bound (sorbed) to surfaces via surface complexation or cation exchange are assumed immobile. This allows the de-coupled solution of transport equations for dissolved species and at the same time ensures charge balance in the liquid phase. Some codes also offer the possibility to solve Nernst-Planck equations for diffusion of charged species with individual diffusion coefficients while maintaining electro-neutrality. Only some no codes currently consider gradient in chemical activity coefficients that typically arise if the ionic strength of solutions shows significant spatial variations.

To provide an accurate description of natural systems at different spatial and temporal scales, the reactive transport code has to deal with the coupling of different physical and chemical phenomena. To allow for full control in the system description, a general-purpose code thus should be able to solve chemical systems of realistic complexity; able to model physical processes for arbitrary complex geometry, numerically accurate and robust, easily scalable in terms of process coupling and system complexity, compatible with HPC architecture, well documented and preferably available as open-source.

Chemical solvers based on Law of mass action (LMA) (e.g. equilibrium constant of chemical reactions) are most commonly used to calculate equilibrium speciation in reactive transport codes due to the simplicity of the algorithm. The LMA solvers have limitations when multicomponent phases (e.g. solid solutions, non-ideal liquid and gaseous phases) have to be considered. The Gibbs Energy Minimization (GEM) algorithm is the method of choice for the simulations of multiphase systems and is based on the standard chemical potentials. Both LMA and GEMS have pros and cons when practical applications are considered. Both approaches are based on different algorithms and assumptions, but are equivalent from the theoretical point of view and must therefore, provide the same result. Recently, developed an innovative approach referred to as xLMA method, which combines the basic algorithms used in the LMA and GEM approach resulting in substantial improvement of the stability and performance of the chemical solver.

The goal of the PSI contribution in WP3 was the development of improved 2D and 3D conceptual and numerical models that consider the influence of charged mineral surfaces on chemical and transport processes. The improved models should be tested and used by analyzing experiments on interactions of concrete with clays or other materials.

2. Studied system

In cooperation with Amphos 21 we conducted a small modelling study on the hydration of the CEBMA reference mix. Furthermore we participated in the WP3 benchmarking study.

We modelled the evolution of cement/clay interfaces investigated in of the Mont Terri Cement Interaction (CI) experiment (in cooperation with Uni Bern). (Kosakowski 2018)

We intensively tested the Fenics-Rektoro framework by comparison with analytical solutions and benchmark studies. In terms of applications, we concentrated on the analysis of electrochemical diffusion experiments conducted at LES. The experimental set up consists of two adjacent reservoirs separated by a cellulose acetate membrane, which represents an uncharged porous medium. It determines the electrochemical flux of KCl between two reservoirs with an initially identical concentration of KCl. The electrochemical flux of KCl is triggered by the HNO_3 concentration gradient imposed between the two reservoirs. (Hax Damiani et al. *submitted*).

3. Main results – Scientific highlights

In the planned Swiss repository, design cement and clay materials are essential parts of the engineered barrier system. To be able to predict or reconstruct the spatial and temporal evolution of such systems, reactive transport codes are commonly applied. There is a variety of different codes available, and each one has specific advantages and limitations.

Within the CEBAMA project, we developed a new reactive transport framework FENICS-Reaktoro that allows modeling reactive transport processes in a more versatile way. We furthermore used OpenGeoSys-GEM and the new framework to model different aspects in the evolution of cement-based materials:

- the electrochemical coupling of solutes migrating in porous media with and without the presence of charged surfaces,
- and the evolution of a low-pH cement (ESDRED) in contact with Opalinus Clay on data from the Mont Terri CI experiment, which is the focus of the work conducted by the Uni Bern group in WP1.

3.1. Electrochemical transport

For the modelling of electrochemically coupled transport, we use our newly developed reactive transport framework FEniCS-Reaktoro. It allows to model reactive electrochemical mass transport in saturated porous media. It combines two state-of-the art simulation codes for solution of partial differential equations and for calculation of chemical equilibria. We implemented the sequential non-iterative approach (SNIA) for coupling transport (FEniCS) and chemical solvers (Reaktoro).

FEniCS (Alnæs et al. 2015) is a Finite Element library that offers an intuitive math-alike scripting interface that allows one to set up the physical processes directly by defining the partial differential equation easily and straightforwardly. Reaktoro (Leal et al. 2017) is a chemical solver that combines advantages of existing law of

mass action (LMA) and Gibbs Energy Minimization (GEM) solvers to speed up the equilibrium calculation. Reaktoro also allows definition of chemical problems by using GEMS (Kulik et al. 2013) and Phreeqc (Parkhurst and Appelo, 2013) files as input.

We implemented the so-called Poisson-Nernst-Planck system of equations in its weak form:

$$\int_\Omega \llbracket \Delta c \rrbracket \_i/\Delta t \cdot V\_i \, dx = \int_\Omega (-D\_i \nabla c\_i - (z\_i \, D\_i \, F \, c\_i)/RT \ \nabla\phi) \cdot \nabla V\_i \ dx \quad \textbf{Eq. 1}$$

$$\int_\Omega \llbracket \nabla \phi \rrbracket \cdot \nabla V\_\phi \, dx - F/\epsilon \int_\Omega (\sum\_(i=1)^{Ns} \llbracket z\_i \, c\_i \rrbracket) \cdot V\_\phi \, dx = 0 \quad \textbf{Eq. 2}$$

where c is the concentration, Δt is the time step, V is the test function, D_i is the diffusion coefficient for species i, z is the charge, F is the Faraday constant, R is the gas constant, T is the temperature, ϕ is the electric potential, and ϵ is the dielectric constant.

To analyze the effect of the electrochemical migration during the diffusion of ions, we model an experiment conducted at PSI by Martin Glaus to investigate the flux of charged species between two reservoirs. The experimental setup consists of two reservoirs separated by a cellulose acetate membrane. Both tanks contain a solution with KCl and HNO_3. A neutral species (HTO) was added as a non-sorbing tracer in one reservoir.

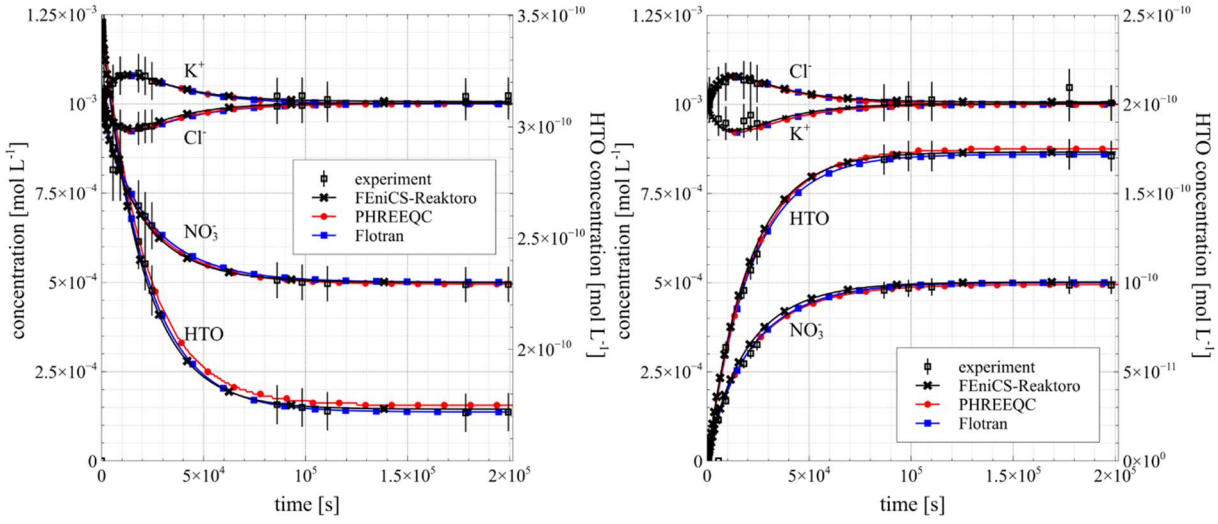

Figure 2: *Left upstream reservoir and right downstream reservoir concentration evolution demonstrating the effect of charge coupling in the K^+ and Cl^- species.*

Figure 1 presents the evolution of the concentration in each reservoir over time. The initial concentrations in the reservoirs correspond to concentrations at $t = 0$ s. In the experiment, fluxes of K^+ and Cl^- are measured during the course of the experiment even though there is no initial concentration gradient present. This so-called "uphill fluxes" are created because of the different mobility (diffusion coefficients) of the ions involved. The electrochemical fluxes of K^+ and Cl^- are triggered by the HNO_3 concentration gradient imposed at time zero. The diffusion of H^+ and NO_3^- induce additional fluxes of K^+ and Cl^- to maintain the charge balance at all times.

It is possible to see a good agreement between our results, other codes and experimental data. The electro-migration term fully controls the transport phenomena observed in this model and, therefore, the traditional Fickian approach is not suitable for describing adequately the short-term fluxes in such setups.

3.2. Hydration of the CEBAMA reference mix and modelling of cement clay interaction

For the WP3 Modelling Task benchmark study (Idiart et al. 2019), the initial state of the hardened low-pH concrete had to be calculated. For the CEBAMA reference mix no modelling study existed and detailed experimental data on the long-term hydration of the concrete were not available at the time the Modelling Task was launched. Amphos 21 and PSI therefore conducted a modelling study on the hydration of the reference mix. While Amphos 21 modelled the system using the Thermochimie thermodynamic database (Giffaut et al. 2014) with Phreeqc, we used the scripting engine of GEM-Selektor V3 and the CEMDATA thermodynamic database (Lothenbach et al. 2019). Details regarding the calculations are reported in Idiart et al. (2019). The hydration of the CEBAMA reference mixture was calculated with an approach successfully tested first by Lothenbach (2011) and later used by Kosakowski (2018) for modelling of cement/clay interaction within the Mont Terri Cement Interaction experiment.

The still ongoing Cement Interaction (CI) experiment is part of the Mont Terri Project, an underground research laboratory in Switzerland that is dedicated to investigating the Opalinus Clay formation, a formation under investigation as host rock for deep geological disposal of radioactive waste. The CI experiment is described in Jenni at al. (2014) and Mäder et al. (2017). Two boreholes in the Opalinus Clay formation were filled with sections of three different concretes and bentonite. After 2.2, 5 and recently 10 years of interaction samples of material interfaces were taken by drilling. Experimental results for up to 5-year-old samples were available when the modeling study was conducted.

The models calculated with OpenGeoSys-GEM improve earlier models (Berner et al. 2014) by using an updated thermodynamic database for cement phases, more clay and zeolites minerals, improved reaction kinetics and an alternative approach to consider cation exchange processes for C-S-H and Opalinus Clay. The model domain was represented in form of a 1D radial symmetric model (Figure 2) which takes the center of the borehole as origin and extents to a distance of 1.4 m into the Opalinus Clay.

Different model variants for the interface between Opalinus Clay (OPA) and Ordinary Portland Cement (OPC), and the interface between OPA and low pH cement (ESDRED) were calculated. The models consider the kinetically controlled hydration of clinker phases and the kinetic control of relatively slowly reacting phases like clays and zeolites.

The biggest difference between calculations for the Mont Terri CI experiment and the WP3 benchmarking study on clay/cement interaction is that for the specific setup of the CI experiment, where fresh concrete mixtures were poured into the boreholes, the explicit consideration of the cement hydration process in the reactive transport model was necessary for reproduction of most experimental observations.

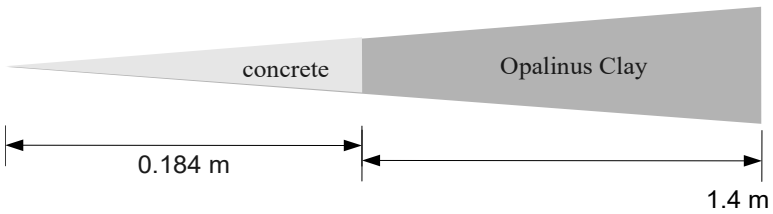

Figure 2: *Conceptual 1D radial symmetric representation of CI Experiment.*

The reactive transport models reproduce the main features reported in Jenni et al. (2014) and Mäder et al. (2017). This includes specifically the precipitation of ettringite and M-S-H in ESDRED near the interface that is visible in the modelled mineralogical profile after 5 years (Figure 3).

The Mg content of Opalinus Clay pore water will promote the conversion of C-S-H to M-S-H and to a lesser degree the formation of hydrotalcite ($MgCO_3 \cdot Fe/Al_2O_3 \cdot 5MgO$). The ingress of sulfate SO_4^{2-} causes the formation of ettringite and at very high sulfate concentrations, gypsum. The dissolution of Afm phases provides the aluminum required for ettringite formation. The precipitation/dissolution processes are linked to long-term changes in porosity, but quantitative comparison with experimental data was not yet possible.

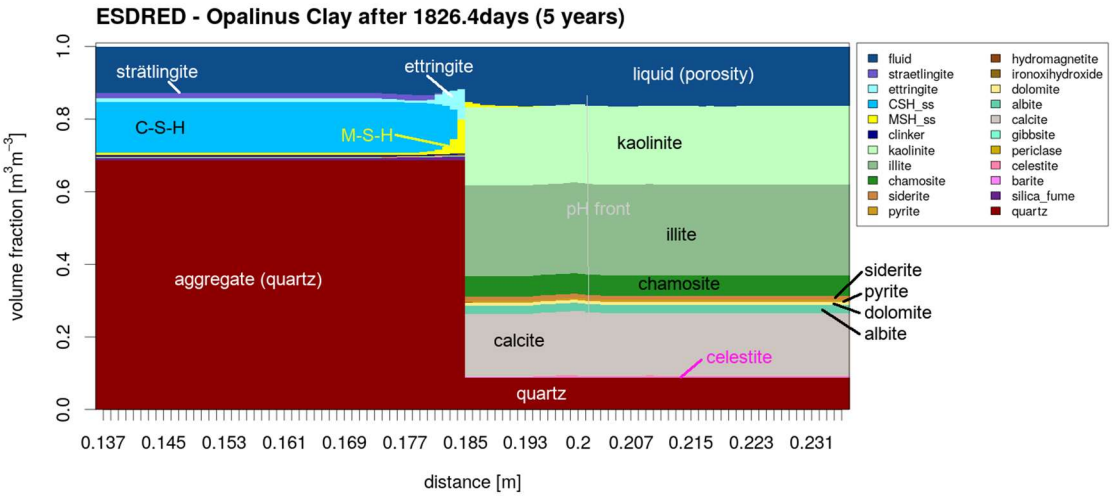

Figure 3: *Calculated mineralogical profile across the ESDRED/Opalinus Clay interface after 5 years of interaction time.*

In order to achieve a good agreement between modelled and experimentally observed behavior it was necessary to include the cement hydration process in the model. This proved to be very successful for the OPC case, as the kinetic model of Lothenbach (2011) in combination with the CEMDATA V14 database proved very successful to describe the hydration of the OPC. In agreement with the results of Lothenbach (2011) the same kinetic model was less good to describe the hydration of ESDRED concrete, because either the kinetic parameters for the dissolution of clinker phases need to be adapted or some relevant intermediately formed cement phases are missing in the thermodynamic setup.

We note that many details of the evolution of clay/cement interfaces are well represented in current state-of-the-art reactive transport models. However, large uncertainties still exist in terms of the temporal evolution of effective parameters like porosity or pH front. This relates to difficulties or even impossibilities to measure in-situ pore water compositions or reaction rates for calibration of reactive surface areas. Very long-term experiments, like the Mont Terri CI-experiment, are inevitable, as they offer the possibility to test the process understanding and knowledge about the system. Such long-term datasets offer the only possibility to calibrate model setups and extend predictability beyond the current limit of a few years.

References:

Alnæs, M., Blechta, J., Hake, J., Johansson, A., Kehlet, B., Logg, A., Wells, G.N. (2015). The FEniCS Project Version 1.5. Archive of Numerical Software, 3(100).

Berner, U., Kulik, D.A., Kosakowski, G. (2013). Geochemical impact of a low-pH cement liner on the near field of a repository for spent fuel and high-level radioactive waste. Physics and Chemistry of the Earth, Parts A/B/C, 64, 46–56.

Giffaut, E., Grivé, M., Blanc, P., Vieillard, P., Colàs, E., Gailhanou, H., Duro, L. (2014). Andra thermodynamic database for performance assessment: ThermoChimie. Applied Geochemistry, 49, 225–236.

Hax Damiani, L., Kosakowski, G., Glaus, M., Churakov, S.V. (*submitted*). A framework for reactive transport modelling using FENICS-REAKTORO: governing equations and benchmarking results.

Idiart, A.E., et al. (2019). Final Report on the Modelling Task. CEBAMA Deliverable D3.07, Brussels, Belgium.

Jenni, A., Mäder, U., Lerouge, C., Gaboreau, S., Schwyn, B. (2014). In-situ interaction between different concretes and Opalinus Clay. Physics and Chemistry of the Earth, 70–71, 71–83.

Kulik, D.A., Wagner, T., Dmytrieva, S.V., Kosakowski, G., Hingerl, F.F., Chudnenko, K.V., Berner, U.R. (2012). GEM-Selektor geochemical modeling package: revised algorithm and GEMS3K numerical kernel for coupled simulation codes. Computational Geosciences, 17(1), 1–24.

Lothenbach, B., Kulik, D.A., Matschei, T., Balonis, M., Baquerizo, L., Dilnesa, B., Myers, R.J. (2019). Cemdata18: A chemical thermodynamic database for hydrated Portland cements and alkali-activated materials. Cement and Concrete Research, 115, 472–506.

Leal, A.M.M., Kulik, D.A., Smith, W.R., Saar, M.O. (2017). An overview of computational methods for chemical equilibrium and kinetic calculations for geochemical and reactive transport modeling. Pure and Applied Chemistry, 89(5), 145–166.

Lothenbach, B. (2011). CI Experiment: Thermodynamic modelling of the hydration of ordinary Portland cement and low-pH cements. Technical note TN 2009-33. Dübendorf, Switzerland, Switzerland: Empa.

Kosakowski, G. (2018). CI experiment: Reactive transport modeling of interface evolution with OpenGeoSys-GEM (Technical Note TM-44-18-5). Paul Scherrer Institut, Villigen, Switzerland.

Kulik, D.A., Wagner, T., Dmytrieva, S.V., Kosakowski, G., Hingerl, F.F., Chudnenko, K.V., Berner, U.R. (2012). GEM-Selektor geochemical modeling package: revised algorithm and GEMS3K numerical kernel for coupled simulation codes. Computational Geosciences, 17(1), 1–24.

Mäder, U., Jenni, A., Lerouge, C., Gaboreau, S., Miyoshi, S., Kimura, Y., Lothenbach, B. (2017). 5-year chemico-physical evolution of concrete–claystone interfaces. Mont Terri rock laboratory (Switzerland). Swiss Journal of Geosciences, 110(1), 307–327.